1-1-2012

Enhancing the mechanical properties of a hydroxyapatite-collagen bone surrogate

Richard Franz Banglmaier
Wayne State University,

ENHANCING THE MECHANICAL PROPERTIES OF A HYDROXYAPATITE-COLLAGEN BONE SURROGATE

by

RICHARD F. BANGLMAIER

DISSERTATION

Submitted to the Graduate School

of Wayne State University,

Detroit, Michigan

in partial fulfillment of the requirements

for the degree of

DOCTOR OF PHILOSOPHY

2012

MAJOR: BIOMEDICAL ENGINEERING

Approved by:

_____

Advisor Date

_____

_____

_____

_____

DEDICATION

I dedicate this Dissertation to my mother and father,
Eileen and Wilhelm Banglmaier,
for their unyielding support and encouragement of my decisions, throughout my life,
and especially during the times I changed the path I was on.

I also dedicate this Dissertation to my wife,
Susan Banglmaier,
and to my son,
Stephen Banglmaier,
both of whom I love very much and thank them for their patience and devotion
during the time spent on this research.

I also dedicate this work to my dear friend,
Kurt Martin,
who's untimely passing leaves a void
Kurt, you will be dearly missed.

ACKNOWLEDGMENTS

I wish to thank all the people who have helped make this achievement possible. I would like to express my deepest gratitude to Dr. Pamela VandeVord for her support at the onset of this project and investing the time to grow this research into a funded work from an independent study. I also would like to thank my committee members, Dr. Constantine Demetropoulos, Dr. Howard Matthew, and Dr. Sam Nasser, for their interest and constructive support.

I like to thank Drs. Howard Matthew and Rangaramanujam Kannan for their early help with the solution chemistry, especially review of the calcium phosphate precursors, and polymer processing, respectively. I like to thank Dr. Therese Bou-Akl for help with protocol development, experimentation, and imaging. Thanks are due Dr. Zhi "Mike" Mei for help with SEM imaging procedures, Mary Jane Heeg for help with XRD scanning and procedure, and Dr. Guangzhao Mao for XRD scanning support.

I would like to thank Li Mao and Bin Wu for histology help and Rebecca Miller for chemistry support.

I would like to thank my family for their support over the years. I would like to especially thank my parents for their unending support to allow me the opportunity for my education. I am so very grateful to my wife for her understanding and support. And, I am grateful to my son, for him just being so awesome.

Lastly, I would like to acknowledge that funding was provided in part by a grant from the Department of Defense (DOD/CDMRP Award #: W81XWH-10-1-0892) and the Wayne State University Graduate School and Biomedical Engineering Department Dissertation Research Award.

TABLE OF CONTENTS

LIST OF TABLES

LIST OF FIGURES

CHAPTER 1 – INTRODUCTION

1.1 Statement of the Problem

Biomaterials research has identified the importance of materials that mimic the composition and morphology of the tissue that they are to replace. In particular, a biomimetic approach to bone tissue surrogates for fracture fixation and defect repair may overcome issues related to conventional biomaterials, such as stress shielding, cytotoxicity and immune response, as well as bioactivity defined as resorption and osteoinductivity. Hydroxyapatite (HAp), a calcium phosphate apatite, has a similar chemical composition as bone and positive biocompatibility. More closely mimicking bone tissue morphology is a hydroxyapatite and collagen (HAp/C) composite having both the inorganic mineral and organic biopolymer phases. HAp/C composites have shown promise as a surrogate bone biomaterial. Previous HAp/C composites exhibit morphological similarities to that of bone with the exception of collagen fiber alignment. Investigators have shown that longitudinal alignment of collagen fibers is preferential to tensile stress *in vivo*. The mechanical strength of current HAp/C composites with random collagen fiber alignment is at or below the strength of cortical bone, precluding the HAp/C composites from load bearing applications in orthopaedics. Load bearing application of HAp/C composites will require increased mechanical strength similar to that of cortical bone. Our hypothesis is that the mechanical strength of the HAp/C composite is dependent on the preferential alignment of bulk collagen fibers and not of the mineral phase. Therefore, there is a need to characterize the morphology of a HAp/C composite with preferential collagen alignment and correlate to the quantified mechanical and structural properties.

1.2 Background and significance

Bone tissue has a complex structural hierarchy of organic and inorganic phases. Bone consists of a nanocrystalline plate-like HAp deposited within the collagen fiber matrix and in alignment with the axis of the collagen fibrils [1-5]. Microscopically, mature bone is organized in concentric lamellae called osteons. These osteons, in turn, have an ordered arrangement of collagen fibers that are preferentially aligned to the stresses applied to the bone [6]. From a biomimetic point of view, a bone surrogate

material should possess comparable mineral chemical composition, fibrillar morphology, and mechanical properties equivalent to those of bone tissue.

Current research shows that HAp materials are the most promising for a bone surrogate material. Chemically, the composition of HAp is similar to the mineral phase of bone. Bone mineralization is a complex process coordinated between the fibrillogenesis of collagen molecules and calcium phosphate apatitic crystals, the constituent building blocks of bone. However, much of the knowledge has been elucidated from work on isolated solutions modeling simplified environments of specific mineralization conditions. Particularly, the solution environment has a significant effect on the mineralization outcome when calcium phosphate is precipitated in the absence or presence of collagen.

It is well known that calcium phosphate precipitation, absent collagen, undergoes phase transitions during mineralization, which may involve an amorphous calcium phosphate (ACP) or octacalcium phosphate (OCP) phase [7-23]. Both of which are dependent on thermodynamic and kinetic factors. The mineralization pH level has a significant effect on thermodynamic factors affecting the initiating precursor phases, temporal phase transitions, surface-solution interactions due to the Debye length at the mineralization front, and crystal growth accelerants [8, 11, 24-26]. The effect collagen has on mineralization is controversial. Some studies suggest it promotes HAp [27] or ACP [13] nucleation, others suggest that it inhibits HAp nucleation [28], while still others claim it has no effect on HAp nucleation [29-32]. The neutral influence of collagen may correctly characterize its affect since environmental and temporal factors (pH, ion concentration, and duration) more specifically affect calcium phosphate mineralization in the presence of collagen [9-11, 28, 33-35]. Ion concentration (speciation), pH, and reaction duration may all affect the resultant calcium phosphate phase [9, 10, 34-37]. The latter two may also affect the mineral content and mineral crystallinity, respectively.

HAp biomaterials may be produced by one of several techniques where the synthesis process can modify the composition, morphology, and material properties. *In-vivo* and *in-vitro* studies show that the synthesized HAp ceramic or composite is biocompatible with the host bone tissue, but resorption and bone ingrowth may be hindered by the solubility of the surrogate HAp biomaterial [38]. Solubility is

retarded in HAp ceramics with high crystallinity and large grain boundaries. A nanocrystalline HAp structure may be achieved by continuous precipitation followed by low temperature cold isostatic compression of the HAp powder or coprecipitation in a collagen matrix [2-5, 38]. These processes form uniform HAp crystals about 20-50 nm in size. While i*n-vitro* and *in-vivo* evaluation shows that low crystallinity nano-HAp ceramics and nano-HAp/collagen (HAp/C) composites are more soluble in the acidic osteoclastic environment during bone resorption and are actively resorbed with ingrowth of new bony tissue when implanted [2, 38], X-ray diffraction (XRD) analysis shows that the latter crystalline HAp structure is comparable to that of bone [2, 3, 38].

Often, the relevance of synthetic composites to bone is typically characterized with a visual comparison of peak intensity and breadth to an arbitrary bone x-ray diffraction pattern or with a side-by-side list of peak locations and known calcium phosphate peaks from powder diffraction files (PDF). A physicochemical comparison of the thermodynamic and kinetic factors affecting calcium phosphate mineralization with bone is needed to illustrate the optimization pathways for a synthetic HAp/C composite.

Bone fibrillar morphology observes a preferred alignment which makes bone inherently anisotropic. The transverse elastic modulus (6-13 GPa) of bone is less than the longitudinal elastic modulus (16-23 GPa) [1]. A number of theories exist for collagen alignment. One theory supports the finding that collagen aligns in response to stress applied to the bone [6]. While bones experience complex combined loading under physiological conditions, their natural occurring curvature predisposes them to undergo eccentric bending even under simple compression. Thus, a bone can simultaneously experience tensile and compressive stresses in certain areas. Martin et al. (1996) [39] showed that the equine third metacarpus exhibited preferential collagen orientation that varies throughout the cross section. Using polarized light microscopy, which suggests collagen alignment parallel to the cross section of the osteon would appear bright and collagen aligned perpendicular to the cross section would appear dark, they showed collagen fibers aligned with the longitudinal axis of the bone in areas exposed to tension and

perpendicular to this axis in areas of compression. In effect, the longitudinal orientation of collagen is suspected to act as a tensile reinforcement allowing the bone to withstand physiologic bending loads.

The current state of HAp/C composite synthesis suggests that while the bioactivity of the composite is ideal for bone graft implantation, the mechanical properties are not sufficient to sustain long-term load bearing applications. The mechanical response to collagen fiber alignment in HAp/C composites is not fully understood. Despite the evidence supporting the influence of collagen fiber alignment on the tensile and flexural strength of bone, research to date has not addressed the influence of fiber alignment in coprecipitated HAp/C composite scaffolds. In order to study the influence of collagen alignment on the strength of a HAp/C composite, a method to achieve the preferential alignment must be developed.

1.3 Specific Aims

A promising extrusion method has been developed by this lab and the resulting Hap/C composite has shown improvement in flexural strength [40]. Our research plan is to quantify the mechanical improvements and relate to the fiber alignment. First, a physicochemical characterization of the material needs to be investigated to determine synthesis parameters to produce a HAp/C composite with bone-like composition, apatitic mineral crystal phase, and crystallinity. Next, synthesis of a composite with preferred collagen alignment must be fabricated and confirmed. Lastly, correlate the fiber alignment morphology contributions to the improvements in mechanical properties. The Specific Aims for this project are to:

1) *Characterize the physicochemical properties of a synthetic HAp/C composite with bone-like composition, apatitic mineral crystal phase, and crystallinity*.

   Hypothesis 1A: The composition of the mineral and organic constituents is sensitive to the pH level of the reaction environment, with an inverse relationship between pH level and mineral content. Mineral content will decrease as the pH increases.

   Hypothesis 1B: HAp mineralization is characterized by a precursor crystalline phase, which is transient and dependent on the reaction (aging) duration. Durations beyond 8 hours will yield a HAp calcium phosphate mineral phase.

Hypothesis 1C: The degree of mineral crystallinity will increase with increased aging.

2) *Quantify the collagen alignment morphology in a HAp/C composite induced by a novel extrusion process.*

   Hypothesis 2A: Increased hydrodynamic shear flow will increase the orientation of collagen fibers.

   Hypothesis 2B: Collagen fiber orientation will be aligned in the direction of the extrudate flow.

3) *Determine the extent to which collagen alignment increases the material properties of a HAp/C composite*.

   Hypothesis 3A: Preferential orientation of collagen fibers in the HAp/C composite will be associated with increased tensile material properties.

CHAPTER 2 – STRUCTURE AND MORPHOLOGY OF BONE

2.1 Structure of the Long Bones

Bone has a hierarchical structure which affects the mechanical function at each level dependent on the length scale. Understanding the structural relationship between the components within and interactions between levels is essential to the mechanical properties observed at the gross level. The hierarchical levels of bone, from largest to smallest length scale are (Figure 1):

> "Level 1: Macrostructure: Whole bone, cancellous and cortical bone
>
> Level 2: Microstructure (from 10 to 500 μm): Haversian systems, osteons, single trabeculae
>
> Level 3: Sub-microstructure (1–10 μm): lamellae
>
> Level 4: Nanostructure (from a few hundred nanometers to 1 μm): Fibrillar collagen and embedded mineral
>
> Level 5: Sub-nanostructure (below a few hundred nanometers): Molecular structure of constituent elements, such as mineral, collagen, and non-collagenous organic proteins." [41]

For ease of discussion, we will start with the sub-nanostructural level because the nomenclature presented will be discussed throughout the other structural levels and will give us a point of reference for how the constituents at this level serve as the building blocks for the next higher structural level.

2.1.1 Sub-nanostructure

The main constituents of bone are mineral, collagen (type-1 collagen), and non-collagenous organic proteins. The mineral phase is a biological apatite crystal that is plate-shaped with dimensions on the order of 45-50 nm long, 20-25 nm wide, and 2-3 nm thick [41, 42]. Collagen molecules, with a high percentage of glycine and significant amounts of proline and hydroxyproline, form the triple helix structure of tropocollagen filaments. These units are 280

nm in length and 1.5 nm in diameter. The tropocollagen filaments are arranged in a revised quarter-stagger array forming collagen fibrils tens of nanometers in diameter. Non-collagenous organic proteins, including phosphoproteins, such as osteopontin, sialoprotein, osteonectin, and osteocalcin, may function to regulate the size, orientation, and spatial location of the HAp mineral deposits.

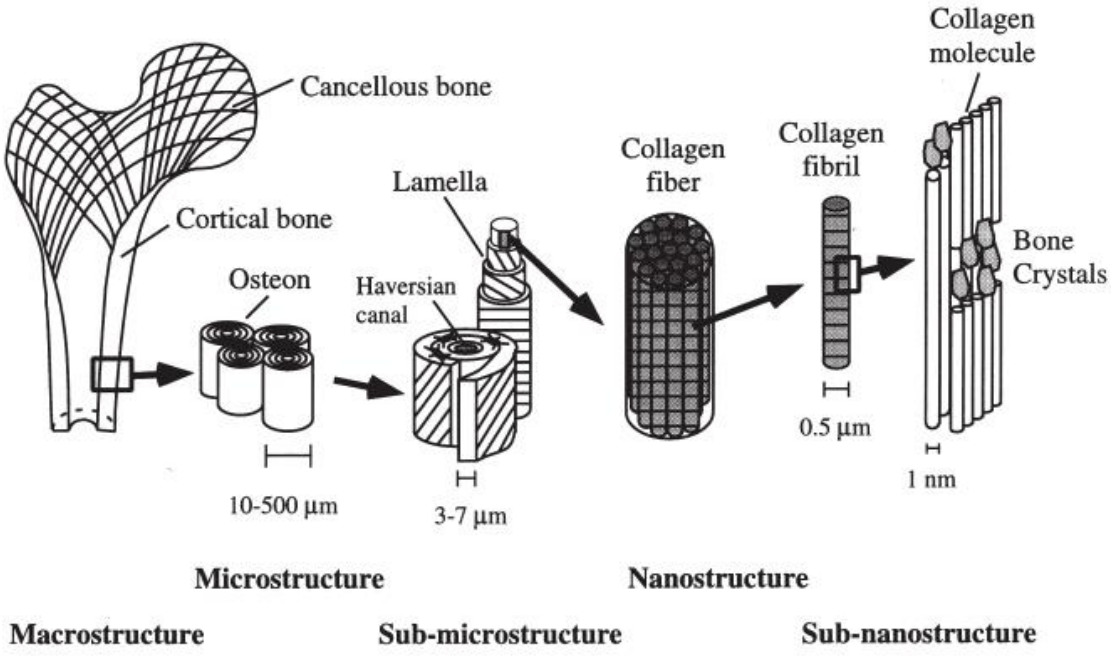

Figure 1: Hierarchical structure of bone. Reprinted from *Medical Engineering & Physics*, 20, Rho, J-Y., Kuhn-Spearing, L., Zioupos, P. "Mechanical Properties and the Hierarchical Structure of Bone", 92–102. Copyright (1998), with permission from Elsevier.

2.1.2 Nanostructure

Collagen fibers are the most prominent structures at this scale. Formed by progressive self-organization of the collagen fibrils, diameters are from hundreds of nanometers to micrometers.

2.1.3. Sub-microstructure

Bone lamellae form the concentric rings of osteons and are 3–7 mm thick. The generally accepted lamellar structure of the osteon is a parallel arrangement of the collagen fibers within a lamella and with a change in the orientation of fibers between one lamella to the next. Osteonal lamellae encompass a central canal.

2.1.4 Microstructure

The concentric arrangement of mineralized collagen fiber lamellae around a central canal form osteons or Haversian system. The osteon looks like a cylinder about 200–250 mm in diameter running roughly parallel [43] to the long axis of the bone. Between concentric lamellae are mineralized zones called cement lines. While current consensus suggests the absence of collagen in osteonal cement lines, the extent of cement line mineralization and the nature of the ground substance within the cement line are unclear [44]. Analytical techniques show that cement lines contain significantly less calcium and phosphorus, but significantly more sulfur, than surrounding bone matrix. Additionally, the Ca/P ratio of cement lines was significantly greater than that of lamellar bone, suggesting that the mineral in cement lines may not be in the form of mature HAp.

2.1.5 Macrostructure

The gross macrostructure of mature long bones is composed of three sections and two types of bone (Figure 2). The sections of the long bones are the epiphysis, metaphysis, and diaphysis. The epiphysis is located at the ends of the long bones between the articular cartilage surfaces and the metaphysis. This section is comprised of cancellous (or trabecular) bone and is encased by a thin layer of cortical (or compact) bone. The metaphysis is the transition region between the epiphysis and diaphysis where the cortical bone thins relative to the diaphysis. The diaphysis is the shaft of the long bone, between the metaphyses, and is comprised of thick cortical bone surrounding the medullary canal (or marrow cavity).

Differentiation between cortical and cancellous bone is visually evident. Cortical bone is denser than the cancellous bone residing in the ends of the long bones. Cancellous bone exhibits a complex network of lattice-like trabeculae (Figure 3a). The trabecular structure allows greater load deflection than the compact structure of cortical bone, which also provides localized energy absorption at the ends of the long bones during dynamic loading. While the strength of cortical bone is derived from its compact structure, cancellous bone strength is imparted by the alignment of the trabecular network along lines of internal stress (Figure 3b).

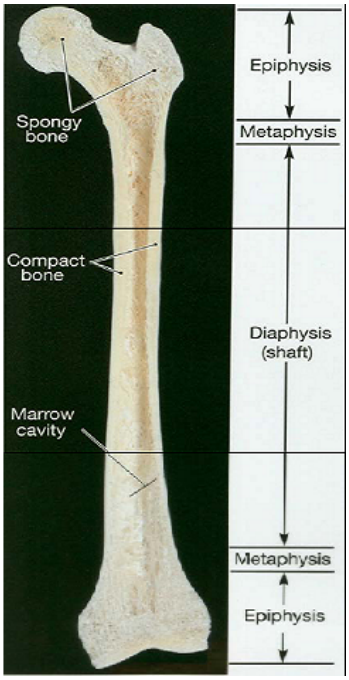

Figure 2: Gross features of the long bones displaying types of bone (cortical and cancellous) and regions.

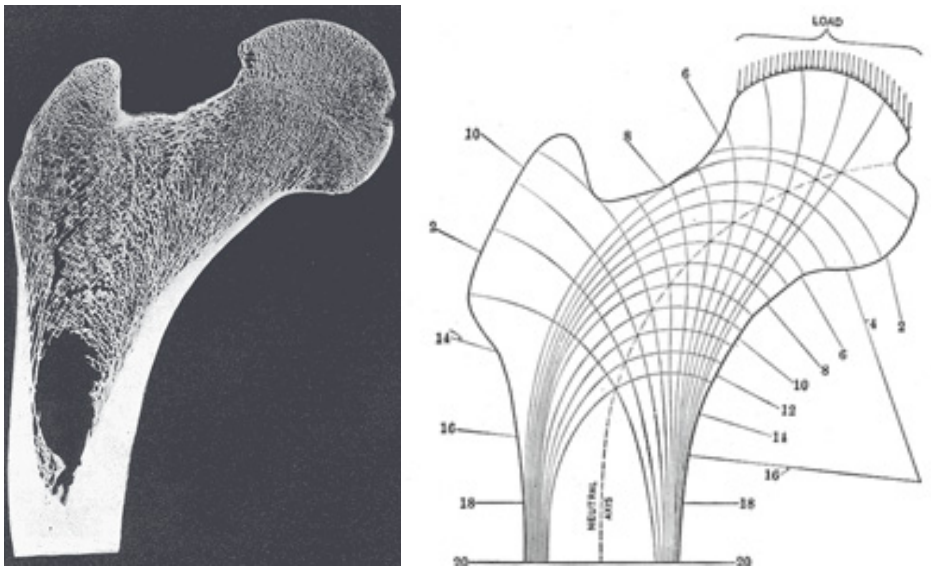

A B

Figure 3: Cancellous bone structure showing network of trabeculae. Trabeculae in the femoral head and neck (A), and schematic of trabeculae alignment along lines of principal stress (B).

2.2 Collagen Morphology

2.2.1 Collagen Structure and Theories of Orientation

Collagen fiber morphology spans several length scales down to the polypeptide chains making up the triple helix tropocollagen filaments. Three left handed helical polypeptide collagen molecules (2 α-1 chains and 1 α-2 chain) wrap around each other producing a triple helix tropocollagen filament (Figure

4). Tropocollagen filaments readily form fibrous crystals in aqueous salt solutions and self-organize into collagen fibrils in the extracellular environment. Type-I collagen fibrils consist of a repetitive tropocollagen structure known as the "revised quarter stagger" model, whereby the filaments are lined head to tail in rows that are offset by 64 nm from the adjacent filament. The staggered substructure of the collagen fibrils has regularly spaced gaps within the array (Figure 5). This arrangement also allows for cross-linking between the carboxyl terminus of one filament to the amino terminus of the adjacent filament (segments 1 and 5, respectively, in Figure 5). Taken together with the other interfilament hydroxypyridinium bridging cross-links, a stable crystal lattice is the result [42]. The gaps, or hole zones, serve as nucleation sites for the apatite crystals. The hole zones are approximately 40 nm in length and 5 nm wide limiting the growth of the crystals to their observed dimensions.

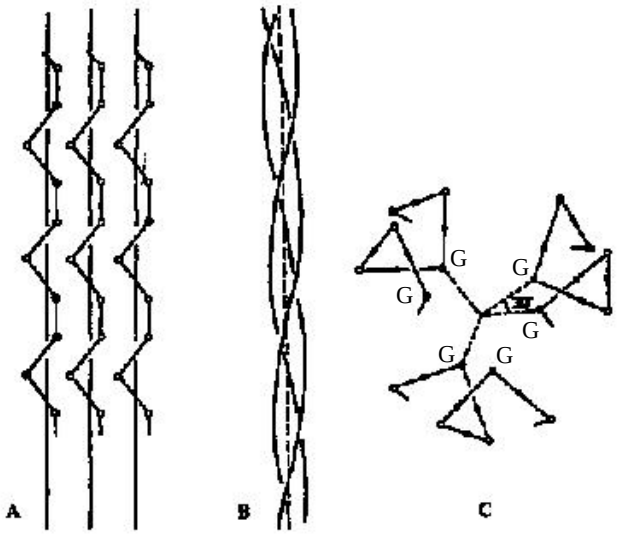

Figure 4: Schematic representation of the triple helix tropocollagen molecule. A) Three left-handed polypeptide chains, B) the assembled right-handed triple helix, and C) end view showing internal packing of glycine (G) residues. Reprinted from *Oxford University Press*, Mann, S. "Biomineralization: Principles and Concepts in Bioinorganic Materials Chemistry", R.G. Compton, S.G. Davies, J. Evans (eds.). Copyright (2001), with permission from Oxford University Press, New York.

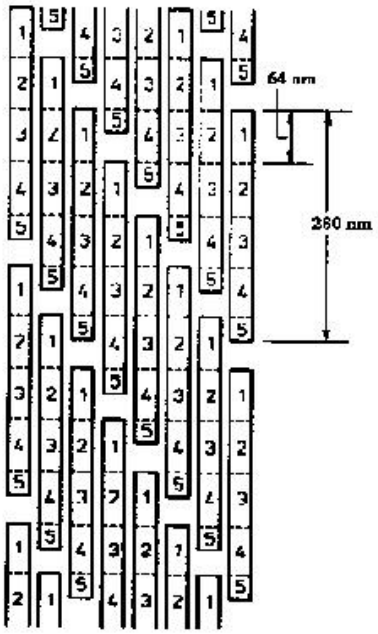

Figure 5: Revised quarter-stagger model of collagen fibrils. Reprinted from *Oxford University Press*, Mann, S. "Biomineralization: Principles and Concepts in Bioinorganic Materials Chemistry", R.G. Compton, S.G. Davies, J. Evans (eds.). Copyright (2001), with permission from Oxford University Press, New York.

2.2.1.1 Parallel Collagen Fiber Orientation

The parallel collagen fiber orientation theory is an early theory that gained acceptance to describe osteonal collagen orientation. This theory is based largely on the work of Ascenzi and Bonucci (1964, 1967, 1968, 1972) [45-48]. Collagen is theorized to have a predominantly parallel arrangement within the same lamellae with a preferred alignment within the lamellae. The collagen fibers may change up to 90º between adjacent lamellae. The result is the definition of three types of osteons, which contain different lamellar sub-structures [6]. The orientation types are: type-T (transverse), type-A (alternating), and type-L (longitudinal) (Figure 6). Type-T osteons contain lamellae with fibers that are aligned parallel to the transverse plane of the osteon cross-section. While parallel to the transverse plane, these fibers further align in the circumferential direction within each lamella. Type-A osteons contain an alternating fiber alignment between lamellae producing transverse and longitudinal direction and causing the light and dark birefringent pattern. Lastly, type-L osteons contain collagen fibers which align parallel to the osteon axis. The fibers in these osteons are extinct in polarized light and the osteon appears dark.

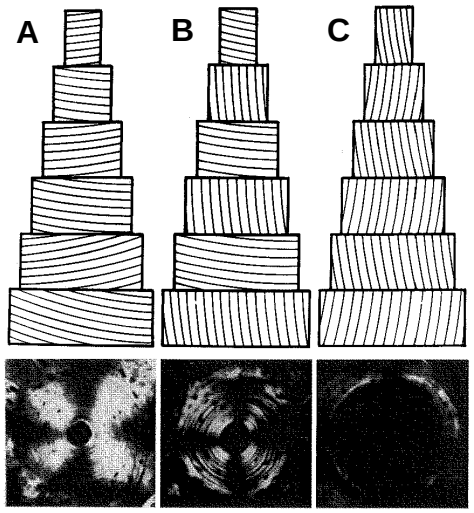

Figure 6: Schematic drawings of collagen fiber orientation patterns within lamellae of the osteon and accompanying polarized light micrograph, A) type-T collagen fiber orientation; B) type-A collagen fiber orientation; and C) type-L collagen fiber orientation. Reprinted from *Anatomical Record*, 161 (3), Ascenzi, A. and Bonucci, E. "The Compressive Properties of Single Osteons", 377-391. Copyright (1968), with permission from John Wiley and Sons [47].

2.2.1.2 Twisted and Orthogonal Plywood Model of Collagen Fiber Orientation

Giraud-Guille (1988) [49] described the lamellar collagen fiber alignment as a twisted or orthogonal plywood model. The twisted plywood model suggested that parallel collagen fibers would rotate by a constant angle between lamellar planes, similar to a helical structure (Figure 7). Similarly, the orthogonal plywood model consists of collagen fibers which are parallel in a given plane, but unlike the twisted

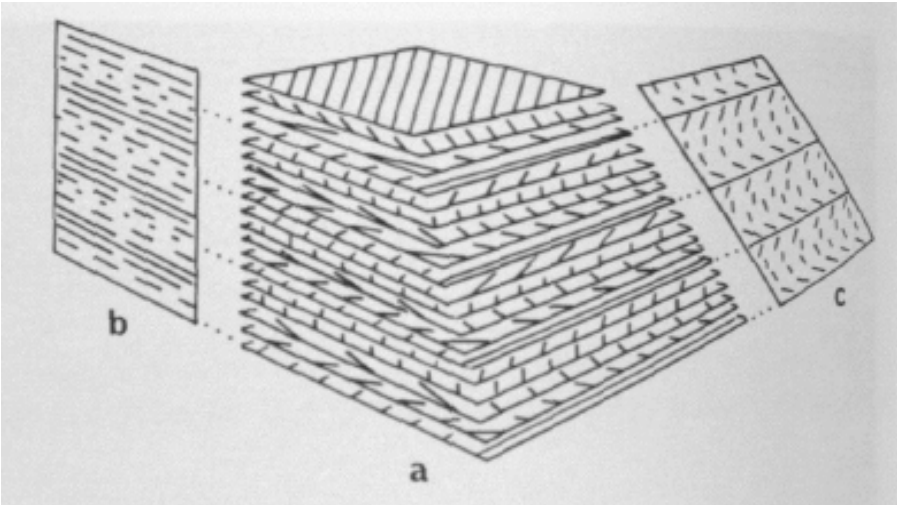

Figure 7: Twisted plywood model of collagen fiber orientation patterns within lamellae of the osteon. Springer and *Calcified Tissue International*, 42 (3), 1988, 174, "Twisted Plywood Architecture of Collagen Fibrils in Human Compact Bone Osteons", Giraud-Guille, MM. Figure 9, copyright 1988 Springer-Verlag New York Inc; with kind permission from Springer Science and Business Media.

plywood model the fibers do not rotate by a continuous angle between lamellae. In this model, the fibers align such that they are out of phase by 90º with each other. The orthogonal plywood model is a close approximation of the type-L and type-T osteons from the parallel collagen orientation model while the twisted plywood model explains the type-A osteons.

2.2.1.3 Random Orientation Packing Density of Collagen Fibers

The previous models define the collagen alignment assuming parallel fibers. However, Marotti and Muglia (1988) [50] suggested that collagen fibers were not parallel to each other, but rather were randomly aligned. Their model proposed alternating densely and loosely packed lamella (Figure 8). The alternating extinct and bright lamellae observed in polarized light microscopy were postulated to be due to the different collagen fiber densities and not the result of changes in fiber orientation. The bright osteonal rings were attributed to the loose packed lamellae while the extinct rings were attributed to the dense packed lamellae. At the time, the packing density lamellar model was thought to correspond better with how bone was formed. It was assumed that the alternating collagen alignment would require that the osteoblasts in order to produce the rotated collagen alignments. This model then suggests that the osteoblasts lay down a random matrix of collagen fibers, where the collagen fiber density would change.

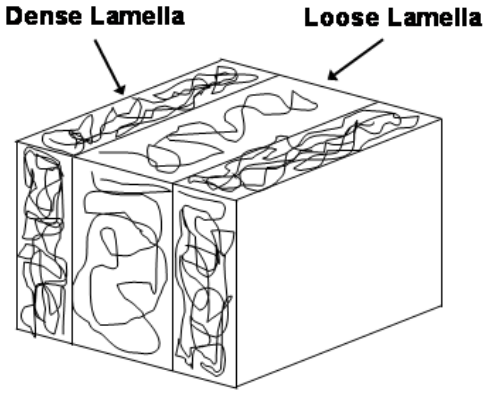

Figure 8: Random orientation packing density model of interlamellar collagen.

2.2.2 Quantification of Collagen Fiber Alignment

Collagen is a birefringent material that exhibits an optical order when examined with polarized light. Images acquired via polarized light microscopy (PLM) can then be analyzed to obtain both qualitative [50-53] and quantitative [39, 54-57] measures of the fiber orientation within a collagenous material. To understand the technique of quantifying collagen orientation, the concept of birefringence must be presented, followed by discussion of techniques used to quantifying fiber orientations.

A birefringent crystal has an optical axis that coincides with the axis of symmetry, parallel to the *c*-axis, and is considered to be an anisotropic crystal. Birefringence can be conceptualized by considering that a light ray entering an optically anisotropic (or birefringent) crystal is doubly refracted into two orthogonal linear rays, an ordinary (*o*) and extraordinary (*e*) ray, where each ray has a separate index of refraction and the ordinary ray vibrates perpendicular to the optical axis while the extraordinary ray vibrates parallel to the optical axis. When the light emerges in this case, one of the rays is retarded with respect to the other by an amount equivalent to the difference between the two indices of refraction multiplied by the thickness of the material. This retardation of the light is the magnitude of birefringence (or path difference) and causes the two rays to be out of phase when they recombine upon exiting the crystal. If the light entering the birefringent crystal is polarized (vibrating in a single plane) by a polarizing filter (polarizer), the out of phase ordinary and extraordinary rays will recombine having a vibration angle between 0º and 90º from that of the polarized light entering the crystal. This concept is illustrated in Figure 9. In cases where the ordinary and extraordinary rays are out of phase by an integer multiple (n, where n = 1, 2, 3 …) of the wavelength (λ), the resultant light emerging will be parallel to the polarizing direction (Figure 9A). If the rays are out of phase by an odd multiple of $^{n}/_{2}\lambda$ (where n = 1, 3, 5 ...), then the resultant light emerging will be perpendicular to the polarizing direction (Figure 9B). Lastly, in cases other than the preceding two, the resultant light emerging will be at an angle other than 0º and 90º from the polarizing direction (Figure 9C).

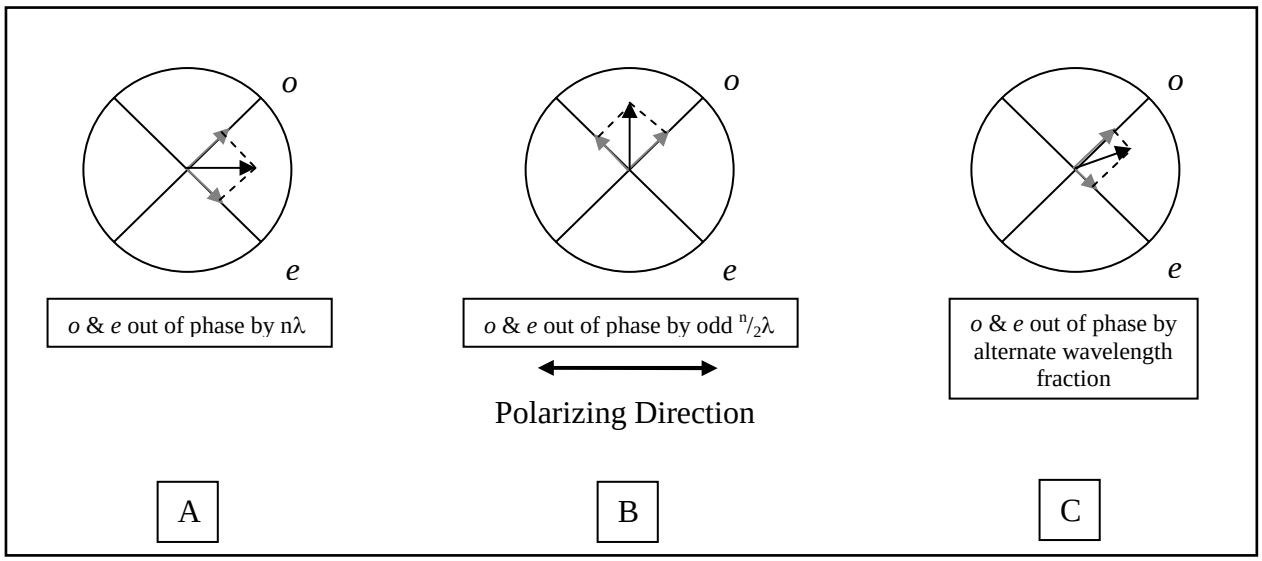

Figure 9: Birefringent double refraction in crystals: three cases of ordinary and extraordinary ray path differences and the resultant light ray recombination (*o* = ordinary ray; *e* = extraordinary ray). Black arrows show the vibration direction of the recombined resultant light ray.

Further, if a second polarizing filter (analyzer) oriented 90º to the first is placed after the light emerges from the crystal, then only components of the recombined light ray parallel to this filter will pass through the analyzer. In the first case (Figure 9A); the emerging light ray will be extinct because it is perpendicular to the analyzer. In the second case (Figure 9B); all of the emerging light ray will pass through the analyzer because it is parallel. In the last case (Figure 9C), only the component of the emerging light ray parallel to the analyzer will pass through.

Birefringent double refraction will only occur when the light entering the crystal does not propagate parallel to optical axis. Polarized light entering a crystal and propagating in the direction of the *c*-axis will not be doubly refracted and will only have an ordinary ray vibrating in the direction of the polarized light. When viewed with crossed polars (polarizer and analyzer 90º to each other) this crystal will appear extinct even when rotated through 360º in the plane of the polarizer and analyzer (Figure 10A). A crystal with a component of its optical axis perpendicular to the propagating light will doubly refract the light into an ordinary ray perpendicular to the optical axis and an extraordinary ray parallel to the optical axis. When viewed with crossed polars this crystal will appear extinct when the optical axis is orientated parallel to the polarizing direction of either the polarizer or analyzer (Figure 10B). The same crystal will become brighter when rotated in the plane of the polarizing direction of the polarizer and analyzer,

reaching a maximum brightness at angles of 45º, 135º, 225º, and 315º to the direction of the polarizer (Figure 10C).

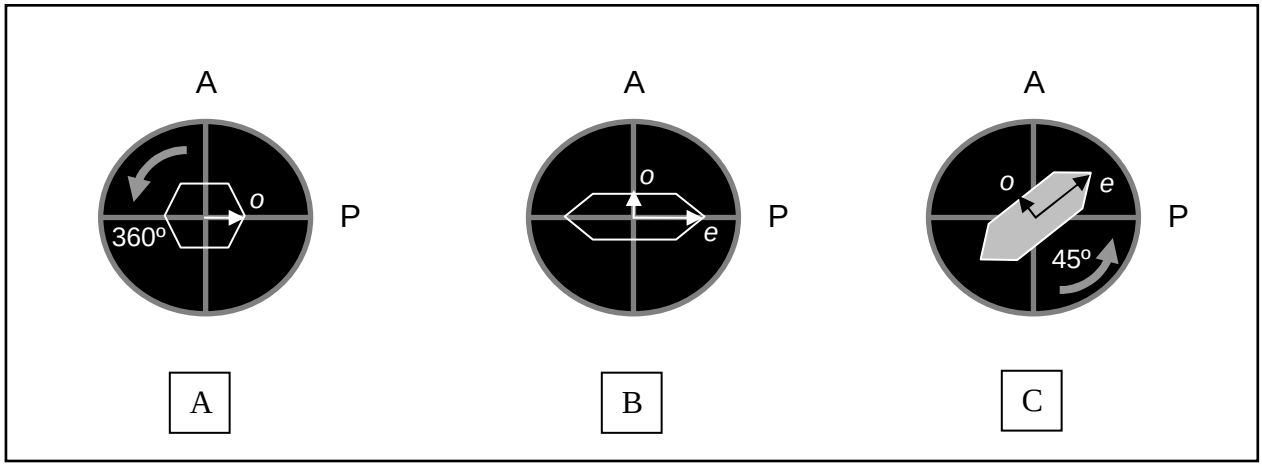

Figure 10: Effects of optical axis orientation when viewed under crossed polars. Optical axis orientation perpendicular to the plane of the crossed polars causes extinction (A). Optical axis orientation parallel to the plane of the crossed polars and parallel to the vibration direction of either the polarizer or analyzer causes extinction (B). Optical axis orientation parallel to the plane of the crossed polars and rotated an angle from the vibration direction of polarizer causes increasing light intensity. A maximum intensity occurs at angles of 45º, 135º, 225º, and 315º to the vibration direction of the polarizer (C). (*o* = ordinary ray; *e* = extraordinary ray).

These concepts hold for collagen molecules, which have been considered a crystal [42] or liquid crystal [50, 51]. PLM has been employed as a technique to quantify the orientation of collagen [39, 54, 56, 57]. Collagen fibrils oriented perpendicular to the polarizing plane (microscope stage) are extinct while those parallel to the plane may be extinct or bright [39, 46, 50, 53, 54, 57]. Collagen fibrils parallel to the vibration direction of the polarizer or analyzer will be extinct and those at an angle to either will have varying degrees of intensity. This has been a limitation of using linearly polarized light when quantifying transverse sections of osteonal collagen. Circularly polarized light has been employed to reduce this in plane extinction artifact of linearly polarized light [39, 53, 56, 57]. Alternatively, microdisection and confocal microscopy techniques have allowed the unrolling of osteon lamellae for greater dimensionality in the measurement of collagen orientation [53, 58, 59]. However, these measurements still provide an indirect measurement of the collagen orientation.

Mathematical quantification of collagen fibers may be obtained using stereological image processing techniques such as mean intercept length (MIL) [60, 61], line fraction deviation (LFD) [62], and discrete Fourier transform (DFT) [63-66]. MIL and LFD have been frequently used in the stereological study of

trabecular bone [67-70]. Sander and Barocas (2008) [71], compared the MIL, LFD, and DFT techniques on simulated fiber orientations. Of the three stereological techniques, they concluded that the DFT method was the most accurate at predicting the principle direction of fiber orientation and the anisotropy or degree of alignment. They also showed that the DFT method successfully quantified collagen orientation directly from grayscale SEM images of collagen fibrils, whereas the MIL and LFD techniques typically conducted on binary images. While MIL and LFD could both be thresholded or formulated to handle grayscale images, this would introduce significant error, sacrifice accuracy, and increase computation time.

Briefly, the DFT technique performs a Fourier transform on the grayscale pixel intensities of an image and produces a centered power spectrum image [72]. There is a radial alignment of the spectral intensities in the power spectrum image, whose angular orientation correlates to the oriented objects in the original image. In this manner, grayscale images of collagen fibers can be mathematically quantified [63-66, 71].

In this study, the DFT technique will be applied to PLM images to quantify collagen orientation. This is a new application of the DFT technique and will provide a direct measure of collagen orientation in PLM images as compared to previous PLM quantification methods. This technique is being employed because it was expected that the collagen fibers of the synthetic HAp/C composites produced in this study would be more porous than in cortical bone and would not possess the morphological features of osteons as observed in PLM studies of cortical bone. Therefore, it was necessary to utilize a direct quantification method with greater sensitivity than previous PLM methods.

2.3 Mineral Morphology

2.3.1 Composition and Orientation

The mineral apatite in bone is a carbonated phosphate apatite resembling HAp. While the chemical composition resembles that of HAp ($Ca_{10}(PO_4)_6(OH)_2$), the hydroxyl group may be absent along with inclusions of small but significant amounts of impurities such as HPO_4, Na, Mg, citrate, CO_3, K, [73]. Consequently, a more appropriate chemical composition for bone apatite would be

$(Ca,X)_{10}(PO_4,CO_3,Y)_6(OH,Z)_2$ with X substituting cations and Y and Z substituting anions – indices 10, 6, and 2 changing according to stoichiometry [38]. Going forward, bone apatite will be referred to as HAp for ease of discussion.

HAp crystals are plate-like having length and width dimensions an order of magnitude greater than thickness – 45-50 nm long, 20-25 nm wide, and 2-3 nm thick [41, 42]. This dimensional aspect ratio plays a significant role in the load borne by the crystals in situ (discussed in the next chapter). The long axis of the crystal (c-axis) is aligned with the long axis of the collagen molecules and the width of the crystal (a-axis) is aligned perpendicular to the plane of the revised quarter-stagger repeated pattern along a groove formed among adjacent tropocollagen filaments (Figure 11). This produces a plane in which the HAp crystals are offset from one and other by the length of the crystal and another plane where the crystals aligned next to each other in a row. The alignment of crystal rows produces the banding seen in collagen fibrils.

HAp crystals are restrained in the hole-zones between tropocollagen filaments, which have dimensions slightly less than the crystals themselves. Dimensions of the hole-zones are 40 nm in length and 5 nm in width. Given that the crystal width is 20 nm and the diameter of tropocollagen filaments are 1-1.5 nm, the crystals overlap in the direction of the groove. Therefore, the HAp crystals may contain collagen molecule inclusions as imperfections as the crystal forms. In addition, bonding of the HAp crystals and collagen are thought to be a function of the non-collagenous proteins. While this is not known for certain, it is known that some non-collagenous proteins bind to collagen, possibly at particular

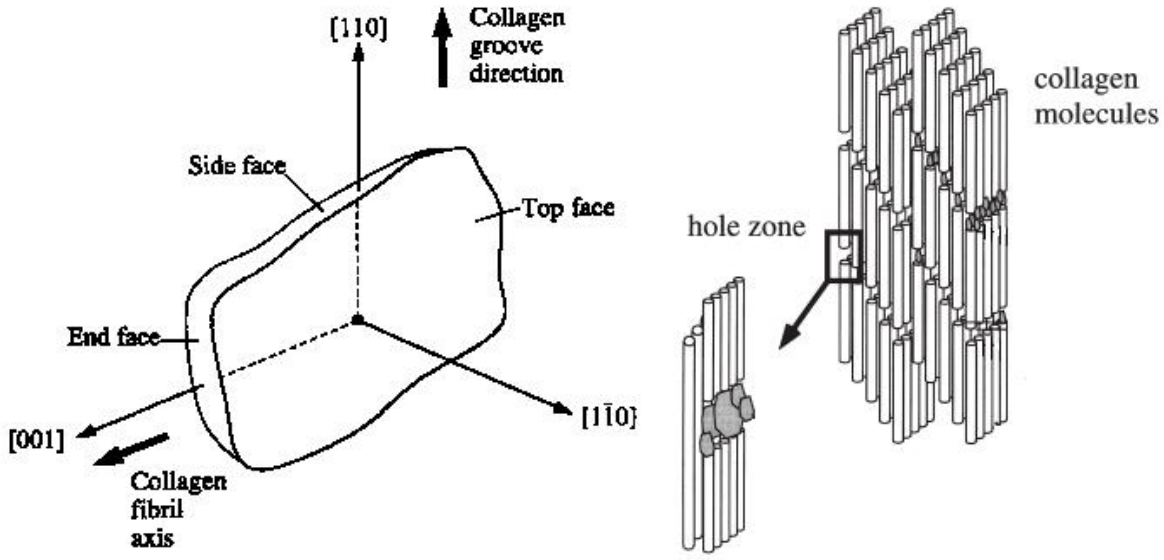

A B

Figure 11: HAp crystal morphology. A) Crystallographic axes and orientation with respect to the collagen molecule axis, and B) packing within the collagen hole zones and grooves.

A Reprinted from *Oxford University Press*, Mann, S. "Biomineralization: Principles and Concepts in Bioinorganic Materials Chemistry", R.G. Compton, S.G. Davies, J. Evans (eds.). Copyright (2001), with permission from Oxford University Press, New York.

B Reprinted from *Medical Engineering & Physics*, 20, Rho, J-Y., Kuhn-Spearing, L., Zioupos, P. "Mechanical Properties and the Hierarchical Structure of Bone", 92–102. Copyright (1998), with permission from Elsevier.

sites in the hole-zones [42]. The non-collagenous proteins have abundant anionic groups that would strongly interact with the Ca^{2+} ions of the HAp crystals.

2.3.2 Crystal Structure and Phase Determination

A number of techniques may be employed to aid in the determination of a crystal's structure and phase. Energy dispersive x-ray spectroscopy (EDS) can yield information regarding the elemental composition of a material and, by way of the atomic content, an estimate of the phase of a calcium phosphate crystallite. Raman and infrared spectroscopy can identify materials based on their characteristic bonding "fingerprints." In this way, these two techniques could yield calcium phosphate phase distinctions since the different phases would have different bonding characteristics. Crystallinity and phase composition analysis has been attempted with infrared spectroscopy [74, 75]. While these techniques offer valuable insight into the composition of a crystallite, x-ray diffraction (XRD) provides physically relevant information of a crystallite's structure and phase.

Briefly, XRD is a measure of the x-ray intensity reflected from the physical planes within a crystallite. As incident x-rays are directed onto a powdered crystallite sample over a range of angles, characteristic peak intensities are observed. These peaks are known as diffraction lines and their angular location is associated with the interplanar spacings of the crystallite, known as *d* spacing. The *d*-spacing is a measure of the interplanar spacing of successive crystal planes. An illustrative representation would be to assume that one of the crystal's exterior surfaces represents a crystal plane, say the [1 0 0] plane, as you pass through the depth of the crystal perpendicular to this plane, each successive [1 0 0] plane will be spaced *d* nanometers apart. The relationship between diffraction line location (θ) and interplanar *d*-spacing is observed in Bragg's Equation:

$$\lambda = 2d\sin\theta \qquad (1),$$

where λ is the wavelength of the x-ray source (CuKα in this study), θ is the incident angle between the x-ray source and sample, and *d* is the *d* spacing. The diffraction line position and intensity are fundamental to identifying the crystallite and subsequently its phase, since the diffraction intensities are ultimately related to both the structure and composition of the crystal phase [76].

In addition to diffraction line position and intensity, crystallographic measures are affected by diffraction line broadening. Diffraction line broadening inversely correlates with the crystal size and lattice perfection where it is used as a measure of crystallinity [77]. Diffraction line breadth is determined from the full width of a diffraction peak at half its maximum intensity – full width at half maximum (FWHM). Measurement of crystallite size can be quantified after correcting for instrumental broadening (*b*) using a Gaussian broadening correction in the form [78]:

$$\beta^2 = B^2 - b^2 \qquad (2)$$

where β is the corrected line broadening and *B* is the experimental line broadening. Using the corrected line broadening, one can determine crystallite size from the Scherrer equation [78]:

$$L = K\lambda / \beta\cos\theta \qquad (3)$$

where L is the mean crystallite dimension and K is a constant that is approximately equal to unity (K=0.89 from Bragg's simplified derivation) and related to the crystallite shape [79].

Measures of a crystallite's lattice constants are ultimately determined from its diffraction line positions. Using the relationship between the *d* spacing and the Miller indices for a hexagonal crystal system, the unit cell lattice constants *a* and *c* are related to the diffraction lines with the corresponding (*hk*0) and (00*l*) indices, respectively:

$$d_{hkl}^2 = (4/3a^2)\,(h^2 + k^2 + hk) + (l^2/c^2) \qquad (4)$$

It is evident from equation (4) that the unit cell lattice dimension *a* is dependent on [*hk*0] crystal planes and the *c* dimension is dependent on [00*l*] crystal planes for a hexagonal crystal system (different relationships exist for the other crystal systems).

CHAPTER 3 – BIOMECHANICAL PROPERTIES OF BONE

Bone is a dynamically adaptive living tissue whose strength is dependent on properties at the structural and constituent levels because of its inherent hierarchy. Generally, structural strength is dependent on geometric and material properties [80]. But, one cannot ignore that in composites the material properties of the whole or sub-structures are dependent on the interactions, organization and material properties of the constituents. Cortical bone strength has been studied at two structural levels (i.e. whole bone and osteon) and at the constituent level.

3.1 Mechanical Properties of Whole Bone and Osteons

Material properties at the whole bone structural level are derived from small uniform specimens. These specimens may be considered for the whole bone because the length scale spans that of the osteons. Modulus and ultimate (failure) stress of cortical bone are directionally dependent (Table 1). It should be noted that materials whose properties are dependent on direction of applied loading are said to be anisotropic and will be discussed further in Section 3.5. The modulus and ultimate stress of whole bone is greater in compression than tension in both longitudinal and transverse directions. The ultimate stress anisotropy is more pronounced in tension than in compression based on the values reported by Reilly et al (1974) [81] and Reilly and Burstein (1975) [82], but others have reported longitudinal compressive stresses exceeding that in tension [83]. The latter is the generally accepted norm.

Table 1: Modulus and Strength of Whole Human Cortical Bone (Femur)

	Tension		Compression	
	Longitudinal	Transverse	Longitudinal	Transverse
Elastic Modulus (GPa)	17.9 ±0.9	10.1 ±2.4	18.2 ±0.9	11.7 ±1.0
Ultimate Stress (MPa)	135 ±16	53 ±11	105 ±17 193[a]	131 ±21

From Reilly et. al. (1974) [27]; Reilly and Burstein (1975) [82]

[a] From Hayes and Gerhart (1985) [83]

On a smaller length scale, the material properties of osteon and lamellar structures have also been evaluated. Most notably is the work of Ascenzi and Bonucci [45-48]. They reported the moduli and ultimate stresses derived from tensile and compressive tests conducted on single osteons (Table 2). The

osteon moduli and ultimate stresses closely follow those values reported for the gross structure, above. The osteon types refer to those presented previously (Section 2.2.1). Note that the ultimate stresses for the type-L osteons (longitudinally aligned collagen) closely approximates the ultimate tensile stresses for the whole bone and the type-T osteons (transversely aligned collagen) approximate the ultimate compressive stresses for the whole bone. However, the osteon moduli are approximately half that of the whole bone, for the same osteon types. The reason may have to do with cement line slippage between lamellae resulting in larger deformation and the lower reported elastic moduli.

Table 2: Modulus and Strength of Osteonal Human Cortical Bone (Femur)

	Tension		Compression	
Osteon Type	Elastic Modulus (GPa)	Ultimate Stress (MPa)	Elastic Modulus (GPa)	Ultimate Stress (MPa)
Type L	11.7 ±5.8	114 ±17	6.3 ±1.8	110 ±10
Type A	5.5 ±2.6	94 ±15	7.4 ±1.6	134 ±9
Type T	-	-	9.3 ±1.6	164 ±12

From Ascenzi and Bonucci (1964, 1967, 1968) [45-47]

Interlamella deformation along the cement lines may have significance given that nanoindentation tests showed that lamellar elastic moduli are greater than the macroscopic moduli. Fan et al. (2001) [84] reported a longitudinal modulus of 24.7 GPa and transverse modulus of 17 GPa in individual lamella. Differences between these results and whole bone results may be explained by inclusion of cement lines in the macroscopic values and are more pronounced in individual osteons. Cement lines lack the presence of collagen and the mineral phase may not be in a crystallized HAp form. Perhaps, the unmineralized, low collagen content composition of the cement line results in greater plasticity and lower stiffness than the adjacent lamellae and acts to reduce the overall strength of the osteonal system compared to individual lamella [81, 85]. Differences between osteonal specimens and whole bone specimens may be the result of a more direct measurement of the single osteon cement line failure properties since it has been noted that "osteon pull-out" frequently occurs [86, 87]. Whereas, measurements at the whole bone level include multiple osteon systems with interspersed remnants of older osteons. The nanoindentation results may also provide more relevant properties of the bone constituents themselves, namely the mineralized collagen composite.

3.2 Geometric Properties

Geometric properties are relevant to bone strength because genetic variation among vertebrate species or regional variations within the cortices of the diaphysis may produce misleading interpretation of bone strength for development of orthopaedic interventions. Geometric properties taken together with the material properties will provide insight to how a bone will respond when exposed to a given load. As a hypothetical example, a transgenic rat femur may have different material and geometric properties versus control animals, yet the structural strength of the compared bones are equivalent [80]. In this particular model, a genetic defect retards the growth of the transgenic rat femur resulting in a smaller cross section and section modulus compared to controls. Given only this information, it may be concluded that the control femurs are structurally stronger for whole bone torsion or bending test. However, the material properties of the transgenic femurs are greater than the controls such that the structural strength of the transgenic femurs is equivalent to the controls. Similarly, Lanyon et al. (1979) [88] postulated that regional variations in material organization of the diaphysis may result from the maintenance of uniform stresses throughout a bone's cross-section. They found that middiaphysis areas of the cortex in compression had a lower elastic modulus than areas in tension for mature ovine radii. Riggs et al. (1993) [89] also reported elastic modulus differences between the tension and compression cortices of the equine radius at mid-diaphysis, despite the similarity in cortical thickness. These material differences were attributed to significant compositional variations, including more oblique-to-transverse collagen fiber orientation, lower mineral content, and increased remodeling with secondary osteons in the compression cortex. However, the composition is a byproduct of bone remodeling caused by non-uniform stress distributions throughout the cross-section of the diaphysis. The non-uniform stresses, in turn, are caused by eccentric loading due to the geometric curvature of the bone. Eccentric loading shifts the neutral axis and amplifies the compressive loading in the compressive cortex [90]. This example shows that the geometry of the bone can alter the stress distribution and subsequently the material properties through remodeling. While the exact mechanisms by which bone adapts are not exactly known, it is known that the material properties are a function of the constituent materials making up bone, their organization, and

their content. This study investigates the material properties of a synthetic bone surrogate based on these parameters, in particular organization. The geometric property adaptation is beyond the scope of the study.

3.3 Mechanical Properties of Collagen and HAp Crystals

Material properties at the constituent level of bone hierarchy have also been reported. Albeit type-I collagen, derived from the collagen of tendons, has been more widely reported than HAp crystals. Landis et al (1995) [91] reported a modulus of 50 MPa, maximum strain of 0.35, and a maximum stress of 20 MPa. These values, except strain, are lower compared to other investigators who put the modulus at over 1 GPa and the ultimate stress at 120 MPa [92, 93]. Gosline et al (2002) [93] reported a strain value of 0.13. It is not exactly clear why there is such a disparity between the reported values except that reported bone properties also have a high degree of variability reported over a large range. Type-I collagen molecules in bone are present in a fibrous crystal form [42], the effect of which is not discussed in the literature. HAp crystal ultimate stress and modulus are estimated to be 3 GPa and 100 GPa, respectively [94, 95]. Jager and Fratzl (2000) [96] suggest that the modulus is three orders of magnitude greater than that of type-I collagen. This order of magnitude difference would suggest that type-I collagen elastic modulus is closer to 1 GPa stated above.

Parameters such as strength, stiffness, or fracture toughness might be ascribed solely to either the HAP crystal or collagen constituents. Review of the literature suggests that strength and stiffness are due to HAp while the fracture toughness is due to collagen [94-97]. The high elastic modulus of HAp crystals imparts stiffness to composite. Strength, which is a measure of a material's failure stress, seems more likely to be due to collagen rather than the mineral phase, as the literature suggests. Consider that type-I collagen has a reported ultimate stress of 120 MPa [93], which is in the range of the ultimate tensile stress of whole bone and type-L osteons with longitudinal collagen fibers. This suggests that the failure of bone is due to collagen failure and not the HAp crystals with an estimated ultimate strength of 3 GPa. Collagen alignment relative to the load direction would therefore significantly affect the strength. Collagen is also believed to play a role in the toughness of bone. It is postulated that a toughening mechanism is fiber

bridging [98-101] whereby the fibers span across the crack opening. In general, toughness is a measure of the work or energy required to fracture a material [6]. Collagen can deform to a greater extent than HAp and remain intact behind the crack tip, thereby absorbing and dissipating the crack energy [6, 94, 95]. The reported fracture toughness of cortical bone is K=2.2-6.3 MPa·√m [6]. Again collagen alignment is presumed to affect the toughness, but the extent to which it does has not been directly quantified [98]. The assignment of these parametric roles for HAp and collagen understates the complex interaction and organization of the constituents.

3.4 Influence of Collagen and HAp on Bone Strength

Bone strength resides in the organization and interaction of the constituent materials – HAp crystals and collagen fibers. HAp and collagen form a composite material whose mechanical properties are considerably different from those of the individual constituents [102]. The resultant composite is able to withstand a variety of tensile and compressive forces where collagen and HAp by themselves could not. However, just the presence of HAp and collagen in composite form is not sufficient to generate the mechanical properties of normal bone. Landis (1995) [102] sought to identify the effect that the structural interaction of HAp and collagen had on the strength of calcified tissues by comparing normal tissue to brittle or weak tissue. Two aspects of HAp crystal formation in the abnormal tissues were found to be unusual, their crystallographic structure and spatial relationship with collagen. In the abnormal tissue, the crystals did not appear as plate, but rather as thick blocks or narrow spear shaped structures. Individual crystal sizes exceeded as much as three- to ten-fold the normal tissue crystal dimensions. The abnormal crystals were more noticeably larger in their length than in any other dimension resulting in observed spear-like abnormalities. The spatial arrangement of HAp crystals in normal calcified tissue exhibit parallel arrays of flat crystal bands or sheets following the pattern of the collagen hole-zones and grooves. On the other hand, abnormal tissue does associate with collagen, but doesn't follow the same obvious pattern of the collagen fibril hole-zones and grooves. Abnormal tissue also shows evidence of inconsistent alignment of the HAP crystal with respect to the collagen fibril axis. Another notable difference in the weakened abnormal tissue is the disorganized arrangement of collagen fibrils. Many

individual fibers are kinked or twisted and the periodicity of the revised quarter-stagger, responsible for the hole-zones and grooves, is out of phase in adjacent fibrils. The mechanism for the weakness or brittleness of the abnormal tissues is believed to arise from disruptions in the orderly arrangement of collagen fibrils. Landis (1995) [102] postulated that the structural deficiency is a consequence of defective assembly of the collagen network where the abnormal fibril period fails to produce the regular overlapping hole zones or parallel grooves that communicate across the entire fibril. The irregular holes and grooves subsequently affect the crystal growth, either arresting the growth of crystal bands across the groove or not restraining crystal growth to the desired size in the abnormal hole-zone. The model proposed by Landis (1995) [102] is shown in Figure 12. It is evident from this model that the orderly arrangement and mineralization of collagen fibrils impart strength to bone.

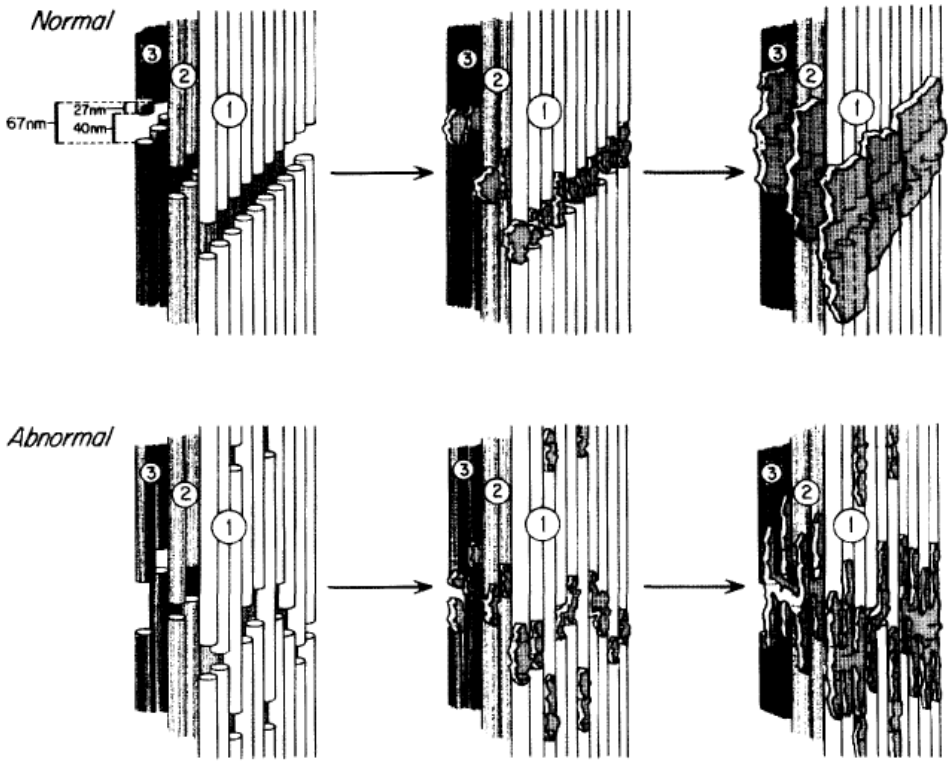

Figure 12: Normal (top) and abnormal (bottom) collagen fiber arrangement with progression of crystal growth within the hole-zone groves along parallel faces of tropocollagen filaments. Normally staggered collagen allows plate-like HAp crystals to form in the hole-zones, which continue to grow into the region of overlapping filaments. Abnormal collagen organization does not result in the staggered pattern and HAp crystal growth is retarded to form spike-like crystals that do not grow to produce crystal bands, as in normal organization and growth. Reprinted from *Bone*, 16(5), Landis, W.J., "The Strength of a Calcified Tissue Depends in Part on the Molecular Structure and Organization of its Constituent Mineral Crystals in the Their Organic Matrix", 533-544. Copyright (1995), with permission from Elsevier.

Mechanical tests and detailed analysis of the collagen-HAp interactions from a study conducted by Kikuchi et al. (2001, 2004) [2, 103] supports those qualitative findings above. These researchers evaluated the effects of pH and temperature on the bending strength and self-organization mechanism of collagen and HAp. Ideal conditions promoting strength and self-organization were pH=9 and 40ºC. They postulate that the HAp crystal structure automatically determines its orientation relative to collagen. Briefly, the mechanism is a result of weakened carboxyl bonds on the collagen caused by the interaction of Ca^{2+} ions on the surface of HAp nanocrystals. These Ca^{2+} sites on the HAp crystal surface are oriented perpendicular to the c-axis. When they interact with a carboxyl group on the collagen they cause the carboxyl group to conform perpendicularly to the long axis of the fiber. Another interesting note was that the content of collagen decreased with lower pH levels and temperature. While the study illustrates the importance of the interaction between collagen and HAp, the changes in collagen content leaves open for discussion the role that collagen plays with respect to the strength of the composite.

Two physical models also detail the importance of organization between collagen and HAp. Jager and Fratzl (2000) [96] and Gao et al (2003) [94] proposed similar models of collagen filaments and HAp crystals idealized under tensile loads (Figure 13 and 14). The organization of both models stressed the overlap of the mineralized collagen filaments. In addition, Jager and Fratzl (2000) [96] also compared their model with an unmineralized collagen overlap model and two serial HAp-collagen model without overlap (results were normalized to the unmineralized collagen model). While the serial model resulted in an increased modulus from the HAp inclusion, the maximum stress decreased 3-30%. The mineralized overlapping model increased the modulus by a factor of 59 and the maximum stress by a factor of 2. The model stresses that it is the interaction and organization of the two constituents that impart the strength seen in bone at the structural level. Mineralization alone did not increase the strength, despite increasing the modulus. The special organization of the mineralized collagen is what gives the increased strength. Gao et al. (2003) [94] suggested that the HAp crystals carried the load in tension while the collagen transferred the load to the crystals by shear. In an extension of the model, the importance of the nano-sized HAp crystals is illustrated [94, 95]. At this length scale, the large aspect ratio of the nanocrystals

causes them to withstand stresses near the theoretical limit even if they are flawed. Flaws are considered to be inclusions of the collagen molecules or other organic proteins within the crystal.

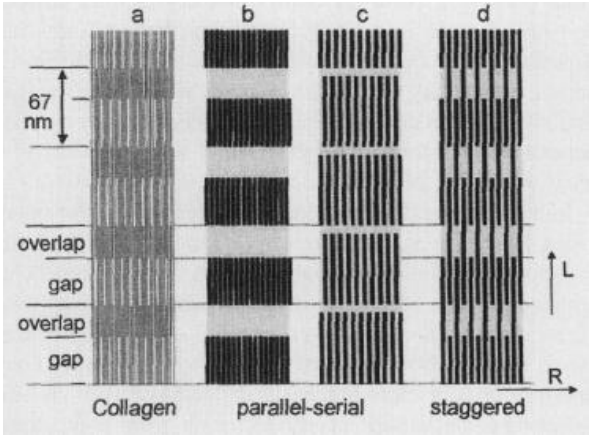

Figure 13: Two dimensional collagen model proposed by Jager and Fratzl (2000). Staggered unmineralized collagen (right) was compared to serial mineralized collagen (center) and staggered mineralized collagen to show the importance of the staggering effect on the mechanical properties. Reprinted from *Biophysical Journal*, 79, Jager, I. and Fratzl, P., "Mineralized Collagen Fibrils: A Mechanical Model with a Staggered Arrangement of Mineral Particles", 1737-1746. Copyright (2000), with permission from Elsevier.

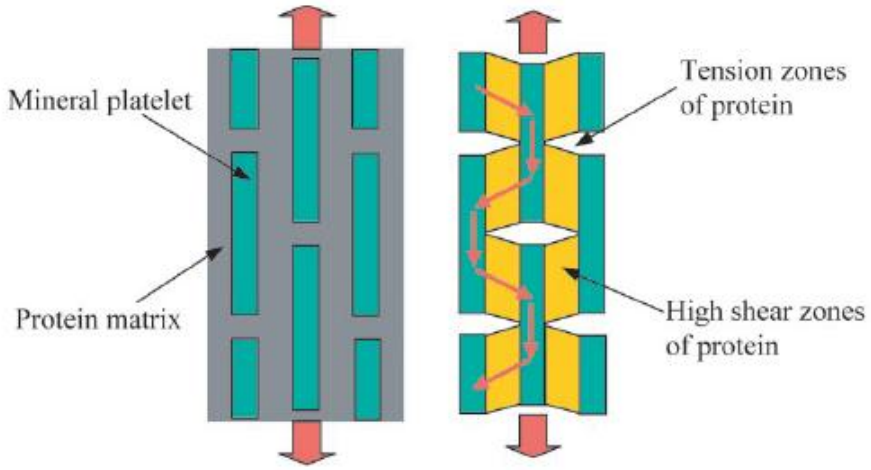

Figure 14: Two dimensional collagen model proposed by Gao et al. (2003). The model suggests that staggered mineralized collagen transfers load to the HAp crystals via shear with the crystals in tension. Unloaded (left). Loaded (right). Reprinted from *Proceedings of the National Academy of Sciences*, 100(10), Gao, H., Ji, B., Jager, I., Arzt, E., Fratzl, P. "Materials Become Insensitive to Flaws at Nanoscale: Lessons from Nature", 5597-5600. Copyright (2003), with permission from Proceedings of the National Academy of Sciences.

While a good start, this is an oversimplified model. One point in particular, the model is formulated as a 2-D planar model reminiscent of a brick and mortar configuration suggesting the entire length of the collagen filaments would be under shear, as described by Gao et al. (2003) [94] (Figure 14). This does not fully account for the periodicity of the collagen filaments where the HAp crystals would not be in linear rows across the plane but would rather be staggered as in Figure 12. This arrangement would place

the HAp crystals in shear and certain portions of the collagen filament in tension. The shear stresses on the surface of the crystals may be negligible given their high aspect ratio as the shear component from many collagen filaments would be acting on a large surface area. Perhaps more importantly, collagen filaments acting on opposite faces of a single crystal would cause a rotation of the crystal as the lines of force through the collagen filaments tried to align along the same axis. This rotation may cause a transverse compression of the interstitial fluid within the unit. As such, the model also does not account for the fluid content and its contributions to bearing loads. The interstitial fluids may bear the transverse compressions described above. The preceding discussion is used to emphasize how the organization of collagen and HAp crystals provide enhanced material properties to the whole structure. An improved model should account for these conditions, but is beyond the scope of this study.

3.5 Anisotropy

Anisotropy is the opposite of homogeneity in all directions. It is a material characteristic of being directionally dependent and can be defined as a difference in a physical property when measured along different axes. The physical properties of composite materials are generally anisotropic in nature. For instance, the elastic modulus of a composite will depend upon the directional orientation of the applied loads. As with bone, material properties are different when measured along different axes.

Bone's highly ordered internal arrangement of collagen and HAp crystals predisposes it to anisotropy. Morphological analyses show that mineralized collagen fibers are approximately parallel within lamellae [46, 49]. Section 3.1 presented the material properties of bone and osteons. The results clearly show the directional dependence, and hence anisotropy, of bone's material properties. Gibson et al. (1995) [54] showed that the lateral cortex of the equine third metacarpal bone exhibited higher bending modulus and failure strength. Using polarized light microscopy and correlating to the data of Gibson et al. (1995) [54], Martin et al. (1996) [39] showed that the lateral cortex had longitudinally aligned collagen fibers. Skedros et al. (2003) [90] suggested that regional variations in the equine third metacarpal material properties were due to collagen alignment. These studies support the idea that anisotropy in bone is a function of collagen orientation. This would suggest that the random orientation packing density theory

does not appear to explain this phenomenon while the parallel collagen orientation and twisted plywood theories do explain the anisotropy observed in bone.

CHAPTER 4 - PHYSICOCHEMICAL CHARACTERIZATION OF A HYDROXYAPAPTITE-COLLAGEN COMPOSITE

4.1 Introduction

Bone is a hierarchical structure comprised of mineral and organic constituents. As an analogue to bone mineral, synthetic hydroxyapatite (HAp) has been studied extensively [104-106]. During mineralization, it is well known that the precipitating calcium phosphate undergoes environmentally and temporally dependent phase transitions prior to the end phase HAp [7-11]. Mineralization may involve an amorphous calcium phosphate (ACP) [12-21] and/or an octacalcium phosphate (OCP) [9, 22, 23] precursor dissolving and remineralizing as HAp over time [8, 11]. Aside from inhibitory factors, the resultant calcium phosphate phase is dependent on thermodynamic factors (supersaturation, pH, ionic strength) [8, 11, 24] and kinetic factors (ion ratios) [8, 11]. Solution pH can alter the solubility of the calcium phosphate phases, where HAp is the most stable calcium phosphate phase at pH >4 [8, 11]. Both high supersaturations and pH favor an ACP precursor, but the phase transitions may occur rapidly without the inclusion of inhibitory species (Mg^{2+}, Zn^{2+}) or proteins [8, 11]. Solution ionic strength may affect the interaction between the crystal surface and solution species due to the response of the double layer Debye length at the mineralization front [11, 25]. Ion ratios may affect a temporal factor like the kinetics of crystal growth, where the ion activities of the species making up the crystal growth units favor the lowest activation barriers [11]. In addition, foreign ions may inhibit or accelerate crystal growth kinetics. Carbonate ions are a calcium phosphate phase transition accelerant [8] and inclusion into the apatitic phase has been shown to increase with pH [26].

Much of the preceding work has been isolated to simplified solution environments which model specific calcium phosphate mineralization conditions. In doing so, the mineralization solution environments have excluded collagen. The effect collagen has on mineralization is controversial, where some studies suggest it promotes HAp [27] or ACP [13] nucleation, others suggest that it inhibits HAp nucleation [28], while still others claim it has no effect on HAp nucleation [29-32]. The latter affect may correctly characterize collagen's influence since environmental and temporal factors (ion concentration,

pH, and duration) more specifically affect calcium phosphate mineralization in the presence of collagen [9-11]. Ion concentration (speciation), pH, and reaction duration may all affect the resultant calcium phosphate phase. The latter two may also affect the mineral content and mineral crystallinity, respectively. Concentration of the calcium and phosphate ions will influence the supersaturation of the respective phases, the ion activities, ionic strength, and the kinetics. In general, the result is the favored precipitation of initial precursor phases and growth pathways with the lowest activation barriers [8, 11]. Bradt et al. (1999) [9] suggested an ideal concentration of calcium and phosphate for the mineralization of collagen which would allow mineralization to proceed in concert with fibrillization. Otherwise, elevated concentrations would result in an unstructured precipitate or lowered concentrations would lead to no calcium phosphate precipitation. Calcium phosphate phase solubility is affected by the solution pH and can alter the respective phase supersaturation levels. Experiments suggest that acidic conditions can result in the precipitation of calcium phosphate phases other than HAp on existing collagen or fibroin templates while physiologic and alkaline environments yield HAp [10, 34-37]. Experiments in acidic pH resulted in calcium phosphate phases of brushite (dicalcium phosphate dihydrate – DCPD) and octacalcium phosphate (OCP) [34, 35, 37]. Calcium phosphate phases included DCPD, OCP and HAp when mineralizing collagen in neutral (pH 7) and physiologic (pH 7.4) environments [34, 35, 37]. Alkaline pH levels were shown to yield HAp only [10, 34, 35, 37]. Additionally, the mineral fraction of HAp coprecipitated with collagen varies with pH [10]. Like solution mediated calcium phosphate mineralization, the phase transitions of mineralizing collagen are also time dependent [9, 28, 35] and if amorphous phases are stabilized in collagen the crystallinity may also be time dependent. Also, incorrect timing of mineralization with collagen fibrillogenesis may lead to no mineralization or to a structureless precipitate [9].

Thermodynamic and kinetic factors affecting calcium phosphate mineralization illustrate the optimization pathways for a synthetic HAp/C composite. The present study aims to optimize the biomimetic coprecipitation of HAp and fibrillogenesis of collagen in a HAp/C composite and characterize the physicochemical properties with respect to bone. Specifically, this study investigates the

environmental and temporal effects on the composition, phase, and crystallography of a biomimetic mineral and compares to that of natural bone.

4.2 Materials and Methods

The current study utilized a biomimetic process of collagen mineralization. The mineralizing calcium and phosphate ions are coprecipitated in an assembling collagen matrix. An optimized starting calcium and phosphate concentration was held constant while varying the reaction pH and duration to quantify environmental and temporal effects.

4.2.1 Precursor Solutions

Mineralization precursor solutions were prepared by separating the calcium and collagen into one solution and the phosphate into another, before combining. Collagen was extracted from rat tail tendons, lyophilized, and was subsequently dissolved in 0.01M HCl, with a concentration of 1 mg/mL. Calcium and collagen were combined by adding 108 μL of 0.4 M $CaCl_2$ to 600 μL of the dissolved collagen. A potassium phosphate solution was prepared by adding a 1.6 M KH_2PO_4 stock solution to a 2.1 M K_2HPO_4 stock solution in a 20:80 volume ratio to achieve a pH of 7.4. Separately, a neutralization buffer was prepared with 160 μL of 0.5 M tris(hydroxymethyl)aminomethane (pH 7.4 with HCl) and 110 μL of 2 M NaCl. The potassium phosphate solution (12.98 μL) was added to the neutralization buffer. The mineralization solutions were estimated to produce a calcium to phosphorus (Ca/P) ratio of approximately 1.67 and a 85:15 mineral:collagen ratio.

4.2.2 Environmental (pH) Experiments

The calcium/collagen and phosphate precursor solutions were slowly combined while monitoring the pH. During precursor mixing, the pH was maintained at one of four pH levels; 6.8, 7.4, 8.0, or 9.0. The separate precursor solutions were pumped into a central reaction vessel with peristaltic pumps (Pulsafeeder, Punta Gorda, FL, USA) at a flow rate of 5 mL/min. The reaction vessel was maintained at 37ºC in a water bath. During mixing, the pH was monitored with an electrode (Pulse Instruments, Van Nuys, CA, USA) and controller (Jenco Instruments, San Diego, CA, USA), and activated micropumps

with a 1 M HCl or 1 M KOH titrant to maintain the pH at the desired level (Figure 15). After mixing, the solutions were allowed to react (age) for 18 hours. At the end of the 18 hour aging period, the mineralized collaged was recovered by vacuum filtration, washed three times with deionized H_2O, and dried by lyophilization. Each pH level experiment was repeated three times.

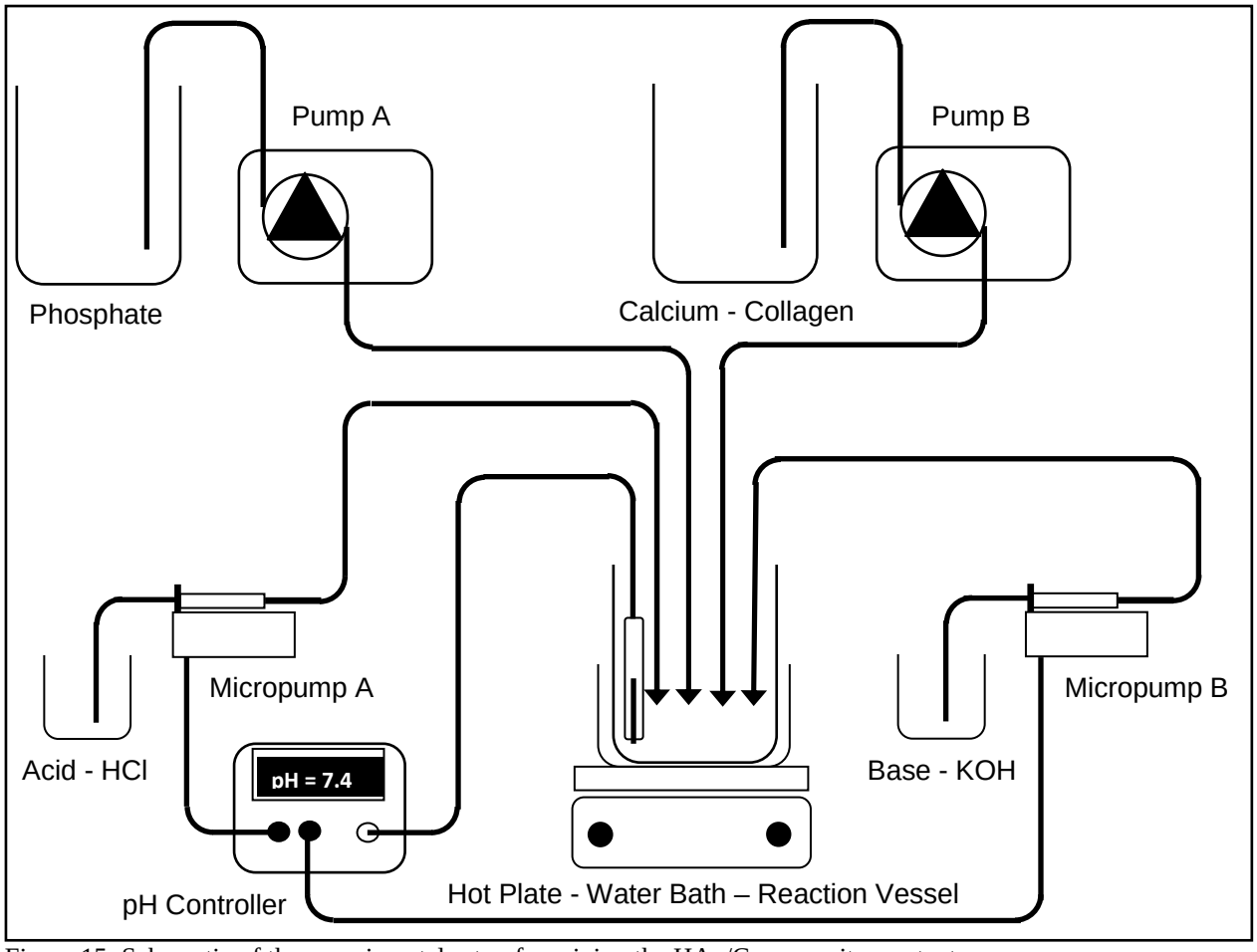

Figure 15: Schematic of the experimental setup for mixing the HAp/C composite reactants.

4.2.3 Temporal (Aging) Experiments

The temporal experiments were designed to study the effects of the post mixing reaction, or aging, duration. Precursor solutions were prepared and mixed as described above. The pH was maintained at 8.0 and the reactants were aged for one of three durations; 6, 12, or 24 hours. Each aging duration experiment was repeated three times.

4.2.4 Mineral-Collagen Composition

Mineral and collagen weight fractions of the composite were determined for the environmental group. After environmental experiment HAp/C composite recovery, a sample from each of the three experiments at each pH level was obtained for composition analysis, with an average initial sample weight of w_{wet} = 360mg. Each sample was placed in a furnace (Nytech 85P, Nytech, Bloomfield, CT, USA) and heated to 200ºF for 24 hours to remove water and weighed for a second time to determine the composite dry weight (w_{dry}). Each sample was then placed back in the oven and heated to 600ºF for 24 hours to oxidize the organic constituent and weighed a final time to determine the remaining mineral weight ($w_{mineral}$). The mineral weight fraction was the ratio of the mineral weight to the composite dry weight:

$$(w_{mineral} / w_{dry}) * 100\% \quad (1).$$

The collagen weight fraction was determined as:

$$(1 - w_{mineral} / w_{dry}) * 100\% \quad (2).$$

4.2.5 Calcium to Phosphorus Molar Ratio

The molar ratio of calcium to phosphorus (Ca/P) in the HAp/C composite was determined by the use of energy-dispersive x-ray spectroscopy (EDS), which enabled molar ratio quantification of the environmental and temporal sample composites. The EDS samples were prepared after vacuum filtration. Wet precipitate was placed onto a carbon tape disk, pressed flat to produce a thin film, and air dried. Samples were placed on a sample holder and then placed in a scanning electron microscope (SEM) with a tungsten filament and equipped with an EDS (JSM-6510LV-LGS, JEOL Ltd, Tokyo, Japan). Calcium and phosphorus x-ray counts were quantified as atomic %. The values of which were then used to derive the Ca/P ratio of the samples.

4.2.6 X-ray Diffraction Analysis

Diffraction patterns were obtained from 30 powder samples from the following groups: hydroxyapatite reference standard (HAp-RS), amorphous calcium phosphate reference standard (ACP-RS), natural bone from the femora of male Wister rats, demineralized bone from the femora of male Wister rats, environmental experiment, and temporal experiment (Table 3). The natural bone served as a

biological mineralization comparator (biological HAp/C). A hydroxyapatite reference standard (HAp-RS) (Sigma-Aldrich Corp., St. Louis, MO, USA) was used for background correction and peak search validation of the Powder4 pattern analysis application [107]. The HAp-RS powder was scanned with identical diffractometer operating parameters as the experimental x-ray diffraction (XRD) patterns and diffraction line positions were obtained. XRD patterns were also obtained for an amorphous calcium phosphate reference standard (ACP-RS) and a demineralized collagen reference. These patterns were obtained for two reasons; (1) it became clear that there was a complex background pattern underlying the biomimetic and biologic samples and (2) to aid in the understanding the characteristics of the background pattern.

Table 3: Summary of powder samples analyzed by XRD

Powder Sample	Sample Size	Experimental Test Levels
Hydroxyapatite Reference Standard (HAp-RS)	1	
Amorphous Calcium Phosphate Reference Standard (ACP-RS)	1	
Natural Bone from Rat Femora	6	
Environmental Experiments	12	pH 6.8 (n=3)
		pH 7.4 (n=3)
		pH 8.0 (n=3)
		pH 9.0 (n=3)
Temporal Experiments	9	6 Hours (n=3)
		12 Hours (n=3)
		24 Hours (n=3)

All experimental and biologic samples were ground with a mortar and pestle and XRD patterns were obtained from a Rigaku, SmartLab, high-resolution XRD system (Rigaku, Tokyo, Japan). The XRD analyses were conducted with the following parameters: the diffractometer was operating at 40 kV and 44 mA, generating graphite-monochromatized CuKa radiation (wavelength, λ = 1.54059 Å); the XRD patterns were obtained over the 2θ range from 5° to 60° with a scan speed of 3° 2θ/min and step size of 0.01° 2θ.

Diffraction line positions (2θ-values) were determined for all biomimetic and biologic samples. After XRD pattern acquisition, pattern smoothing was performed with a Savitzky-Golay filter (105 points) using the MDI Jade application (Jade, MDI, Livermore, CA, USA). Filtered patterns were exported and

the lines were obtained from each background subtracted and corrected XRD patterns using the Powder4 application.

Experimental XRD patterns were prepared for analysis by, first, conducting an automatic background search with parameters for all samples set to a sampling interval of 28, a curvature of 3.0, and a search iteration of 100. The sampling interval selection allowed the background to closely follow the XRD patterns of the samples and the selected number of iterations minimized the background peaks. The curvature value had minimal affect on background selection. Next, a cursory peak search was performed with search parameters across all samples set to a minimum height percent of 9.11% ±1.77% and a minimum width (2θ) of 1.02. Lastly, additional peaks were manually identified and peaks outside of the range of interest (10°-55° 2θ) were deleted.

Once the line positions and intensities were obtained, the 2θ line positions were converted to *d* spacing using Bragg's Equation:

$$\lambda = 2d\sin\theta \qquad (3),$$

where λ is the wavelength of the x-ray source (CuKα), θ is the angle between the x-ray source and sample, and *d* is the *d* spacing. The relative intensity of each line was obtained by dividing the line intensity by the strongest intensity in the pattern and multiplying by 100. The *d* spacing and relative intensities were compared to the published HAp Powder Diffraction File (PDF) card #9-432 [108] using the Hanawalt, Rinn, and Frevel (HRF) [109] method described by Klug and Alexander, 1974 [78]. After validating the Powder4 application with the HAp-RS, the biologic and experimental samples were similarly compared to the HAp PDF 9-432 to verify the presence of HAp. Sample diffraction lines that did not conform to the locations given for HAp were compared to the PDF cards for carbonated HAp (CHAp - PDF 19-272), dicalcium phosphate dehydrate (DCPD - PDF 9-077), octacalcium phosphate (OCP - PDF 26-1056), and tricalcium phosphate (TCP - PDF 9-169) [110] to identify traces of these other calcium phosphate phases.

After the diffraction lines were found from the corresponding peak intensities and *d* spacing derived from the 2θ line positions, the peak broadness was extracted from the XRD patterns. Diffraction line broadening inversely correlates with the crystal size and lattice perfection where it is used as a measure of crystallinity [77]. The breadths of the XRD diffraction lines were determined from the full width of a diffraction peak at half its maximum intensity – full width at half maximum (FWHM).

Crystallographic measures of crystallite size and unit cell lattice constants were quantified after correcting for instrumental broadening. The HAp-RS served to obtain the instrumental broadening (b) using the Gaussian broadening correction equation [78]:

$$\beta^2 = B^2 - b^2 \qquad (4)$$

where β is the corrected line broadening and B is the experimental line broadening. Then, the crystallite size and unit cell lattice constants *a* and *c* for each environmental, temporal, and biological sample could be calculated. Crystallite size was determined from the Scherrer equation [78]:

$$L = K\lambda / \beta \cos\theta \qquad (5)$$

where L is the mean crystallite dimension and K is a constant that is approximately equal to unity (K=0.89 from Bragg's simplified derivation) and related to the crystallite shape [79]. Unit cell lattice constants *a* and *c* are determined from diffraction lines with the corresponding (*hk*0) and (00*l*) indices, respectively, using the relationship between *d* spacing and the Miller indices for a hexagonal crystal system:

$$d_{hkl}^2 = (4/3a^2)(h^2 + k^2 + hk) + (l^2/c^2) \qquad (6)$$

It is evident from equation (6) that the unit cell lattice constant *a* is dependent on [*hk*0] crystal planes and *c* is dependent on [00*l*] crystal planes for a hexagonal crystal system.

4.2.7 Thermodynamic Model

Solution chemistry affects the thermodynamics of calcium phosphate precipitation. The precursor solutions used to produce the environmental samples were modeled with chemical equilibrium calculation software (Chemist 1.0.3, Micromath, St. Louis, MO, USA). Mineralization solutions were built up from

the compounds and reagents specified in the Environmental (pH) Experiment section. Each mineralization experiment was solved and the response of the thermodynamic factors – driving force, reaction chemical potential, and ionic strength – was reported for each pH level and each calcium phosphate phase expected to precipitate – DCPD, HAp, OCP, TCP. Supersaturation is the thermodynamic driving force and affects the stability of the phases nucleating in the bulk solution, as well as the mode of crystal growth (spontaneous nucleation or step incorporation). Supersaturation, expressed as the relative supersaturation (σ), allows comparison between the different expected calcium phosphate phases and is normalized by the number of growth units (n) in the unit cell,

$$\sigma = (IAP^{1/n} - K_{sp}{}^{1/n}) / K_{sp}{}^{1/n} \quad (7)$$

where IAP is the ion activity product and K_{sp} is the solubility product for the mineralization reactions [8, 11]. The chemical potential of the precipitation reactions, or work performed by the system, is measured by the Gibb's free energy (ΔG),

$$\Delta G = -(RT/n) \ln(IAP/Ksp) \quad (8)$$

where R is the gas constant and T is the absolute temperature (in Kelvin) [8]. The free energy may be considered a measure of the reaction spontaneity where a reaction with a negative free energy is favored and will release energy to the surroundings. Ionic strength affects the screening length of ion-ion interactions in the bulk solution and the Debye length of the mineral surface-solution interactions.

4.2.8 Statistical Analysis

The Ca/P molar ratios determined in the calcium to phosphorus composition analysis, by EDS, were separately analyzed with an ANOVA for main effects due to pH or Aging. Subsequently, *post hoc* analyses to identify significant differences between groups were conducted utilizing Tukey HSD, all pair wise comparison test, when the main effects were significant.

The analysis of the XRD data was designed so that the environmental and temporal effects could be assessed relative to natural bone. First, the presence of the HAp mineral phase was assessed by correlation of the biomimetic and biologic specimen *d* spacings to the Hap PDF 9-432 standard. Next,

environmental and temporal effects on the resultant biomimetic HAp/C composites were compared to the biologic HAp/C composites. Full profile intensity and *d* spacing data extracted from the specimen XRD patterns were tested via a repeated measures ANOVA. A repeated measures treatment of the data was used to account for the multiple diffraction lines within each specimen sample in order to compare the entire diffraction pattern. The last XRD pattern analysis assessed crystal structure related measures – intensity and FWHM. Intensity and FWHM values were obtained from the strongest peaks present in all specimens. The values were then normalized relative to the maximum intensity or FWHM value across all specimens in each group in order to assess the entire specimen profile instead of individual peaks. The resultant number of peaks included in the analysis was 7 for the environmental group comparisons and 8 for the temporal group comparisons.

Analyses of crystallographic measures, crystallite size and unit cell dimensions, were conducted using a one-way ANOVA for main effects due to pH or Aging. When necessary, *post hoc* analyses were conducted utilizing an all pair wise test (Tukey HSD).

All statistical analyses were performed using commercially available software (SAS JMP, SAS Institute, Cary, NC, USA) and significance was set to 0.05.

4.3 Results

Biomimetically mineralized collagen composites were fabricated with controlled environmental pH levels and duration of mineralization reactions. The composites were created to mimic the crystallographic nature of biologically occurring bone. Precursor solutions were prepared to be supersaturated with respect to HAp and to obtain a mineral to collagen ratio of 85:15 wt%. Four levels of pH and three levels of reaction aging were studied to investigate their effects on a mineralized, self assembling, collagen composite. Bone from rat femora were analyzed to serve as a biologic HAp/C composite comparator. In addition, thermodynamic modeling was performed to evaluate the preferential precipitation of HAp formation in the solution preparations used in these experiments.

4.3.1 Mineral-Collagen Composition

Mineral weight fractions of the composite were determined for 12 samples in the environmental experiments. The samples that were collected from the biomimetic HAp/C composite filtrate were still highly hydrated, with 88.43% ± 2.38% water content. After dehydration and organic oxidation, the mineral weight fraction was 83-84wt% at pH levels below 9, at which point the mineral weight fraction of the composite increased to 88wt% (Figure 16). Based on the concentrations of the precursor solutions, the calculated composition for complete calcium and phosphate precipitation in the collagen matrix would be 85.8 wt% mineral and 14.2 wt% collagen.

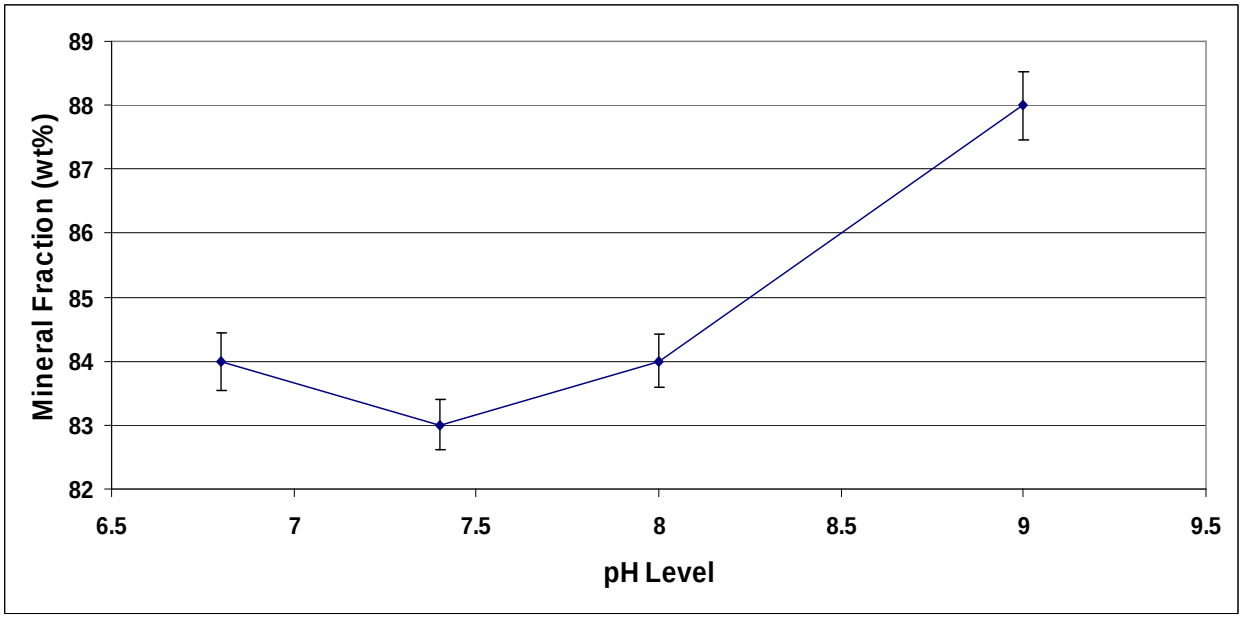

Figure 16: HAp/C composite composition response to pH change.

4.3.2 Calcium to Phosphorus Molar Ratio

Calcium to phosphorus ratios were determined for the 12 environmental and 9 temporal samples, by EDS. The Ca/P ratio increased with increasing pH. The ratio was 1.51, 1.55, 1.75, and 1.85 for the pH level 6.8, 7.4, 8.0, and 9.0, respectively (Figure 17). The two basic pH levels of 8.0 and 9.0 produced Ca/P ratios of 1.75 and 1.85, respectively, which were greater than the stoichiometric molar ratio of HAp, at 1.67. These two alkaline induced Ca/P ratios were both significantly different than the acidic and physiologic ratios ($p<0.05$). When the pH was held constant during the temporal experiments the Ca/P

ratio remained constant (Figure 18). The Ca/P ratio was approximately 1.8 across the three aging durations (6 hours, 12 hours, and 24 hours).

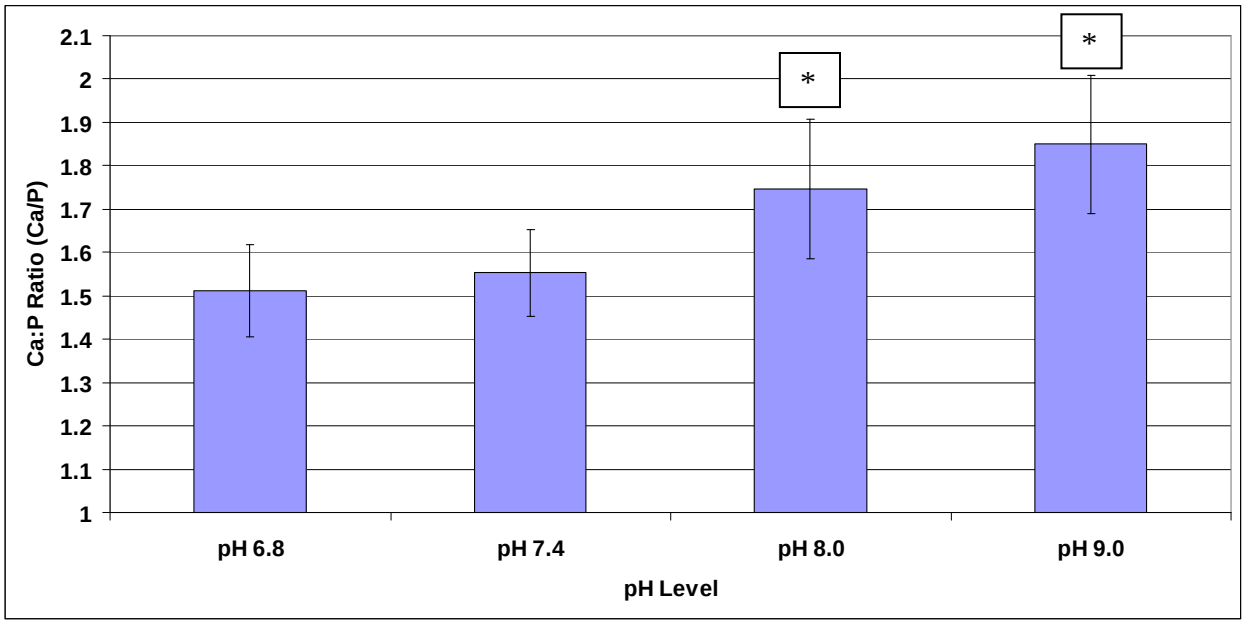

Figure 17: HAp/C composite Ca/P ratio response to pH.
* Significantly different than pH 6.8 and pH 7.4 ($p<0.05$).

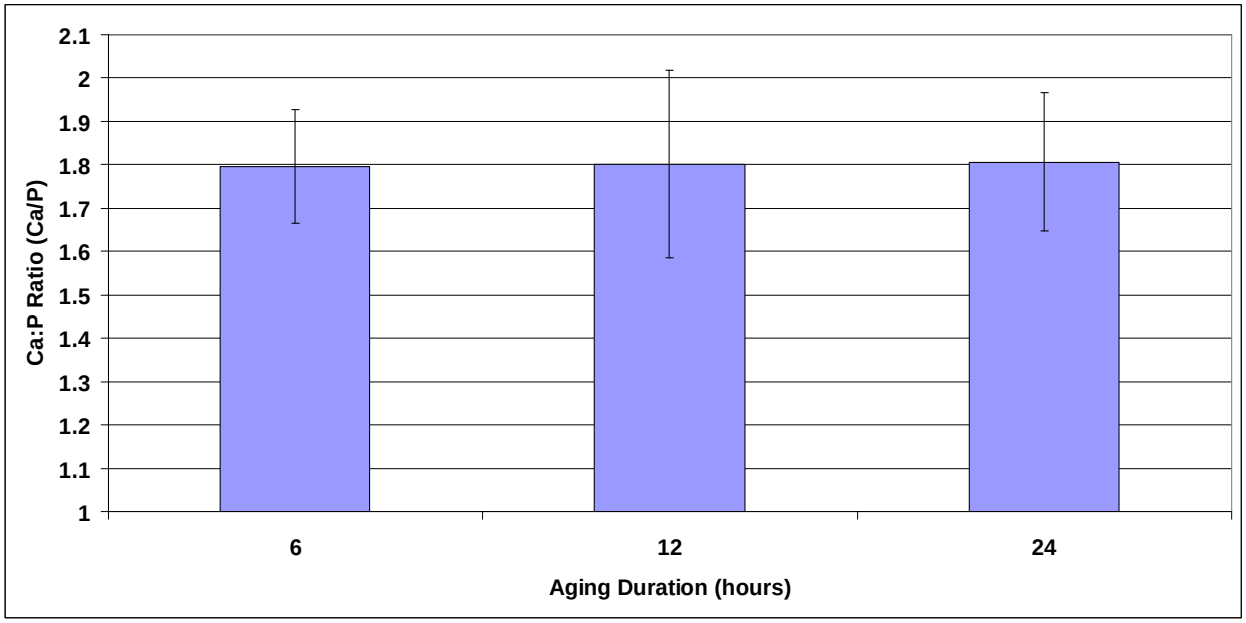

Figure 18: HAp/C composite Ca/P ratio response to aging duration.

4.3.3 X-ray Diffraction Analysis

Diffraction patterns were obtained from 30 powder samples. Examples of typical XRD patterns from the reference standard, biologic, and biomimetic HAp/C samples after pattern smoothing, background subtraction, and peak identification are shown in Figures 19-22 (all patterns are exhibited in Appendix A). The biologic and biomimetic patterns exhibited broader and less intense diffraction peaks than the HAp-RS. Peak overlap is present in the biologic and biomimetic samples where broad peaks overlap in several regions and obscure neighboring peaks. This is most notable in the 2θ range of 31º-33º, where the three most intense diffraction peaks overlap, and between 46º-53º, where only three to four of the seven peaks are visible. One other visible observation is the shape of the background curve. The biomimetic HAp/C composite background has characteristics of ACP-RS while the biologic HAp/C composite background has characteristics of ACP-RS and collagen. ACP-RS has broad peaks between 10º-15º and 20º-35º (Figure 23) while collagen has a peak at 7.605º and a broad peak from 10º-35º (Figure 24). The XRD patterns of the biologic and biomimetic HAp/C composites appear to be riding on a background pattern that resembles ACP-RS and collagen.

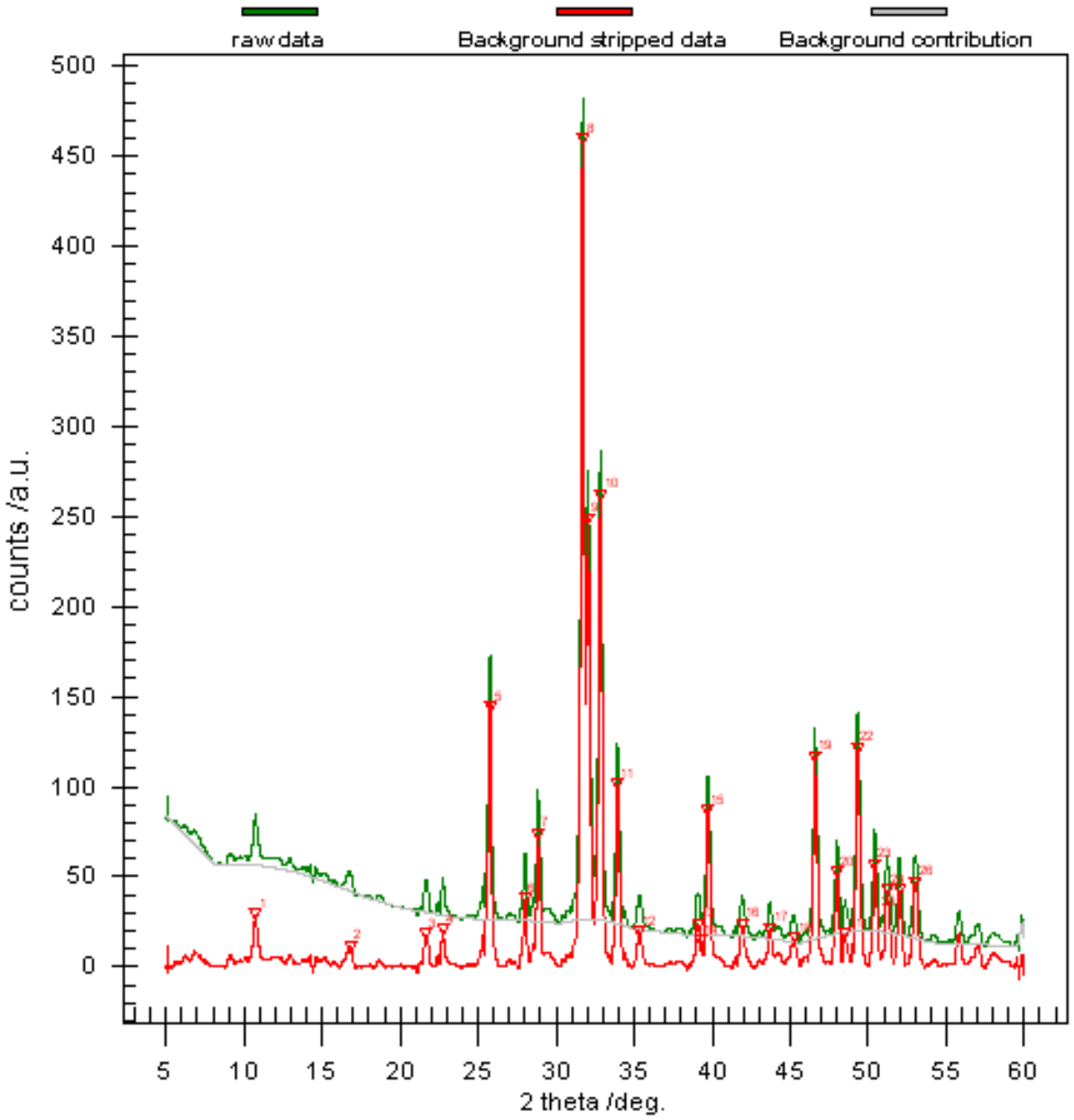

Figure 19: Typical XRD pattern for HAp-RS. The green curve is the original Savitzky-Golay smoothed XRD pattern, the grey curve is the calculated background, and the red curve is the background subtracted pattern (red inverted triangles are the peak identifiers).

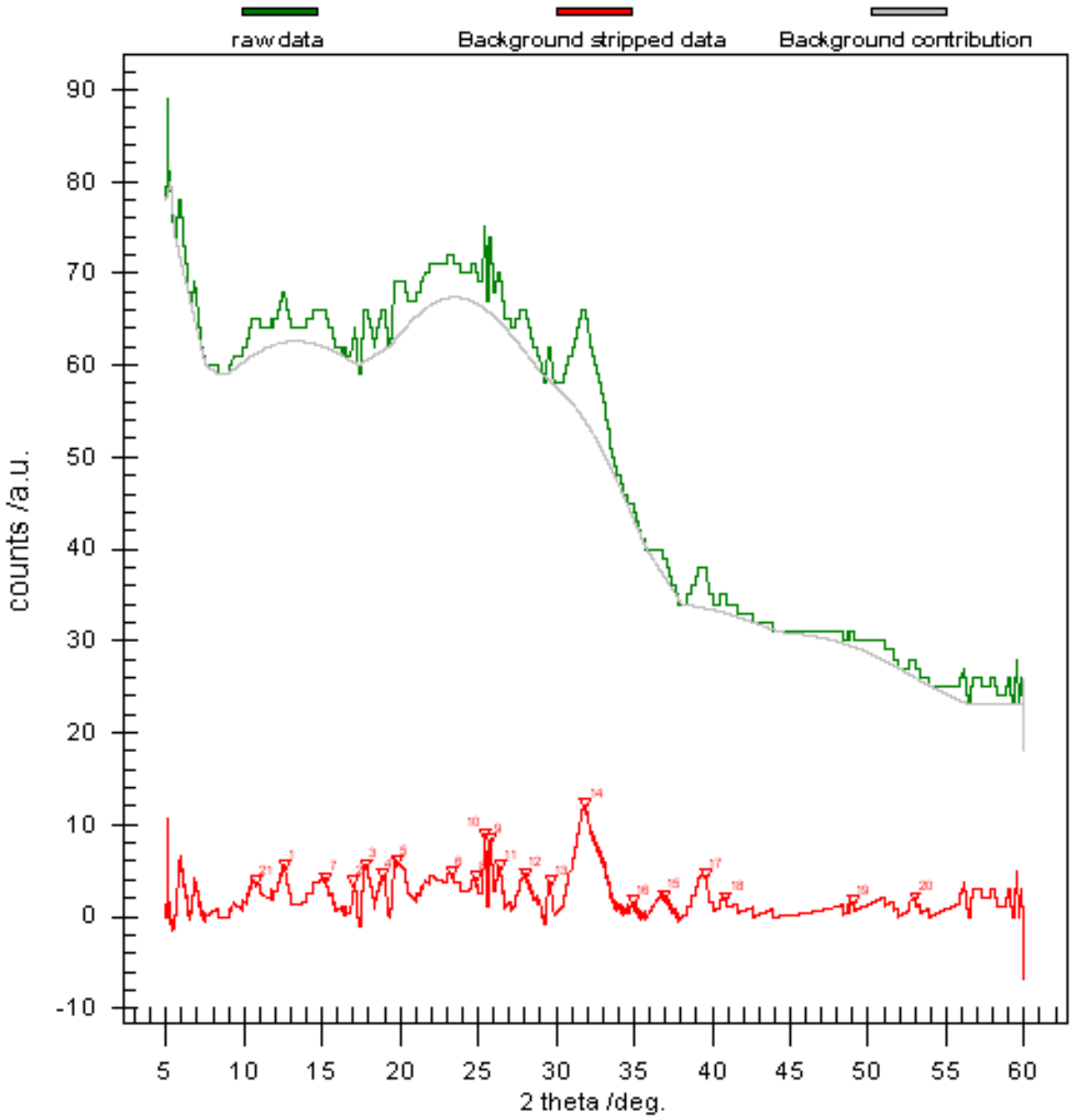

Figure 20: Typical XRD pattern for biological sample from rat femora. The green curve is the original Savitzky-Golay smoothed XRD pattern, the grey curve is the calculated background, and the red curve is the background subtracted pattern (red inverted triangles are the peak identifiers).

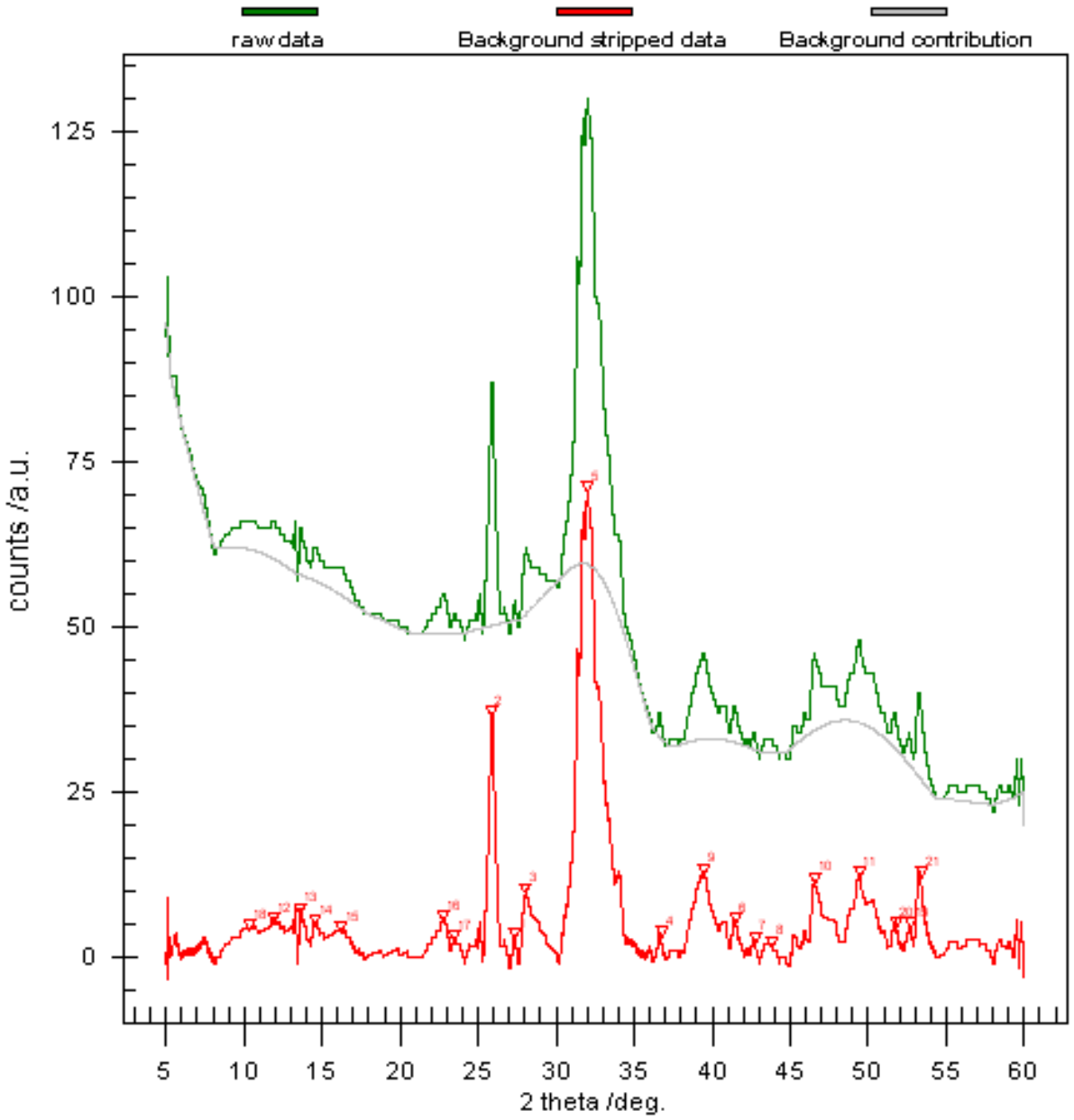

Figure 21: Typical XRD pattern for environmental sample. The green curve is the original Savitzky-Golay smoothed XRD pattern, the grey curve is the calculated background, and the red curve is the background subtracted pattern (red inverted triangles are the peak identifiers).

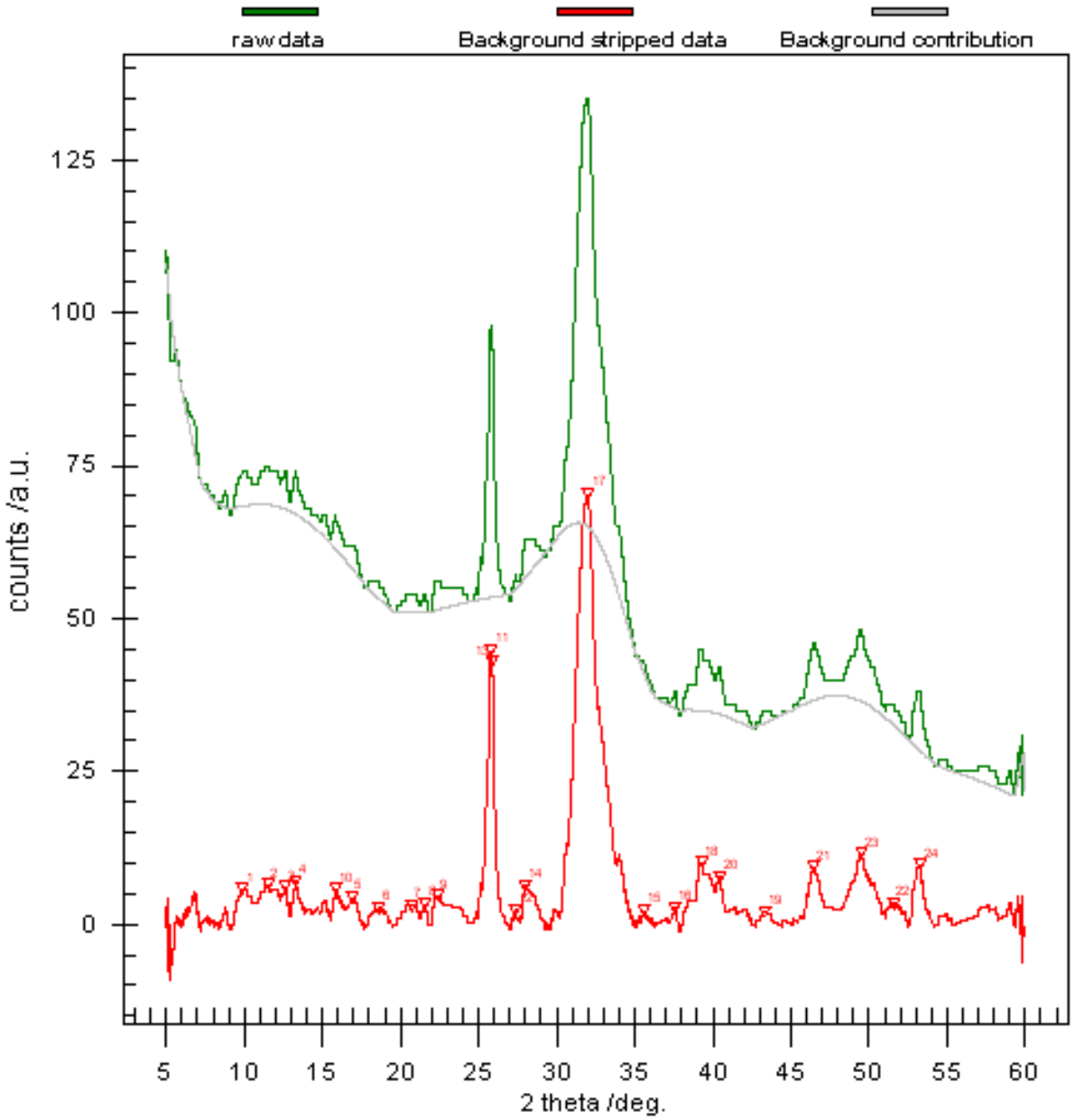

Figure 22: Typical XRD pattern for temporal sample. The green curve is the original Savitzky-Golay smoothed XRD pattern, the grey curve is the calculated background, and the red curve is the background subtracted pattern (red inverted triangles are the peak identifiers).

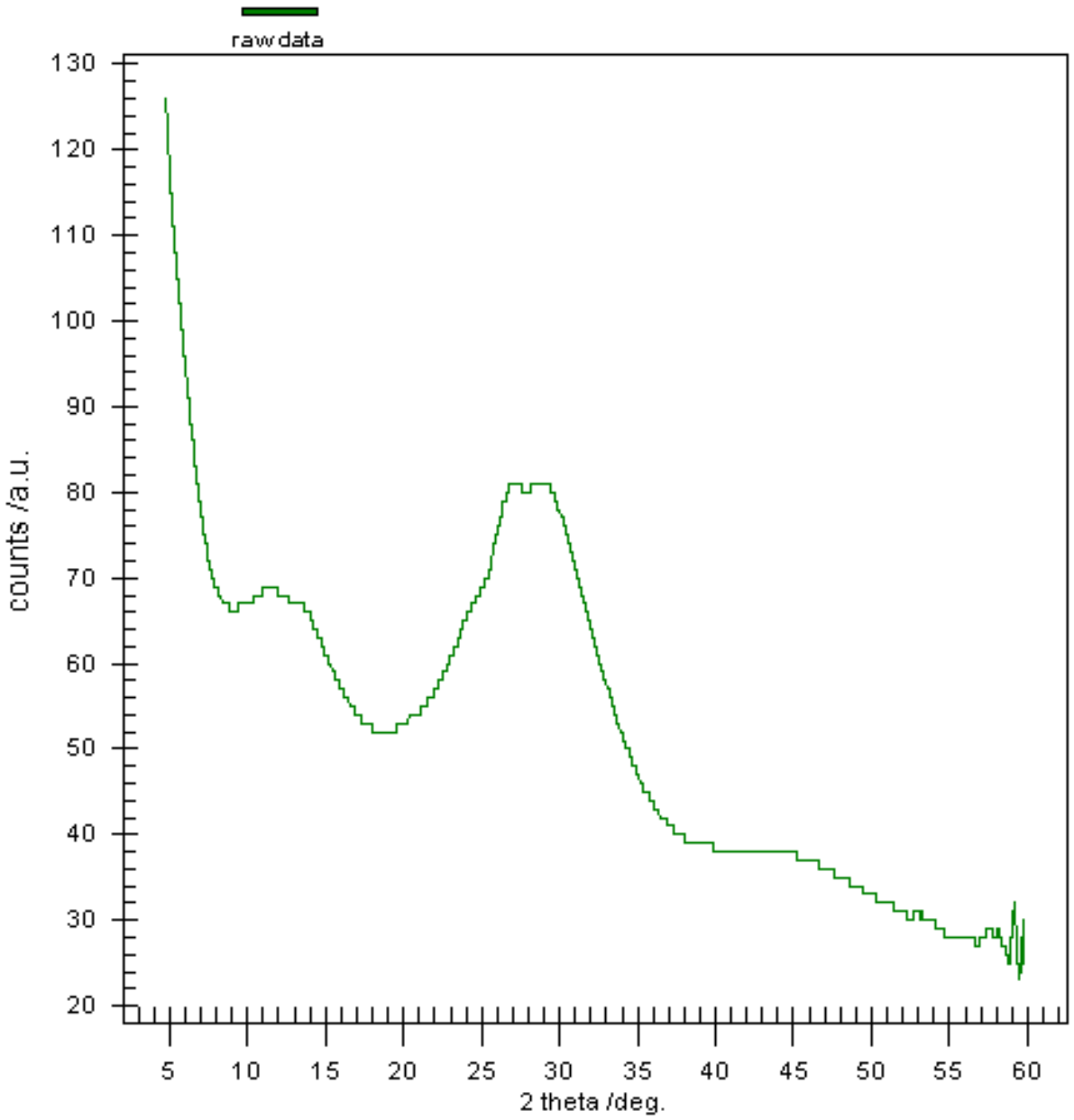

Figure 23: XRD pattern of ACP-RS. The XRD pattern of ACP exhibits characteristics of the background for biomimetic and biologic HAp/C composites.

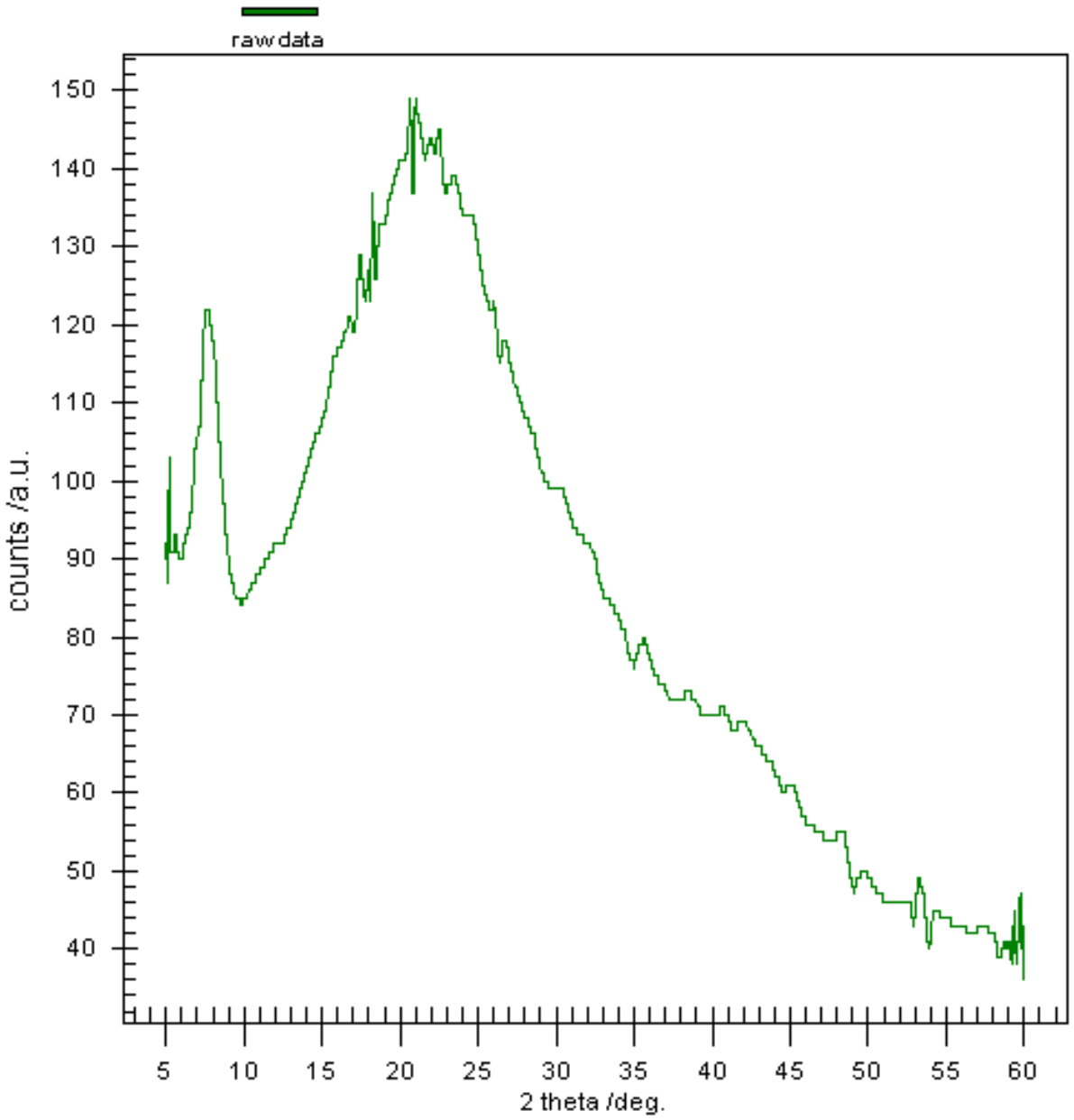

Figure 24: XRD pattern of demineralized collagen from rat femora. The XRD pattern of collagen exhibits characteristics of the background for biomimetic and biologic HAp/C composites.

The HAp-RS diffraction pattern was used to validate the Powder4 application's ability to identify the diffraction lines of interest in the current study. Twenty three out of 26 diffraction lines identified for the HAp-RS were matched to the 29 diffraction lines of the HAp PDF 9-432 [108], in the 2θ range of interest 10º-55º (Table 4). The average *d* spacing difference between the 23 matched diffraction lines was 0.008 Å, ± 0.008 Å. The HAp-RS diffraction lines are positively correlated to the HAp PDF 9-432 standard [108] (correlation coefficient 0.99999), but have a greater *d* spacing. This is equivalent to the HAp-RS

diffraction lines being shifted to lower 2θ values compared to the HAp PDF 9-432 standard [108]. The results confirmed that the Powder4 application was sufficiently capable of discerning the diffraction line locations.

Table 4: Comparison of HAp reference standard to HAp PDF 9-432 and difference in *d* spacing

PDF 9-432 [108]		HAp-RS		*d* spacing Difference
Rel Intensity	*d* (Å)	Rel Intensity	*d* (Å)	*d* (Å)
100	2.814	100	2.820	0.006
60	2.778	54	2.791	0.012
60	2.720	57	2.725	0.005
40	3.440	31	3.453	0.013
40	1.841	26	1.847	0.006
30	1.943	25	1.948	0.005
20	2.262	19	2.269	0.007
20	1.806	12	1.809	0.003
20	1.722	10	1.726	0.004
18	3.080	16	3.095	0.015
16	1.890	11	1.893	0.003
16	1.754	9	1.756	0.002
12	8.170			
12	3.170	8	3.183	0.012
12	1.780	9	1.782	0.002
10	4.070	4	4.107	0.037
10	3.880	4	3.905	0.026
10	2.148	5	2.152	0.004
8	2.296	3	2.293	0.003
8	2.065	5	2.070	0.005
6	5.260	2	5.269	0.009
6	2.528	4	2.538	0.010
6	2.000	3	2.001	0.001
6	1.871	4	1.875	0.004
4	4.720			
4	2.134			
2	3.510			
2	2.228			
2	2.040			
			Average Difference (SD)	0.008 (0.008)

The environmental and temporal samples both exhibited, on average, 12 of the HAp PDF 9-432 [108] diffraction lines. The difference in *d* spacing was similar to the difference observed for the HAp-RS with an average environmental difference of 0.009Å, ±0.006Å and an average temporal difference of 0.009Å, ±0.007Å. The biologic HAp/C composite exhibited an average of 13 of the HAp PDF 9-432 [108] diffraction lines with an average *d* spacing difference of 0.018Å, ±0.023Å. The d spacing of the

environmental, temporal, and biologic diffraction lines was positively correlated to the HAp PDF 9-432 [108] (Table 5). The biologic HAp/C samples had the highest correlation to the PDF 9-432 standard [108], followed by the temporal samples, and then the environmental samples.

Table 5: Environmental, temporal, and biologic correlation results

	Environmental HAp/C vs HAp PDF 9-432 [108]	Temporal HAp/C vs HAp PDF 9-432 [108]	Biologic HAp/C vs HAp PDF9-432 [108]
Correlation Coefficient	0.9978	0.9988	0.9990

After evaluating the samples for the presence of HAp, environmental and temporal samples were compared to biologic HAp/C composite samples, from bone, to determine crystallographic differences due to the sample preparation of the biomimetic HAp/C composite. The *d* spacing was not significantly different between the environmental, or temporal, specimens and the biologic HAp/C composite ($p>0.05$). Crystal structure related measures (intensity and FWHM) were obtained from the strongest peaks present in all specimens and analyzed for their effects. The pH was found to have a significant effect on the intensity, where all pH levels were greater than the biologic HAp/C composite ($p\leq0.0377$). A linear trendline fit to the data shows the inversely proportional relationship between pH and intensity (Figure 25). The data for bone are plotted on the same chart showing its relative pH if its intensity followed the trendline equation, where the bone intensities were representative of the alkaline environment above a pH of 9.0. As the pH increased, the FWHM breadth increased but the effect was not significant ($p=0.4898$). Again, bone is plotted showing its relative pH if its FWHM followed the trendline (Figure 26). Bone FWHM values were representative of the acidic environment below a pH of 6.8. Aging effects on intensity were also significant. All aging durations had intensities greater than the biologic HAp/C composite ($p<0.0001$) and they increased with the duration (Figure 27). The FWHM effects were inversely proportional to aging (Figure 28), but were not significant ($p=0.1734$). Bone was plotted in both figures, as before, showing its relative aging duration should its intensity and FWHM follow the trendlines. All aging intensities are well above bone which is closest to 6 hours. The FWHM of bone is representative of the 24 hour aging duration.

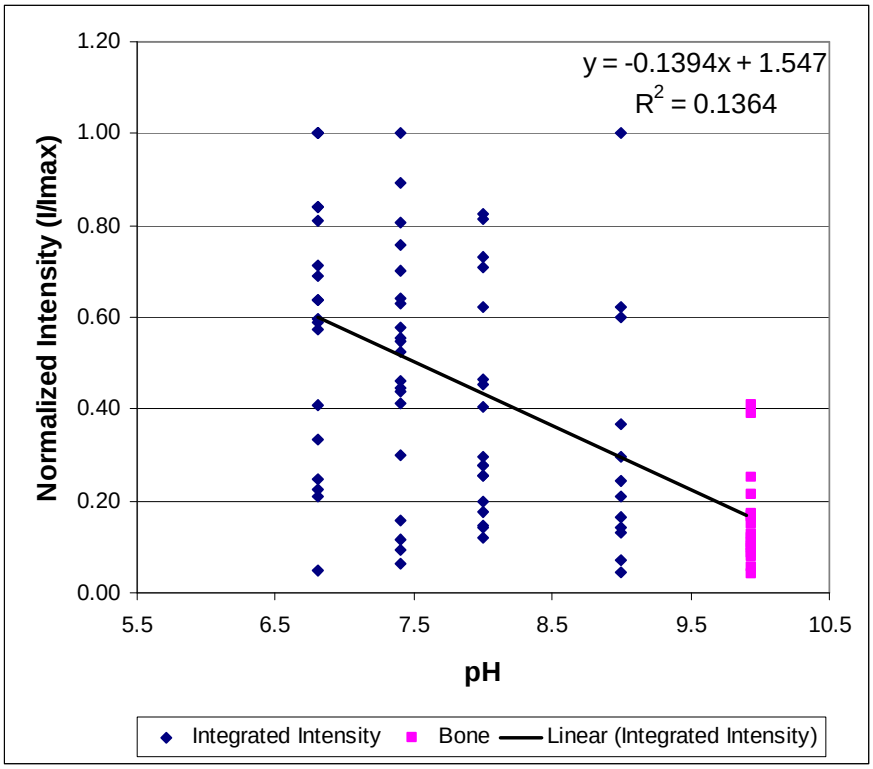

Figure 25: Response of the normalized XRD intensities to changes in the pH of the mineralization solution. Normalized intensity of bone is shown at a representative pH.

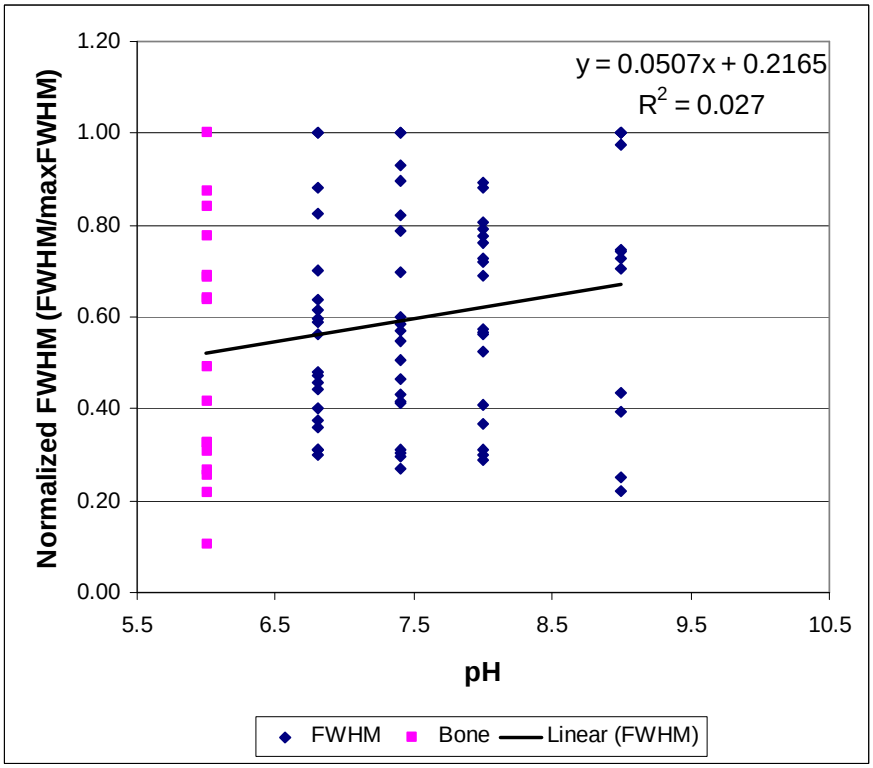

Figure 26: Response of the normalized XRD FWHM to changes in the pH of the mineralization solution. Normalized FWHM of bone is shown at a representative pH.

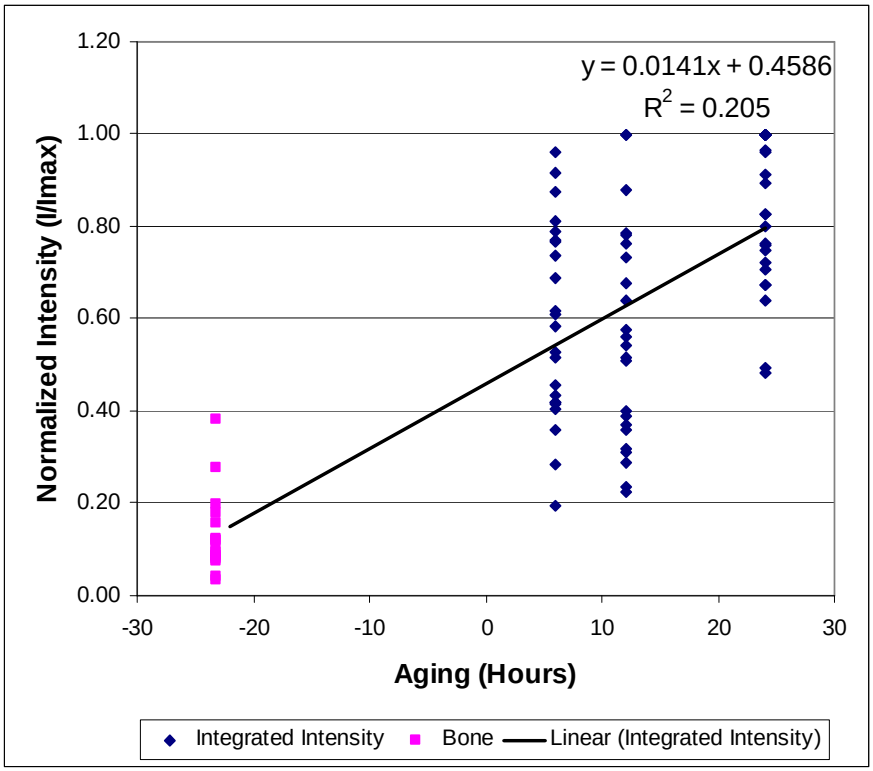

Figure 27: Response of the normalized XRD intensity to changes in the duration of the mineralization reaction. Normalized intensity of bone is shown at a representative aging.

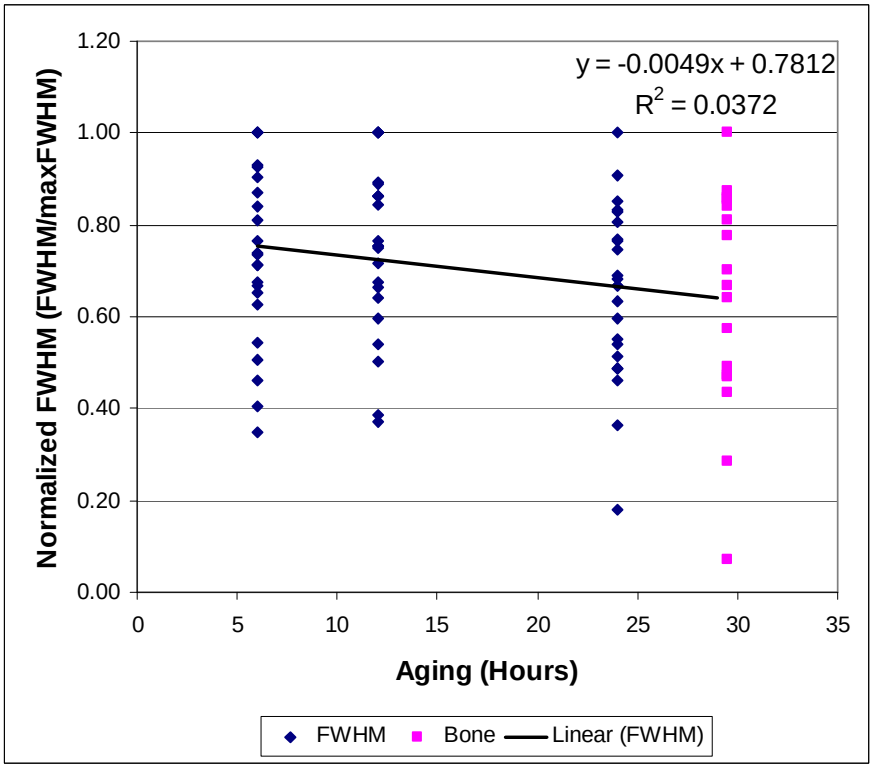

Figure 28: Response of the normalized XRD FWHM to changes in the duration of the mineralization reaction. Normalized FWHM of bone is shown at a representative aging.

Further crystallographic examination was performed by analyzing the crystallite size and unit cell lattice constants. Figures 29-32 show the environmental and temporal effects on the crystallite size and the unit cell lattice constants *a* and *c*, respectively. Crystallite size and unit cell lattice constants were also determined for the biologic HAp/C composite. Environmental treatments decreased the crystallite size with increasing pH (Figure 29). Bone's crystallite size was representative of a pH 8.0. Aging increased the crystallite size, where bone was representative of the 24 hour aging treatment level (Figure 30). However, the environmental and temporal crystallite sizes were not significantly different ($p>0.05$).

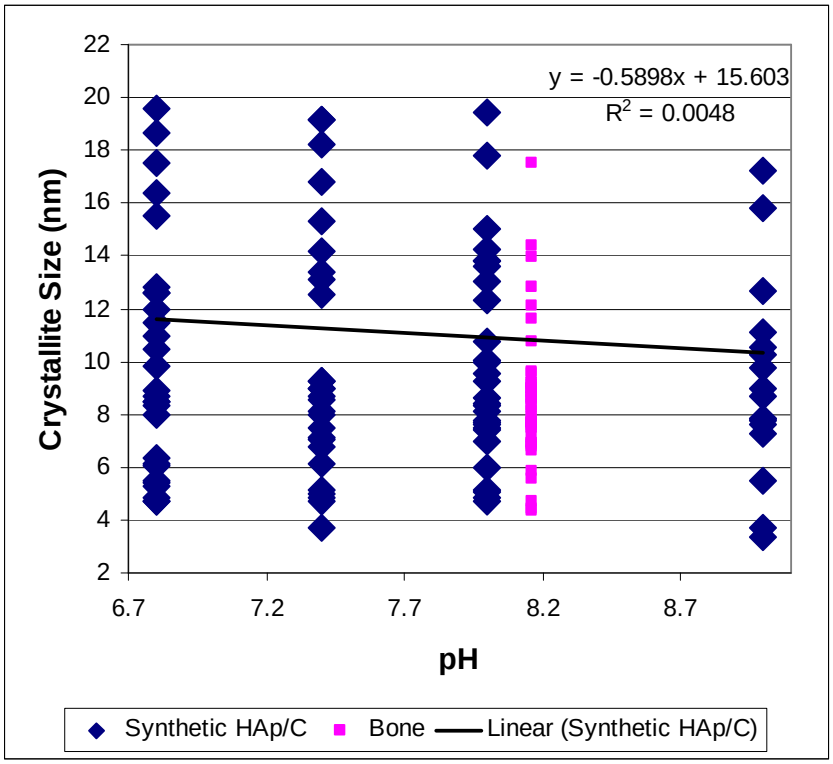

Figure 29: Crystallite size effects due to variation of the environmental conditions used to synthesize the biomimetic HAp/C composites. Crystallite size of bone is shown at a representative pH.

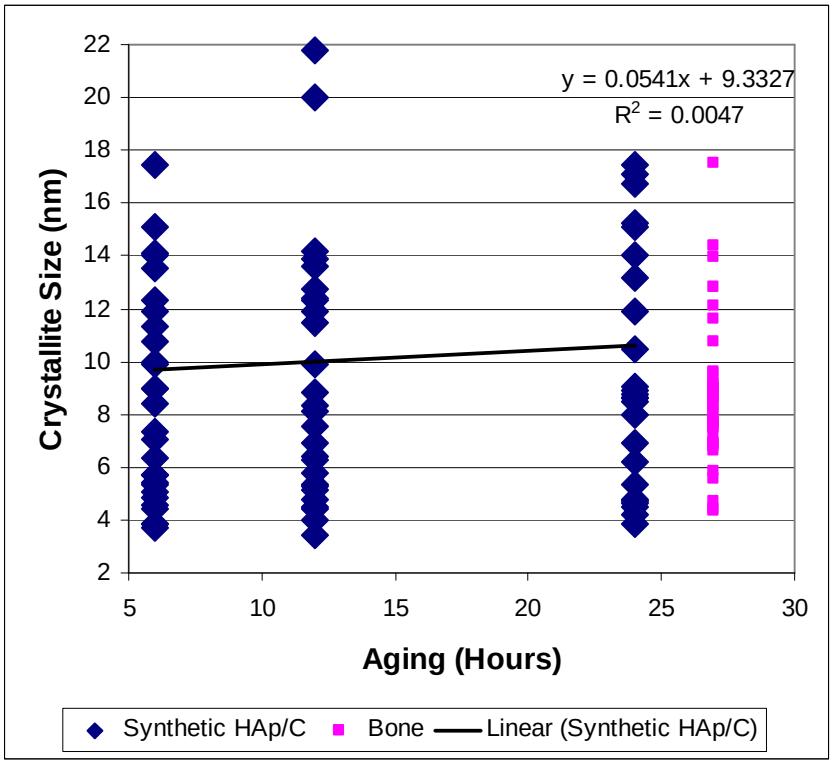

Figure 30: Crystallite size effects due to variation of the temporal conditions used to synthesize the biomimetic HAp/C composites. Crystallite size of bone is shown at a representative pH.

The HAp unit cell lattice constants *a* and *c*, derived from the environmental experiments, showed an increasing trend up to a pH of 8.0 and then dropped at a pH of 9.0 (Figure 31). The environmental lattice constant *a* was not significantly different than the biologic HAp/C composite, but the biomimetic HAp/C composite produced at a pH of 6.8 had a significantly smaller lattice constant *c* ($p=0.0075$). The biologic HAp/C composites were representative of a pH between 7.4 and 8.0. Temporal effects on the HAp unit cell lattice constant *a* increased with aging while the lattice constant *c* decreased. The only significant effect was on the lattice constant *c* at an aging duration of 24 hours ($p=0.0161$). The biologic HAp/C composites were representative of an aging duration less than 6 hours (Figure 32).

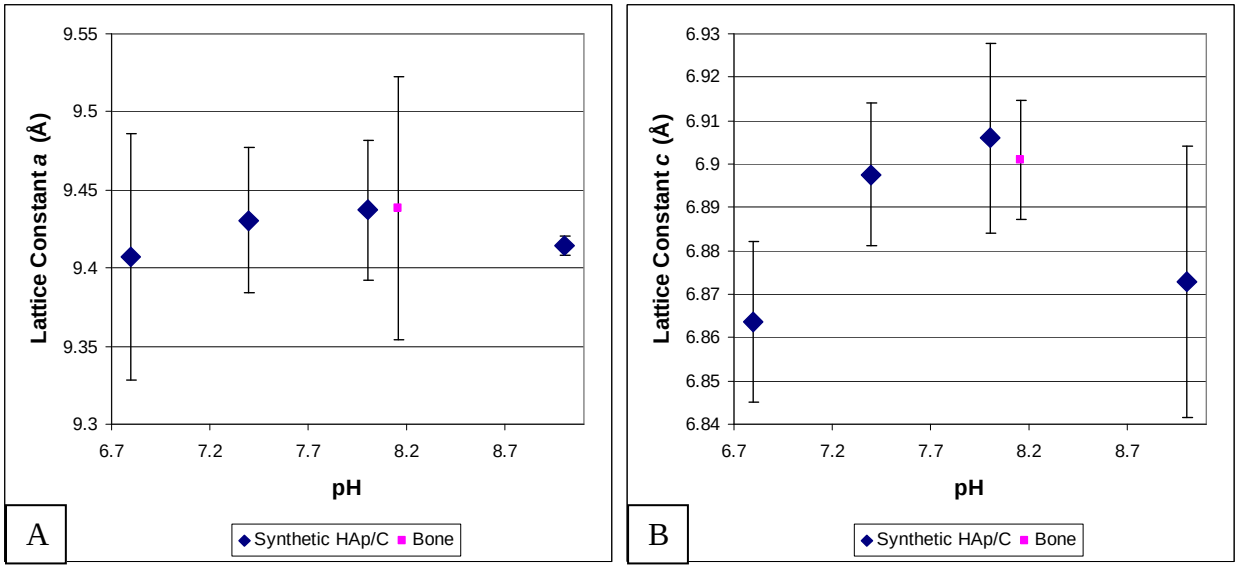

Figure 31: Unit cell lattice constant *a* (A) and *c* (B) effects due to variation of the environmental conditions used to synthesize the biomimetic HAp/C composites.

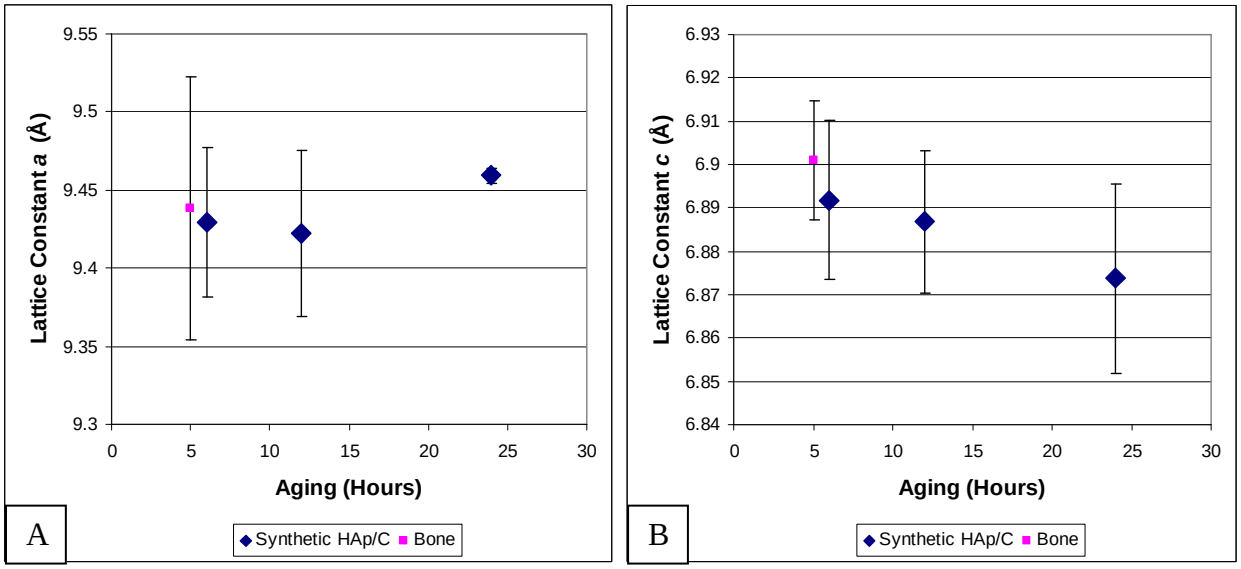

Figure 32: Unit cell lattice constant *a* (A) and *c* (B) effects due to variation of the temporal conditions used to synthesize the biomimetic HAp/C composites.

4.3.4 Thermodynamic Model

Solution chemistry and thermodynamic factors were modeled based on the HAp/C precursor solutions and expected solid precipitates formed. The mineralization solution was supersaturated ($\sigma>0$) with respect to the calcium phosphate phases: DCPD, HAp, OCP, and TCP (Figure 33). The relative supersaturations for these 4 phases all increased with increased pH except for DCPD, which decreased after reaching a maximum at pH 7.4. The relative supersaturation of HAp exhibited an exponential

increase with increased pH. The reaction chemical potential, as measured by the Gibb's free energy (ΔG), decreased for HAp, OCP, and TCP as the pH increased (Figure 34). HAp had the lowest ΔG of all the expected calcium phosphate phases. The ionic strength of the mineralization solution increased from a pH of 6.8 to a maximum at pH 7.4, then decreased as the pH increased to 9.0 (Figure 35).

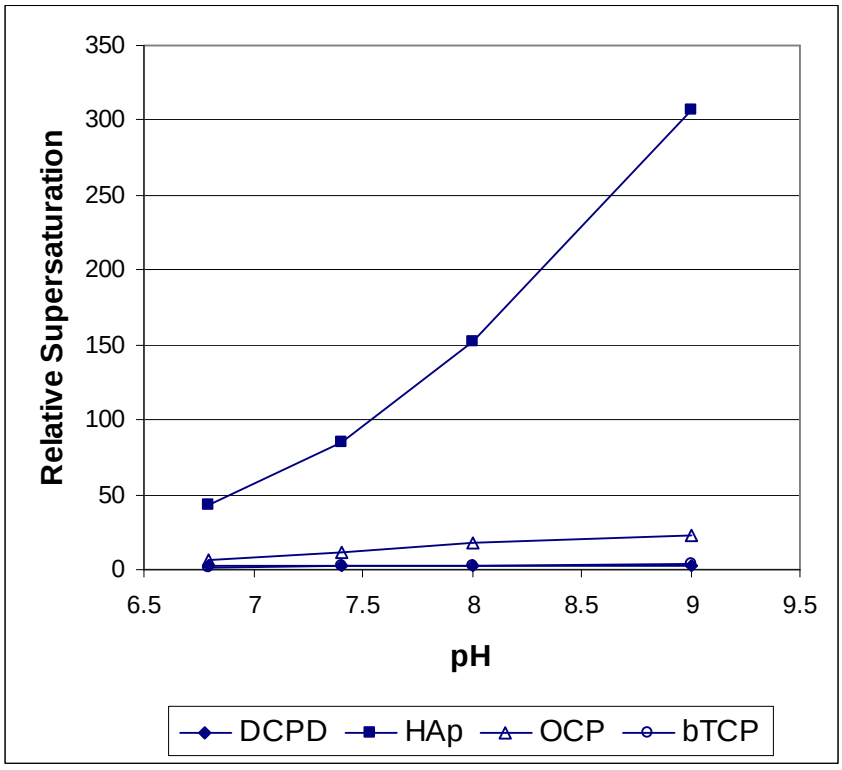

Figure 33: Influence of the solution pH on the relative supersaturations of the expected calcium phosphate phases in the thermodynamic models.

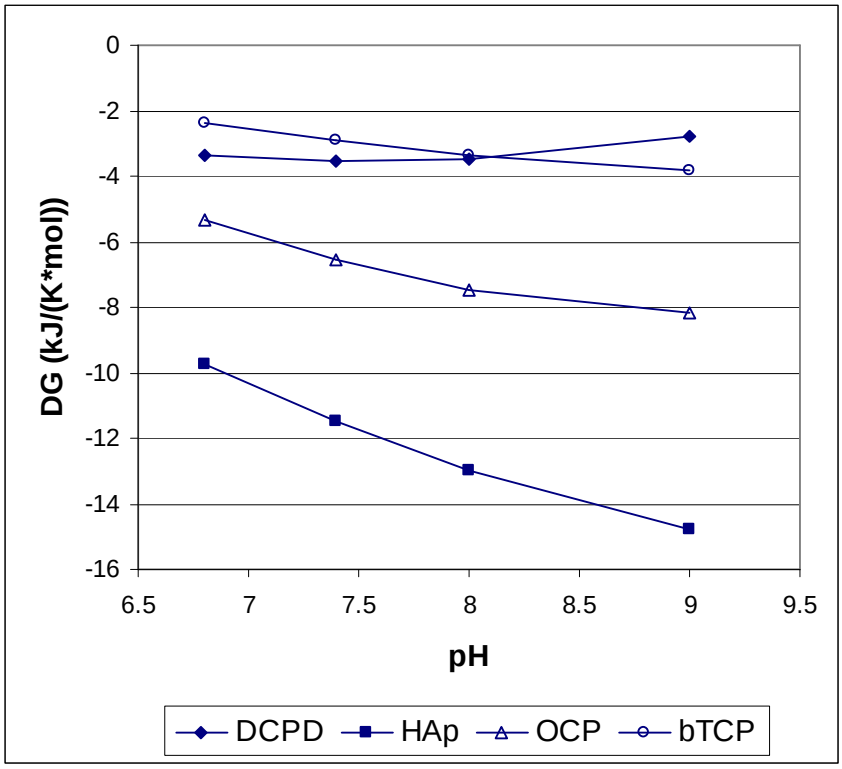

Figure 34: Influence of the solution pH on the reaction chemical potential (ΔG) of the expected calcium phosphate phases in the thermodynamic models.

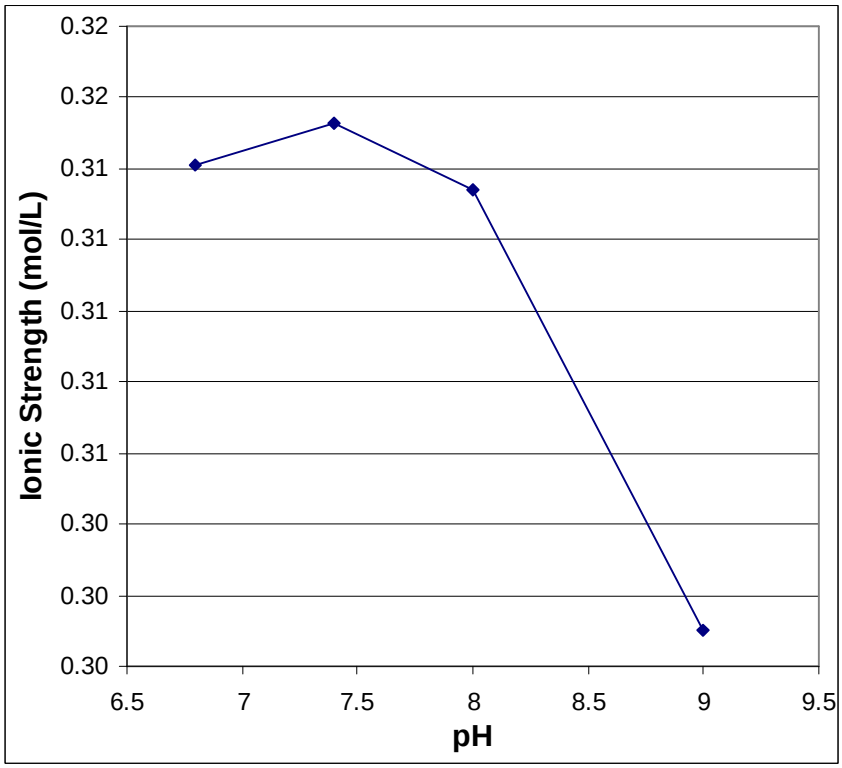

Figure 35: Influence of the solution pH on the ionic strength of the thermodynamically modeled mineralization solutions.

4.4 Discussion

The study aimed to characterize physicochemical and crystallographic properties of a biomimetic coprecipitation of calcium, phosphate, and collagen, with respect to bone. Environmental and temporal effects were investigated with respect to the composition, phase, and crystallography of a biomimetic HAp/C composite as it compares to that of natural bone.

Environmental changes in solution pH significantly impacted the composition of the biomimetic HAp/C composite. The mineral fraction of the biomimetic HAp/C composite was stable at or below a pH of 8.0, but increased when the pH increased to 9.0. The mineral fraction was 83-84% when the pH was below 9 and was in agreement with calculations of the final mineral to collagen composition of approximately 85:15, based on the starting concentrations of the precursor solutions. At these percentages of mineralization, a portion of the available calcium and phosphate would be expected to remain in solution when equilibrium was reached and balanced the ion adsorption and dissolution rates [8, 11, 111]. When the pH was increased to 9, the mineral fraction also increased. An increased mineral fraction may result from the increased alkalinity slowing the dissolution event [111]. Thermodynamic modeling supports the increased mineral fraction, whereby the increased alkalinity predicted an exponential increase in the supersaturation and a decrease in the free energy, both of which would favor a greater driving force for the precipitation of HAp. However, the 88% mineral fraction of the HAp/C composite at a pH of 9 was greater than which could be accounted for by calcium phosphate precipitation alone. Two factors may contribute to the increased mineral content: (1) increased pH produces a net negative surface charge [11] and (2) the decrease in ionic strength at pH 9 increases the Debye length [11, 33]. Together, these two factors may increase the affinity for K^+ and Na^+ ions. EDS measurements did note the presence of potassium, sodium, and chlorine, although these foreign ion inclusions were not quantified [154]. The foreign ion inclusions may have been significant enough to increase the measured mineral fraction.

X-ray diffraction analysis of samples produced in the environmental and temporal experiments indicated a predominant HAp phase. Dominant diffraction lines in these samples correlated to those from

the PDF 9-432 HAp standard [108]. Additional peaks corresponding to DCPD, TCP, OCP, and CHAp were found in the samples, but it was not clear which of these phases were prevalent among the different treatment levels in the biomimetic composites because there was significant peak overlap due to line broadening. These results were not unexpected as the pH range favored the more stable HAp formation. A more acidic environment would be required to favor a DCPD phase or stabilize an OCP phase [8, 11]. If calcium phosphate phases other than HAp presented, it would be expected in the temporal experiments conducted with aging durations of 6 and 12 hours. However, mineralization experiments have shown that complete transformation to HAp can be achieved in 12 hours or less in physiologic or alkaline environments [7, 9, 35]. A confounding factor that may make it difficult to discern the presence of additional phases is the inclusion of collagen. Collagen exhibits an XRD pattern with a peak located at approximately 8° degrees and a very broad peak at approximately 20° [113-115]. The broad peak at 20° may create significant peak overlap and contribute to the increased background profile that was subtracted using automated detection methods. The result could include obscuring the presence of small quantities of additional phases because, as quantitative phase analysis methods indicate, the relative intensity of a particular phase is proportional to the amount of that phase present [76, 116]. Ultimately, small quantities of alternate calcium phosphate phases may be lost to noise. The results from this analysis suggest that the phase of the composite produced by our methods was not sensitive to environmental or temporal effects.

While the XRD results indicated that the calcium phosphate phase was not affected by the environment or aging duration, the Ca/P molar ratio was sensitive to environmental but not temporal effects. The Ca/P molar ratio may be an indicator of the phase. As the pH increased, the Ca/P molar ratio increased. At physiologic pH and below, the mineralized HAp/C composite exhibited a calcium deficient HAp phase or ACP or TCP phases, which both have a stoichiometric Ca/P molar ratio of 1.5. The Ca/P molar ratio increased above the stoichiometric ratio for HAp when the pH was alkaline. ACP content may influence the Ca/P molar ratio across all pH levels. ACP is favorable at high supersaturation [8] and may achieve a ratio >1.5 depending on foreign ion incorporation, the pH and supersaturation levels [117]. The XRD patterns and the thermodynamic models support this finding. The XRD patterns of these

samples indicated a HAp phase for all pH levels, a decreased crystallinity at increasing pH, and it was observed that the background mimicked an ACP-RS reference in both shape and intensity across all pH levels. At acidic and physiologic pH the resultant phase may be a mixture of ACP and HAp. Mixtures of DCPD, OCP, or TCP are not supported by the data since their associated peaks were not of high intensity or quantity. At the alkaline pH levels, the increased Ca/P molar ratio is readily explained by foreign ion inclusions, specifically carbonate ions [11, 112, 117-119]. Carbonate inclusions have been observed arising from dissolved CO_2 gas in the mineralization solutions [120]. Carbonate has also been shown to be more readily included at elevated pH levels [26]. No precautions were taken to exclude dissolved CO_2 in the mineralization solutions from forming carbonate in these experiments. Other evidence supporting the role of carbonate substitutions for increasing the Ca/P molar ratio is provided by the analysis of the unit cell lattice constants. Carbonate substitutions for the phosphate ion, type B carbonate, yields a decrease in the unit cell lattice constant *a* and increase in *c* [112, 121, 122]. The lattice constant *c* was observed to increase with increasing pH. However, the lattice constant a increased from pH 6.8 to 8.0 and then decreased at a pH 9.0, which is suspected of having the greatest carbonate content due to its highest Ca:P ratio. Although the unit cell lattice constant *a* did not behave according to the preceding description, both it and the lattice constant *c* were observed to have similar values as those reported by Ivanova (2001) [123]. Unfortunately, confirmation of a CHAp phase from the experimental conditions of the obtained XRD patterns is difficult due to the proximity of the CHAp diffraction peak locations with respect to the HAp diffraction peaks, especially where peak overlap occurs. The Ca/P molar ratio was not sensitive to temporal effects, as the ratio was constant across the three aging levels.

The study also examined crystallographic changes of the HAp/C composite due to environmental and temporal effects and compared those to that of natural bone. Analysis of the X-ray diffraction patterns suggested that the diffraction line broadness (FWHM) of biomimetic HAp/C composites were not different than the biologic HAp/C composite. No differences were detected between the biomimetic HAp/C composite and biologic HAp/C composite. However, increased diffraction intensities were observed between environmental samples produced at a pH of 6.8, 7.4, and 8.0 and bone, as well as

between temporal samples aged 6, 12, and 24 hours and bone, suggesting that the only biomimetic HAp/C composite that was not more crystalline than the biologic HAp/C composite was those samples prepared in an alkaline environment with a pH of 9. No crystallite size or unit cell lattice constant *a* differences were detected between biomimetic and biologic composites Although no differences were found, the crystallite size of the pH 8.0 and 24 hour samples and the lattice constant *a* of pH 8.0 and 6 hour samples most closely approximately the crystallite size and lattice constant *a* of bone, respectively. There were differences found for the unit cell lattice constant *c*. Environmental samples prepared at pH 6.8 and temporal samples aged 24 hours both had a significantly smaller lattice constant *c* compared to bone. The lattice constant c of the pH 7.4 and 6 hour samples most closely approximated that of bone. On the basis of the crystallographic characteristics, an environment with a pH between 7.4 – 8.0 and an aging duration of 6 hours may possess the most bone-like crystallographic characteristics. However, these environmental and temporal treatment levels possessed significantly greater crystallinity, given their XRD intensity levels. The contributions of ACP and collagen to the XRD background profile of bone may be responsible. Their broad peaks and intensity, relative to the crystalline phase, were subtracted as background, which may have significantly reduced the crystalline intensities relative to the experimental samples.

Within the environmental and temporal treatment groups the observed trends in intensity and FWHM were coupled as expected. As the pH increased the diffraction intensity decreased and the FWHM increased. Decreased intensity and increased broadness are associated with lower crystallinity. In contrast, as the aging duration increased the diffraction intensity increased and the FWHM decreased indicating increased crystallinity. The elevated pH levels, if accompanied by a high supersaturation, could lead to increased ACP content and the decreased crystallinity [8]. In this study, the increased amorphous phase may be responsible for the observed broad background peaks, which are an indication of the non-crystalline ACP phase [117, 124-126]. These observations suggest that crystallinity was inversely proportional to pH and proportional to aging.

4.5 Conclusions

Solution environment has a greater effect on the mineral fraction and the calcium to phosphorus ratio than the resultant mineral phase. Unlike other reports [34-37], these results demonstrate that the effects of pH on the resultant calcium phosphate phase appear to be desensitized by the simultaneous fibrillogenesis of collagen in the mineralizing solution (i.e. no alternate calcium phosphate phases were found aside from HAp). While the phase was not sensitive to changes in pH, the crystallinity, unit cell lattice constant *c* and Ca/P ratio were all affected. The changes in Ca/P ratio may be indicative of the carbonate content. Mineralization duration does not influence the calcium phosphate phase, but does affect the crystallinity and unit cell lattice constant *c*. This study showed that a HAp/C composite, synthesized in an environment with a pH between 7.4 to 8.0 and aged for 6 hours, can be tailored to approximate the physicochemical properties of a biologic HAp/C composite.

CHAPTER 5 - QUANTIFICATION OF COLLAGEN FIBER ALIGNMENT IN A THREE DIMENSIONAL HAP/C COMPOSITE SCAFFOLD

5.1 Introduction

Hydroxyapatite-collagen (HAp/C) composites are biocompatible materials that exhibit bonelike physicochemical characteristics, of which the latter was shown in the previous chapter. However, the mechanical properties of these composites are one or more orders of magnitude less than bone. One physical characteristic of bone that is not present in these HAp/C composites is an ordered arrangement of the collagen fibers.

In bone, there is an ordered arrangement of collagen within osteons. This ordered arrangement gives rise to the extinct or bright appearance of successive lamellae when examined under polarized light [127]. It is generally accepted that there is a change in the collagen orientation from lamella to lamella [49, 53] and also within lamellae [58]. Thus, it is collagen's orientation that causes the extinct or bright appearance of the lamellae.

Collagen fibers will appear brightest in linearly polarized light when oriented at 45º to the crossed polarizer and analyzer (crossed polars) of a polarized light microscopy (PLM) system [50, 55, 128, 129]. The brightness of the fibril will diminish as it is aligned out of the polarizing plane or at an angle less than 45º to the crossed polars. Collagen fibers will become extinct when perpendicular to the polarizing plane or parallel to a polarizing axis [50]. Given this pattern of extinction, an extinct lamella could only have longitudinally oriented collagen fibrils when it is extinct throughout all of the observable positions relative to the polarizing plane. In this manner, prior research has shown that collagen fibers in bone are organized in their alignment within osteons.

Experimental correlation of collagen alignment and mechanical properties shows that the aligned fibers have an impact on the resultant mechanical properties. Collagen acts to both toughen [94-97] and strengthen [81, 130] bone. The latter property is evident in bending and tensile loading environments. Studies of collagen alignment in the cortices of long bones suggest that the collagen fibers preferentially align to the loading environment [39, 46, 54, 56], where longitudinal collagen alignment dominates in the

tensile cortex of cortical bone. Mechanical tests indicate an increased tensile strength in areas of greater longitudinally aligned collagen [39, 46, 54, 56, 130].

Preferred collagen fiber alignment is hypothesized to produce incremental tensile strength in preparations of three dimensional HAp/C composite scaffolds. The goal of this study was to induce a preferential collagen alignment in a HAp/C composite scaffold. Polarized light microscopy is used to evaluate the degree of alignment in the scaffold. The correlation of collagen alignment to the mechanical properties is the subject of a subsequent investigation and will be presented in the next chapter.

5.2 Materials and Methods

A biomimetic process of collagen mineralization was used, where the mineralizing calcium and phosphate ions are coprecipitated in an assembling collagen matrix. The starting calcium and phosphate concentrations and pH where chosen based on the stoichiometric calcium to phosphorus ratio of HAp and physiologic pH, respectively. Three dimensional (3D) HAp/C composite scaffolds were produced by a novel extrusion method developed to induce a varying degree of collagen alignment. Taking advantage of the birefringent properties of collagen, PLM techniques were employed to analyze and quantify fiber alignment.

5.2.1 Mineralization Solutions

Mineralization precursor solutions were prepared by separating the calcium and collagen into one solution and the phosphate into another, before combining. Collagen was extracted from rat tail tendons, dried, and was subsequently dissolved in 0.01M HCl, having a collagen concentration of 1 mg/mL. Calcium and collagen were combined by adding 72 mL of 0.4 M $CaCl_2$ to 400 mL of the dissolved collagen. A potassium phosphate solution was prepared by adding a 1.6 M KH_2PO_4 stock solution to a 2.1 M K_2HPO_4 stock solution in a 20:80 volume ratio to achieve a pH of 7.4. Separately, a neutralization buffer was prepared by combining 107 mL of 0.5 M tris(hydroxymethyl)aminomethane (pH 7.4 with HCl) and 73 mL of 2 M NaCl. The potassium phosphate solution (8.6 mL) was added to 108 mL of the neutralization buffer and 211 mL of ddH_2O. The mineralization reactions were initiated by combining 328 mL of the phosphate neutralization buffer to 427 mL of the calcium/collagen solution, with a starting

pH of 7.4, which decreased to 6.8. The concentrations were estimated to produce a calcium to phosphate (Ca:P) ratio of approximately 1.67 and a mineral:collagen content of 85:15.

5.2.2 HAp/C Specimen Preparation

The calcium/collagen and phosphate precursor solutions were combined in a central reaction vessel. The reaction vessel was maintained at 37ºC in a water bath. After combining, the solution was allowed to react, or age, for 18 hours. At the end of the 18 hour aging period, the mineralized collagen was recovered by vacuum filtration. Wet slurries of HAp/C were placed in the barrel of a custom made screw extruder and extruded into a 5 × 5 × 30 mm mold (Figure 36). Specimens were extruded to produce one of three expected levels of collagen alignment: 1) high longitudinal alignment (HLA); 2) low longitudinal alignment (LLA); and 3) random alignment (RA). The alignment levels corresponded to the type of breaker plate, or lack of plate, placed in the path of the extrudate. Breaker plates are screens that impart an increase in the extrudate flow resulting in the induction of fiber alignment (is there reference for this statement?). Reducing the hole dimension of the breaker plate is associated with increased alignment. The HLA and LLA fabrication methods utilized breaker plates with different sized hole dimensions (HLA holes < LLA holes) and the RA method did not use a breaker plate. Each group consisted of 7 specimens for a total sample size (n) of 21. The 5 × 5 × 30 mm molded beam specimens were compacted under a static pressure of 2.04 MPa for 17 hours. After molding and compaction, the beams were removed from the mold and placed in a -80ºC freezer until they were dried by lyophilization.

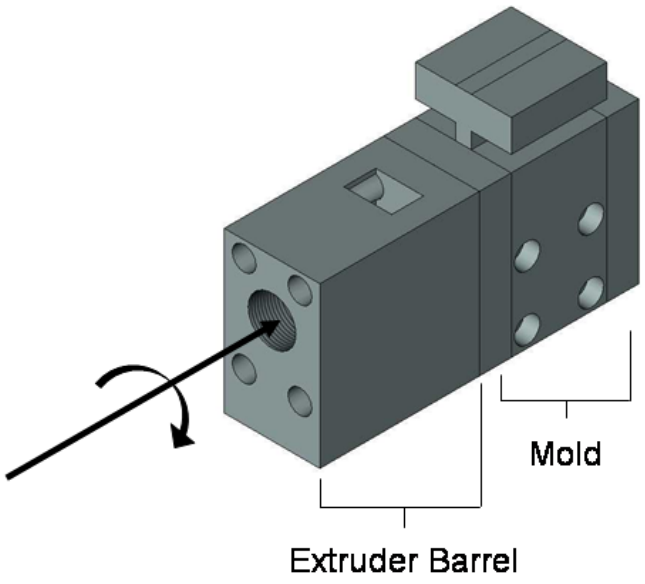

Figure 36: HAp/C composite extruder and mold assembly showing direction of screw ram travel when extruding the wet composite slurry into the mold.

Sections of the dried specimens were then obtained and prepared for PLM analysis. Each specimen was successively sectioned along half the length to obtain PLM sections in the three planes; transverse plane (T-plane), compaction plane (C-plane), and extrusion plane (E-plane) (Figure 37). To orient the reader: the direction of extrusion was the longitudinal direction of the beam in the x-direction; the compaction direction was perpendicular to the x-y plane; and the transverse direction was perpendicular to the length of the beam in the y-z plane. Each of the three specimen sections were embedded in the Technovit embedding media (EXAKT Advanced Technologies GmbH, Norderstedt, Germany). Prior to embedding the sections were prepared by: 1) fixing in 10% neutral buffered formalin (NBF) for 48 hours; 2) washed; 3) demineralized in 10% EDTA for 24 hours; 4) washed; 5) dehydrated in successive alcohol concentrations for 1 hour each (75%, 95%, 100%, 100%, 100%); 6) infiltrated in 50:50 solution of Technovit and alcohol for 8 hours; 7) and then infiltrated in 100% Technovit for 16 hours; at which point the specimens were ready for embedding. Cut sections were placed in the embedding mold and covered

with the liquid Technovit media and placed under a blue light to cure for 24 hours. Embedded sections were mounted to slides, then ground and polished to a thickness of 200 μm.

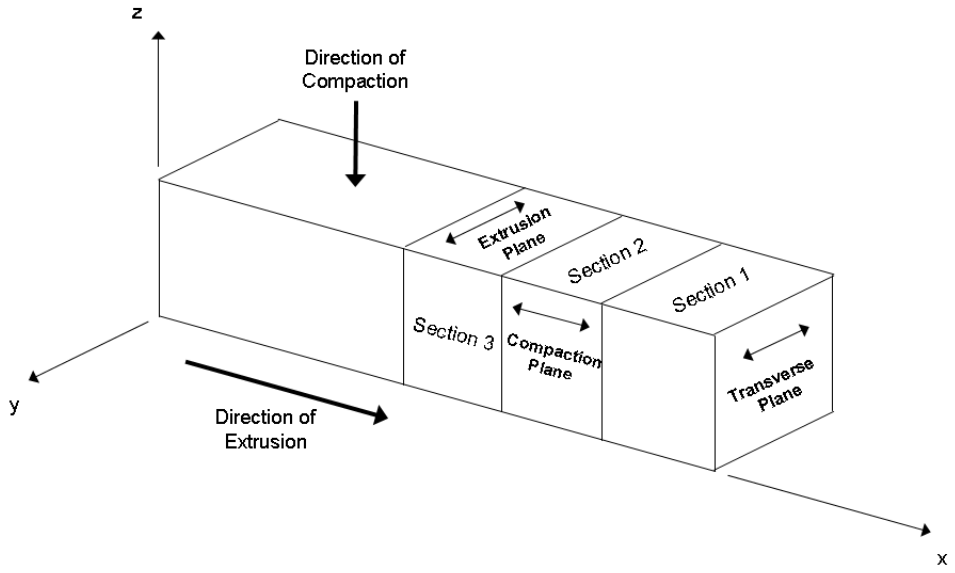

Figure 37: Schematic drawing of extruded HAp/C composite beams illustrating the PLM sections. Sections were prepared to analyze the transverse, compaction, and extrusion planes.

Specimen sections mounted to the slides were oriented such that the section faces containing the analysis plane were parallel to the microscope stage and perpendicular to the direction of the light path. The section planes allowed quantification of the fiber alignment in each of the three planes: extrusion, compaction, and transverse. Imaging the E-plane enabled quantification of the collagen fiber alignment due to the extrusion method. The T-plane enabled quantification of the fiber alignment due to the compaction while the C-plane quantified a combination of the two.

5.2.3 Polarized Light Microscopy Image Analysis

Specimen planar sections were viewed under microscope (Nikon Optiphot-2, Tokyo, Japan) with linearly polarized light at a magnification of 100x. Two polarizing filters, a polarizer and analyzer (Nikon Optiphot-2, Tokyo, Japan), were placed above and below the specimens with their polarizing directions crossed at 90° to each other (crossed polars). Each specimen planar section was imaged twice, once at an

angle of 0° relative to the polarizer and the other at an angle of 45°. Digital images were captured by a high resolution digital CCD color camera (Evolution MP Color, Media Cybernetics, Bethesda, MD, USA) in a montage sequence via commercial image acquisition and stage control software (Image Pro Plus, Media Cybernetics, Bethesda, MD, USA). Each image in the montage sequence had a resolution of 1280 x 960 pixels. Total image size was on the order of 5000 x 5000 pixels, or greater.

In theory, when viewed with crossed polars the collagen fibers will appear extinct when their optical axis (long axis) is aligned parallel (0°) to the polarizing direction of the polarizer. The fibers will be brightest when their optical axis at an angle of 45º to the direction of the polarizer. However, if the thickness of the section retards the light by a full integer of a wavelength (i.e.: $n\lambda$, where n = 1, 2, 3 …), then the fibers lying in plane will appear extinct (Figure 38). The extinct fibers are visible due to the background light intensity and exposure duration. Thus, the polarized light images allow us to visualize the collagen fiber alignment and to apply mathematical techniques to quantify the degree of alignment.

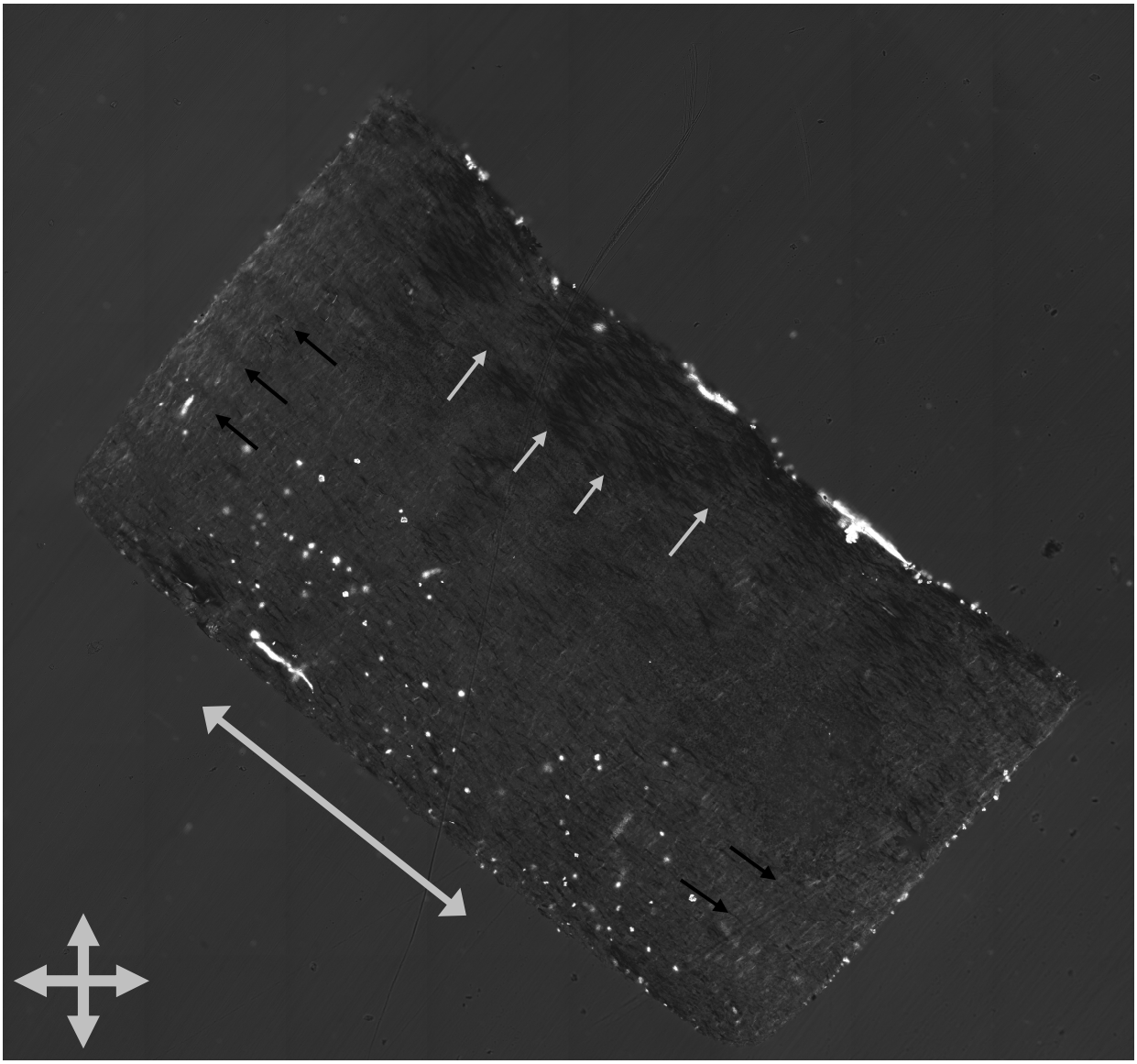

Figure 38: PLM image of specimen section oriented at 45° relative to the polarizer. Note the bright fibers at the upper left and bottom right of the specimen (black arrows) while there are extinct fibers along the upper right (grey arrows). Crossed arrows indicate polarizer and analyzer orientation. Long arrow at bottom of specimen section indicates the direction of preferred fiber alignment.

Fiber alignment analysis utilized the discrete Fourier transform (DFT) method [71, 72]. Prior to applying the DFT method directly to the polarized light grayscale images, they were background corrected, rotated if necessary, and cropped using digital image processing software (ImageJ, http://imagej.nih.gov/ij, National Institutes of Health, Bethesda, MD, USA). Briefly, the DFT technique performs a Fourier transform on the grayscale pixel intensities of an image and produces a centered power spectrum image [72] (Figure 39). There is a radial alignment of the

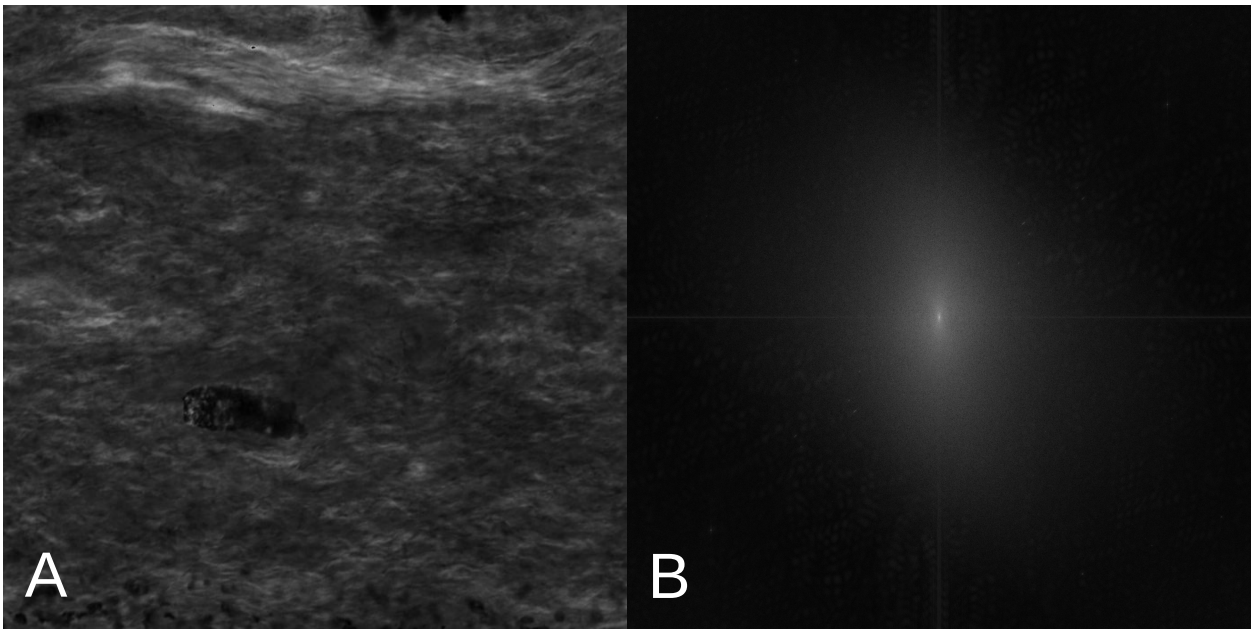

Figure 39: DFT of the grayscale image (A) to the centered power spectrum image (B). Note the hour glass shape of the power spectrum oriented vertically (B). The DFT rotates peaks due to the original object orientation by 90º in the frequency domain. Also, original objects with a curvature generate an hour glass spectrum in the frequency domain [65].

spectral intensities of the power spectrum in frequency space, whose angular orientation correlates to the oriented objects in the original image. From the spectral image, the intensities can be radially averaged and bandpass filtered to obtain a radial orientation distribution of the original image that is offset by 90° [65, 71]. The radial distribution can then be integrated to obtain an orientation tensor in the following form [71]:

$$F = \int_{-\pi/2}^{\pi/2} \mathbf{r}(\theta) \otimes \mathbf{r}(\theta)\, DFT(\theta)\, d\theta \qquad (1),$$

where $\mathbf{r}(\theta) \times \mathbf{r}(\theta)$ is the dyad product equal to:

$$\mathbf{r}(\theta) \otimes \mathbf{r}(\theta) = \begin{vmatrix} \cos^2\theta & \cos\theta\sin\theta \\ \cos\theta\sin\theta & \sin 2\theta \end{vmatrix} \qquad (2)$$

The eigenvalues and eigenvectors can be obtained when the orientation tensor (F) is solved. The eigenvalues allow computation of the anisotropy index (α), which is a measure of the degree of alignment [71]:

$$\alpha = 1 - \lambda 1 / \lambda 2 \qquad (3),$$

where $\lambda 1$ and $\lambda 2$ are the eigenvalues and $\lambda 1$ is less than $\lambda 2$. An anisotropy index of 1 indicates perfect alignment while an index of 0 indicates isotropic alignment. Obtaining these values from the image pixel

data is done by applying the DFT to the original cropped image using the 2D DFT plug-in for ImageJ [72], which produces the power spectrum image. Bandpass filtering and obtaining the radial distribution function is accomplished using the Azimuthal Average plug-in for ImageJ. The lowpass and highpass cutoff frequencies were estimated to be 60 Hz and 300 Hz, respectively. This corresponded to image fiber diameters of 5 to 25 pixels.

5.2.4 Data Analysis

At the onset of this study, it was expected that the synthetic HAp/C composites would be more porous than in cortical bone and would not possess the morphological features of osteons as observed in PLM studies of cortical bone. It was also anticipated that the fibers would possess a degree of alignment in more than just the preferred longitudinal direction of interest. Therefore, it was necessary to utilize a direct quantification method with greater sensitivity than previous PLM methods [39, 56, 57], which the DFT method provided, and to quantify the degree of alignment in an alternate section orientation other than the preferred orientation. The 0° section orientation was chosen because the fibers aligned in the preferred direction would be extinct and could be reduced to the background intensity with a reduction in the exposure duration so that they would not contribute to a measure of the anisotropy at this angle. If the degree of anisotropy then increased in the preferred direction when the section was oriented at 45°, this would indicate that there was a preferential inducement of the collagen fiber alignment. Thus, the 0º section orientation served as a measure of the specimen baseline degree of alignment and the 45º orientation was a measure of the preferred degree of alignment.

Radial distribution functions, eigenvalues, and anisotropy indices were obtained for each specimen plane at both image orientations. The radial polar plots provided a visual observation of the quantified planar alignment of the collagen fibers while the anisotropy indices were used for comparison between specimen planes at both of the orientations. Initial anisotropy index comparisons were made between the E-, C-, and T-planes and within the plane orientations at 0º and 45º to first assess in-plane changes in the anisotropy index due to the specimen section orientation. Next, the data was grouped by the extrusion fabrication methods RA, LLA, HLA to assess the extrusion effects. In both cases, a repeated measures

ANOVA was performed using commercially available software (SAS JMP, SAS Institute, Cary, NC, USA). and significance was set to 0.05.

5.3 Results

Radial orientation distributions were obtained from the power spectrum images and plotted in polar coordinates. The resultant polar plots give a visual interpretation of the frequency data (Figures 40 & 41). Specimen planar sections oriented at 0º typically produced circular (Figure 40A) or square (Figure 41A) radial orientation distributions. Those same planar sections oriented at 45º produced circular or elliptical (Figure 40B and Figure 41B) radial orientation distributions. The square distributions have their corners oriented at 45º in each quadrant while the elliptical distributions are closely aligned to the horizontal direction or vertical direction and both are associated with a higher anisotropy index than the circular distributions. The PLM image and associated power spectrum for the square radial distribution of Figure 41 is shown in Figure 42. Note the increased intensities on the two approximately 45º diagonals in the frequency domain (Figure 42B).

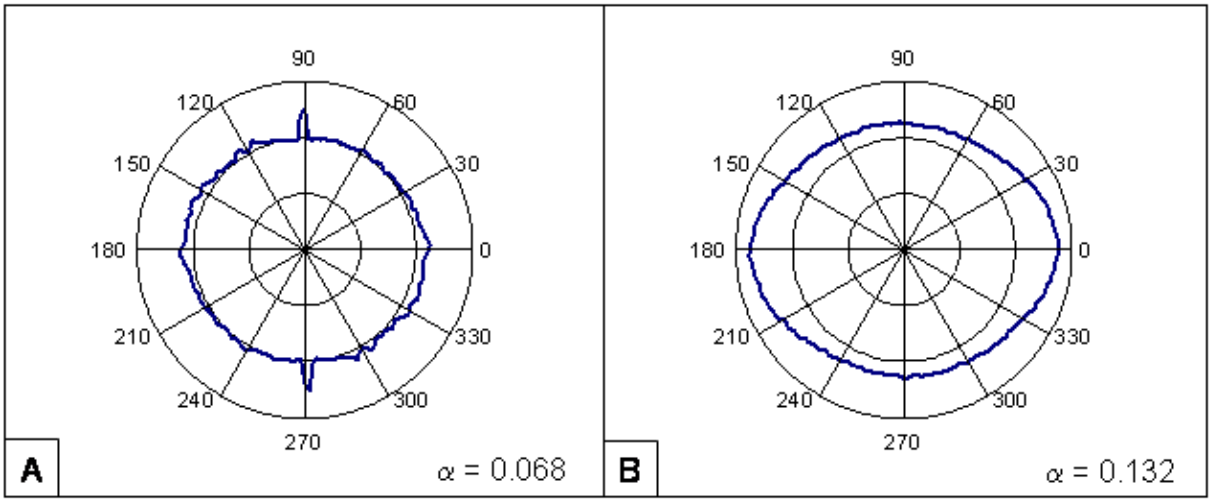

Figure 40: Polar plots showing the change in the radial orientation distribution from a planar section oriented at 0º (A) and 45º (B). Planar section is from the same specimen shown in Figure 4, which was oriented at 45º.

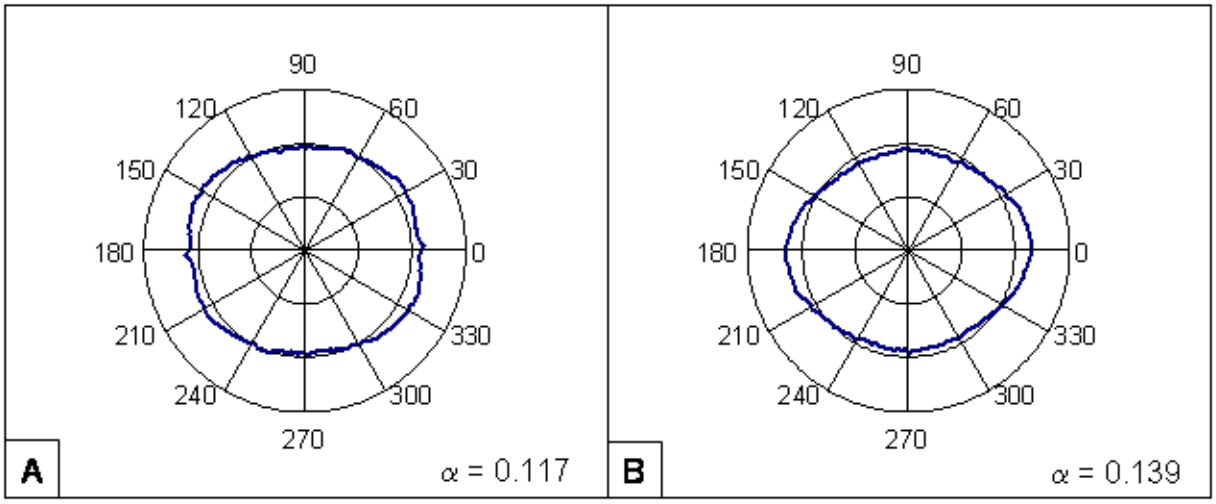

Figure 41: Polar plots showing the alternative square radial distribution from a planar section oriented at 0º (A) and the corresponding elliptical distribution at 45º (B). Square and elliptical distributions are associated with a higher anisotropy index compared to circular distributions.

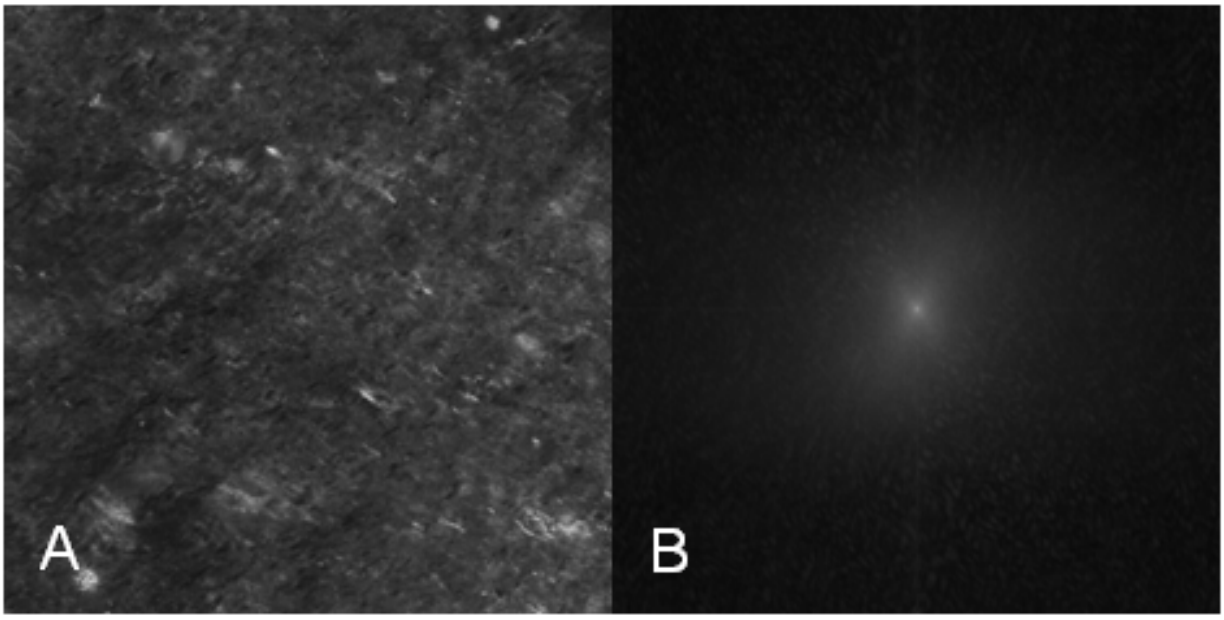

Figure 42: DFT of the grayscale image (A) to the centered power spectrum image (B) for the specimen planar section shown in Figure 41, with a square radial distribution at 0º.

The anisotropy indices (α) for each planar section at both imaging orientations were obtained for all specimens. An initial comparison was made between the three specimen planes (E-plane, C-plane, and T-plane) and within the plane orientations at 0º and 45º to assess in-plane changes in the anisotropy index due to the specimen section orientation (Figure 43). The average anisotropy index of the planar sections increased from the 0º orientation to the 45º orientation ($p=0.0171$), but of all the planes the anisotropy

index was lowest in the E-plane ($p>0.0001$). The increased anisotropy in the C-plane from the 0º orientation to the 45º orientation was the only statistically significant intraplanar anisotropy increase ($p=0.0031$).

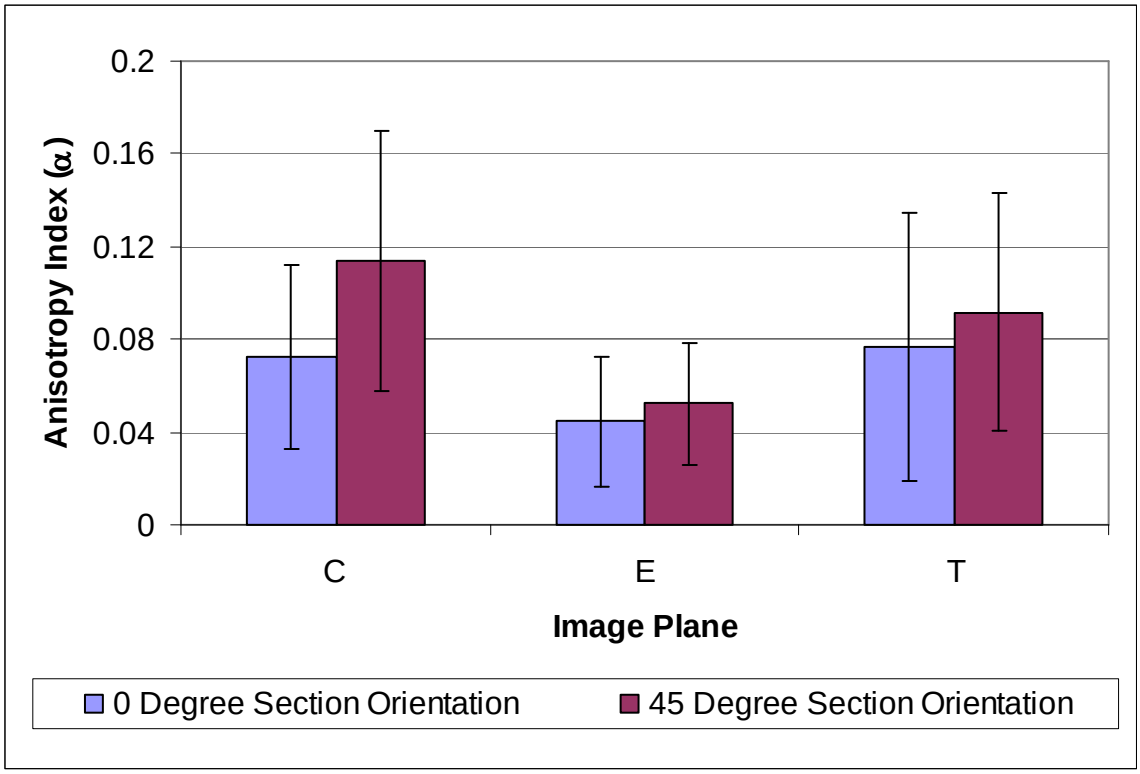

Figure 43: Intraplanar anisotropy chart of the individual and combined effects of extrusion and compaction.

Planar sections orientated at 45º to the crossed polars in the PLM setup indicated the extent to which the degree of alignment was due to the composite fabrication. The T-plane anisotropy is representative of the specimen compaction induced fiber alignment while the E-plane anisotropy is representative of the extrusion induced fiber alignment. C-plane anisotropy is a combination of the compaction and extrusion and the anisotropy was the highest of all the planes. Anisotropy in the T-plane was the next highest. These data indicate that compaction was responsible for the preferred fiber alignment to a greater extent than extrusion ($p=0.0052$). Also, compaction and extrusion together further increased the extent of fiber alignment in the preferred direction, but was only significantly greater than extrusion alone ($p<0.0001$).

Next, the HAp/C composite extrusion method was included in the analysis to determine the effects of the RA, LLA, and HLA methods on the preferred collagen fiber alignment (Figure 44). The extrusion

methods generally followed the intraplanar trends noted above. C-plane and T-plane anisotropies were higher than in the E-plane and the anisotropies increased in the 45º orientation. These trends held except in the case of the RA fabrication method where the anisotropy in the E- and T-plane decreased for the 45ºorientation. Overall, the analysis showed that the extrusion effects alone were not different between the RA, LLA, or HLA extrusion methods (p=0.3447). However, within the fabrication methods, the C-plane anisotropy of the RA method and the T-plane anisotropy of the HLA method were significantly greater in the 45º orientation, p=0.0177 and p=0.0473, respectively. Of the three fabrication methods, the LLA method produced the largest extrusion related anisotropy increase in the E-plane.

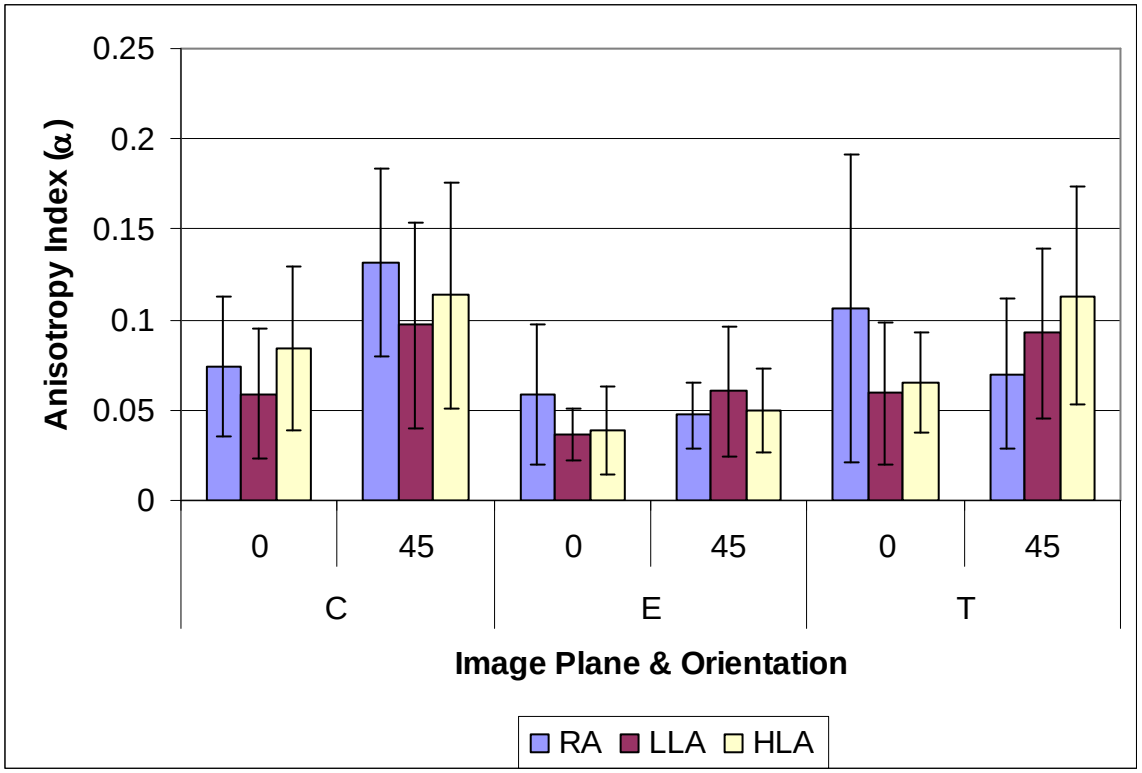

Figure 44: Intraplanar anisotropy chart of the individual and combined effects of extrusion and compaction for each of the HAp/C composite fabrication methods: RA, LLA, and HLA.

5.4 Discussion

Preferred collagen fiber alignment is a possible factor for increasing the tensile strength in synthetic 3D HAp/C composite scaffolds. The goal of this study was to quantify the extent to which a novel extrusion process would induce a preferential collagen fiber alignment in a HAp/C composite scaffold. The study hypothesized that increased hydrodynamic shear flow would increase the alignment of collagen

fibers and that the alignment would be in a preferred direction. Preliminary scaffold fabrication trials resulted in the modification of the fabrication protocol. Initially, the extruded scaffolds retained an excessive water content that left them too porous and as a result, too fragile for lyophilization and post drying handling. The solution was to modify the molds to allow the excess water to be driven off by compaction. Compaction had also been shown to have the benefit of increasing the mechanical properties in other HAp applications, but with mineral preparations only or in preparations without concern for collagen fiber alignment [2, 131]. A second protocol modification arose after the original SEM image modality was abandoned due to specimen preparation issues. Specifically, SEM imaging of collagen alignment required demineralization which resulted in excessive fiber matrix shrinkage when dried. The solution was to embed the demineralized collagen network and pursue a new polarized light microscopy based quantification protocol, the one used in this study. Polarized light microscopy was successfully used and combined with quantitative methods to evaluate the degree of alignment in the scaffold.

Polarized light microscopy was successfully used to visualize collagen fiber alignment in a synthetic 3D HAp/C composite scaffold. Birefringent fiber patterns were observed, imaged, and resolved for quantitative analyses. The degree of collagen fiber alignment from PLM images was then quantified using established techniques for fibrous networks [65, 71, 72]. The level of anisotropy was shown to increase in the preferential direction as a result of the combined effects of extrusion and compaction fabrication methods.

The goal of extruding the HAp/C composite was to increase the degree of fiber alignment in the longitudinal direction of the specimens. Results from analyzing the fiber alignment in the E-plane of the three extrusion process types showed that the use of the breaker plates while extruding the LLA and HLA specimens increased the anisotropy in this direction relative to the baseline anisotropy. Extrusion without the breaker plate actually showed a decreased anisotropy in the longitudinal direction relative to the baseline. This was to be expected, but it was not expected that the LLA specimens would exhibit a greater anisotropy than the HLA specimens and a greater change in anisotropy from the baseline. This may be a result of extrusion instabilities or fractures [132-135] occurring during extrusion of the HLA

specimens. An instability commonly referred to as “sharkskinning” occurs when surface cracks occur and curl perpendicular to the direction of flow. The surface cracks appear “saw-toothed” and are caused by surface accelerations at the exit of the die (or breaker plate in this study) that increases the surface tensile stresses beyond the tensile strength of the extrudate [136]. A more severe instability is gross fracture where high shear rates are developed between the extrudate surface and wall of the die causing compression of the extrudate beyond the exit of the die [133]. These defects may lead to distortions in the fiber alignment and the decreased anisotropy of the HLA specimens. This phenomenon is supported by the results from the T-plane data. The HLA specimen alignment in this direction was significantly increased over the baseline. In fact, the anisotropy was the highest for the HLA group compared to the LLA and RA specimens. Overall, the data suggest that the LLA extrusion method produced a higher degree of alignment than the other two methods in the preferred direction of the extrudate flow, corresponding to the longitudinal direction of the specimens.

Modification of the extruder may eliminate the extrusion instabilities attributed to causing the reduction in the HLA fiber alignment. Extruder modification may improve the degree of fiber alignment for both the HLA and LLA extrusion process types. The instabilities arise from the excessive surface shear and tensile stresses at the wall of the die and after the exit, respectively. The stresses cause turbulent flow in the extrudate exiting the die, which might be eliminated by a funneled approach to the die opening and creating laminar flow [135]. Modifying the extruder breaker plate would require a funneled approach to the breaker plate holes. The funnel would create a gradual increase in the extrudate stresses, thus initiating the fiber alignment further upstream from the onset of the breaker plate and prevent the extrudate fracture instabilities from distorting the fiber alignment. However, it is unknown whether this type of funneled breaker plate could feasibly be manufactured for the 0.3 mm hole size used for the HLA method or even for the 1.0 mm hole size for the LLA method. Therefore, the optimal hole size and design may be that used with the LLA method since it produced the highest degree of fiber alignment in the preferred direction.

The E-plane and T-plane alignment responses are indicative of the individual extrusion and compaction contribution to changes in the degree of fiber alignment, respectively. Both planes exhibited increased alignment over their respective baseline measures, but the increases were not statistically significant. The compaction only contribution to fiber alignment was significantly greater than the extrusion only contribution. The breakthrough finding was that the combination of the two, measured in the C-plane, contributed to a statistically significant increase over the baseline anisotropy. This significant anisotropy increase was preferentially aligned in the longitudinal axis of the specimens, which would provide a direct relationship with the resultant mechanical properties. The goal of inducing a preferential collagen fiber alignment in a HAp/C composite scaffold was achieved. The hydrodynamic shear flow produced an incremental alignment and when coupled with the compaction process the resultant fiber alignment was induced and increased in a 3D HAp/C composite scaffold.

5.5 Conclusions

The application of extrusion and compaction fabrication methods was successfully employed to induce a preferred collagen fiber alignment in a synthetic 3D HAp/C composite scaffold. The combination of extrusion and compaction significantly increased the collagen fiber alignment in the preferential direction over baseline measures. Extrusion breaker plates imparted an increased degree of alignment versus not using them. The larger hole dimension used in the LLA extrusion method induced greater alignment than the smaller hole dimension in the HLA method. The optimal hole size and design may be the current LLA extrusion process method. Although the resultant anisotropies in the study were found to be relatively low ($\alpha = 1$ is completely aligned and $\alpha = 0$ is isotropic alignment), it is expected that the degree of alignment can be increased with incremental compaction and modification to the extruder design, as discussed above. Design modification may initiate fiber alignment earlier in the extruder body and prevent the extrudate fracture instabilities from distorting the fiber alignment. Also, compaction pressures two orders of magnitude greater than the compaction pressure used in this study were shown to produce composite mechanical properties less than an order of magnitude lower than

cortical bone [2]. The PLM technique was successfully employed with quantitative methods to analyze and evaluate the degree of collagen fiber alignment in 3D HAp/C composite scaffolds.

CHAPTER 6 - MECHANICAL PROPERTIES OF A PREFERENTIALLY ALIGNED HYDROXYAPATITE-COLLAGEN COMPOSITE SCAFFOLD

6.1 Introduction

Bone's hierarchical structure lends to its mechanical properties. Collagen molecules are ordered in a close packed arrangement that is mineralized by crystals observing a longitudinal orientation in concert with the collagen [41, 42, 102]. Further up the length scale, concentric lamellar sheets of mineralized collagen align to the applied physiologic stresses [39, 54, 56]. The result is a composite material that maximizes its strength and toughness in preferred orientations concomitant with the applied loading conditions.

Hydroxyapatite-collagen (HAp/C) composites are a synthetic bone analogue that closely resembles the constituent materials of bone, namely hydroxyapatite mineral crystals and collagen fibers. Several precipitation techniques have been employed to synthesize HAp/C composites: 1) HAp precipitation onto a collagen matrix [36, 37], 2) HAp precipitation onto single collagen fibers [34], and 3) coprecipitation of HAp and collagen [2, 137, 138]. Ideally, a biomimetic bone analogue should mimic not only the constituent materials, but the composition of those constituents (mineral fraction) and, to the extent possible, the morphology (collagen alignment). Mineralization of existing collagen gels, sheets, or individual fibers result in compositions with mineral fractions less than that of bone. Coprecipitation addresses the issue of reduced mineral fraction but the collagen alignment is often random within the composite. One coprecipitation alignment method employed a freezing technique to induce collagen alignment, but the resultant composite was very porous [138], to the point that the collagen orientation would not aid in the improvement of the mechanical properties.

This chapter reports on the mechanical response to preferred collagen fiber alignment. This is the second part of the collagen alignment study conducted in the previous chapter. That previous study synthesized a HAp/C composite that was compositionally similar to bone and employed a novel extrusion process that induced a preferred orientation of the collagen fibers. The objective of the current study was

to determine the extent that the preferred collagen alignment would increase the mechanical properties of the HAp/C composite.

6.2 Materials and Methods

The current study builds upon the biomimetic mineralization process and three dimensional (3D) HAp/C composite scaffold fabrication method examined in Chapter 5 - Quantification of Collagen Fiber Alignment in a Three Dimensional HAp/C Composite Scaffold. The mineralizing calcium and phosphate ions were coprecipitated in an assembling collagen matrix with conditions mimicking the physiologic environment. During the fabrication of the 3D HAp/C composite, the degree of collagen alignment was varied in order to study the effects of collagen alignment on mechanical strength.

6.2.1 Mineralization Solutions

Mineralization precursor solutions were prepared as in Chapter 5 - Quantification of Collagen Fiber Alignment in a Three Dimensional HAp/C Composite Scaffold. Briefly, an acidic solution of calcium and collagen was combined with a phosphate containing neutralization buffer. The mineralization reactions were initiated by combining 328 mL of the phosphate neutralization buffer to 427 mL of the calcium/collagen solution, with a starting pH of 7.4, which decreased to 6.8. The concentrations were estimated to produce a calcium to phosphate (Ca:P) ratio of approximately 1.67 and a mineral:collagen content of 85:15.

6.2.2 HAp/C Specimen Preparation

The calcium/collagen and phosphate precursor solutions were combined in a central reaction vessel. The reaction vessel was maintained at 37ºC in a water bath. After combining, the solution was allowed to react, or age, for 18 hours. At the end of the 18 hour aging period, the mineralized collaged was recovered by vacuum filtration. Wet slurries of HAp/C were placed in the barrel of a custom made extruder and extruded into a 5 × 5 × 30 mm mold (Figure 45). Specimens were extruded to produce one of three expected levels of collagen alignment: 1) high longitudinal alignment (HLA); 2) low longitudinal alignment (LLA); and 3) random alignment (RA). The alignment levels corresponded to the type of breaker plate, or lack of plate, placed in the path of the extrudate. Breaker plates are screens that impart

an increase in the extrudate flow resulting in the induction of fiber alignment. Reducing the hole dimension of the breaker plate is associated with increased alignment. The HLA and LLA fabrication methods utilized breaker plates with different sized hole dimensions (HLA holes < LLA holes) and the RA method did not use a breaker plate. Each group consisted of 7 specimens for a total sample size (n) of 21. The 5 × 5 × 30 mm molded beam specimens were compacted under a static pressure of 2.04 MPa for 17 hours. After molding and compaction, the beams were removed from the mold and placed in a -80ºC freezer until they were dried by lyophilization. The dried beams were then machined into dog bone mechanical test specimens, with a width (w) of 2.20 mm (±0.21 mm), thickness (t) of 2.15 mm (±0.64 mm), and gage length (l_g) of 7.06 mm (±0.12 mm) (Figure 46).

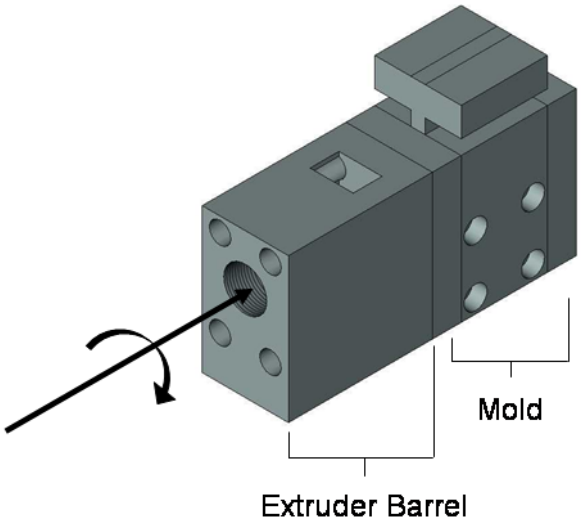

Figure 45: HAp/C composite extruder and mold assembly showing direction of ram travel when extruding the wet composite slurry into the mold.

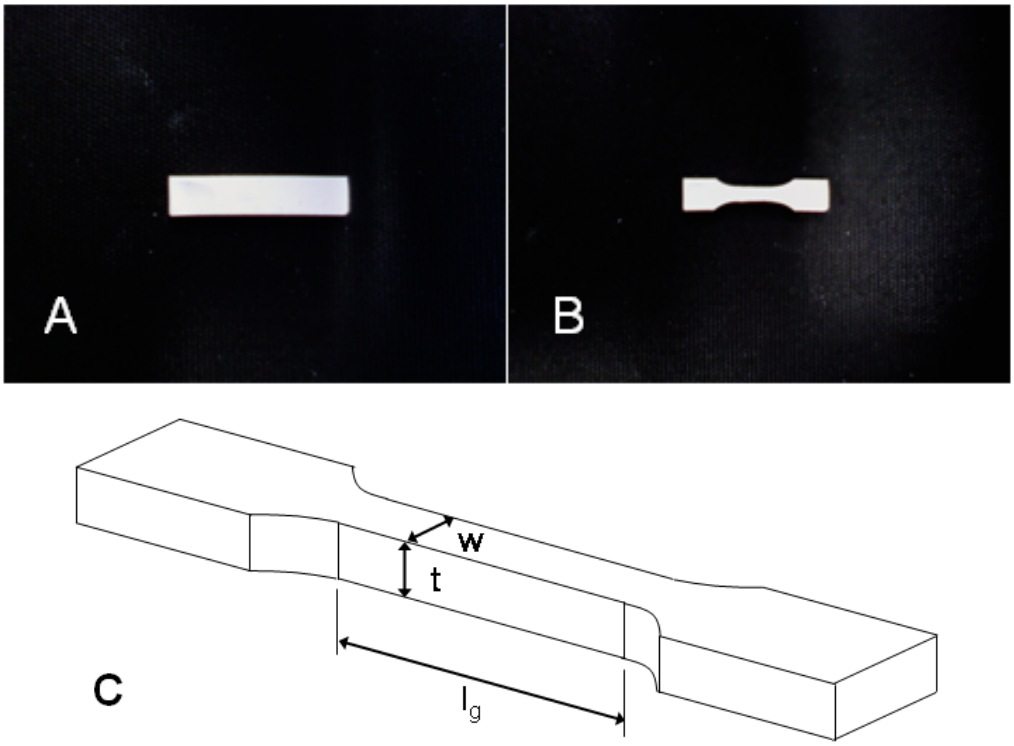

Figure 46: HAp/C composite dogbone mechanical test specimen preparation. As molded 5 x 5 x 30 mm HAp/C specimen (A). Machined dogbone mechanical test specimen (B). Schematic drawing of the dogbone mechanical test specimen dimensions (C).

6.2.3 Mechanical Tests

Tensile tests were conducted on 21 dog bone mechanical test specimens, evenly divided into the three alignment groups (n=7 HLA, n=7 LLA, n=7 RA). Each specimen was potted separately in the cup of the upper test grip, using a two part polyester resin and hardener (Dynalite, Dynatron, 3M, St. Paul, MN, USA). The upper test grip was installed to a servohydraulic materials test machine (Instron 8501, Walther, MA, USA). Next, the lower test grip was installed to the test machine, the cup filled with potting material, the specimen was lowered into the cup, and the potting material was allowed to cure (Figure 47). The tensile tests were conducted at a loading rate of 0.02 mm/s until failure. Load and displacement data was captured on a PC at a rate of 100 Hz. These data were then used to calculate the mechanical properties: maximum load, stiffness, maximum strain, ultimate tensile stress (UTS), Young's elastic modulus, and the work to fracture (toughness).

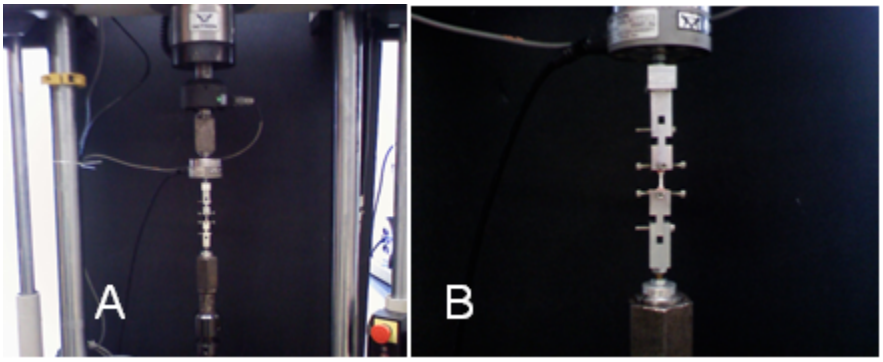

Figure 47: Mechanical test setup in materials test machine (A) and close up showing specimen potting (B).

6.2.4 Statistical Analysis

The effects of the type of extrusion process were determined by conducting a one-way ANOVA test on each of the 6 mechanical properties identified in the previous section. In addition, a regression analysis was conducted to determine whether the degree of alignment, or anisotropy, affected the mechanical properties of the HAp/C composites. The degree of alignment could be influenced by the extrusion process (E-plane), the compaction process (T-plane), or a combination of the two (C-plane), as described in the preceding chapter. Briefly, each specimen was successively sectioned along half the length to measure the degree of collagen fiber alignment in the extrusion plane (due to extrusion alone), transverse plane (due to compaction alone), and the compaction plane (due to a combination of the two) (Figure 48). To orient the reader: the direction of extrusion was the longitudinal direction of the beam in the x-direction; the compaction direction was perpendicular to the x-y plane; and the transverse direction was perpendicular to the length of the beam in the y-z plane. All statistical analyses were performed using commercially available software (SAS JMP, SAS Institute, Cary, NC, USA) and significance was set to 0.05.

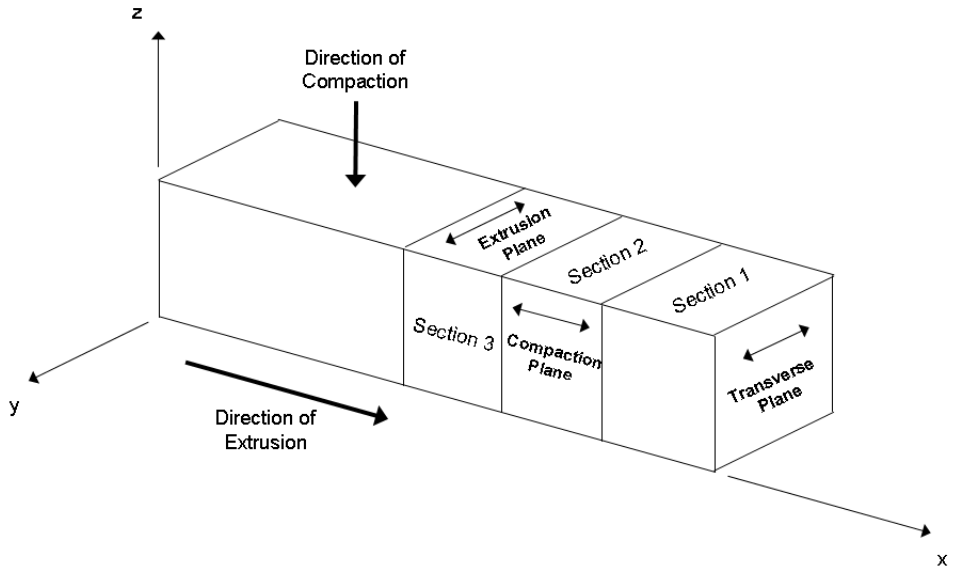

Figure 48: Schematic drawing of extruded HAp/C composite beams illustrating the fiber alignment sections. Sections were prepared to analyze the transverse, compaction, and extrusion planes.

6.3 Results

Uniaxial tensile tests were conducted on the 3D HAp/C composite scaffolds fabricated by an extrusion process that used three types of breaker plates to induce varying degrees of collagen fiber alignment in a preferred direction. The preferred direction corresponded to the longitudinal direction of the test specimens and the tensile axis under examination. The mechanical properties of the HAp/C composite scaffolds were quantified to determine the effects of the extrusion process type and dependence on the degree of collagen fiber alignment.

Fracture patterns were nearly identical for all test specimens in all groups. The fractures occurred within the narrow section of the gage length (Figure 49). The fractures were transversely aligned, but most fractures were not completely perpendicular to the long axis of the specimen. They were at an oblique angle.

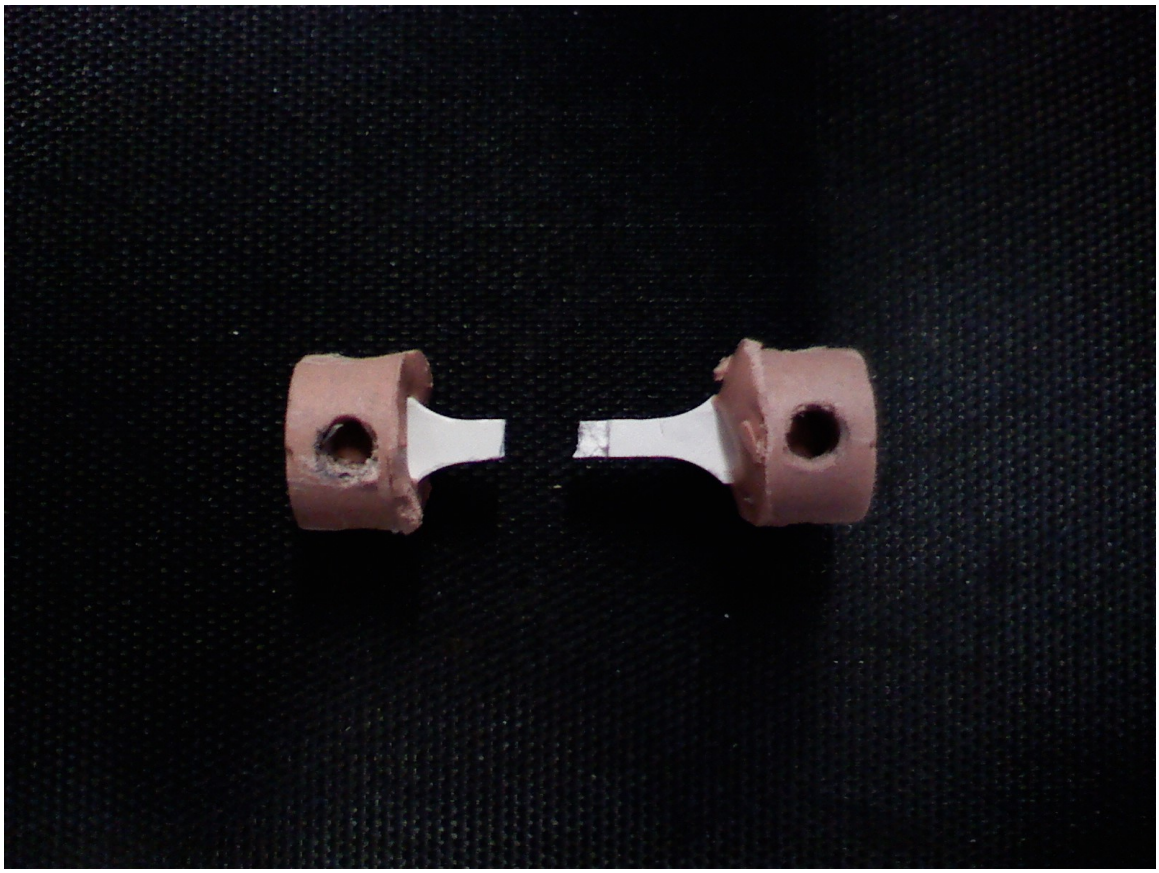

Figure 49: Post fracture specimen removal from the test fixture showing the typical fracture pattern.

Load-time and displacement-time histories were recorded for all specimen tensile tests. The load and displacement histories were combined into a load-displacement curve (Figure 50), from which the maximum load, stiffness, strain, UTS, Young's modulus, and work to failure could be computed. The specimens behaved in a brittle manner with little post yield displacement. Loads increased linearly, having a constant slope, until the yield point where the slope decreased but did not have a large displacement prior to failure.

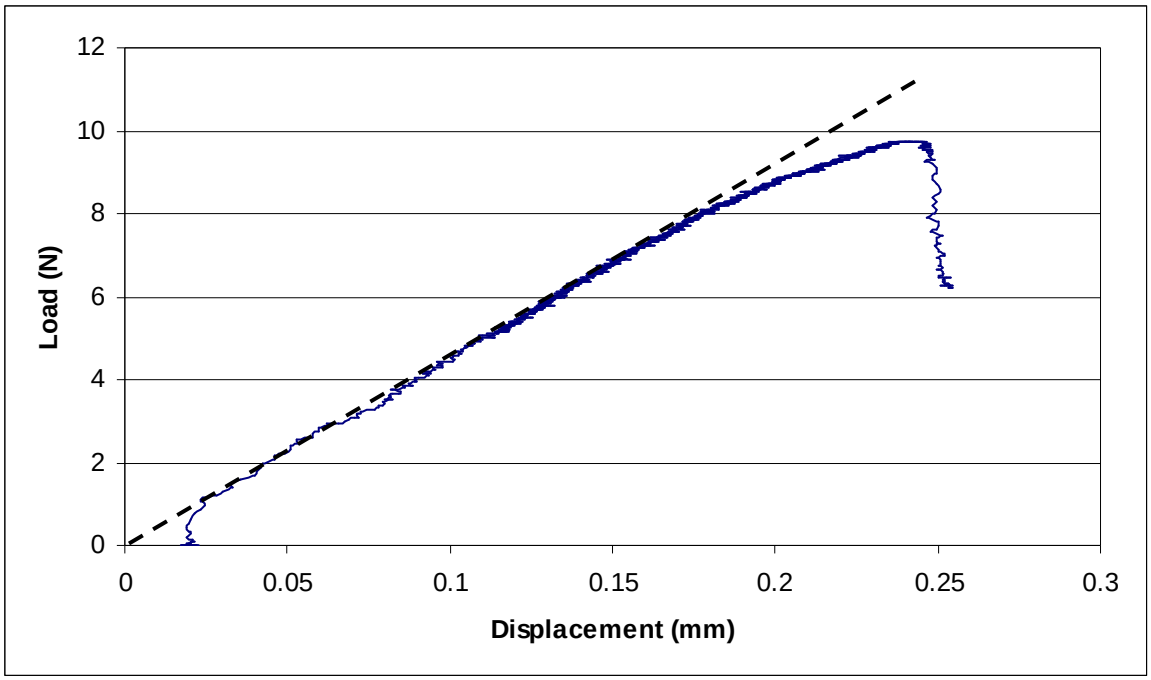

Figure 50: Typical load-displacement curve. Dashed line added to emphasize the linear loading phase prior to yielding where the slope of the curve decreases prior to failure.

Figures 51-56 shows the mechanical properties of the HAp/C composites fabricated by the three different extrusion process types. The average load, stiffness, UTS, and modulus of the HLA fabricated specimens were greater than the other two extrusion types. The LLA extrusion method exhibited a greater maximum strain and work to failure response than the other extrusion methods. Each of the six measured mechanical properties were compared between the three extrusion types to determine the effect, but the analysis did not find a statistically significant effect from the type of extrusion process employed ($p>0.05$).

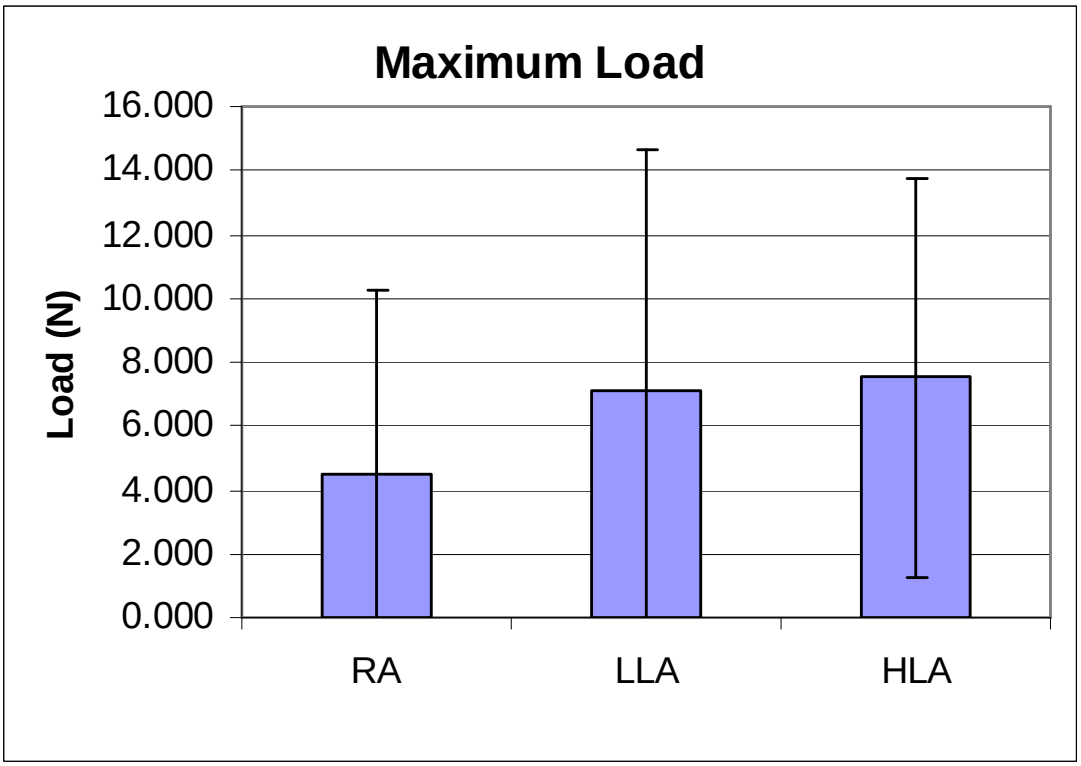

Figure 51: HAp/C composite mechanical response of the maximum load.

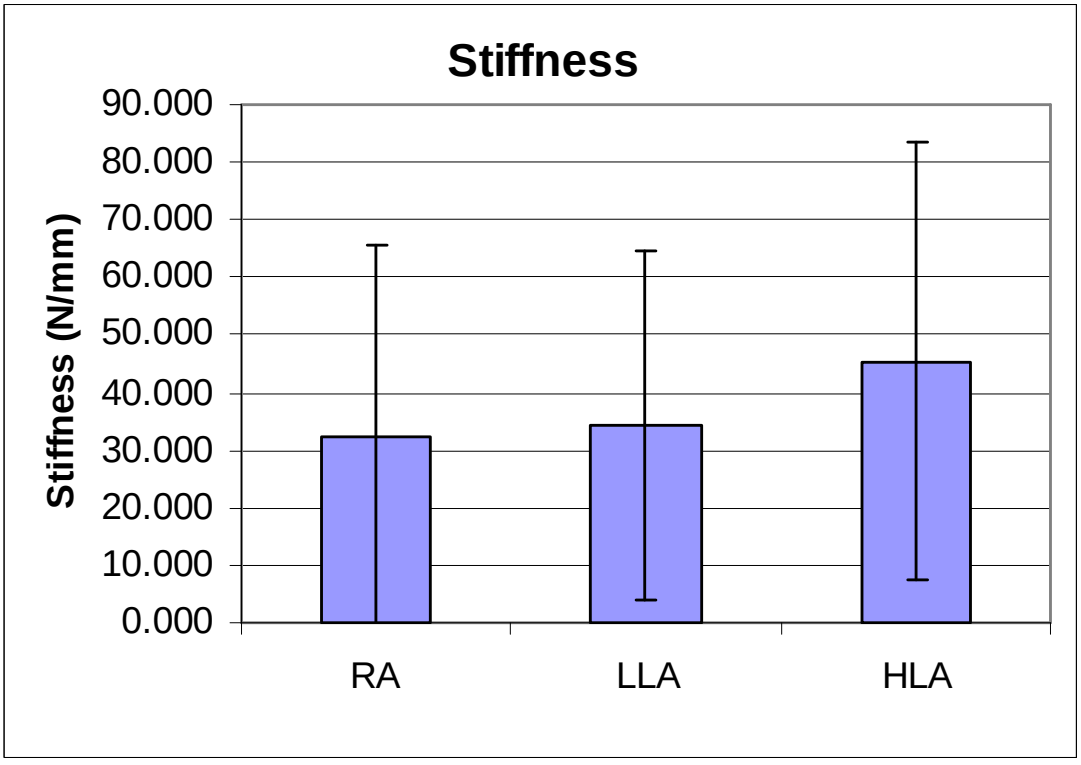

Figure 52: HAp/C composite mechanical response of the stiffness.

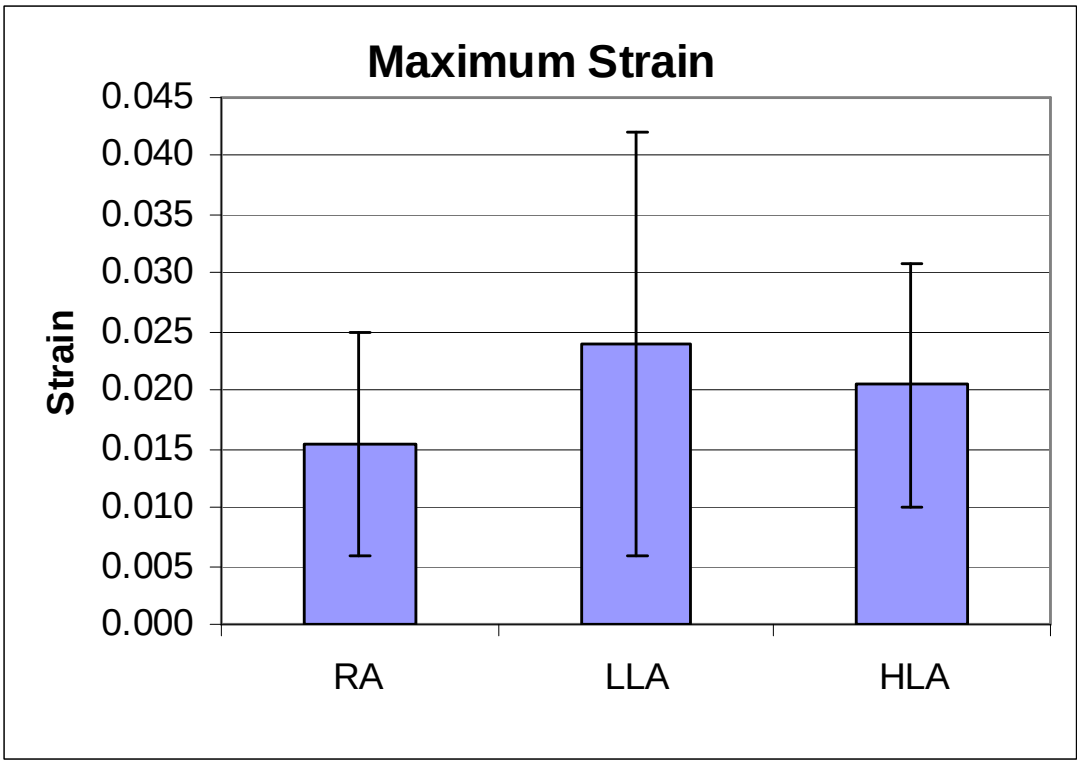

Figure 53: HAp/C composite mechanical response of the strain.

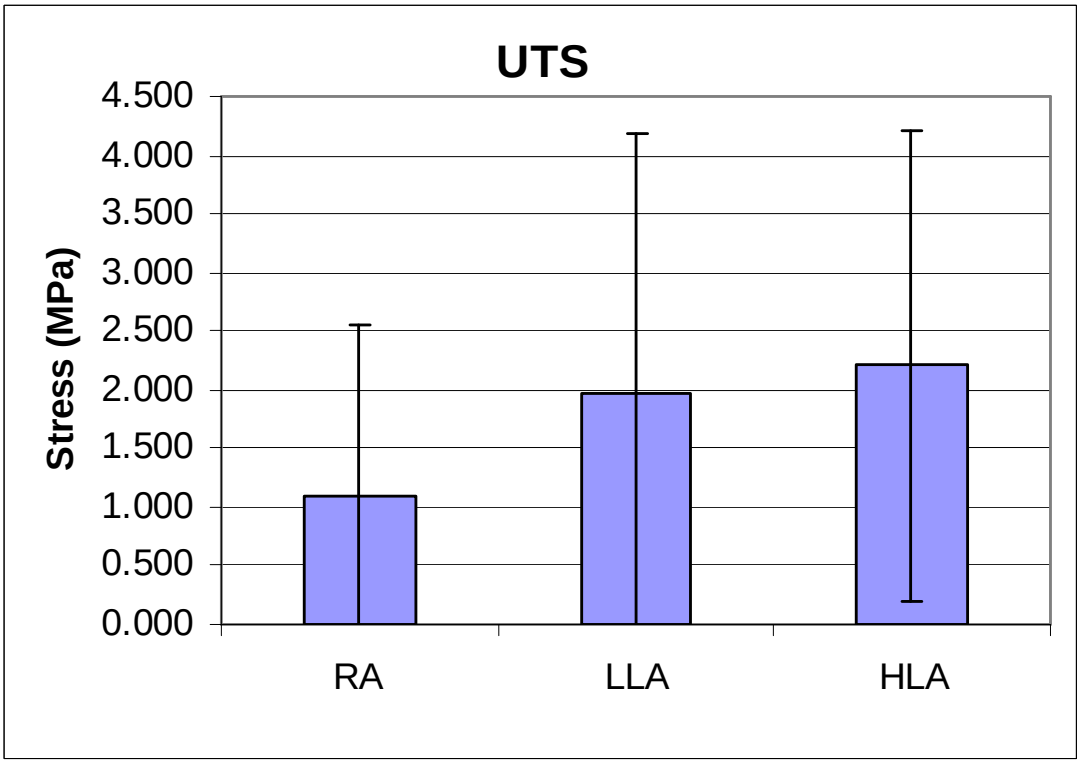

Figure 54: HAp/C composite mechanical response of the UTS.

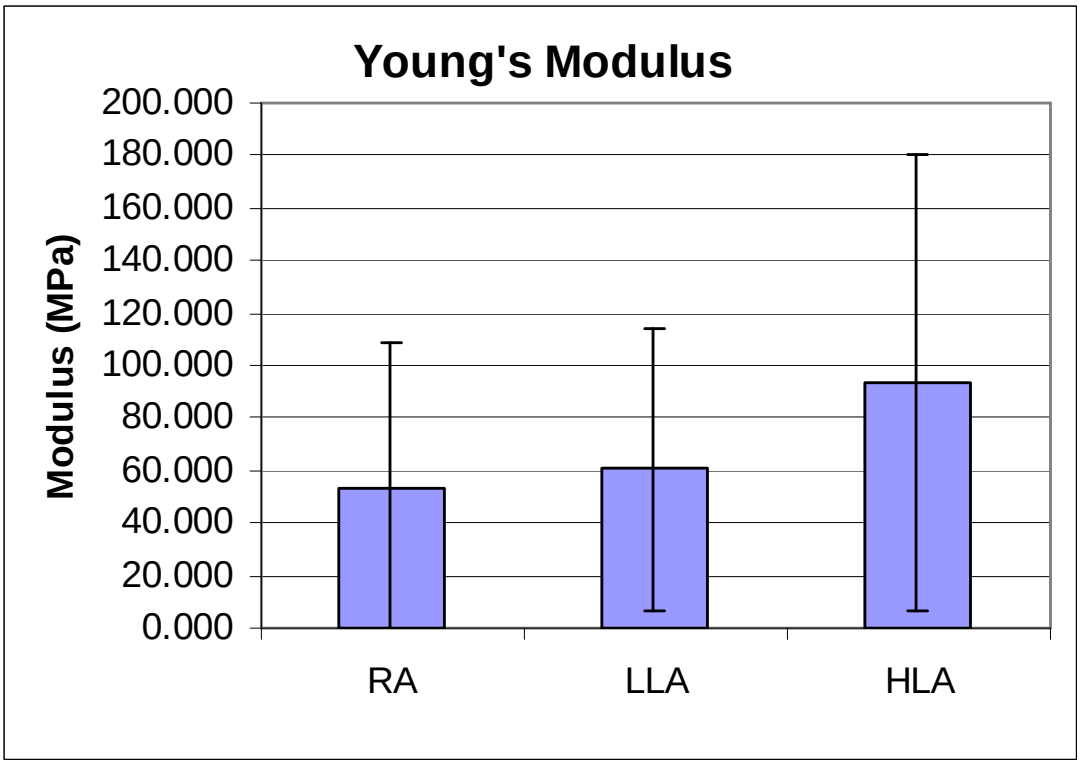

Figure 55: HAp/C composite mechanical response of the elastic modulus.

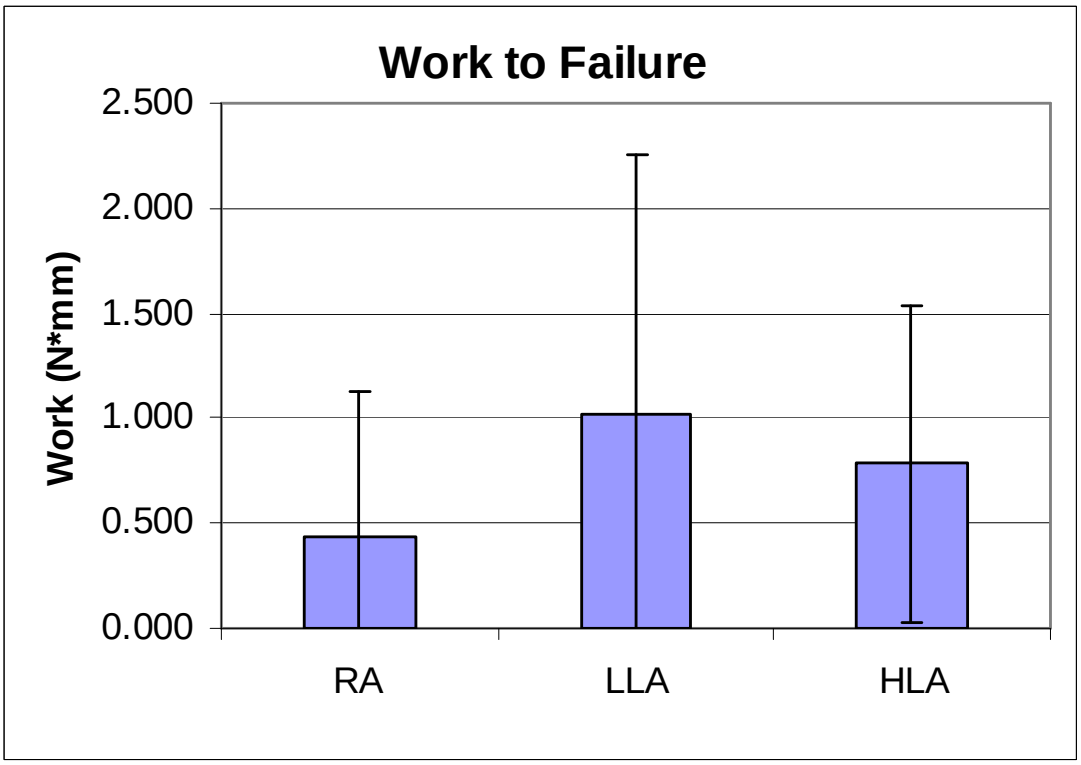

Figure 56: HAp/C composite mechanical response of the work to failure.

In addition to the types of extrusion process used to fabricate the HAp/C composite scaffolds, they were all subjected to a compaction process. The degree of collagen fiber alignment was shown to be influenced by the fabrication processes described in Chapter 5 - Quantification of Collagen Fiber Alignment in a Three Dimensional HAp/C Composite Scaffold. Each of the quantified mechanical properties from the three types of extrusion was evaluated for their dependence on the degree of alignment, or anisotropy. A regression analysis was conducted to demonstrate whether the dependence of the mechanical properties were due to extrusion alone, compaction alone, or a combination of the two (Figures B1-B18 in Appendix B). The regression analysis showed two distinct characteristics of the relationship between the mechanical properties and the degree of alignment in the planes representing the fabrication processes: 1) the individual mechanical properties were either positively or negatively affected by the anisotropy of the plane, defined by the direction of the slope of the linear fit line; and 2) the mechanical properties associated with each type of extrusion process were significantly dependant on a particular planar anisotropy. Table 6 summarizes the positive, negative, and significant relationships between the planar anisotropies and the mechanical properties from the extrusion type used to fabricate the HAp/C composite scaffolds. The mechanical properties of the RA and HLA extruded specimens were positively associated with the anisotropies in all planes, with the exception of the RA maximum strain in the C-plane that had a negative association. The mechanical properties of the LLA

Table 6: Mechanical property dependence on the degree of fiber alignment for the three groups of extrusion process type

Anisotropy Extrusion	**Maximum Load**	**Stiffness**	**Maximum Strain**	**UTS**	**Modulus**	**Work to Failure**
E-plane						
RA	+	+	+	+	+	+
LLA	-	-	-	-	-	-
HLA	+	+	+	+ p=0.0322	+	+ p=0.0340
T-plane						
RA	+ p=0.0277	+	+	+ p=0.0083	+ p=0.0144	+ p=0.0373
LLA	+	+	+	-	+	-
HLA	+	+	+	+	+	+
C-plane						
RA	+	+	-	+	+	+
LLA	+ p=0.0142	+	+ p=0.0376	+ p=0.0020	+ p=0.0087	+ p=0.0044
HLA	+	+	+	+	+	+

+ = positive correlation between mechanical response and planar anisotropy
- = negative correlation between mechanical response and planar anisotropy

specimens were positively associated with the anisotropy in the C- and T-planes with the exception of the negative UTS and work to failure in the T-plane. All of the mechanical properties of the LLA specimens were negatively associated with the anisotropy in the E-plane.

UTS and work to failure were significantly dependent on the E-plane anisotropy of the HLA specimens. Load, UTS, modulus, and work to failure were all significantly dependent on the T-plane anisotropy of the RA specimens. All of the LLA mechanical properties, except stiffness, were significantly dependent on the C-plane anisotropy.

6.4 Discussion

Uniaxial tensile tests were conducted on the 3D HAp/C composite scaffolds fabricated by three extrusion process types that induced varying degrees of collagen fiber alignment in a preferred direction. This study investigated the association between the HAp/C scaffold mechanical properties and the quantified extent of collagen fiber alignment from the combined extrusion and compaction fabrication process. The aim was to determine the extent that the preferred collagen alignment would increase the mechanical properties of the HAp/C composite.

The fabrication processes employed in producing the 3D Hap/C composite scaffolds were chosen for their simplicity in effecting changes in the mechanical properties of the scaffold. Extrusion was chosen as the scaffold fabrication method due to the simplicity of the techniques used to align fibers in the load bearing direction and vary the degree of fiber alignment. Extruded fiber reinforced matrices were shown to increase fiber alignment in a preferred direction [139] with simple techniques that increased the shear and compressive forces during extrusion [140]. Compaction was chosen as an additional processing technique because it had been shown to increase the mechanical properties of HAp and HAp/C scaffolds [2, 38, 131] and incrementally increased extruded HAp/C scaffolds [40].

The extrusion process types used in this study showed that the mechanical properties can be increased by the type of process used. Both the LLA and HLA extrusion processes produced specimens that increased the mechanical strength and toughness relative to the RA process. However, the increases measured were not significantly different. Compaction could have influenced the response of the RA

specimens. The compaction induced alignment in the specimens was greater than the alignment produced by extrusion alone. This finding was supported by four of the six mechanical properties being significantly dependent on compaction induced alignment, which may account for the RA specimens having mechanical properties that were not significantly less than the other extruded samples. The expected random alignment in the specimens were significantly influenced by the compaction process.

The expected increased alignment in the HLA group was not present because of possible extrudate instabilities which caused an increase in the transverse fiber alignment and not an increase in the preferred longitudinal direction. This was evident when only two of the mechanical properties were shown to be dependent on the collagen alignment from extrusion. While the HLA specimens had increased transverse alignment, the significant effects on its mechanical properties were from extrusion.

LLA prepared specimens exhibited mechanical properties on par with the HLA group and, to an extent, greater for those properties whose response has been shown to be dependent on the collagen alignment, namely toughness [56, 141-144] and strain [56, 130, 145-148]. These specimens also showed the highest degree of alignment due to extrusion. However, the response of this group was a special case since the mechanical properties had a negative relationship with the degree of alignment due to extrusion. On the other hand, all of the mechanical properties, except stiffness, were dependent on the combined fiber alignment seen in the C-plane anisotropy. The latter finding suggests that the LLA specimens were influenced to the greatest extent by the combined effects of the extrusion and compaction. It is not clear as to why there was not a significant effect from the extrusion process when this group showed the highest degree of alignment due to the extrusion process. The only explanation would be that there was a preexisting fabrication flaw, such as a crack, that reduced the mechanical response of the group as a whole. In fact, the specimen with the highest E-plane anisotropy supported the lowest load applied and the specimen with the second highest E-plane anisotropy only supported a below average load.

While enhancements were shown, the mechanical properties were one or more orders of magnitude less than those of natural bone. Additional methods during scaffold preparation, such as collagen fiber crosslinking, may provide further improvements to the upper load limits. Crosslinking is

responsible for increasing the mechanical properties of collagen fibers [149]. However, the relationship between the mineral-fiber interactions and fiber alignment were not masked by including crosslinking as a factor in the current study. Compaction was necessary due to the fragility of the specimens without this added fabrication process. The compaction process was deemed not to be confounding since it is additive in nature by affecting only the degree of alignment in the preferred direction. Large variations in the mechanical properties are suspected to be a result of the specimen fragility noted above. In future embodiments of the fabrication process, it is anticipated that modified extruder design [135], compaction pressure [2, 40, 131], and collagen crosslinking [149, 150] will all act in concert to increase the collagen fiber alignment and mechanical properties.

6.5 Conclusions

The application of extrusion and compaction fabrication methods were successfully employed to induce a preferred collagen fiber alignment in a synthetic 3D HAp/C composite scaffold and influence the mechanical properties. Extrusion breaker plates with larger hole dimensions induced greater fiber alignment in a preferred direction than smaller hole dimensions, resulting in a significant interdependence between mechanical properties and fiber alignment. Fiber alignment dependent mechanical properties (strain and toughness) were increased. While the results suggest that the larger hole dimension improved fiber alignment which significantly influenced its mechanical properties, the optimal hole size can not be concluded from this study because initial expectations were for the smaller hole size to increase fiber alignment and extruder design modifications may support this outcome in the future.

CHAPTER 7 – CONCLUSIONS

7.1 Discussion

The subject of this body of work was centrally focused on the alignment of collagen fibers in a hydroxyapatite-collagen composite as it relates to optimizing the composition and mineral phase, increasing the degree of alignment, and ultimately enhancing the mechanical properties. To achieve the end goals, the research anticipated that the three following Specific Aims needed to be addressed: 1) characterize the physicochemical properties of a synthetic HAp/C composite with bone-like composition, apatitic mineral crystal phase, and crystallinity; 2) quantify the collagen alignment morphology in a HAp/C composite induced by a novel extrusion process; and 3) determine the extent to which collagen alignment increases the material properties of the HAp/C composite.

Discussion of the results that addressed each of these three aims was previously presented in detail in their respective chapters. The discussion presented here will summarize those findings in relation to the original hypotheses for each of the aims, above.

7.1.1 Physicochemical Characterization of a Hydroxyapatite-Collagen Composite

The experimental section on the physicochemical characterization of a HAp/C composite addressed the first aim. The study aimed to characterize the physicochemical and crystallographic properties of a biomimetic coprecipitation of calcium, phosphate, and collagen, with respect to bone. Specifically, the study investigated the environmental and temporal effects on the composition, phase, and crystallography of a biomimetic HAp/C composite as it compares to that of natural bone. The hypotheses were: 1) the mineral content will decrease as the pH increases; 2) precipitation reaction aged for durations beyond 8 hours will yield a HAp calcium phosphate mineral phase; and 3) the degree of mineral crystallinity will increase with increased incubation duration.

Environmental changes in the solution pH significantly impacted the composition of the biomimetic HAp/C composite. The mineral fraction of the biomimetic HAp/C composite was stable at or below pH 8, but increased when the pH increased to 9. This satisfied the first part of the original hypothesis that stated the mineral fraction was sensitive to changes in pH, but counter to the second part that stated the

mineral fraction would decrease with increased pH. The mineral fraction was 83-84% when the pH was below 9, but when the pH was increased to 9, the mineral fraction increased to 88%. These findings do not suggest that the hypothesis was refuted, but rather that the original hypothesis may have been incorrectly based on a dissimilar HAp/C coprecipitation process [2]. The hypothesis was based on a prior study that used H_3PO_4 + Collagen and $Ca(OH)_2$ precursors which differed from those used in the current study.

The second hypothesis of this aim stated that aging durations beyond 8 hours will yield a HAp calcium phosphate mineral phase. XRD phase analysis of samples produced in the environmental and temporal experiments indicated a predominant HAp phase. The majority of the specimen diffraction lines, from samples at all levels of pH and aging duration, coincided with those of HAp, from the PDF card file 9-432 and the HAp-RS reference. Additional peaks corresponding to DCPD, TCP, OCP, and CHAp were found in the samples. However, there was no clear trend to distinguish whether any of these phases were prevalent among the different treatment levels in the biomimetic composites. If calcium phosphate phases other than HAp presented, it would be expected in the temporal experiments conducted with aging durations of 6 and 12 hours. Mineralization experiments have shown that complete transformation to HAp can be achieved in 12 hours or less in physiologic or alkaline environments [7, 6, 35]. The results from this analysis satisfied the second hypothesis and showed that aging effects on calcium phosphate phase were not as rigorous as had been assumed since an aging duration as low as 6 hours still transformed to the HAp phase.

The last hypothesis stated that the crystallinity will increase with increased aging duration, but made no provision for environmental effects. The study did address both factors in its analysis and compared the crystallography of the HAp/C composite to that of natural bone. Increased diffraction intensities were observed between environmental samples produced at a pH of 6.8, 7.4, and 8.0 and bone, as well as between temporal samples aged 6, 12, and 24 hours and bone, suggesting that the only biomimetic HAp/C composite that was not more crystalline than the biologic HAp/C composite was those samples prepared

in an alkaline environment with a pH of 9. These observations suggest that crystallinity was inversely proportional to pH and proportional to aging, confirming the original hypothesis.

7.1.2 Quantification of Collagen Fiber Alignment in a Three Dimensional HAp/C Composite Scaffold

The study of extrusion induced preferential collagen fiber alignment addressed the second aim in this body of research. The goal was to quantify the extent to which a novel extrusion process would induce a preferential collagen fiber alignment in a HAp/C composite scaffold. It was hypothesized that increased hydrodynamic shear flow would: 1) increase the alignment of collagen fibers; and 2) that the alignment would be in a preferred direction.

The goal of extruding the HAp/C composite was to increase the degree of fiber alignment in the longitudinal direction of the specimens. Results from analyzing the fiber alignment in the E-plane of the three extrusion process types showed that the use of the breaker plates while extruding the LLA and HLA specimens increased the anisotropy in this direction relative to the baseline anisotropy. Extrusion without the breaker plate actually showed a decreased anisotropy in the longitudinal direction relative to the baseline. This was to be expected, but it was not expected that the LLA specimens would exhibit a greater anisotropy than the HLA specimens and a greater change in anisotropy from the baseline. Overall, the data suggested that the LLA extrusion method produced a higher degree of alignment than the other two methods in the preferred extruded direction.

The E-plane and T-plane alignment responses are indicative of the individual extrusion and compaction contribution to changes in the degree of fiber alignment, respectively. Both planes exhibited increased alignment over their respective baseline measures, but the increases were not statistically significant. The compaction-only contribution to fiber alignment was significantly greater than the extrusion-only contribution. The breakthrough finding was that the combination of the two, measured in the C-plane, contributed to a statistically significant increase over the baseline anisotropy. This significant anisotropy increase was preferentially aligned in the longitudinal axis of the specimens, which would provide a direct relationship with the resultant mechanical properties. The goal of inducing a

preferential collagen fiber alignment in a HAp/C composite scaffold was achieved. The hydrodynamic shear flow produced an incremental alignment and when coupled with the compaction process the resultant fiber alignment was induced and increased in a 3D HAp/C composite scaffold.

7.1.3 Mechanical Properties of a Preferentially Aligned Hydroxyapatite-Collagen Composite Scaffold

Uniaxial tensile tests were conducted on the 3D HAp/C composite scaffolds fabricated by the three extrusion process types that induced varying degrees of collagen fiber alignment in a preferred direction. This study investigated the association between the HAp/C scaffold mechanical properties and the quantified extent of collagen fiber alignment from the combined extrusion and compaction fabrication process. The goal was to determine the extent that the preferred collagen alignment would increase the mechanical properties of the HAp/C composite. The hypothesis was that preferential alignment of collagen fibers in the HAp/C composite will be associated with increased tensile material properties

The extrusion process types used in this study showed that the mechanical properties can be increased by the type of process used. Both the LLA and HLA extrusion processes produced specimens that increased the mechanical strength and toughness relative to the RA process. However, the increases measured were not significantly different. LLA prepared specimens exhibited mechanical properties on par with the HLA group and, to an extent, slightly greater for those properties whose response has been shown to be dependent on the collagen alignment, toughness [56, 141-144] and strain [56, 130, 145-148]. These specimens also showed the highest degree of alignment due to extrusion. All of the mechanical properties, except stiffness, were dependent on the combined extrusion and compaction fiber alignment seen in the C-plane anisotropy. The degree of alignment was preferential in the direction of the tensile loading axis and confirmed the hypothesis.

7.2 Limitations

Each of the study aims presented with experimental limitations, such as solution chemistry, analytical methods, fabrication processing techniques, and omitted processing. The limitations taken in whole or in part may have affected the results observed in this work.

Solution chemistry limitations involved foreign ion inclusions and substitutions. Foreign ion inclusions consisted of potassium, sodium, and chloride ions. EDS measurements noted the presence of potassium, sodium, and chloride ions in the precursor solutions and buffers. These ions were thought to be residual salts that remained after washing and were not incorporated into the mineral crystal. However, it has been reported that these ions can be adsorbed into the crystal structure [112]. Their possible inclusion became evident when the mineral fraction exceeded the theoretical fraction limit at pH 9. The inclusions could have skewed the Ca/P ratios observed, increased XRD peak broadening (crystal strains), and act to weaken the crystalline phase of the composite by producing internal distortion (crystal strains) and dislocation with the apatite crystals. Ca/P ratio and XRD broadening effects may have masked the presence of fractional calcium phosphate phases other than HAp. Use of Fourier transform infrared (FTIR) spectroscopy may discern phase related changes in phosphate P-O bonding to confirm apatite phase and obtain another level of certainty. Any affects on the mechanical properties may be minimized since the specimens were produced with a pH of 7.4 and these ions may not have been as readily adsorbed given the observed mineral fraction reflected the calculated fractions. Further prevention of these foreign ions may require changing the precursor solutions, which rely heavily on HCl for dissolving collagen and buffering with Tris. An alternative is to utilize H_3PO_4 for dissolving collagen and $Ca(OH)_2$ as precursor solutions [2]. Foreign ion substitutions, such as that of CO_3, may account for the Ca/P ratios observed. This is not necessarily a detriment since bone is a carbonated apatite. The concern, however, is that the techniques used were either not sensitive enough to detect (XRD) or that this ion was not specifically quantified (EDS). Peak overlap in the XRD profiles and the close proximity of carbonated apatites to HAp made it difficult to discern one from the other. New tools [151] have been found with the knowledge gained that would allow revisiting the XRD profiles for better peak determinations overall. Also, FTIR may again be employed to observe the CO_3 bonding patterns. Together, these two additional approaches would enhance the present phase analysis.

Analytical technique limitations may manifest in errors quantifying the degree of fiber alignment using PLM. The quantification of the degree of alignment broadly followed previous application on SEM

or other idealized images [65, 71]. The applications used to quantify the degree of alignment were ImageJ plug-ins that may not have explicitly followed the desired quantification algorithms. The result may be an averaging effect that smoothed the data and reduced the observable effects between test groups.

Fabrication processing limitations included the fragility of the specimens and the associated compaction process. After consolidating the wet HAp/C composite by vacuum filtration to the consistency of a paste, the composite still maintained a water content of 88%. Extruding, molding, and drying specimens in this state would leave the resultant HAp/C composite too porous and fragile to conduct mechanical test, let alone handle for machining, potting, and other setup. The compaction process was introduced to overcome these issues by driving excess water out of the specimen while in the mold. While the compaction process improved the fragility, there were still issues with sample frailty. An explanation for the remaining fragility was that specimen compaction may be uneven. Several specimens were compacted at the same time in a hydraulic press. If there was an unbalanced fraction of water between the specimens, then the specimens with the higher water content would not be compacted to the extent of the other specimens present during that compaction cycle. Care was taken to eliminate specimens when it was obvious there was uneven compaction. This was evident in either the thickness differences between specimens in the same compaction cycle or differences in the displacement of the mold compactor. Specimens were eliminated when these differences were observed. This and other fragility issues were prevalent. Eighty four specimens were produced and only 21 specimens were mechanically tests. Other processing steps that may introduce inaccuracies were the freezing and handling during machining. The fragility of the specimens is postulated to have caused the large variation in the mechanical properties. Despite this, statistically significant relationships were observed. One method to overcome the fragility is speculated to be increasing the compaction pressure. The current compaction pressures used were approximately 2 MPa. Others have used 200 MPa [2] or 400 MPa [131]. Further optimization of the compaction process should be conducted

While the current study may have been limited by omitting other strengthening processes, the results presented provide a baseline strength which needed to be established for the extrusion process, with minimal influence from compaction and without collagen crosslinking. Future work can be directed at studying the effects of compaction in greater detail and the effects of crosslinking.

7.3 Future Work and Direction

The limitations described present new challenges and opportunities for future study. Work related to the mineral phase characterization of calcium phosphate mineralization of collagen, reduction of foreign ion inclusions, PLM analytical techniques, scaffold fabrication, and mineralization methodologies could all be expanded.

One area of research envisioned is an improved phase profiling and quantification of the relative fractions of calcium phosphate phases present in collagenous scaffolds. The presence of collagen and possibly ACP were deemed responsible for the background XRD profile observed in the current work. The large broad peaks of the background collagen and ACP may have masked the observation of other calcium phosphate phases. This may occur since quantitative phase analysis methods rely on the fact that the relative intensity of a particular phase is proportional to the amount of that phase present [76, 116]. This work proposes to quantify the fractions of calcium phosphate phases and the contribution of collagen to the background XRD profile by varying known amounts of different calcium phosphate phases from powder standards (ACP, CO3HAp, DCPD, HAp, OCP, and TCP) with and without collagen. XRD patterns would be obtained with a decreased scan speed than in the current study, in order to obtain better resolution of the acquired pattern. Computational methods [151] for individual peak extraction from overlapped peaks would be used to determine peak locations. These computational methods would be applied to the existing composite patterns and compared to those from the known calcium phosphate powder mixtures for an improved analysis of the phase response to the HAp/C composite synthesis environment.

The analytical technique used to quantify the degree of fiber alignment from the PLM images presents an opportunity to study the ability of this method to accurately quantify fiber alignment. A study

to address this is could involve incorporating electrospun collagen fiber processing techniques. The aim would be to determine the extent to which PLM quantified collagen fiber anisotropy differs from that of collagen fiber anisotropy derived from SEM imaging. Collagen fibers can be electrospun with varied orientations based on flow rate and collector RPM [152]. The electrospun fibers samples could subsequently be imaged by PLM and then by SEM. DFT algorithms have been validated against SEM images [71]. Both images could be analyzed by the DFT to obtain the degree of alignment for each imaging modality and compared to determine the accuracy of the PLM application.

Fabricated HAp/C composite scaffolds exhibited a high degree of fragility resulting in observed mechanical properties that were approximately two orders of magnitude less than that of bone. Compaction [2, 38, 40, 131] and crosslinking [150] have been to shown to increase the mechanical properties of HAp scaffolds and collagen fibers, respectively. Use of polyaspartate in the synthesis of the HAp/C composite during mineralization may improve the mineralization within the collagen fibers and the mineral interaction with the collagen fibrils [9, 153]. Thus, inclusion of polyaspartate assisted mineralization may also aid the improvement of the mechanical properties. Future work in this area envisions two aims that would determine the individual and combined effects of these three synthesis and fabrication processes on a three dimensional HAp/C composite scaffold. This future direction would build upon the current body of work, utilize the currently developed methodologies and fabrication processes, and it is hypothesized that the mechanical properties could be tuned to approach that of bone.

In addition to compaction and crosslinking studies building upon the current work, a feasibility study to assess the extent that modification of the extruder may eliminate extrusion instabilities would also seem beneficial. Extruder modification may improve the degree of fiber alignment for both the HLA and LLA extrusion process types. Instabilities arise from the excessive surface shear and tensile stresses at the wall of the die and after the exit, respectively. The stresses cause turbulent flow in the extrudate exiting the die, which might be eliminated by funneling the interior of the extruder body as it approaches the die opening in order to create laminar flow [135]. Modifying the extruder breaker plate with a funneled approach design may address these issues. The funnel would create a gradual increase in the

extrudate stresses, thus initiating the fiber alignment further upstream from the onset of the breaker plate and prevent the extrudate fracture instabilities from distorting the fiber alignment. This work could be included in the previously defined compaction and crosslinking scaffold fabrication studies to best optimize the composite.

7.4 Conclusions

7.4.1. Physicochemical Characterization of a Hydroxyapatite-Collagen Composite

The research concludes that the solution environment had a greater effect on the mineral fraction and the calcium to phosphorus ratio than the resultant mineral phase. Unlike other reports [34-37], these results demonstrate that the effects of pH on the resultant calcium phosphate phase appear to be desensitized by the simultaneous fibrillogenesis of collagen in the mineralizing solution (i.e. no alternate calcium phosphate phases were found aside from HAp). While the phase was not sensitive to changes in pH, the crystallinity, unit cell lattice constant *c* and Ca/P ratio were all affected. The changes in Ca/P ratio may be indicative of the carbonate content. Mineralization duration does not influence the calcium phosphate phase, but does affect the crystallinity and unit cell lattice constant *c*. This study showed that a HAp/C composite, synthesized in an environment with a pH between 7.4 to 8.0 and aged for 6 hours, can be tailored to approximate the physicochemical properties of a biologic HAp/C composite.

7.4.2 Quantification of Collagen Fiber Alignment in a Three Dimensional HAp/C Composite Scaffold

The application of extrusion and compaction fabrication methods was successfully employed to induce a preferred collagen fiber alignment in a synthetic 3D HAp/C composite scaffold. The combination of extrusion and compaction significantly increased the collagen fiber alignment in the preferential direction over baseline measures. Extrusion breaker plates imparted an increased degree of alignment versus not using them. The larger hole dimension used in the LLA extrusion method induced greater alignment than the smaller hole dimension in the HLA method. The optimal hole size and design may be the current LLA extrusion process method. Although the resultant anisotropies in the study were found to be relatively low ($\alpha = 1$ is completely aligned and $\alpha = 0$ is isotropic alignment), it is expected

that the degree of alignment can be increased with incremental compaction and modification to the extruder design, as discussed above. Design modification may initiate fiber alignment earlier in the extruder body and prevent the extrudate fracture instabilities from distorting the fiber alignment. Also, compaction pressures two orders of magnitude greater than the compaction pressure used in this study were shown to produce composite mechanical properties less than an order of magnitude lower than cortical bone [2]. The PLM technique was successfully employed with quantitative methods to analyze and evaluate the degree of collagen fiber alignment in 3D HAp/C composite scaffolds.

7.4.3 Mechanical Properties of a Preferentially Aligned Hydroxyapatite-Collagen Composite Scaffold

The application of extrusion and compaction fabrication methods were successfully employed to induce a preferred collagen fiber alignment in a synthetic 3D HAp/C composite scaffold and influence the mechanical properties. Extrusion breaker plates with larger hole dimensions induced greater fiber alignment in a preferred direction than smaller hole dimensions, resulting in a significant interdependence between mechanical properties and fiber alignment. Fiber alignment dependent mechanical properties (strain and toughness) were increased as a result of increased fiber alignment. The results of the study confirm the hypothesis that the induced alignment would result in increased mechanical properties. The larger hole dimension improved fiber alignment which significantly influenced the related mechanical properties and may serve to be the optimal hole size, despite initial expectations that the smaller hole size would be optimal.

APPENDIX A

X-RAY DIFFRACTION PATTERNS OF ALL SAMPLES

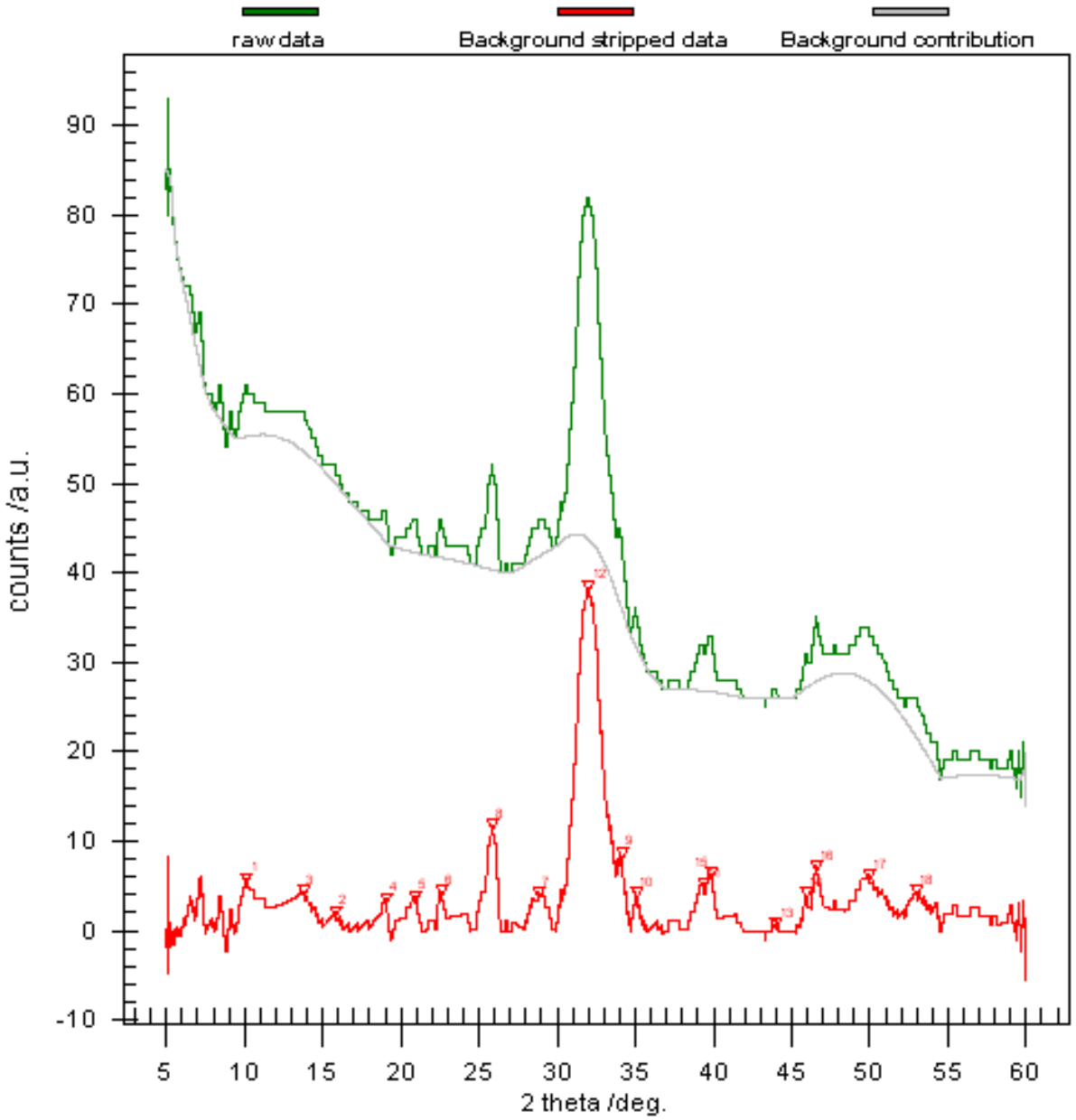

Figure A1: XRD pattern of sample 49LA. The green curve is the original Savitzky-Golay smoothed XRD pattern, the grey curve is the calculated background, and the red curve is the background subtracted pattern (red inverted triangles are the peak identifiers).

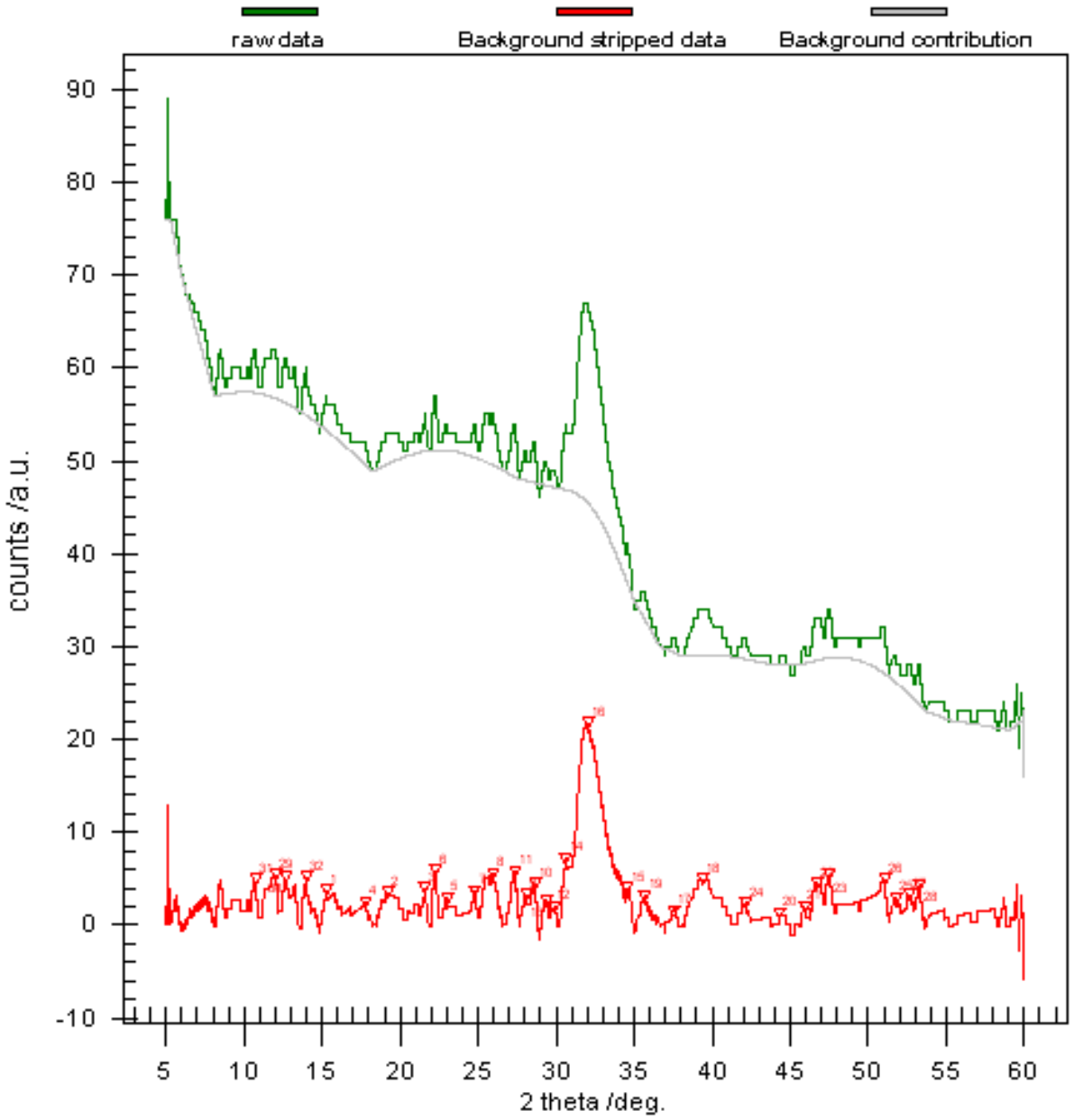

Figure A2: XRD pattern of sample 51LA. The green curve is the original Savitzky-Golay smoothed XRD pattern, the grey curve is the calculated background, and the red curve is the background subtracted pattern (red inverted triangles are the peak identifiers).

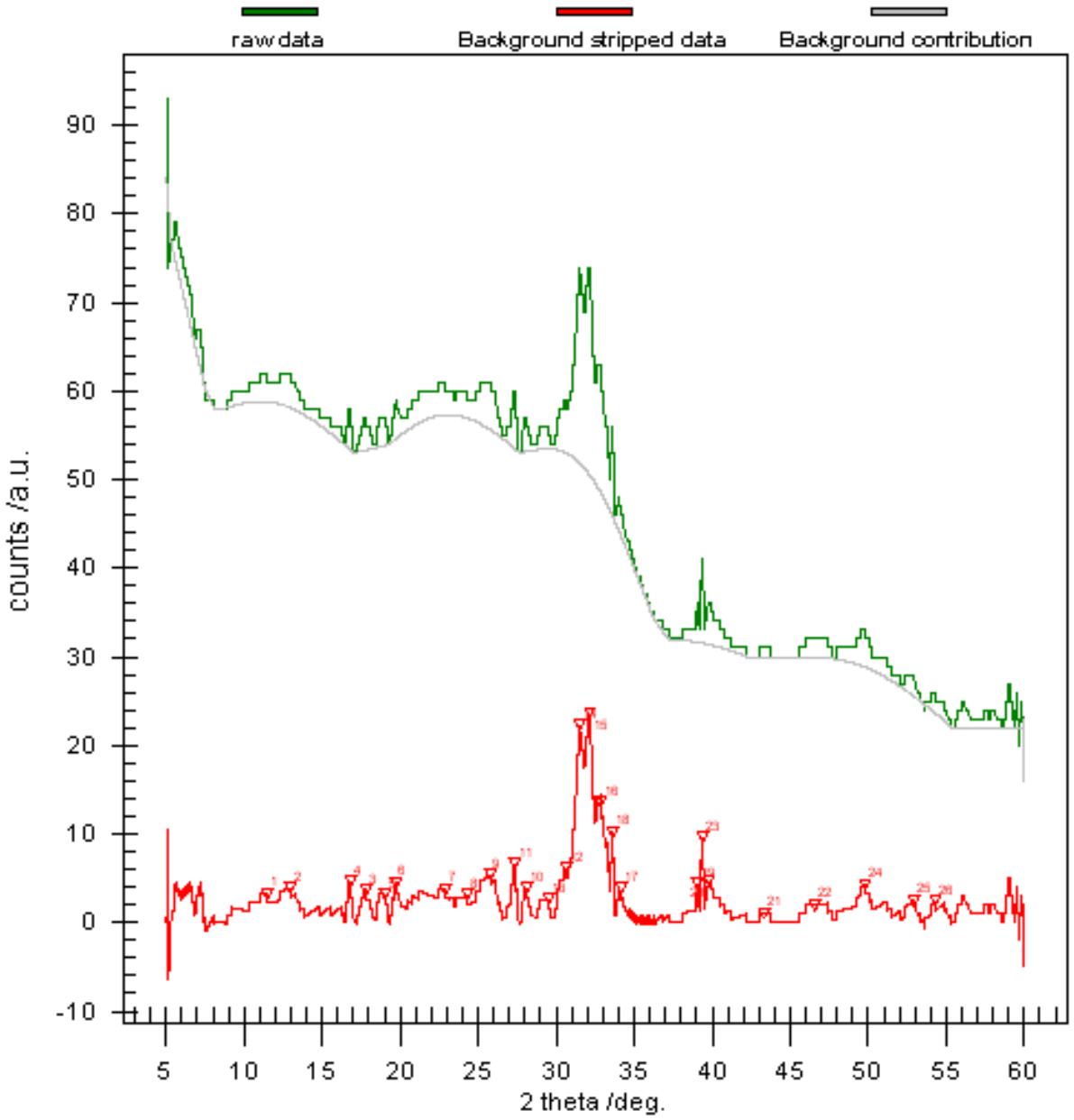

Figure A3: XRD pattern of sample 53RP. The green curve is the original Savitzky-Golay smoothed XRD pattern, the grey curve is the calculated background, and the red curve is the background subtracted pattern (red inverted triangles are the peak identifiers).

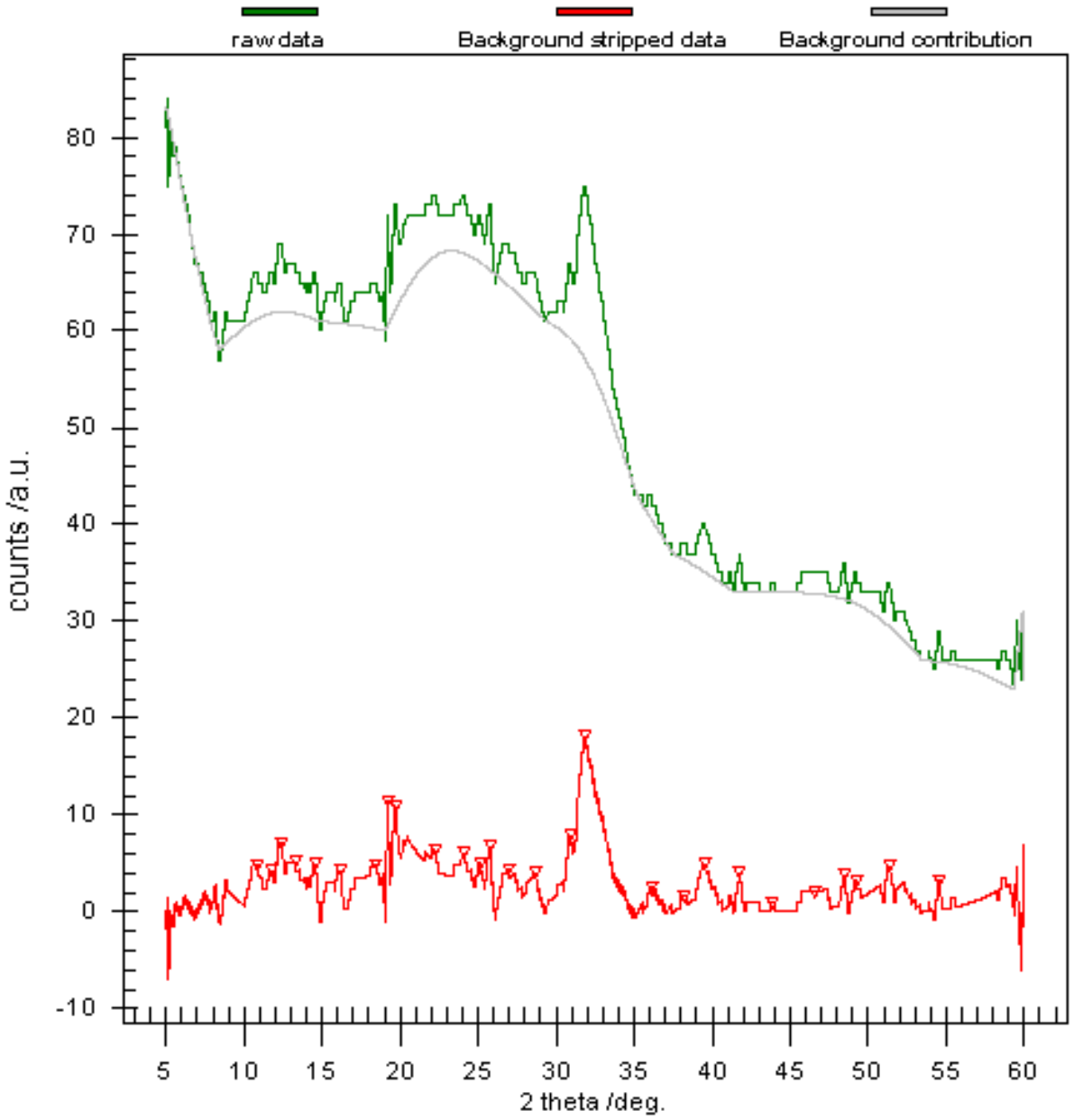

Figure A4: XRD pattern of sample 55LA. The green curve is the original Savitzky-Golay smoothed XRD pattern, the grey curve is the calculated background, and the red curve is the background subtracted pattern (red inverted triangles are the peak identifiers).

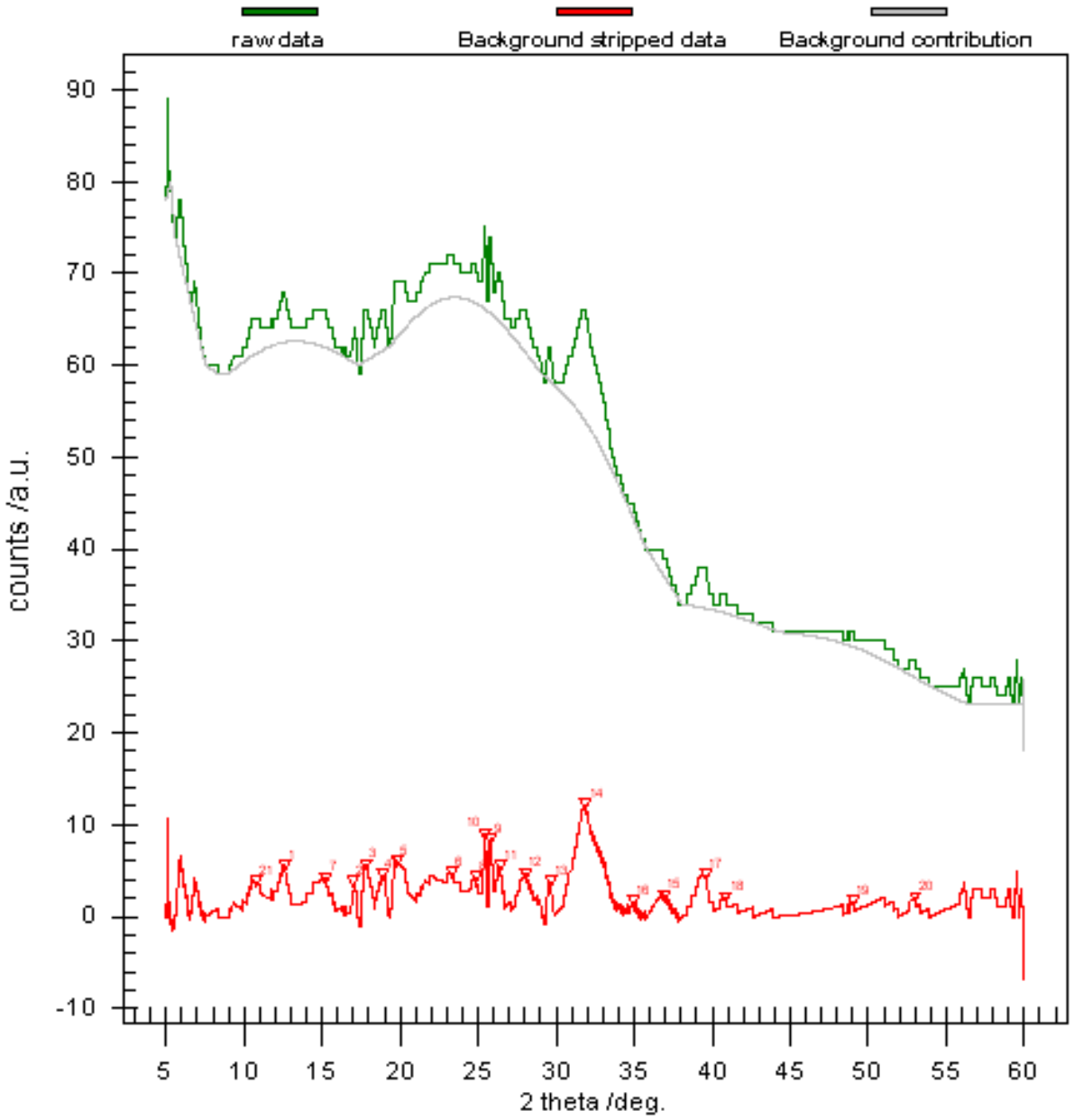

Figure A5: XRD pattern of sample 57LP. The green curve is the original Savitzky-Golay smoothed XRD pattern, the grey curve is the calculated background, and the red curve is the background subtracted pattern (red inverted triangles are the peak identifiers).

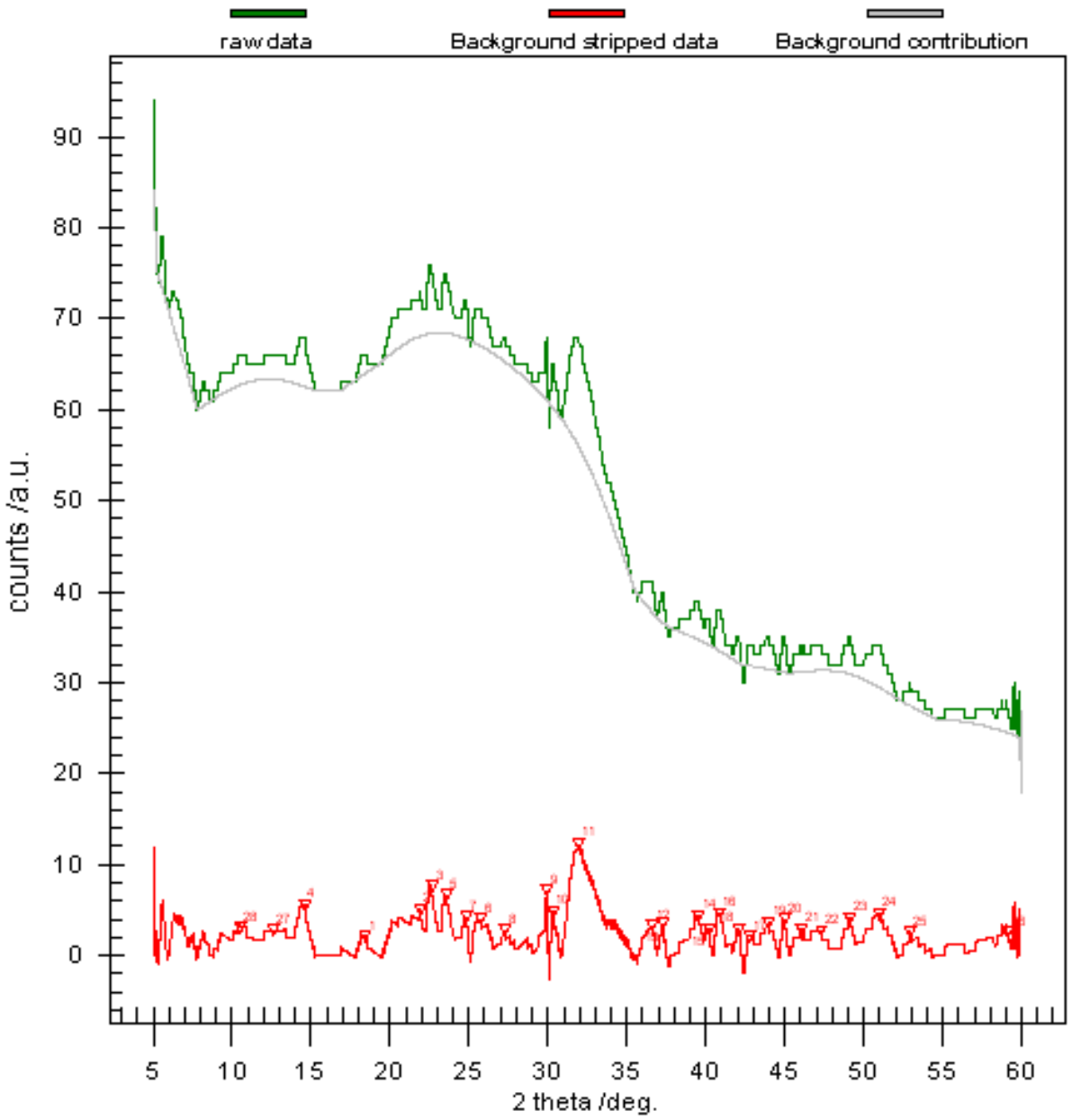

Figure A6: XRD pattern of sample 58RP. The green curve is the original Savitzky-Golay smoothed XRD pattern, the grey curve is the calculated background, and the red curve is the background subtracted pattern (red inverted triangles are the peak identifiers).

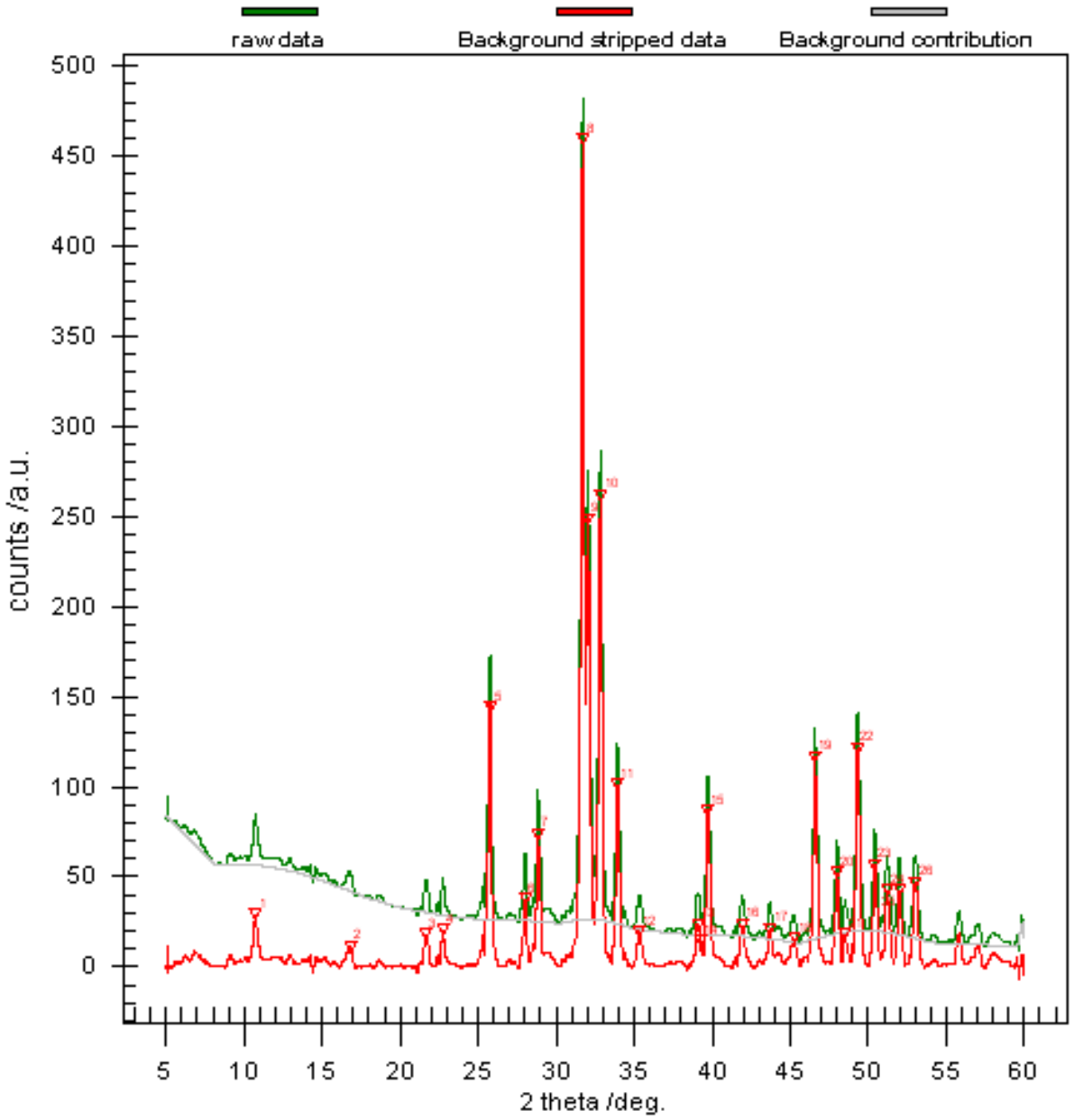

Figure A7: XRD pattern of sample HAp-RS. The green curve is the original Savitzky-Golay smoothed XRD pattern, the grey curve is the calculated background, and the red curve is the background subtracted pattern (red inverted triangles are the peak identifiers).

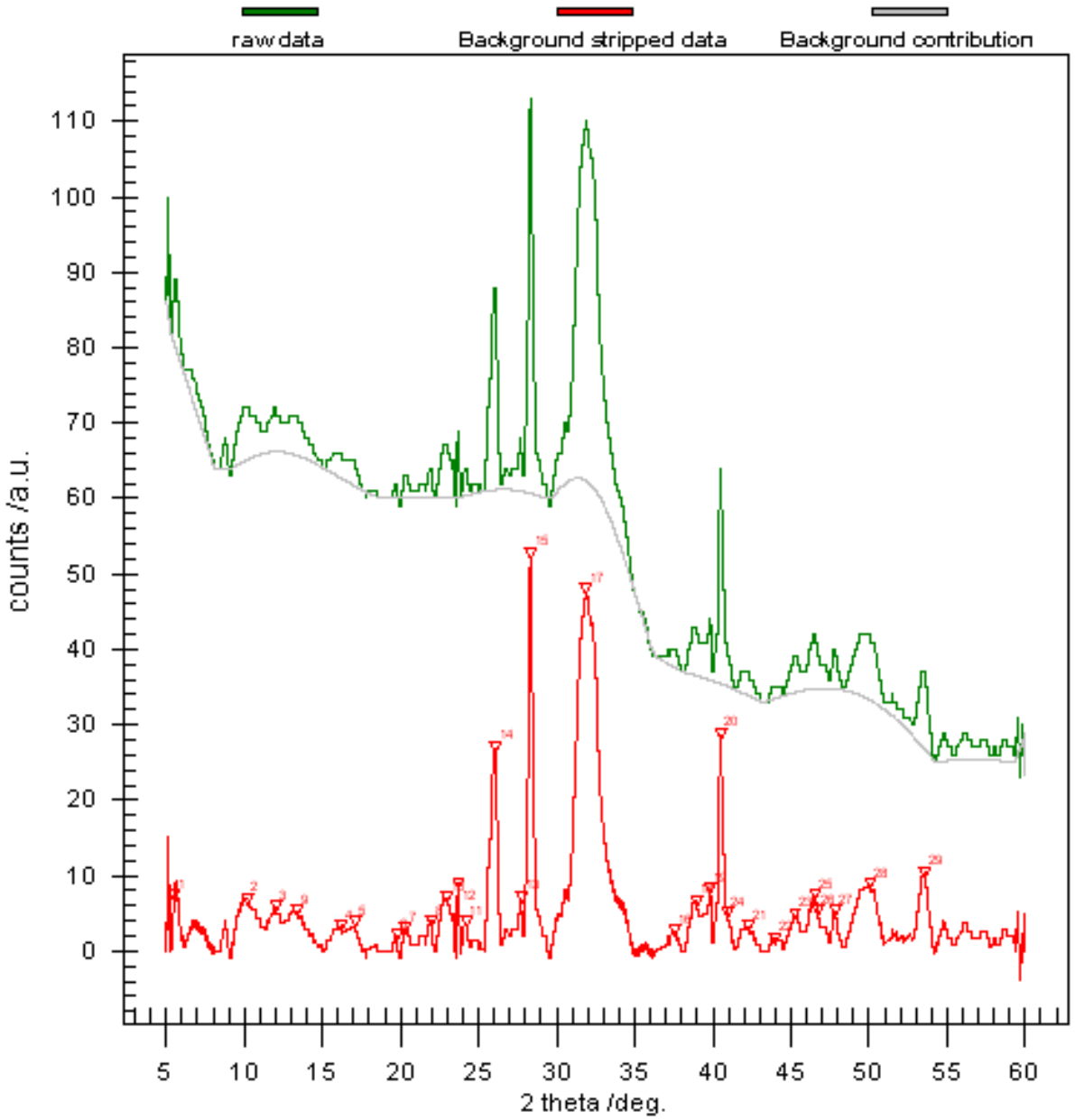

Figure A8: XRD pattern of sample pH68HApC1. The green curve is the original Savitzky-Golay smoothed XRD pattern, the grey curve is the calculated background, and the red curve is the background subtracted pattern (red inverted triangles are the peak identifiers).

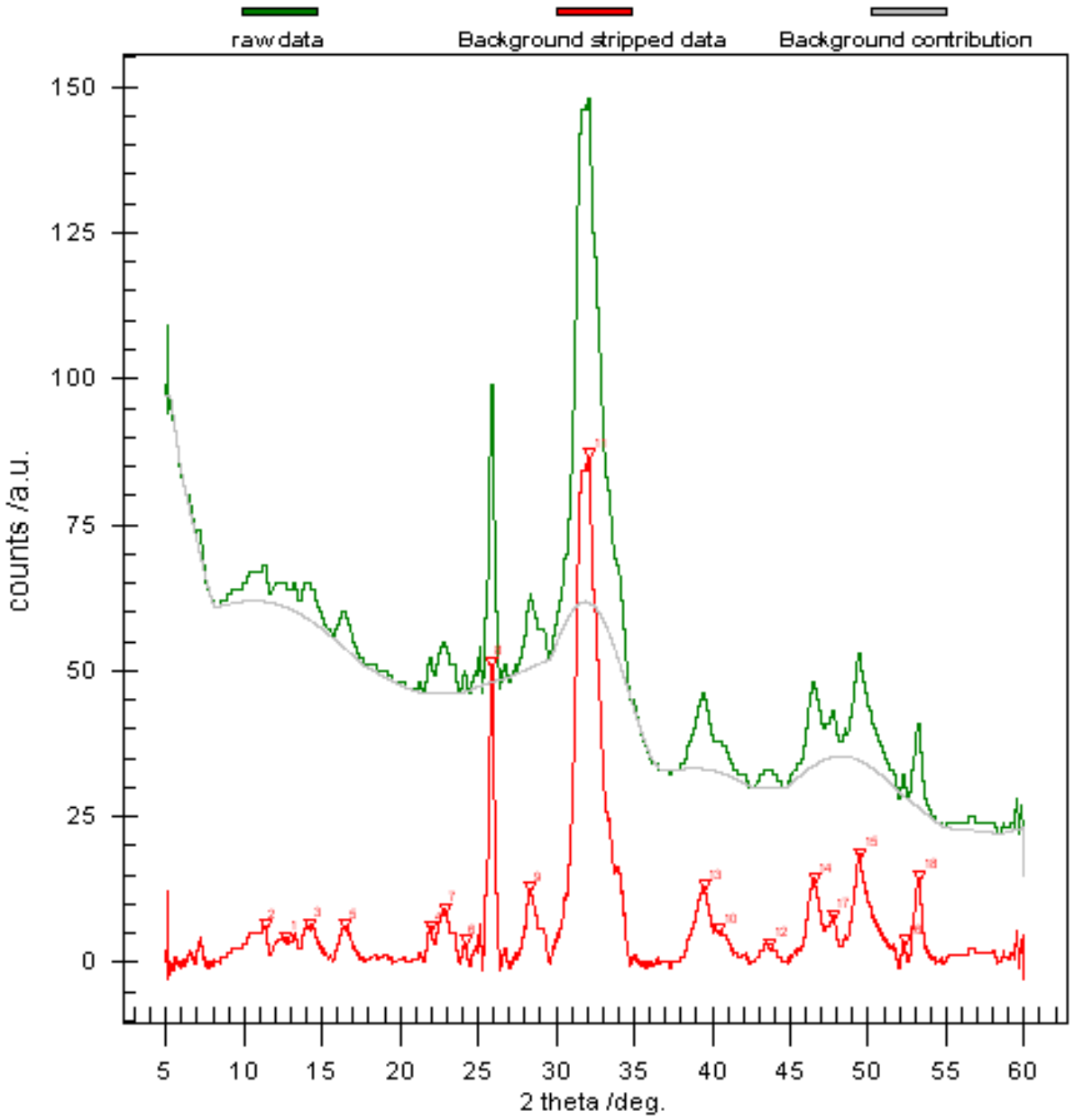

Figure A9: XRD pattern of sample pH68HApC2. The green curve is the original Savitzky-Golay smoothed XRD pattern, the grey curve is the calculated background, and the red curve is the background subtracted pattern (red inverted triangles are the peak identifiers).

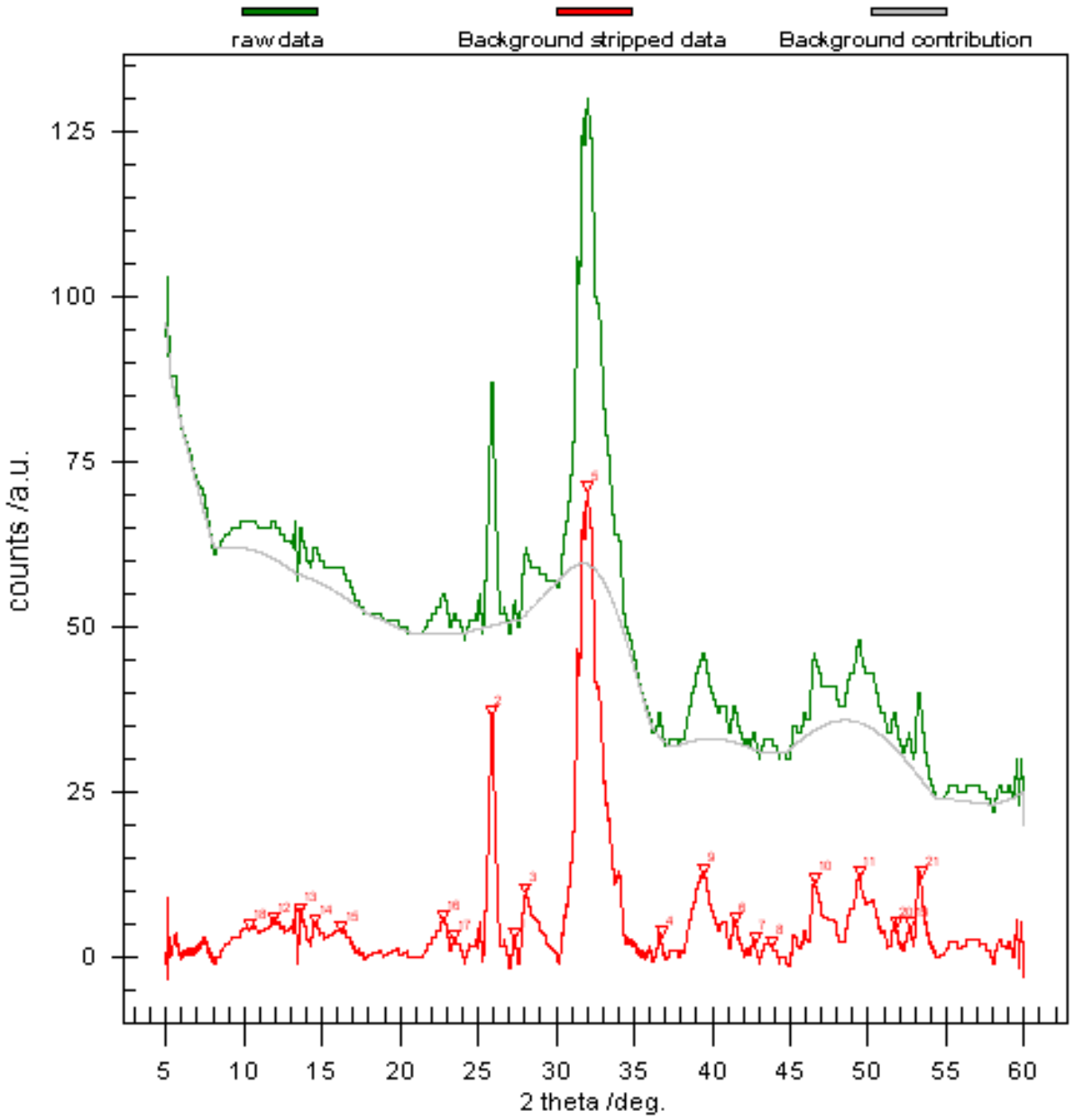

Figure A10: XRD pattern of sample pH68HApC3. The green curve is the original Savitzky-Golay smoothed XRD pattern, the grey curve is the calculated background, and the red curve is the background subtracted pattern (red inverted triangles are the peak identifiers).

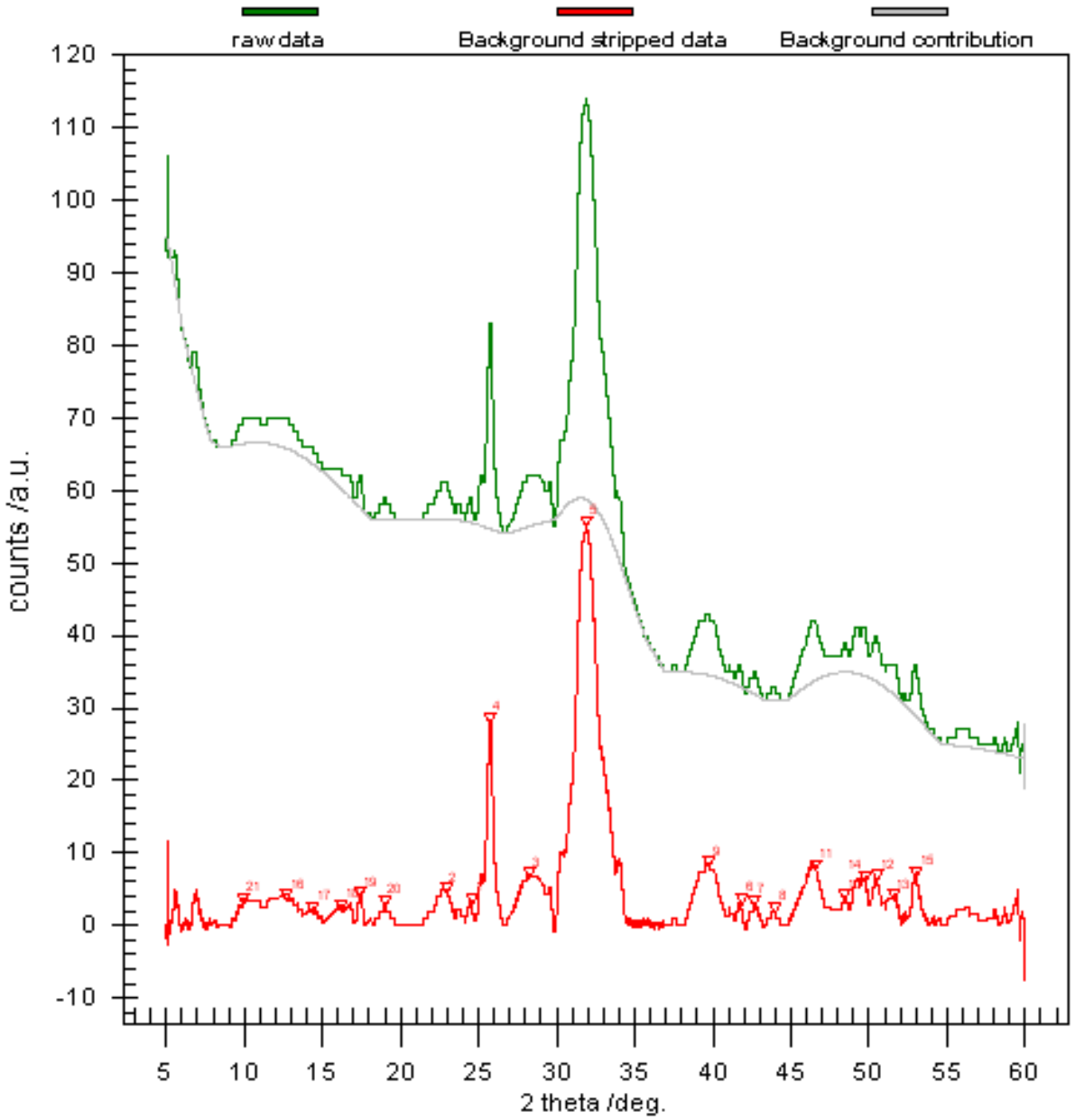

Figure A11: XRD pattern of sample pH74HApC1. The green curve is the original Savitzky-Golay smoothed XRD pattern, the grey curve is the calculated background, and the red curve is the background subtracted pattern (red inverted triangles are the peak identifiers).

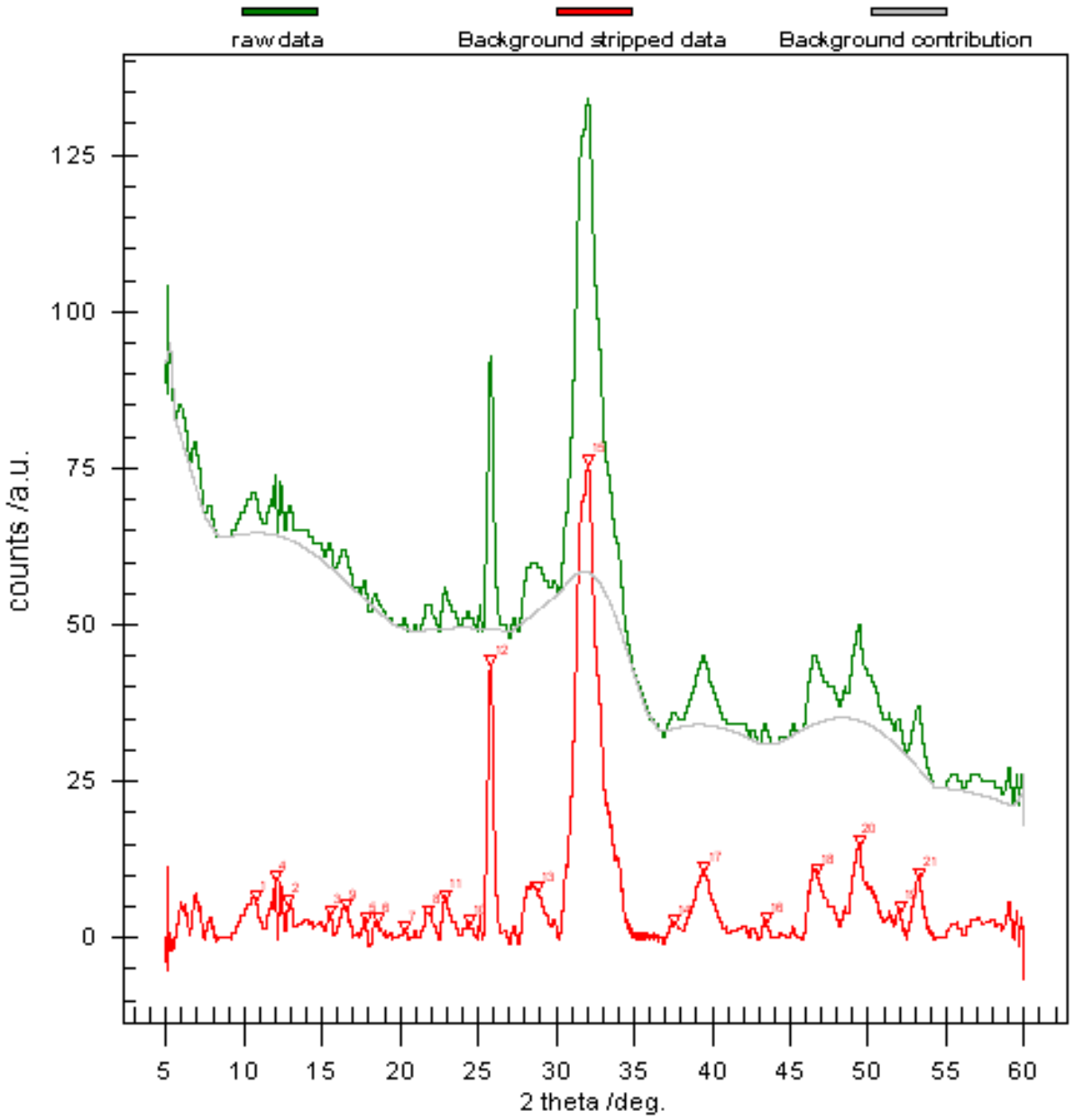

Figure A12: XRD pattern of sample pH74HApC2. The green curve is the original Savitzky-Golay smoothed XRD pattern, the grey curve is the calculated background, and the red curve is the background subtracted pattern (red inverted triangles are the peak identifiers).

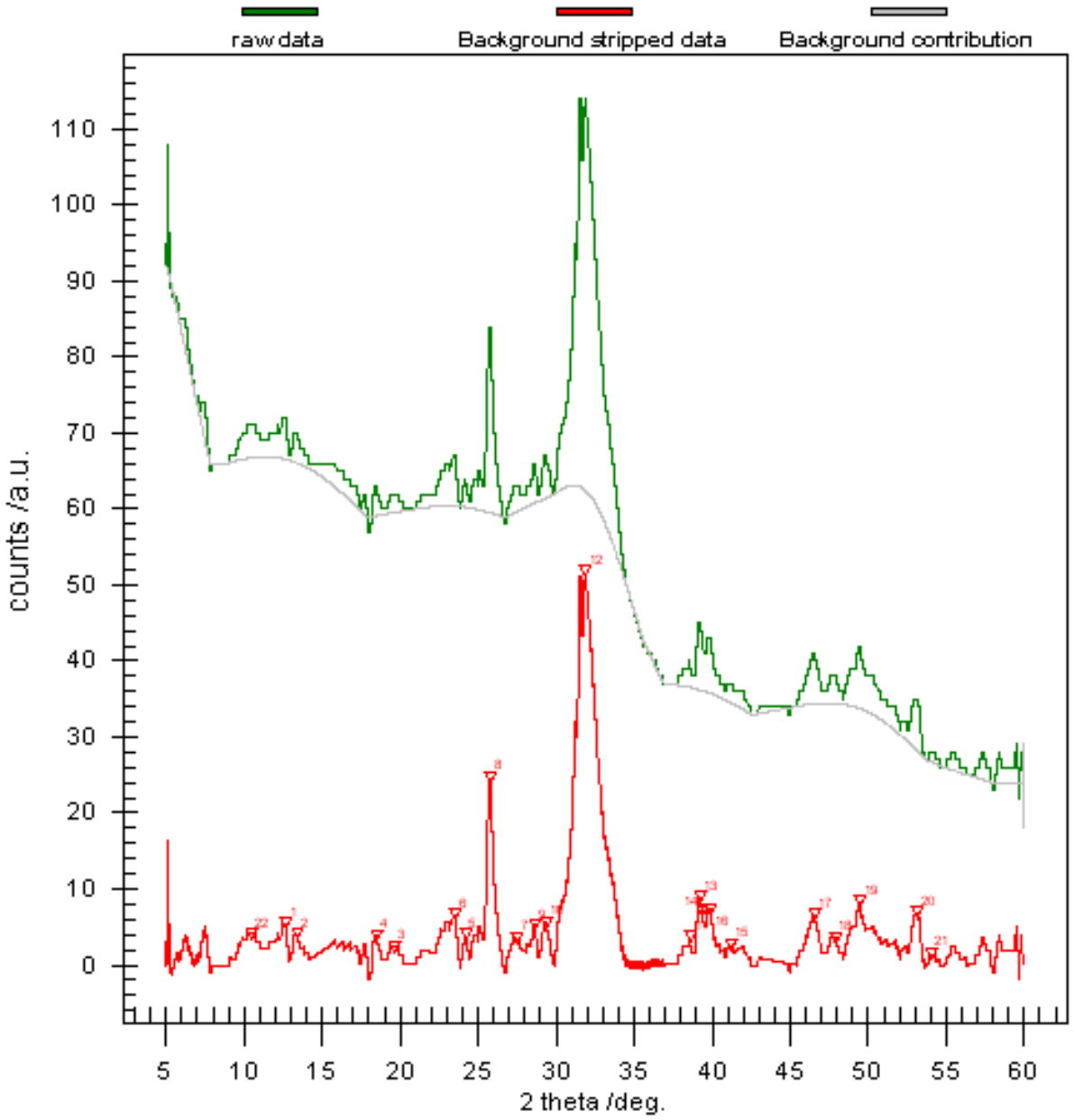

Figure A13: XRD pattern of sample pH74HApC3. The green curve is the original Savitzky-Golay smoothed XRD pattern, the grey curve is the calculated background, and the red curve is the background subtracted pattern (red inverted triangles are the peak identifiers).

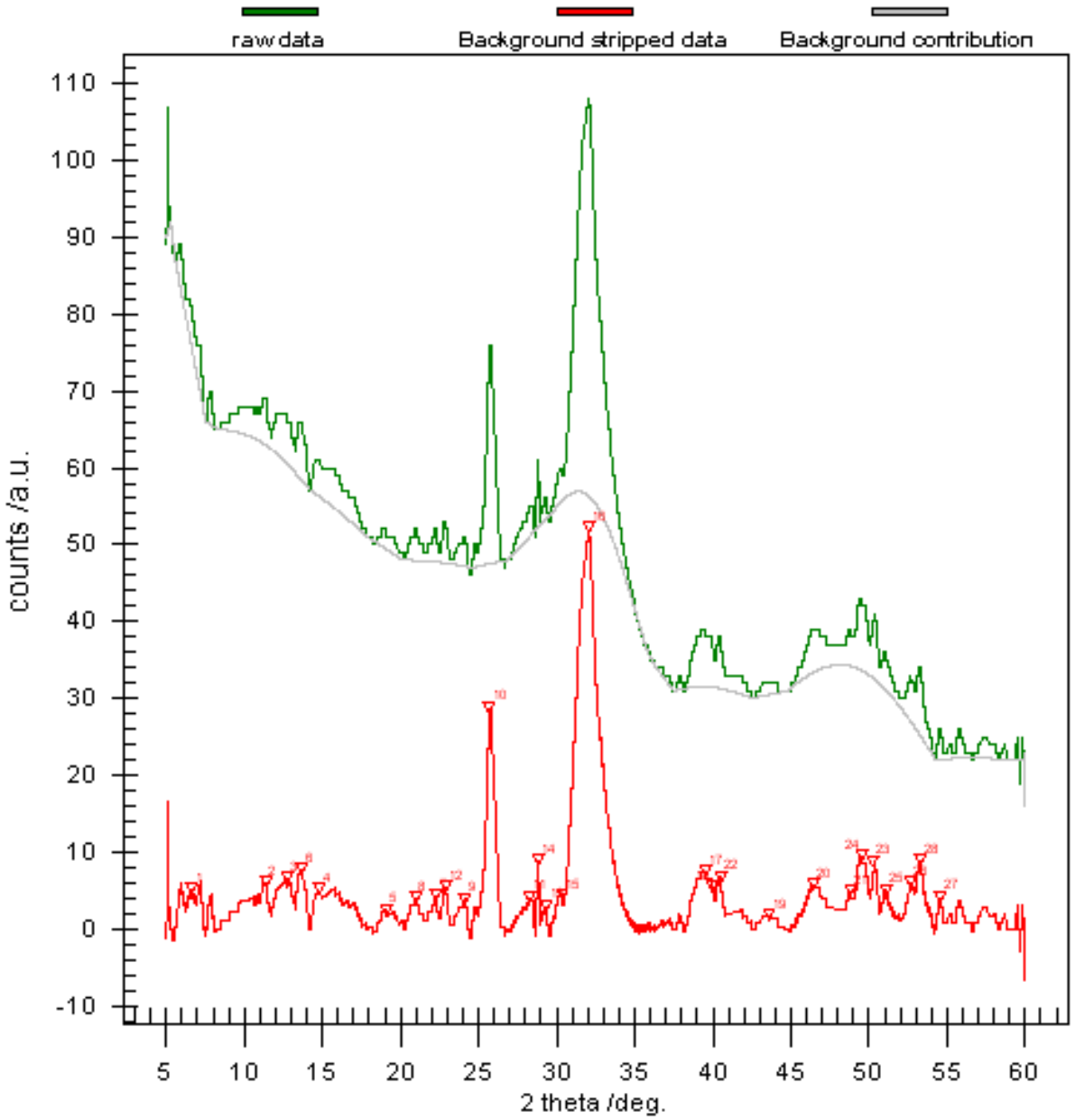

Figure A14: XRD pattern of sample pH80HApC1. The green curve is the original Savitzky-Golay smoothed XRD pattern, the grey curve is the calculated background, and the red curve is the background subtracted pattern (red inverted triangles are the peak identifiers).

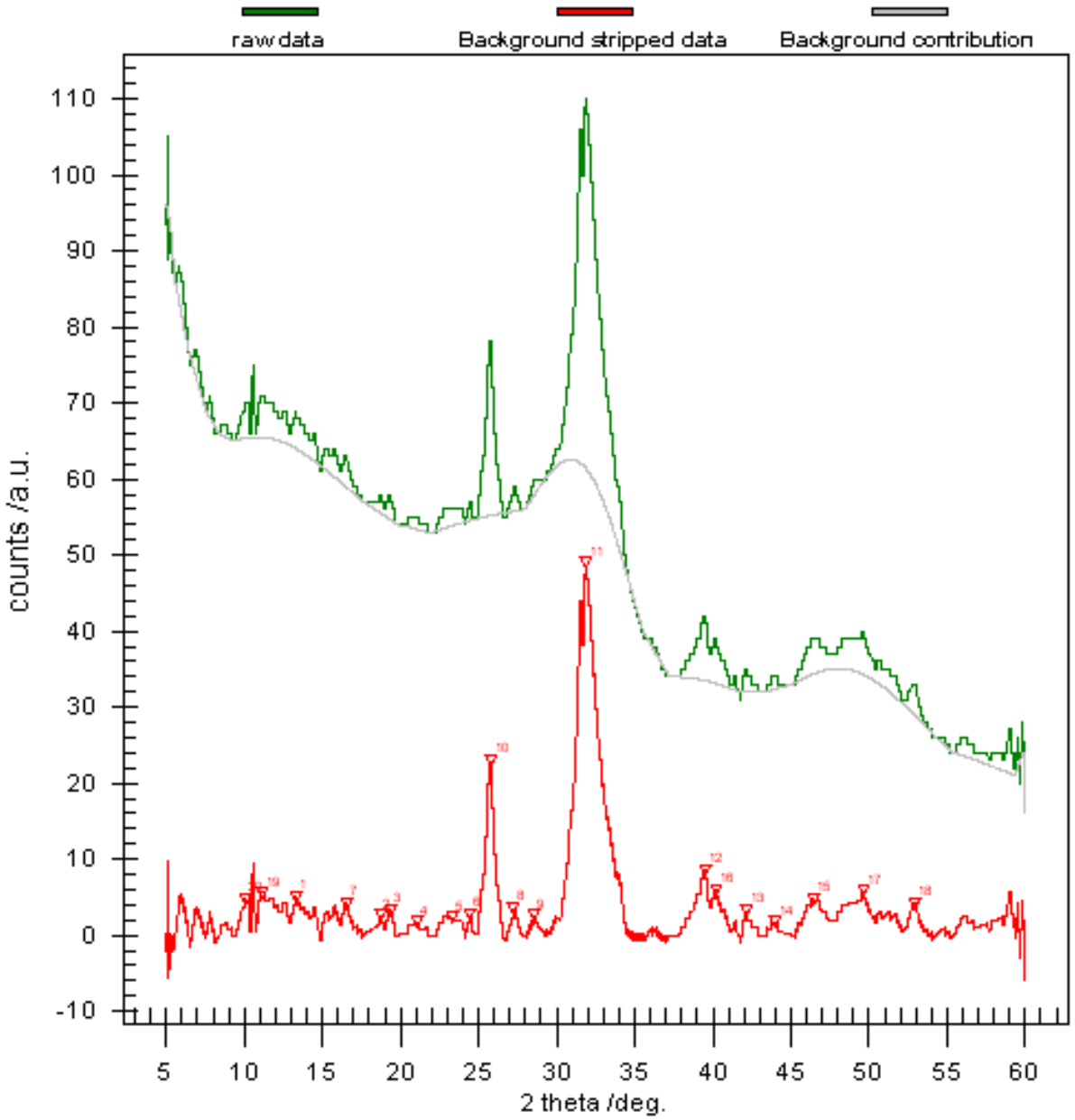

Figure A15: XRD pattern of sample pH80HApC2. The green curve is the original Savitzky-Golay smoothed XRD pattern, the grey curve is the calculated background, and the red curve is the background subtracted pattern (red inverted triangles are the peak identifiers).

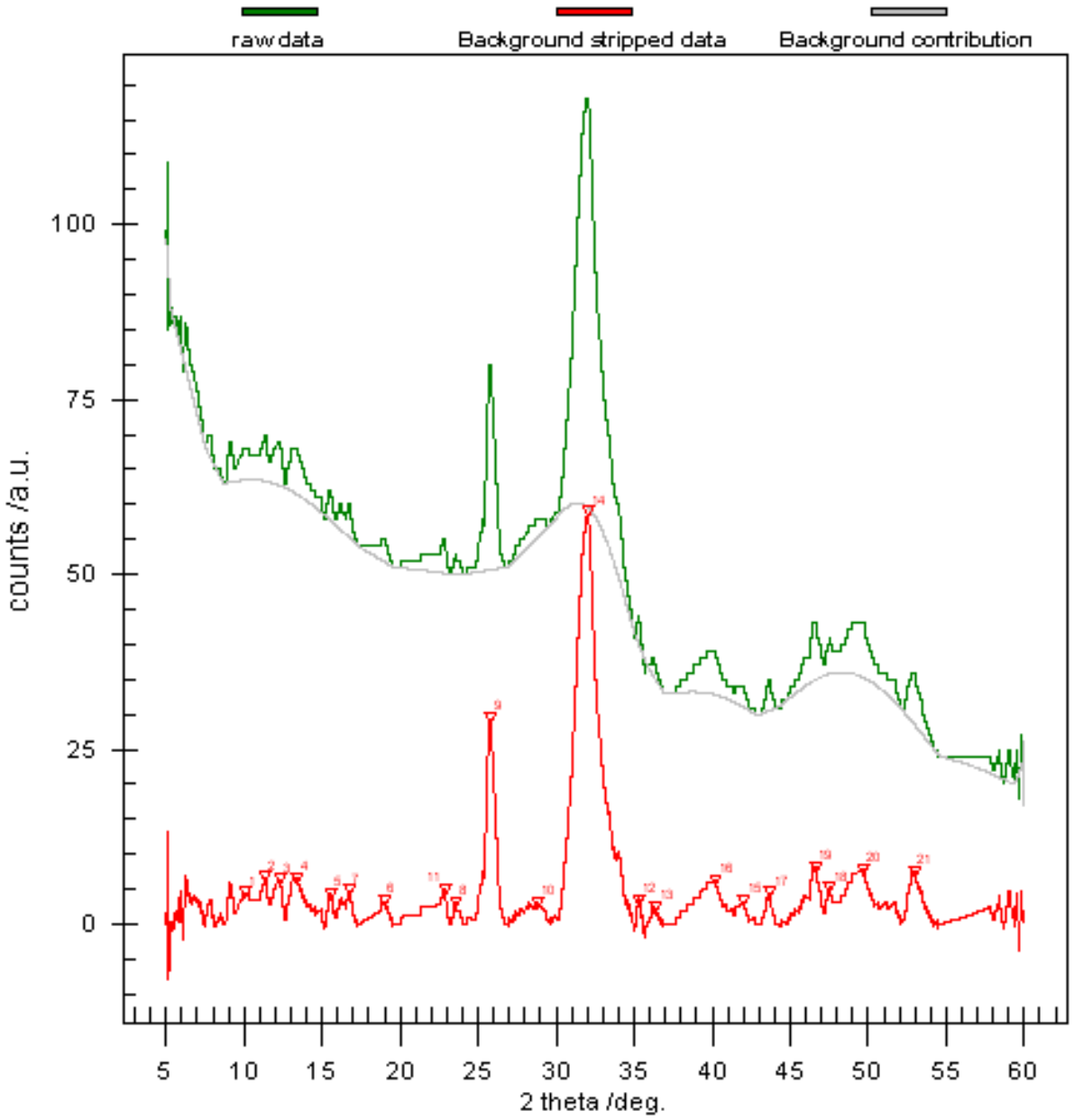

Figure A16: XRD pattern of sample pH80HApC3. The green curve is the original Savitzky-Golay smoothed XRD pattern, the grey curve is the calculated background, and the red curve is the background subtracted pattern (red inverted triangles are the peak identifiers).

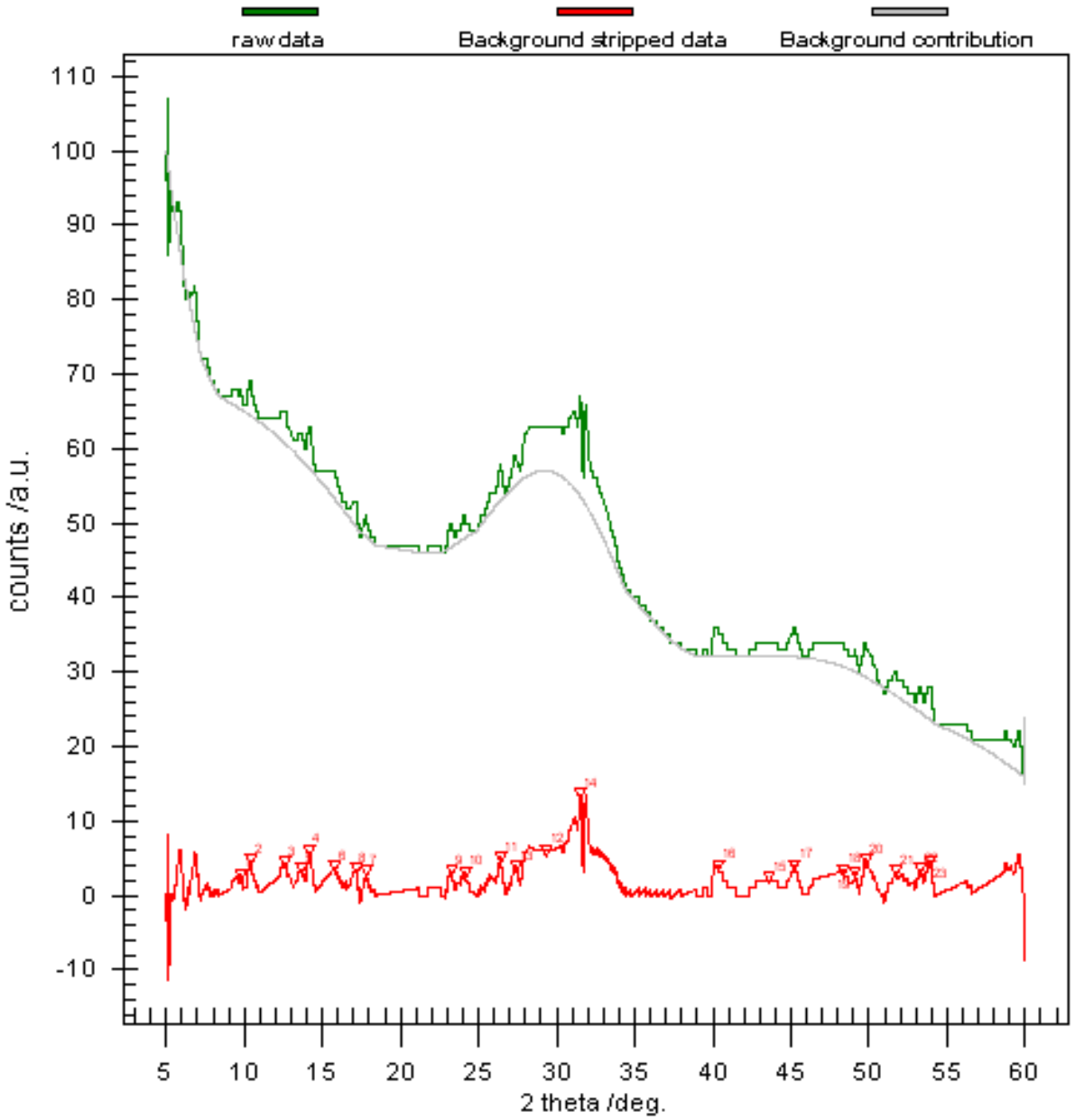

Figure A17: XRD pattern of sample pH90HApC1. The green curve is the original Savitzky-Golay smoothed XRD pattern, the grey curve is the calculated background, and the red curve is the background subtracted pattern (red inverted triangles are the peak identifiers).

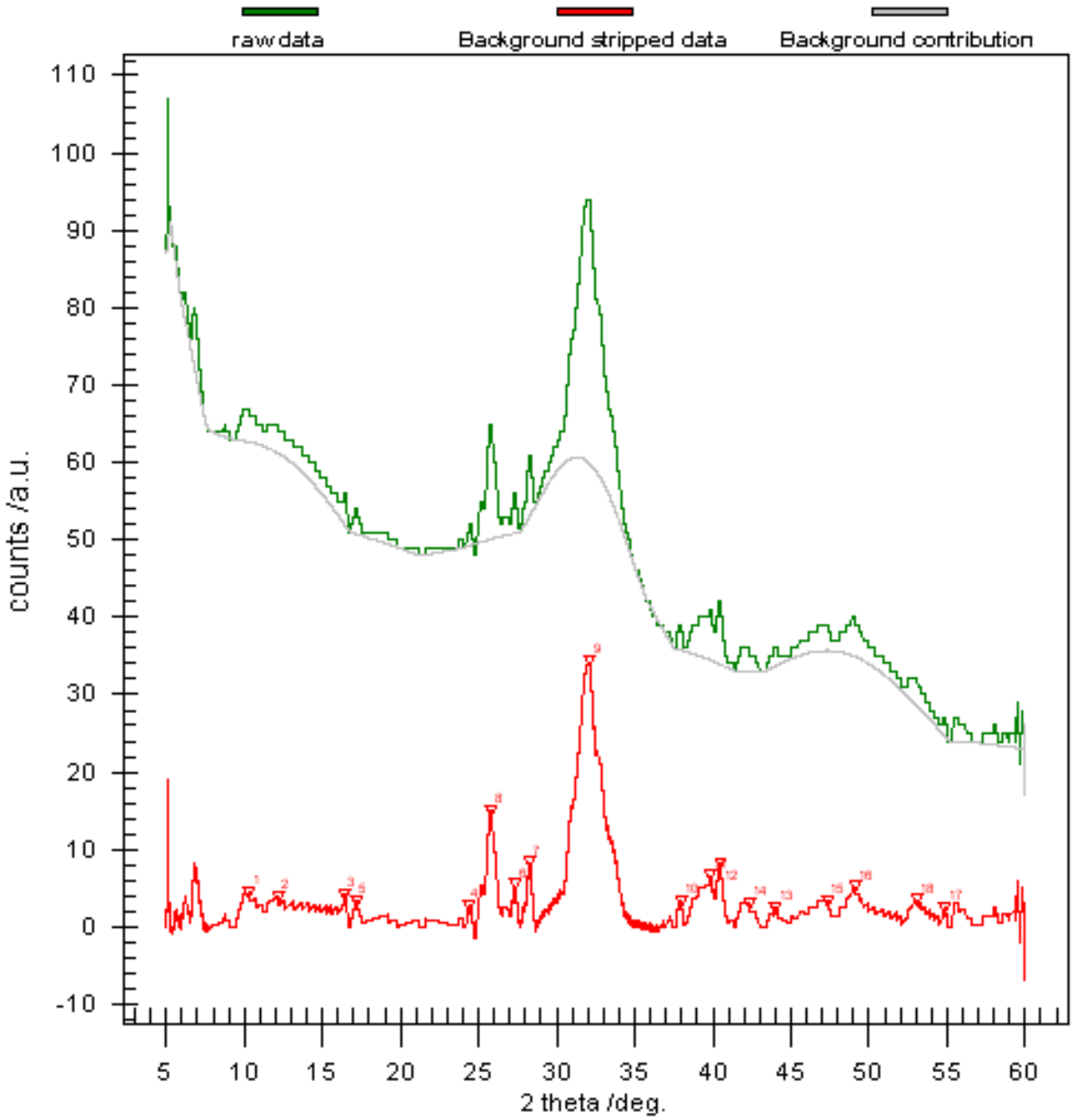

Figure A18: XRD pattern of sample pH90HApC2. The green curve is the original Savitzky-Golay smoothed XRD pattern, the grey curve is the calculated background, and the red curve is the background subtracted pattern (red inverted triangles are the peak identifiers).

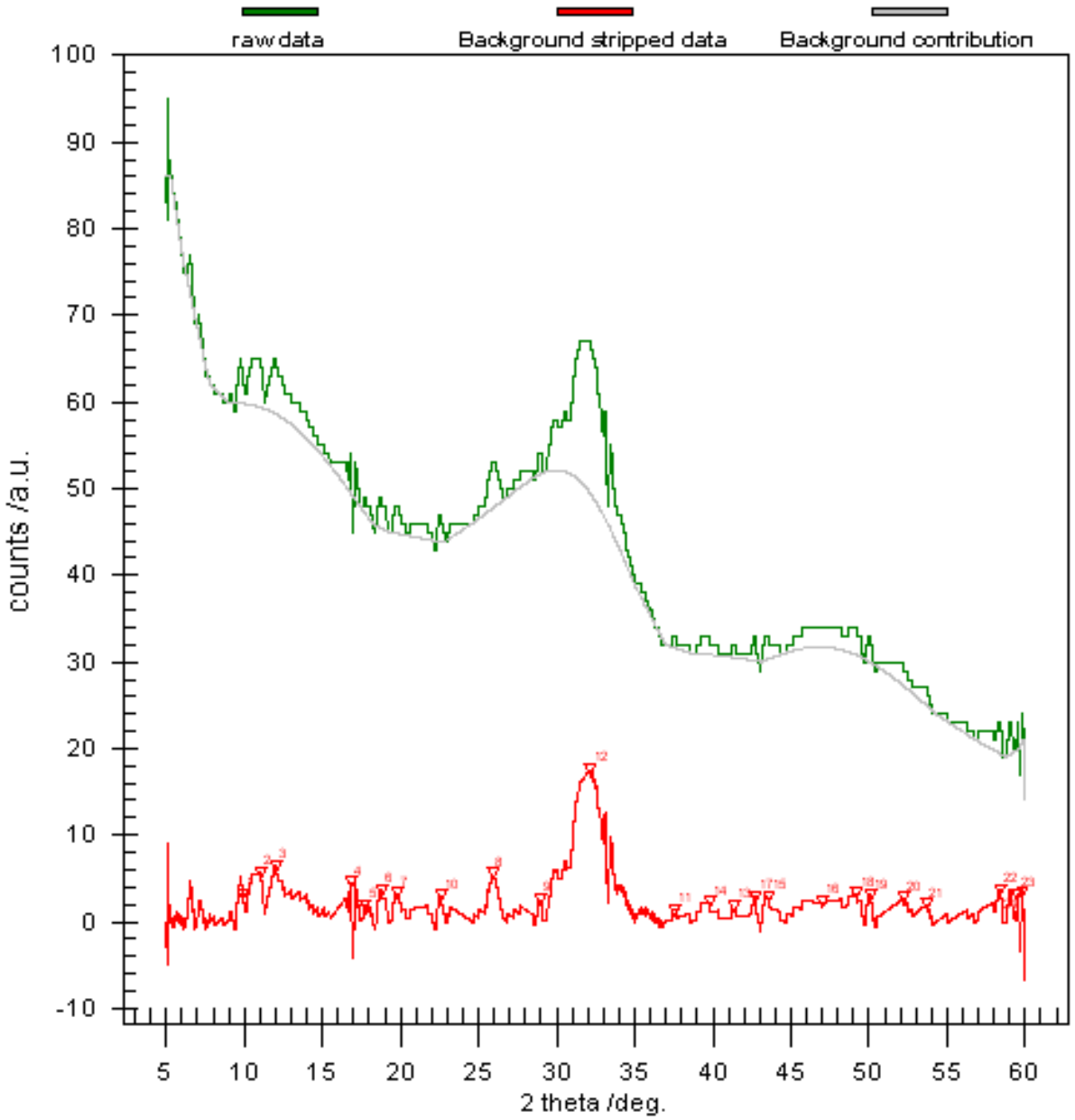

Figure A19: XRD pattern of sample pH90HApC3. The green curve is the original Savitzky-Golay smoothed XRD pattern, the grey curve is the calculated background, and the red curve is the background subtracted pattern (red inverted triangles are the peak identifiers).

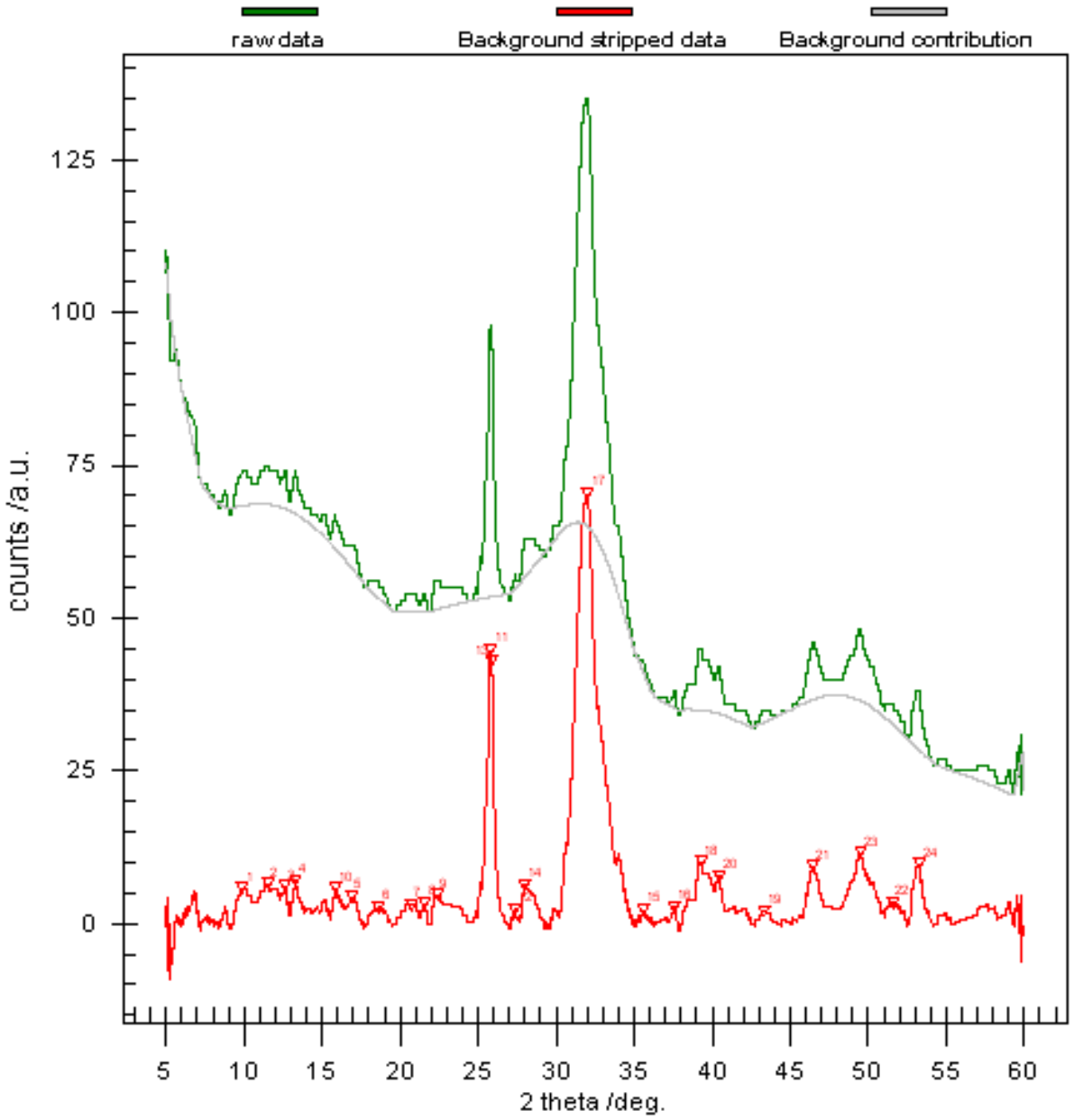

Figure A20: XRD pattern of sample 6HRpH80HApC1. The green curve is the original Savitzky-Golay smoothed XRD pattern, the grey curve is the calculated background, and the red curve is the background subtracted pattern (red inverted triangles are the peak identifiers).

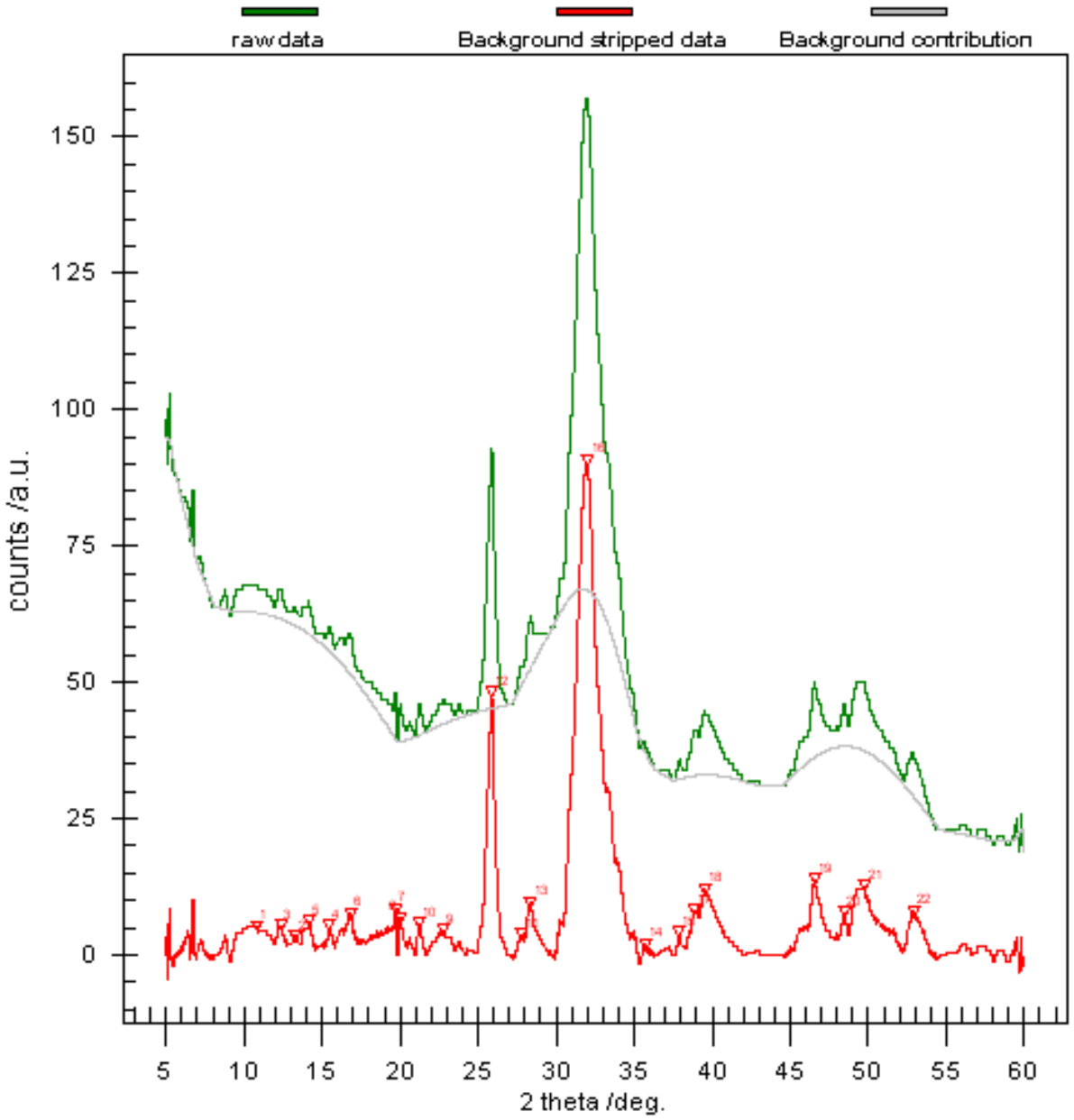

Figure A21: XRD pattern of sample 6HRpH80HApC2. The green curve is the original Savitzky-Golay smoothed XRD pattern, the grey curve is the calculated background, and the red curve is the background subtracted pattern (red inverted triangles are the peak identifiers).

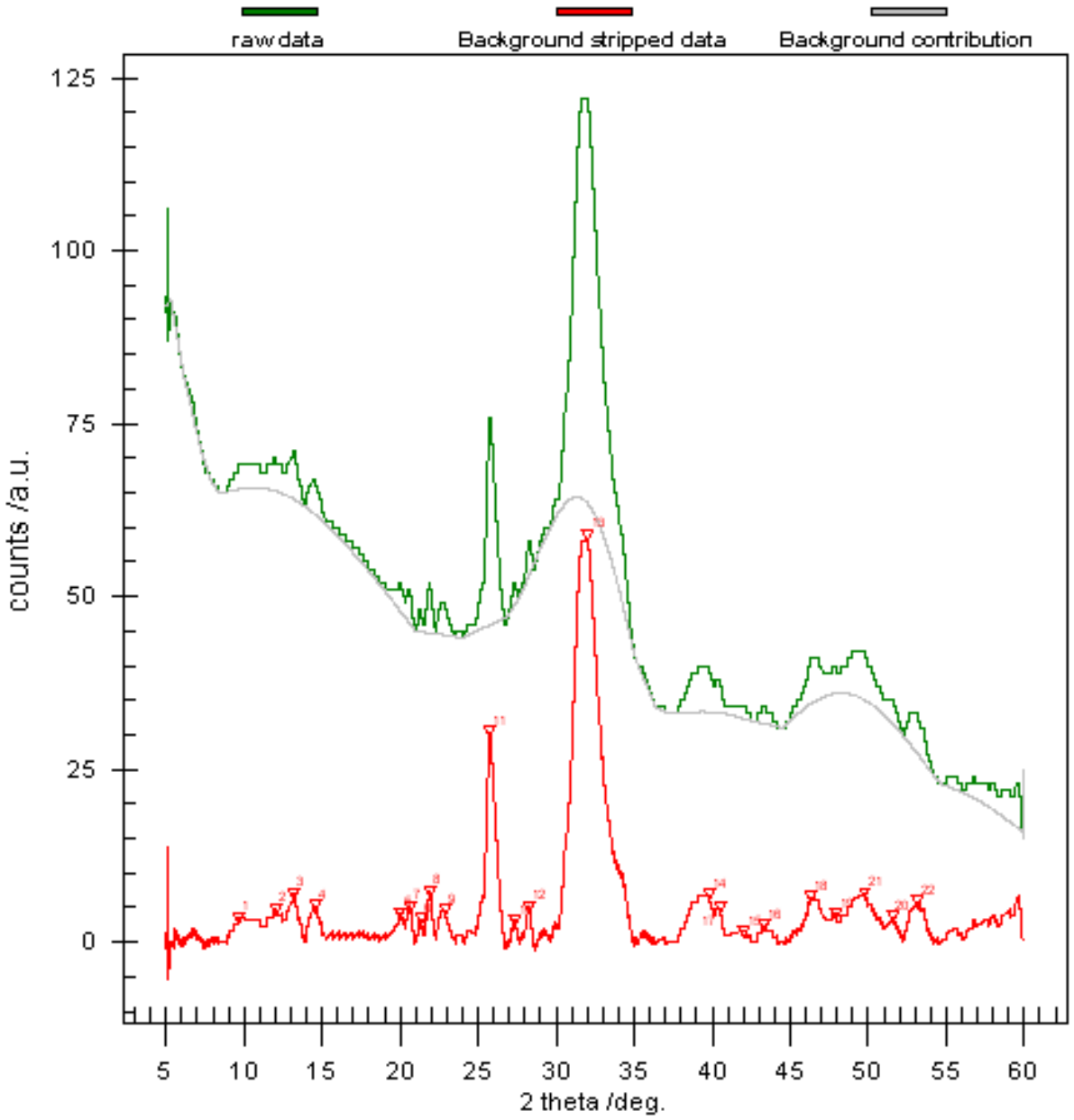

Figure A22: XRD pattern of sample 6HRpH80HApC3. The green curve is the original Savitzky-Golay smoothed XRD pattern, the grey curve is the calculated background, and the red curve is the background subtracted pattern (red inverted triangles are the peak identifiers).

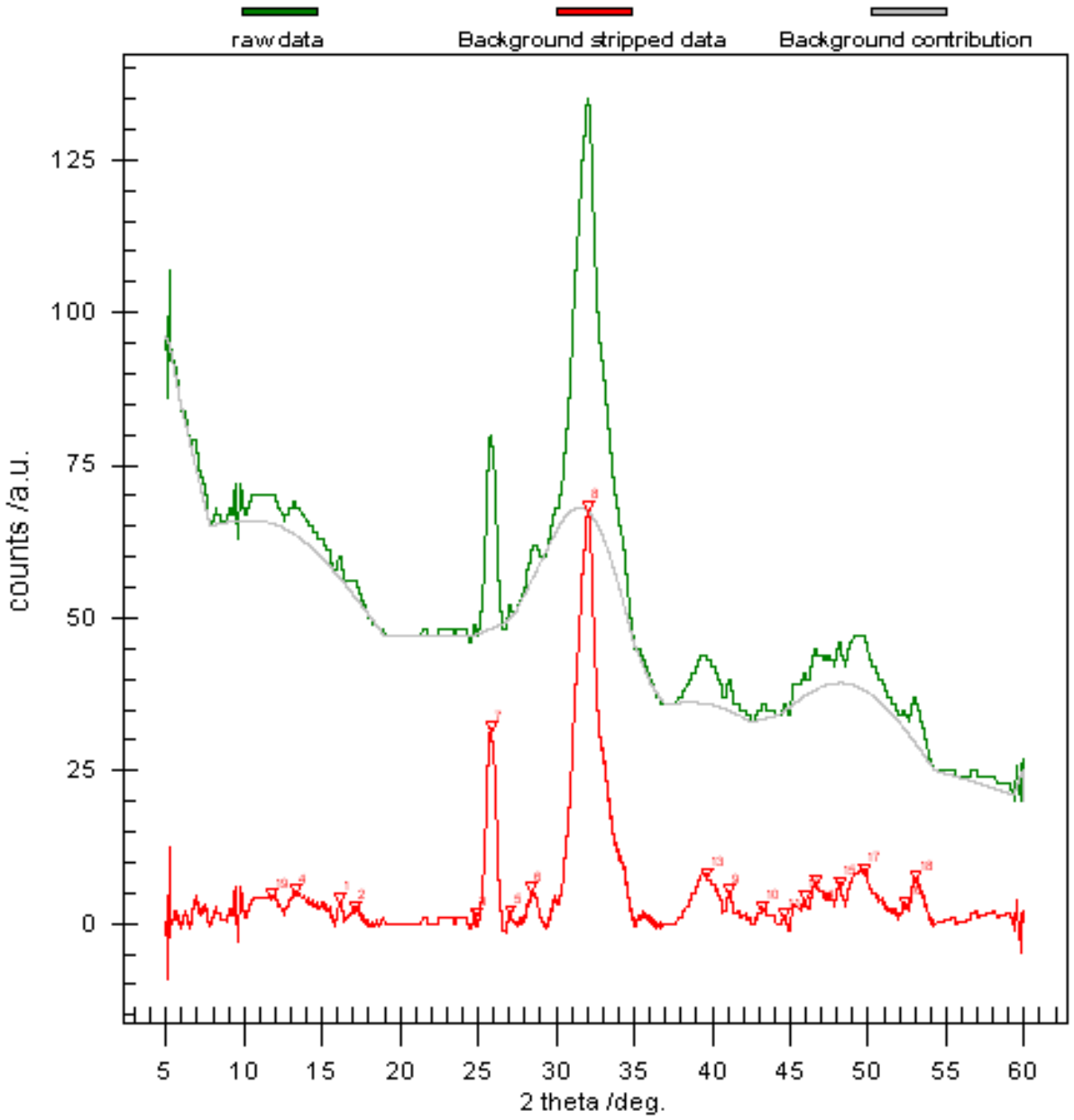

Figure A23: XRD pattern of sample 12HRpH80HApC1. The green curve is the original Savitzky-Golay smoothed XRD pattern, the grey curve is the calculated background, and the red curve is the background subtracted pattern (red inverted triangles are the peak identifiers).

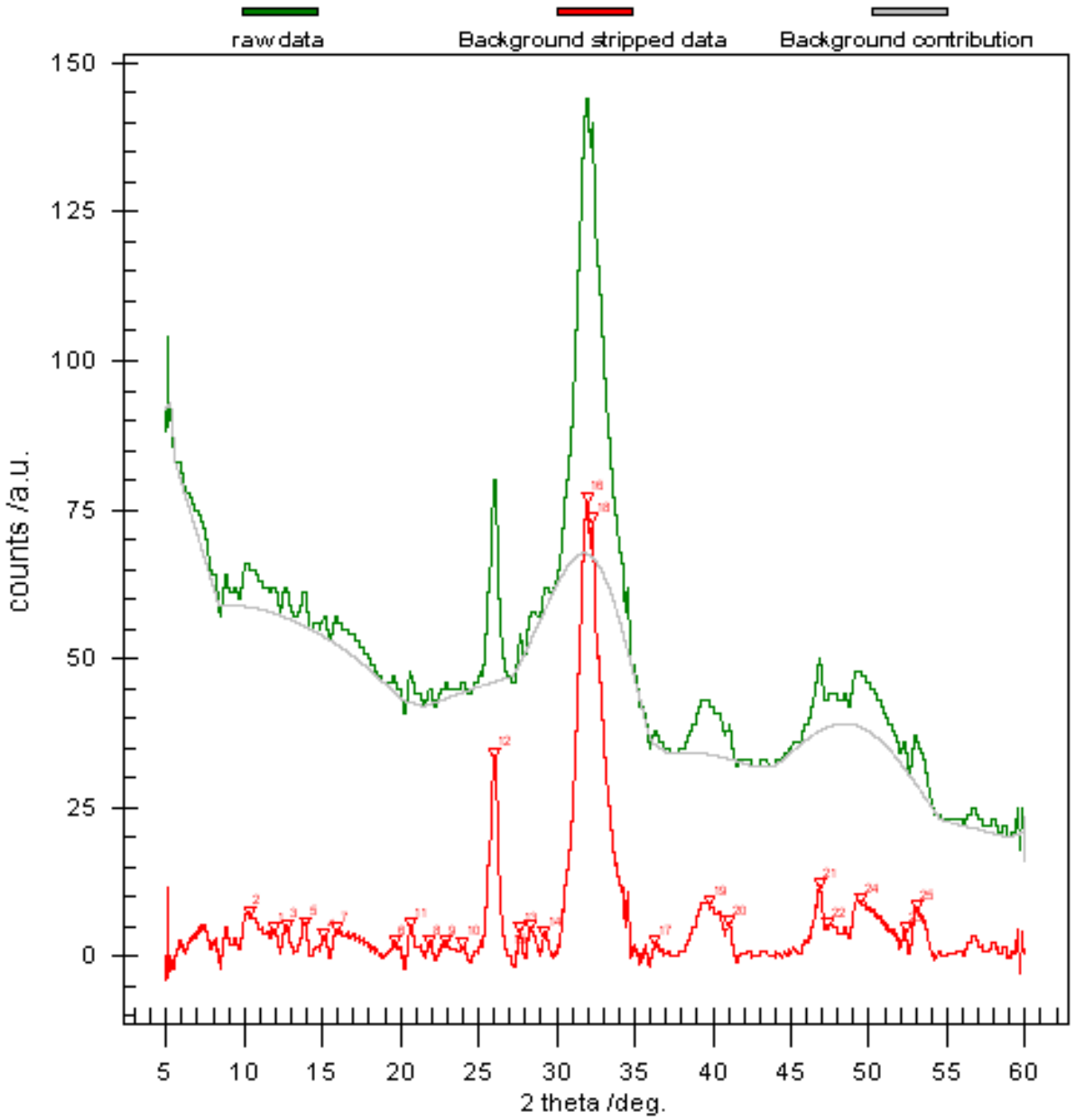

Figure A24: XRD pattern of sample 12HRpH80HApC2. The green curve is the original Savitzky-Golay smoothed XRD pattern, the grey curve is the calculated background, and the red curve is the background subtracted pattern (red inverted triangles are the peak identifiers).

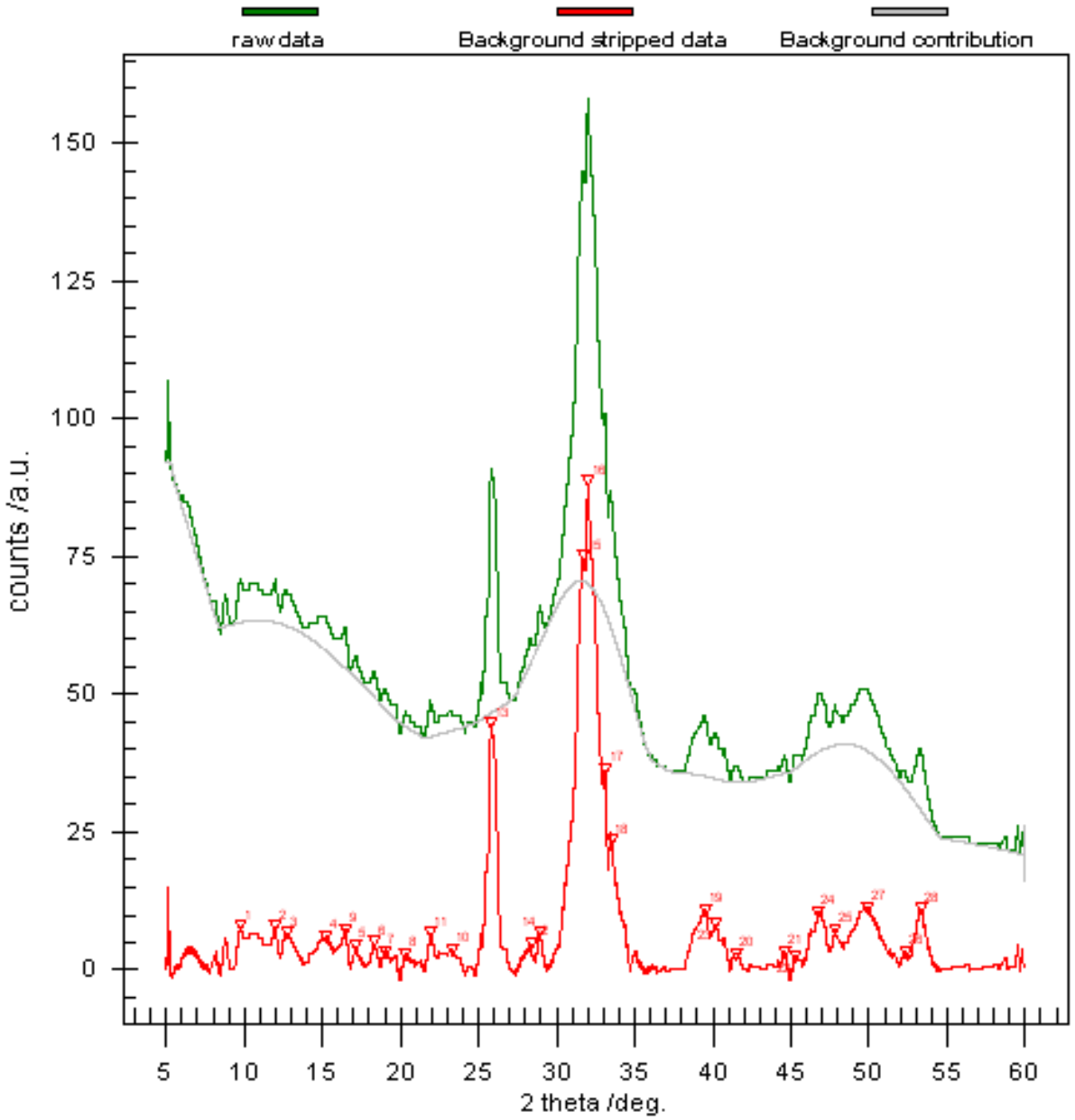

Figure A25: XRD pattern of sample 12HRpH80HApC3. The green curve is the original Savitzky-Golay smoothed XRD pattern, the grey curve is the calculated background, and the red curve is the background subtracted pattern (red inverted triangles are the peak identifiers).

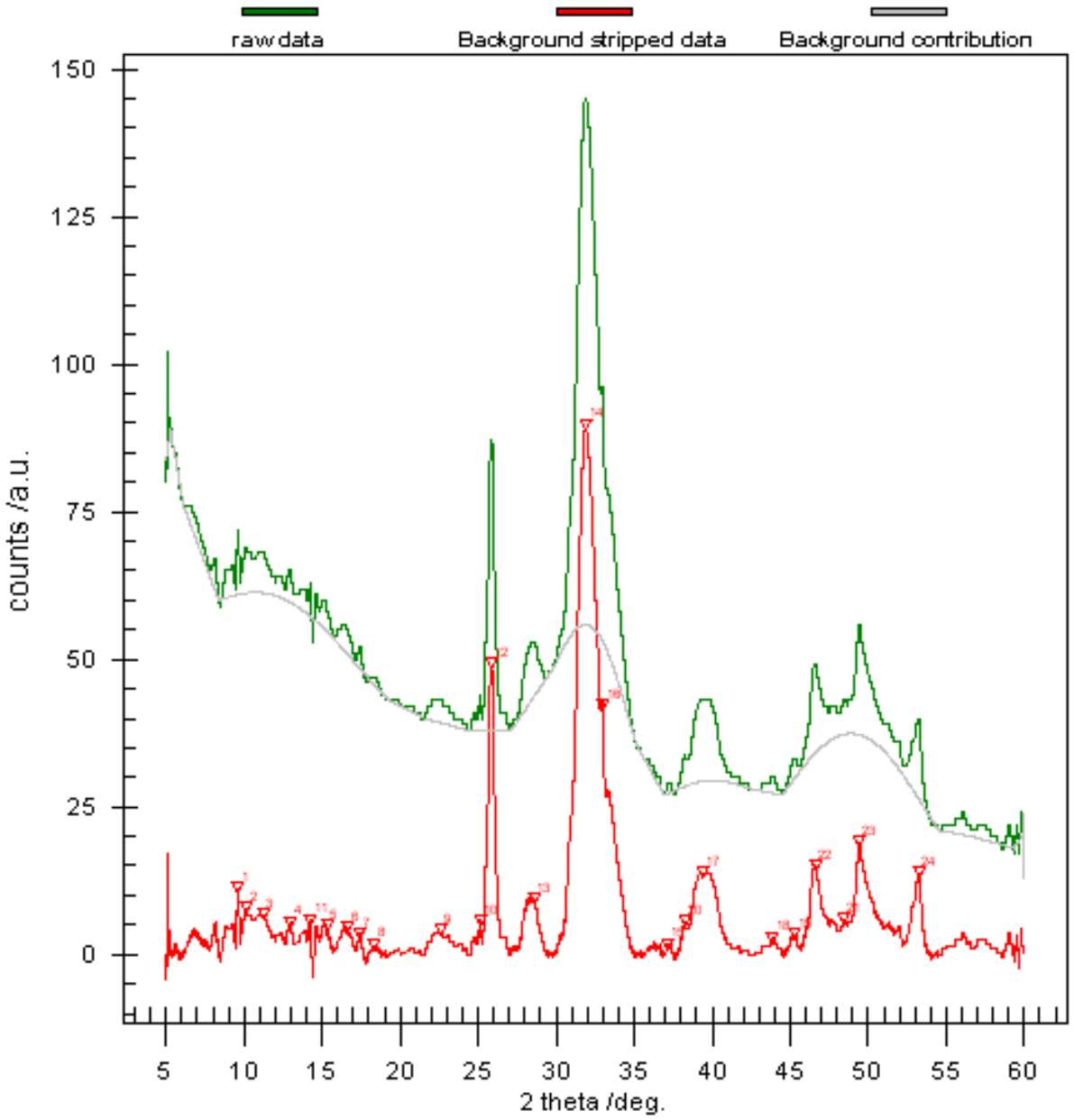

Figure A26: XRD pattern of sample 24HRpH80HApC1. The green curve is the original Savitzky-Golay smoothed XRD pattern, the grey curve is the calculated background, and the red curve is the background subtracted pattern (red inverted triangles are the peak identifiers).

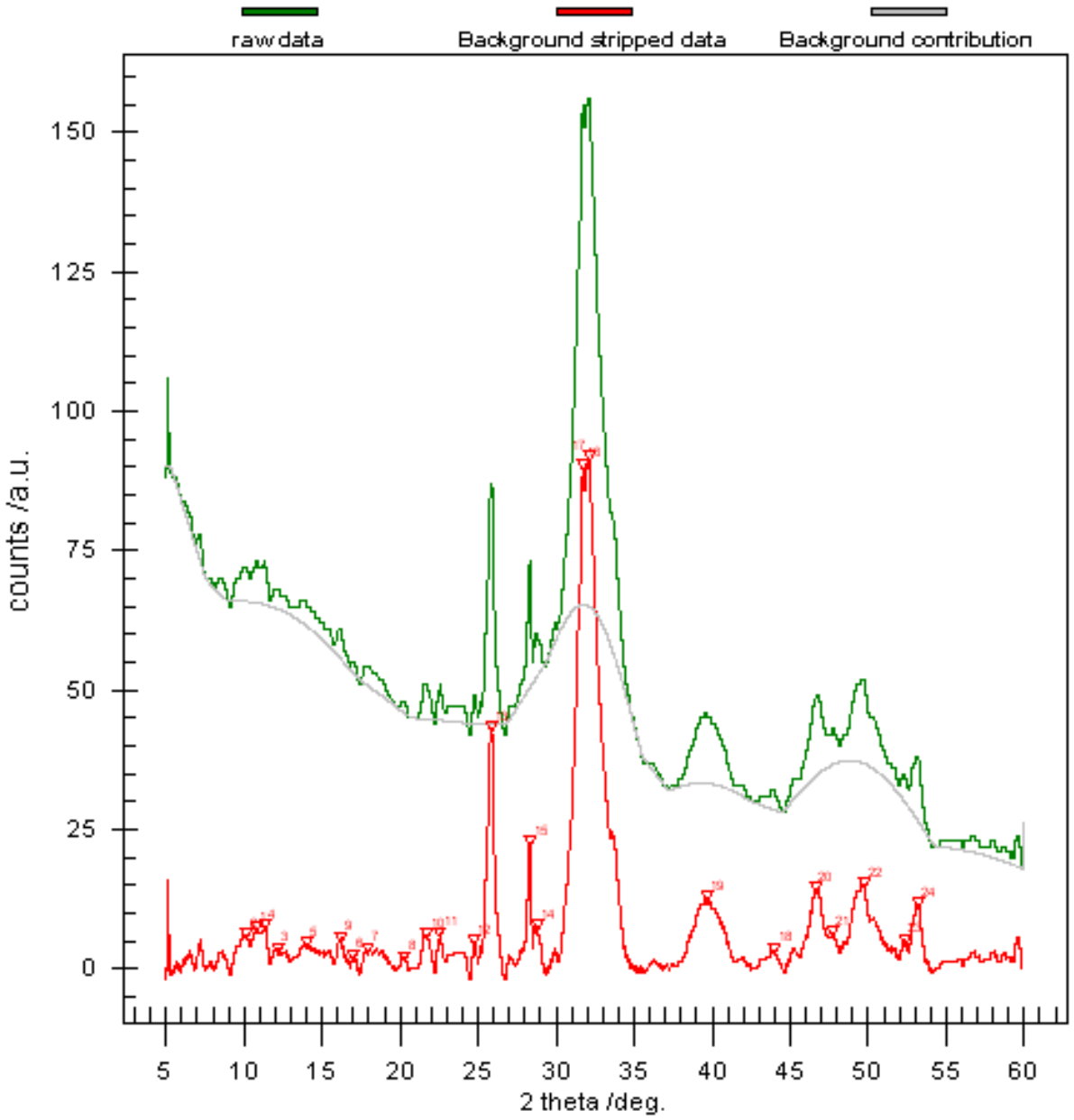

Figure A27: XRD pattern of sample 24HRpH80HApC2. The green curve is the original Savitzky-Golay smoothed XRD pattern, the grey curve is the calculated background, and the red curve is the background subtracted pattern (red inverted triangles are the peak identifiers).

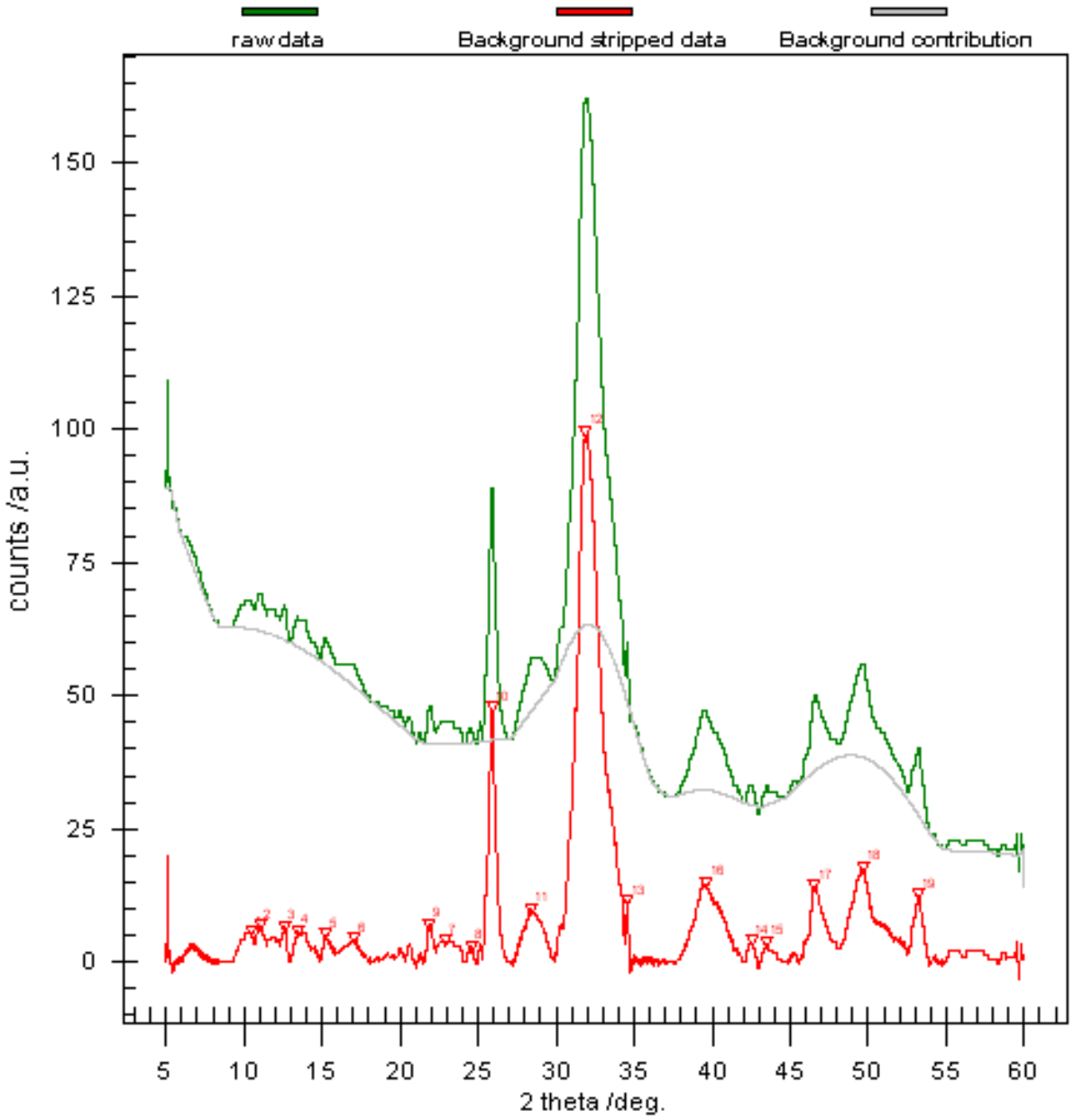

Figure A28: XRD pattern of sample 24HRpH80HApC3. The green curve is the original Savitzky-Golay smoothed XRD pattern, the grey curve is the calculated background, and the red curve is the background subtracted pattern (red inverted triangles are the peak identifiers).

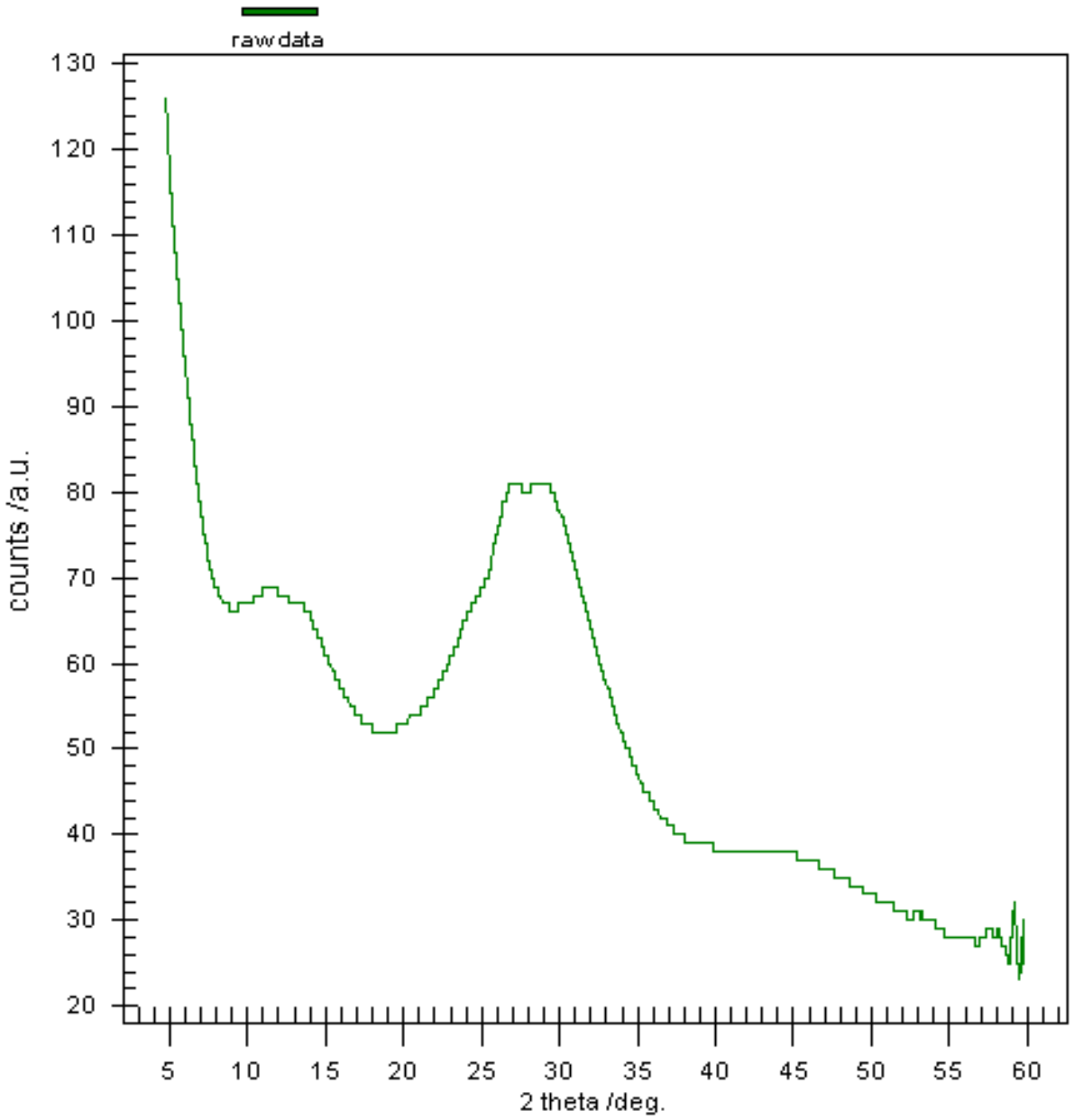

Figure A29: XRD pattern of sample ACP-RS.

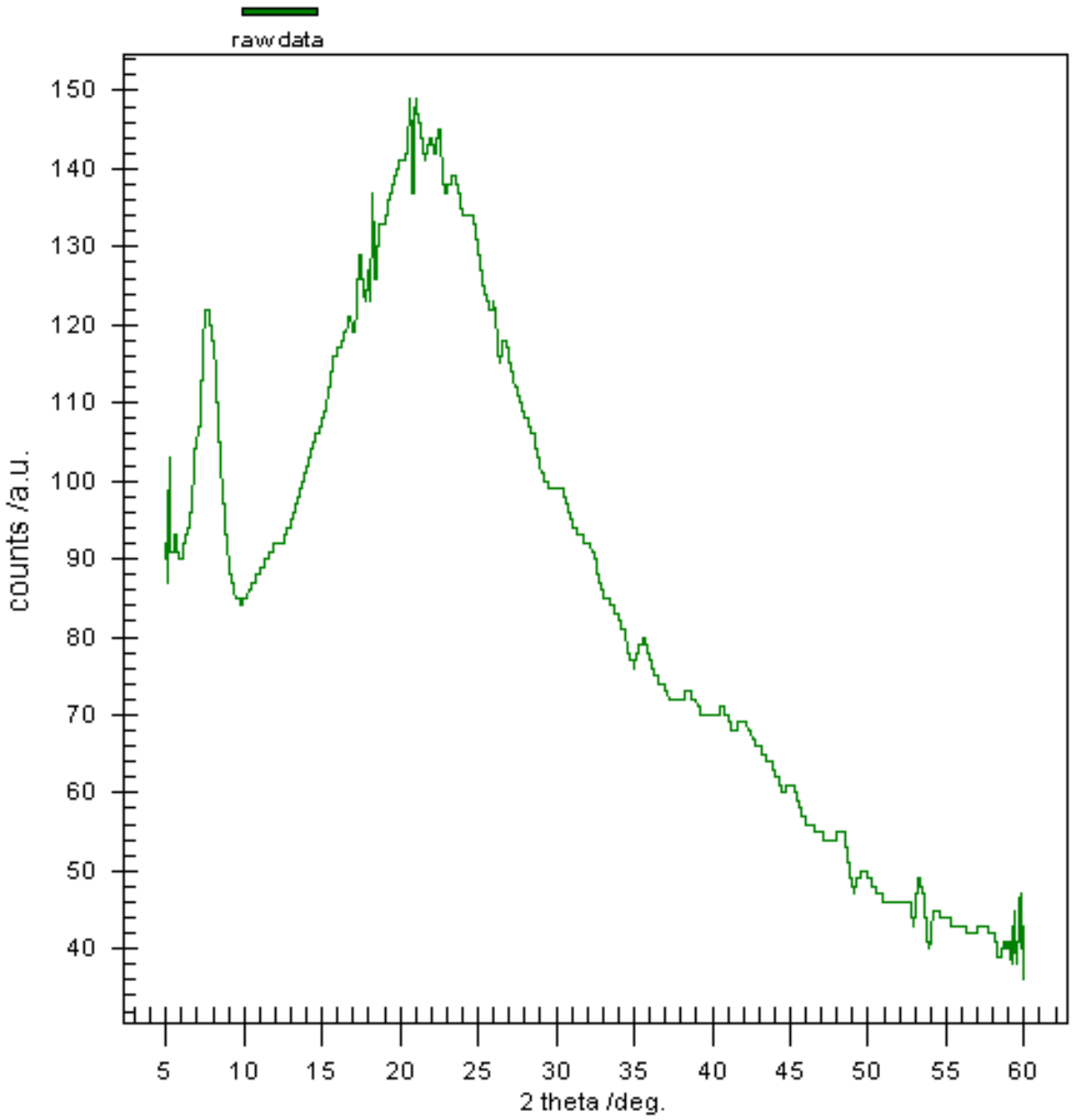

Figure A30: XRD pattern of sample of demineralized collagen from rat femora.

APPENDIX B

MECHANICAL TEST DATA: REGRESSION ANALYSIS

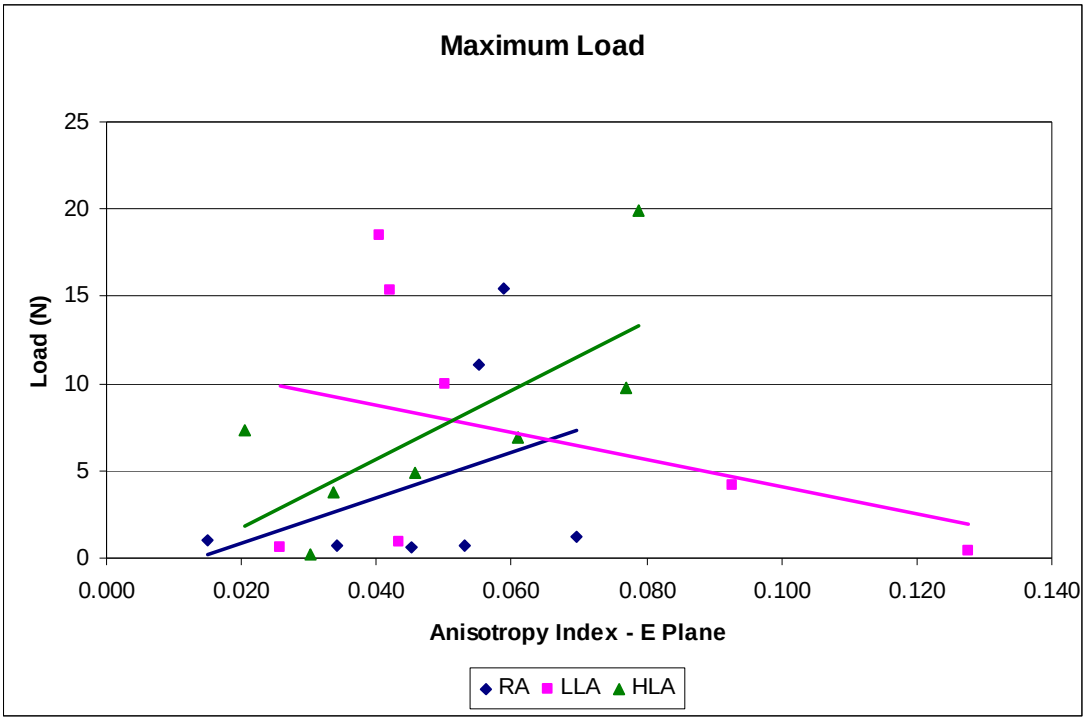

Figure B1: Maximum load versus anisotropy in the E-plane.

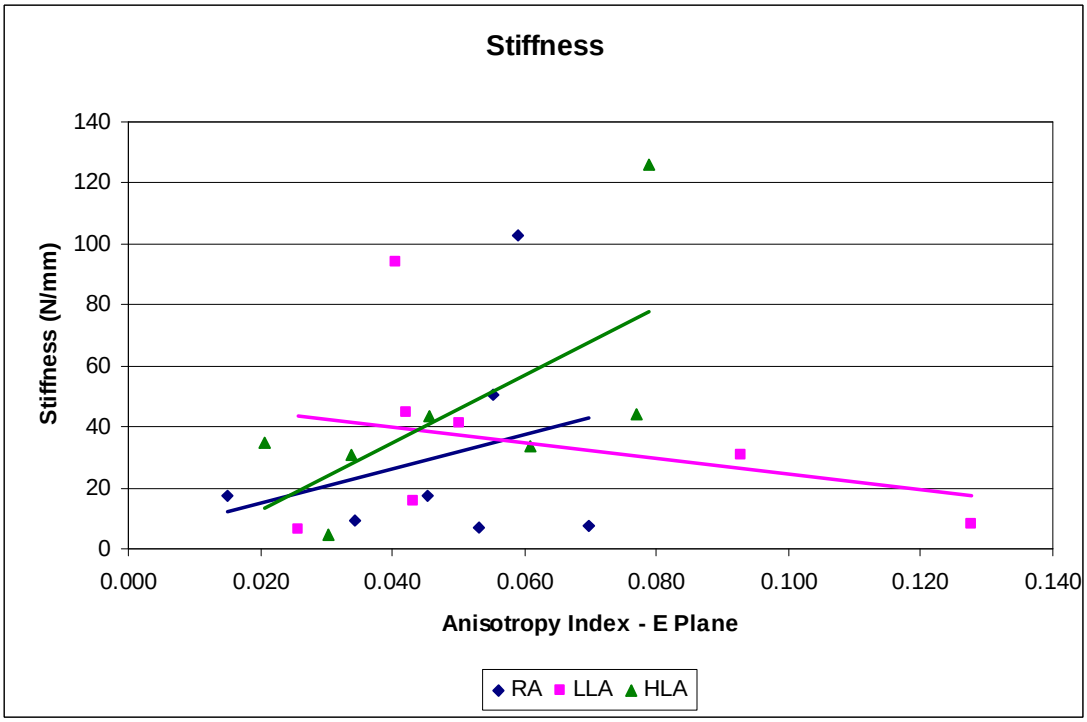

Figure B2: Stiffness versus anisotropy in the E-plane.

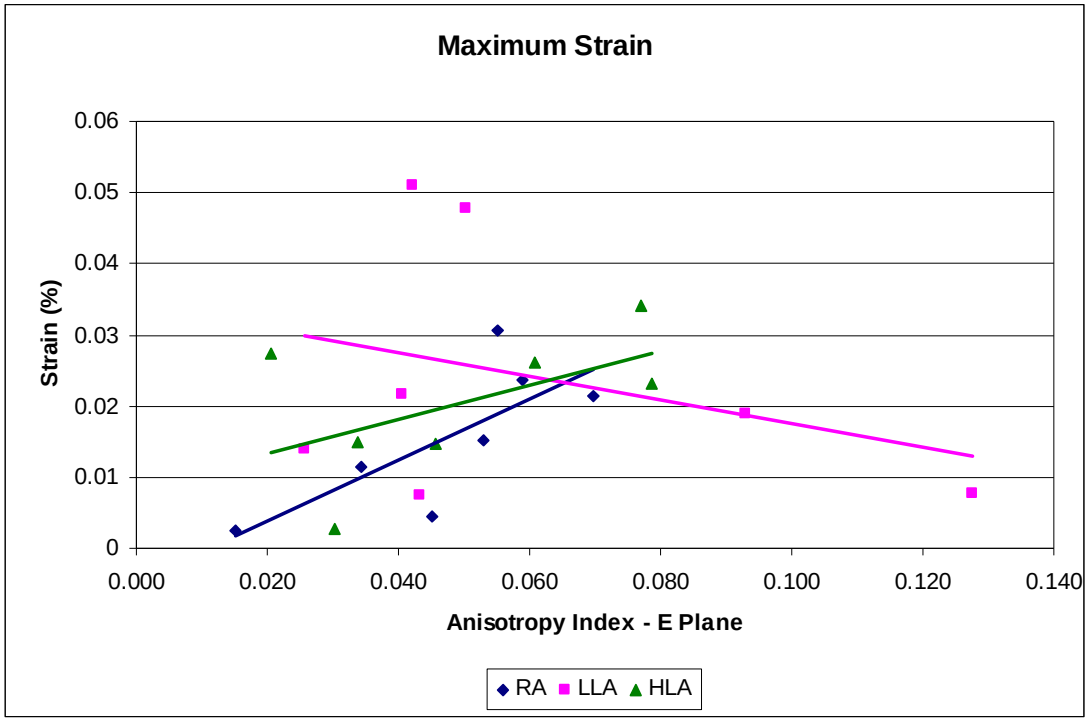

Figure B3: Maximum strain versus anisotropy in the E-plane.

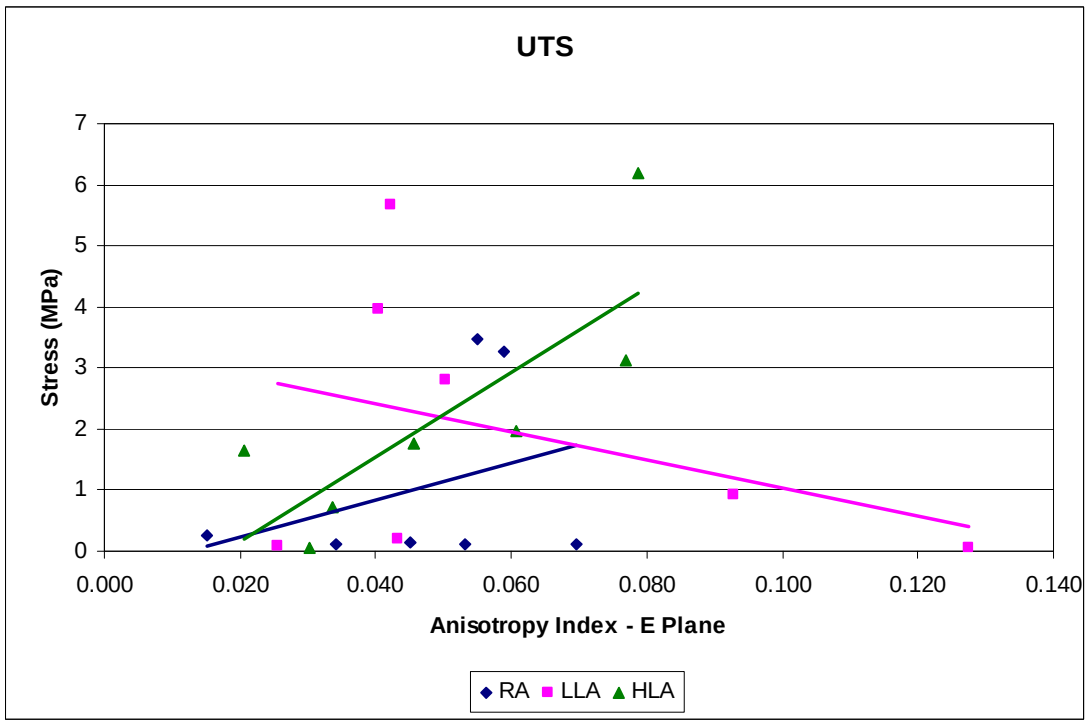

Figure B4: UTS versus anisotropy in the E-plane.

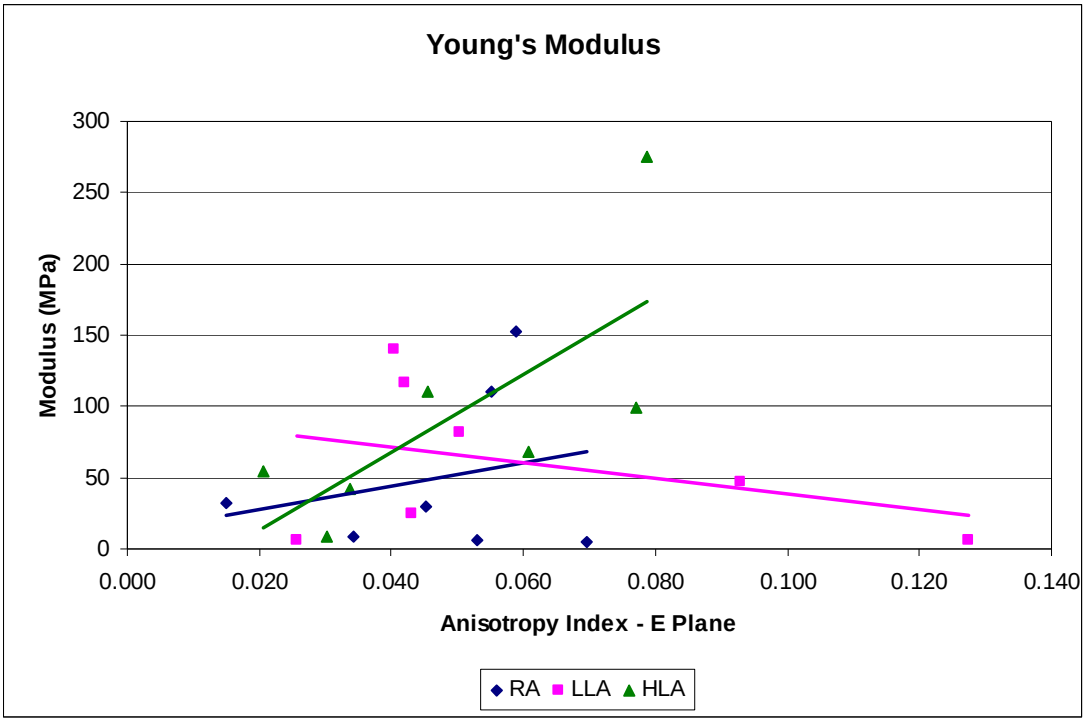

Figure B5: Young's modulus versus anisotropy in the E-plane.

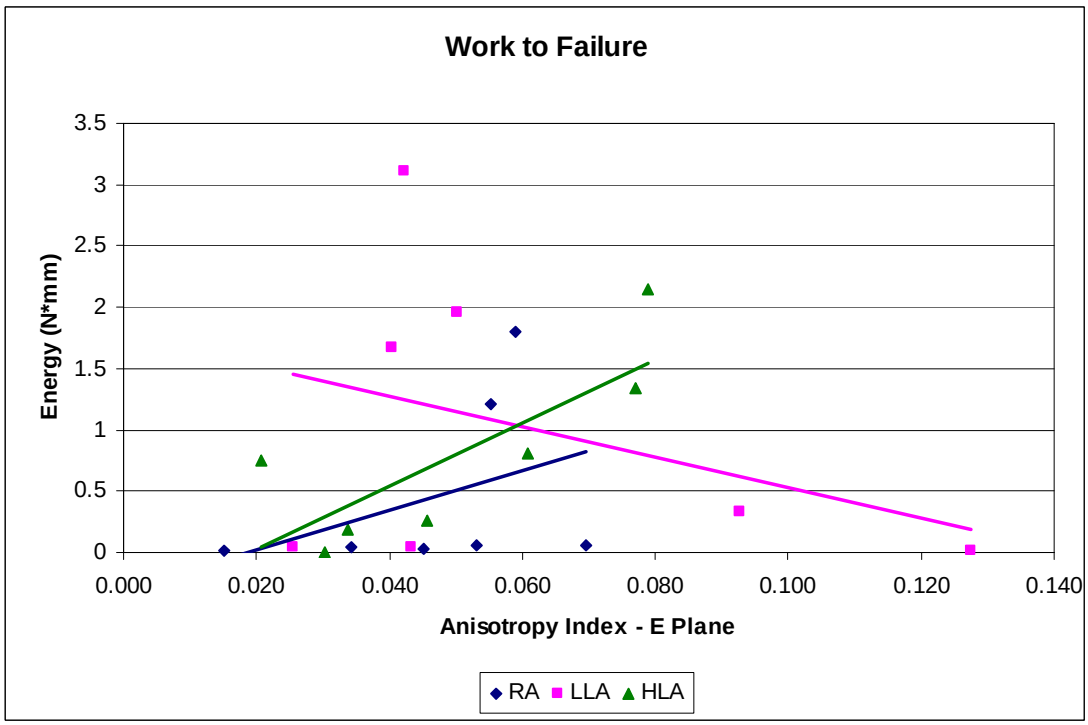

Figure B6: Work to failure versus anisotropy in the E-plane.

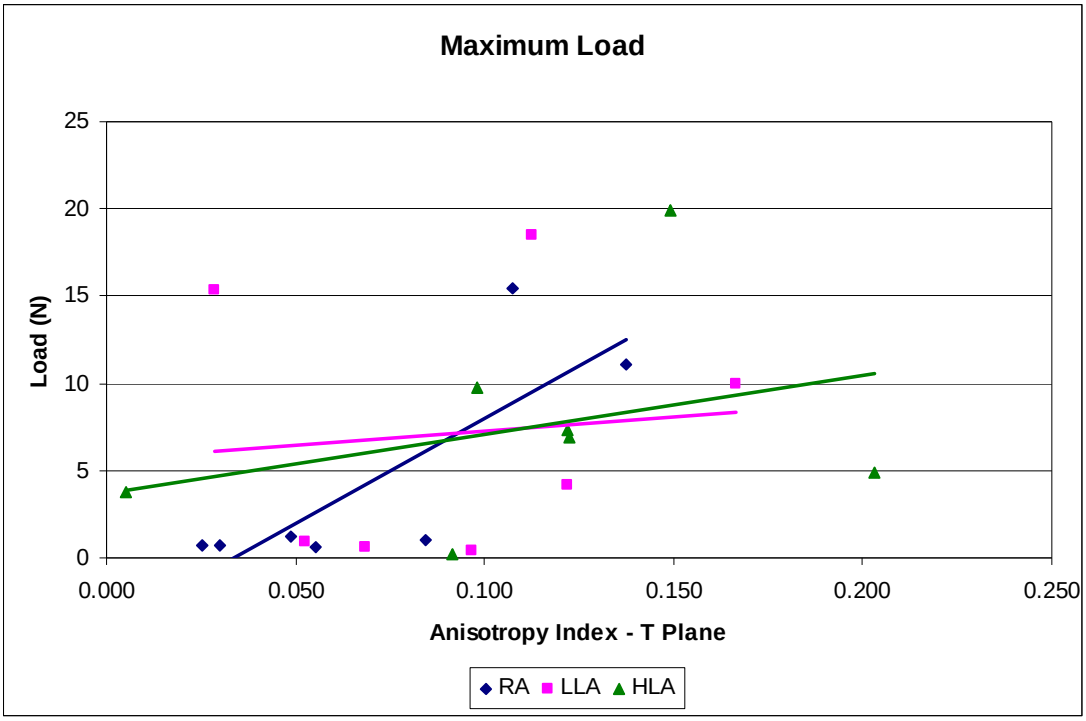

Figure B7: Maximum load versus anisotropy in the T-plane.

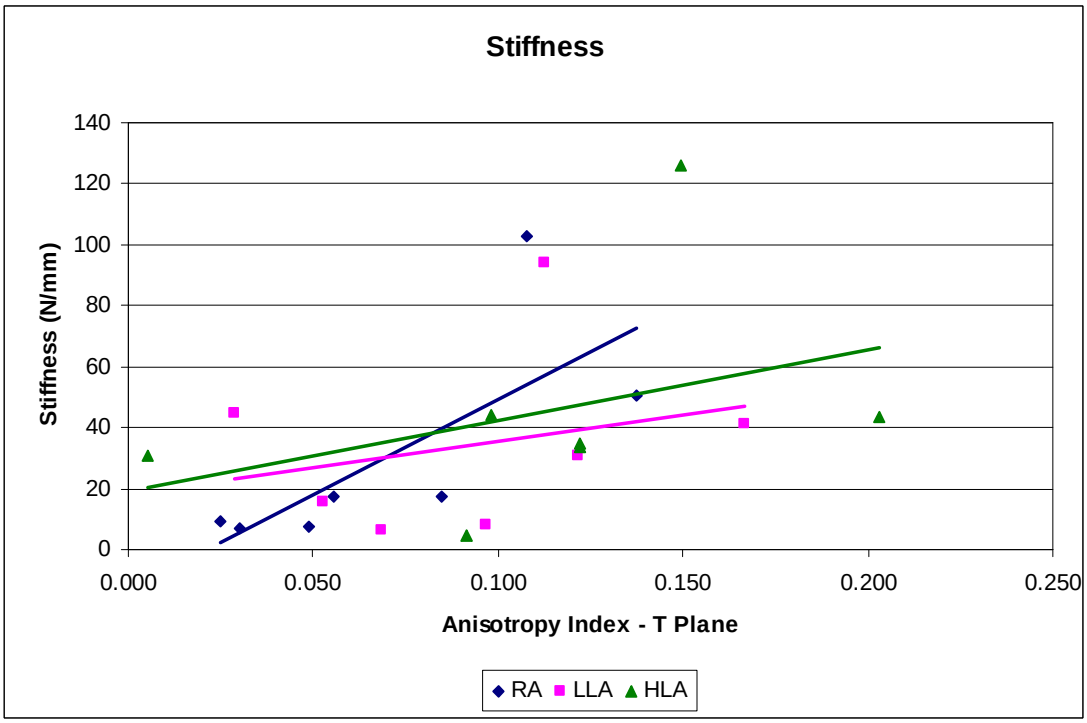

Figure B8: Stiffness versus anisotropy in the T-plane.

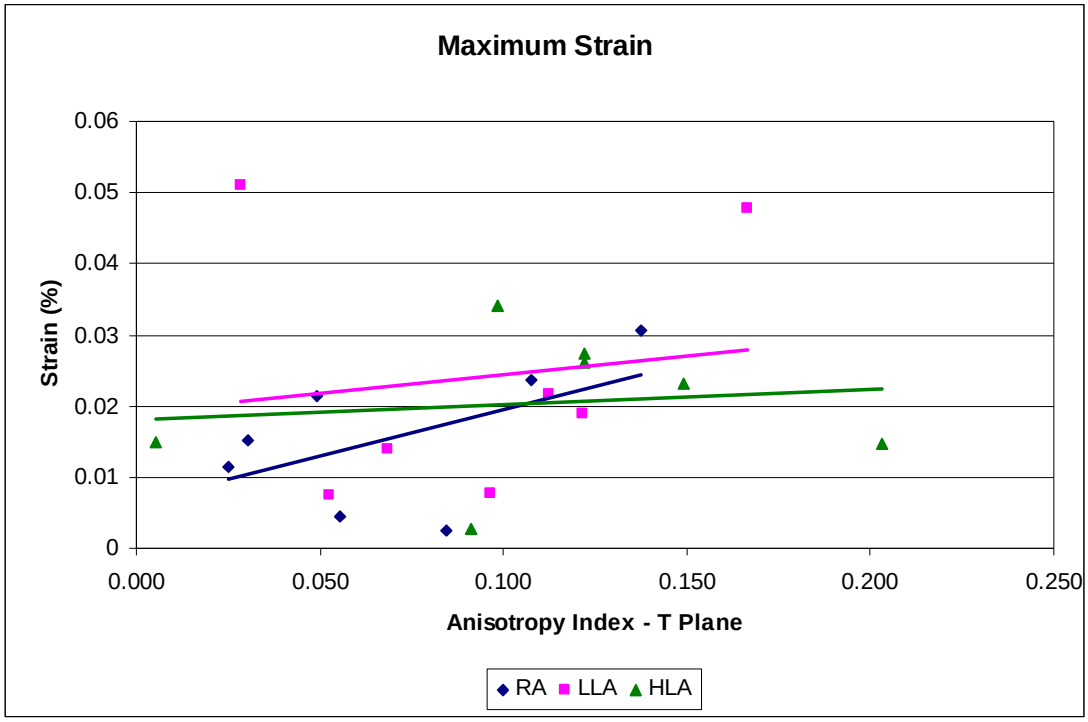

Figure B9: Maximum strain versus anisotropy in the T-plane.

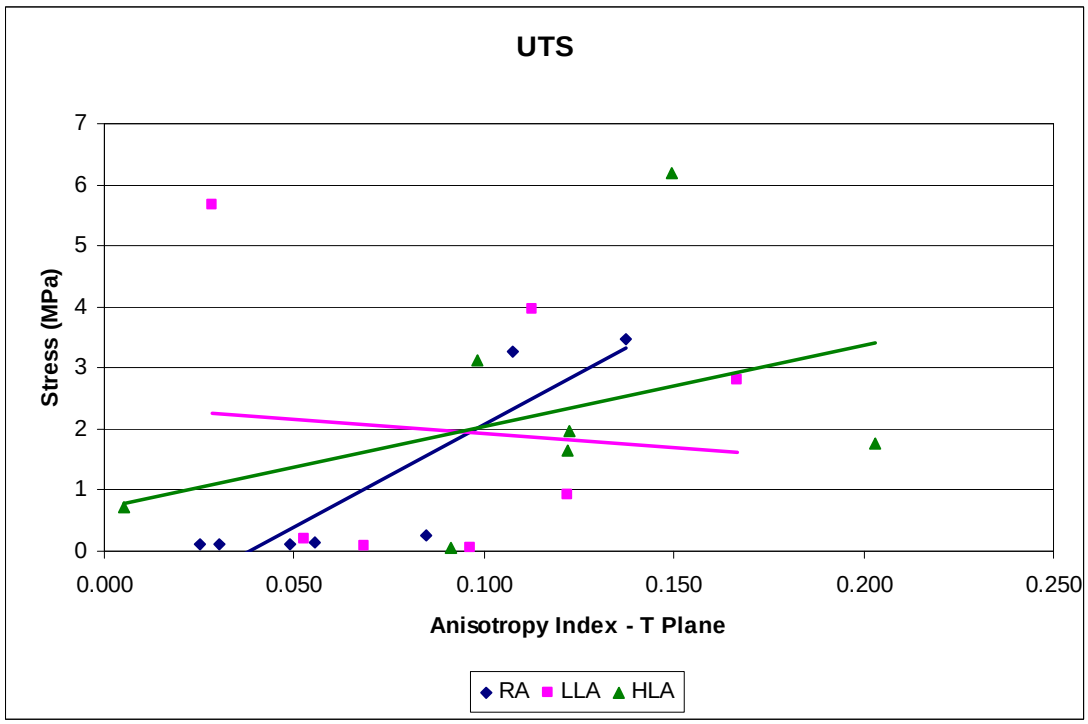

Figure B10: UTS versus anisotropy in the T-plane.

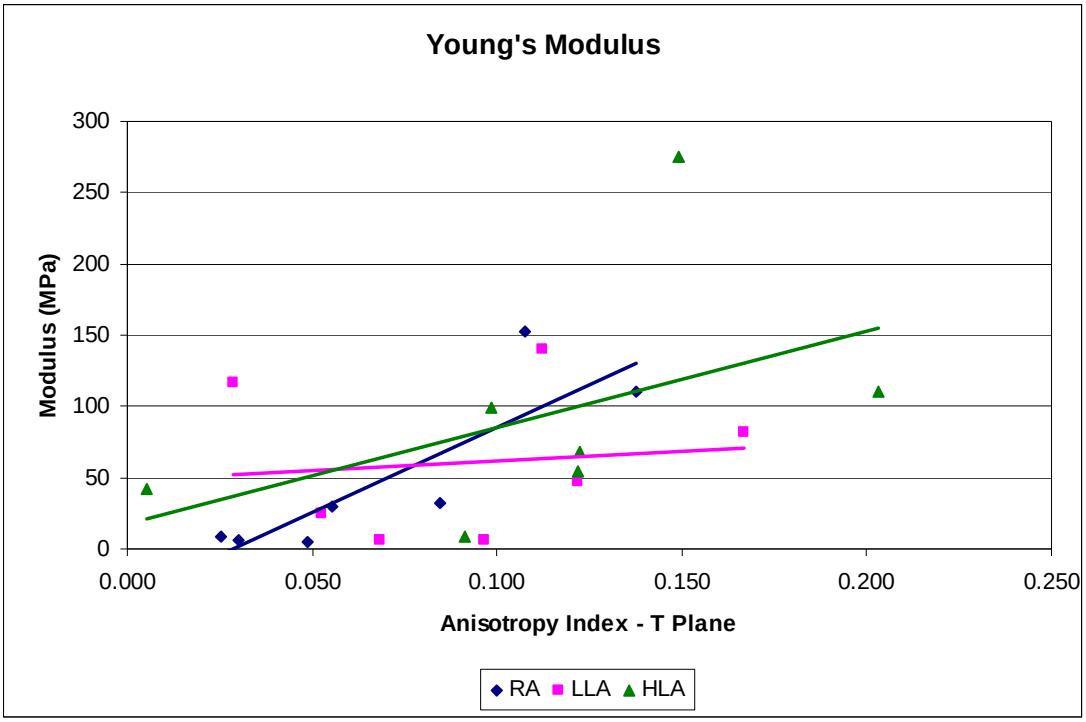

Figure B11: Young's modulus versus anisotropy in the T-plane.

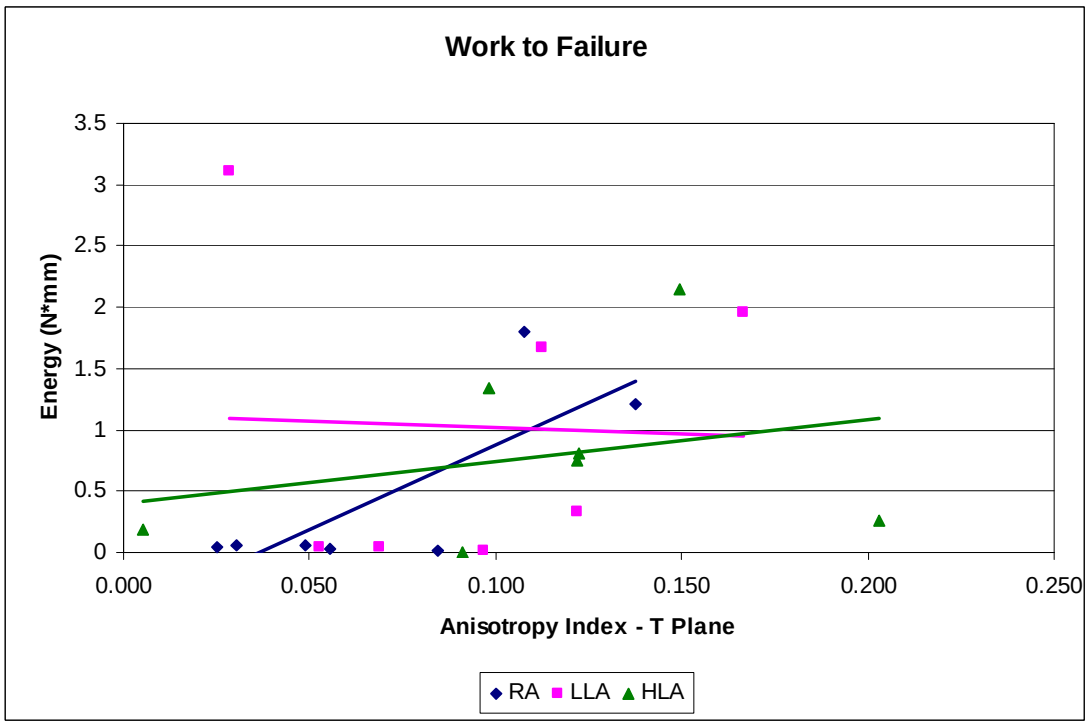

Figure B12: Work to failure versus anisotropy in the T-plane.

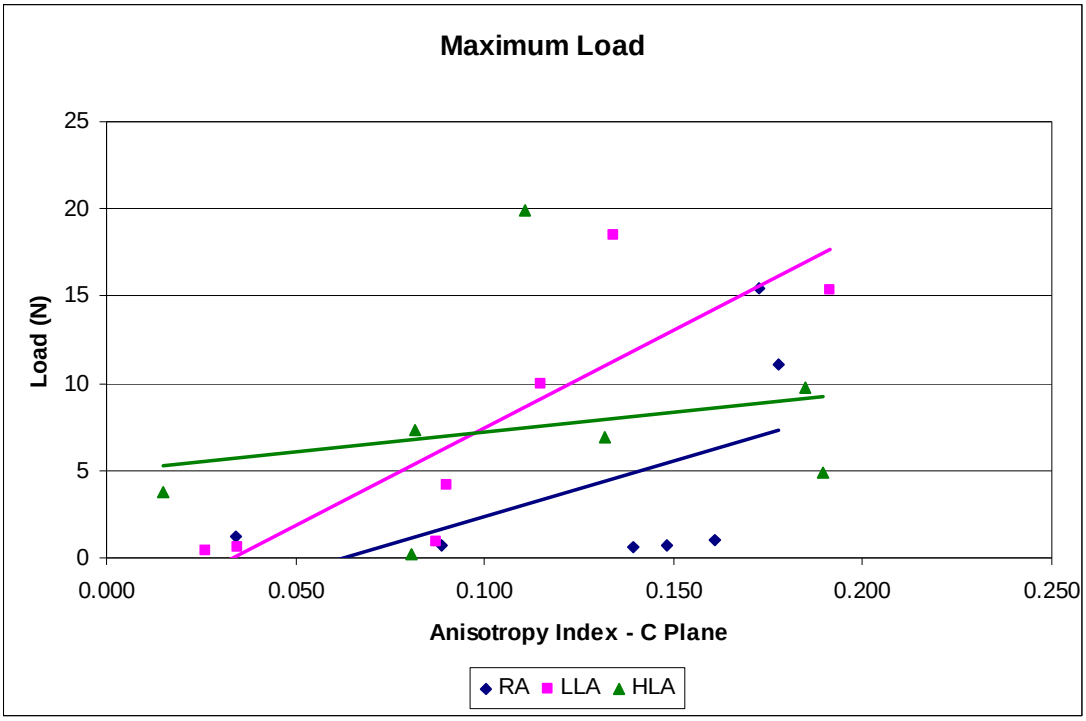

Figure B13: Maximum load versus anisotropy in the C-plane.

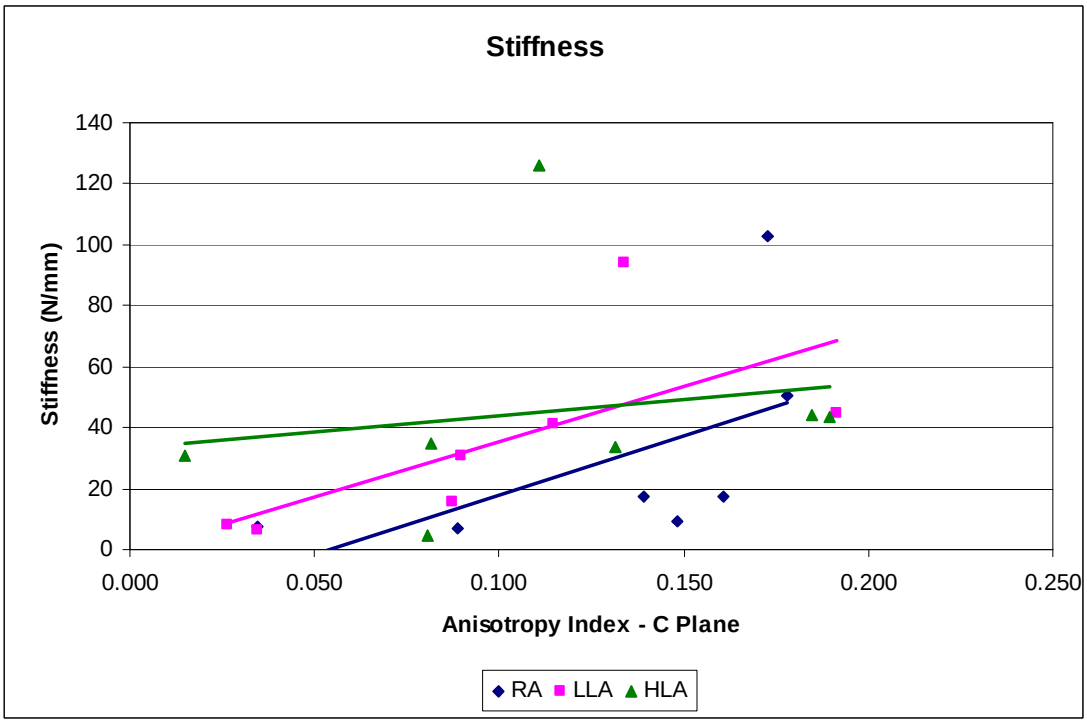

Figure B14: Stiffness versus anisotropy in the C-plane.

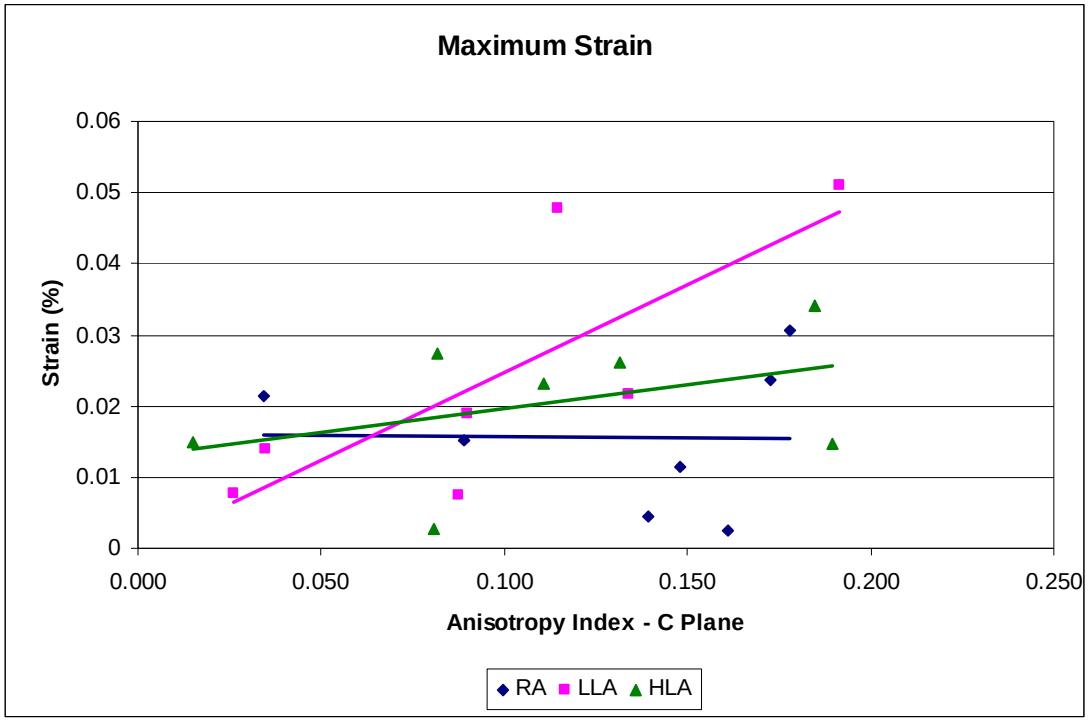

Figure B15: Maximum strain versus anisotropy in the C-plane.

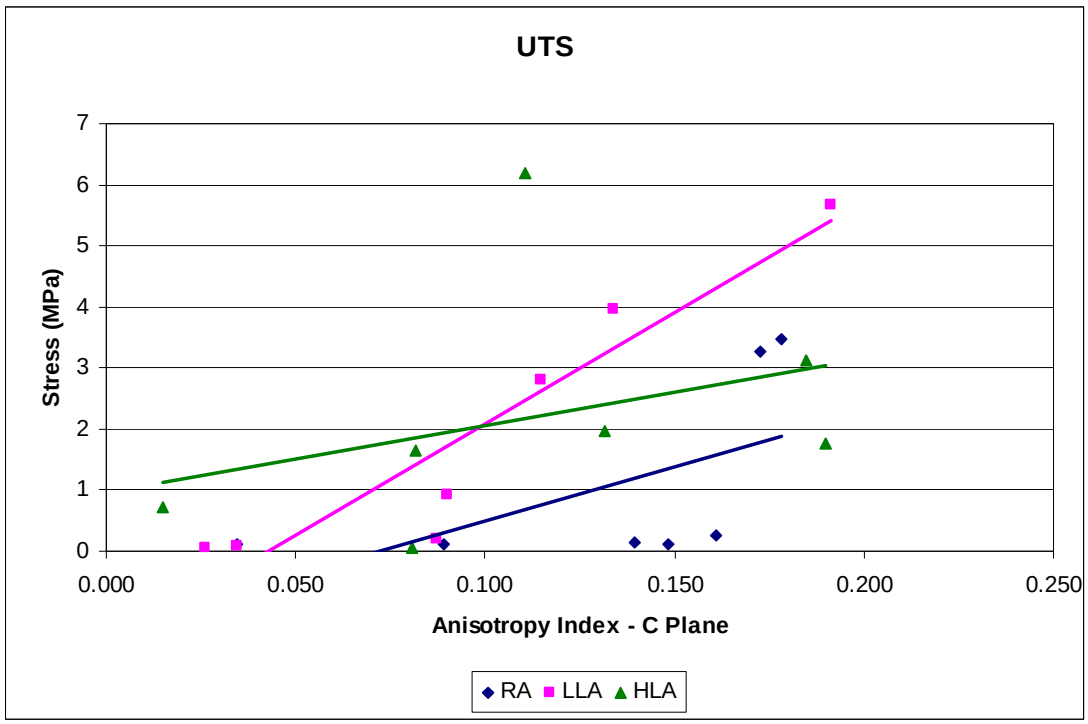

Figure B16: UTS versus anisotropy in the C-plane.

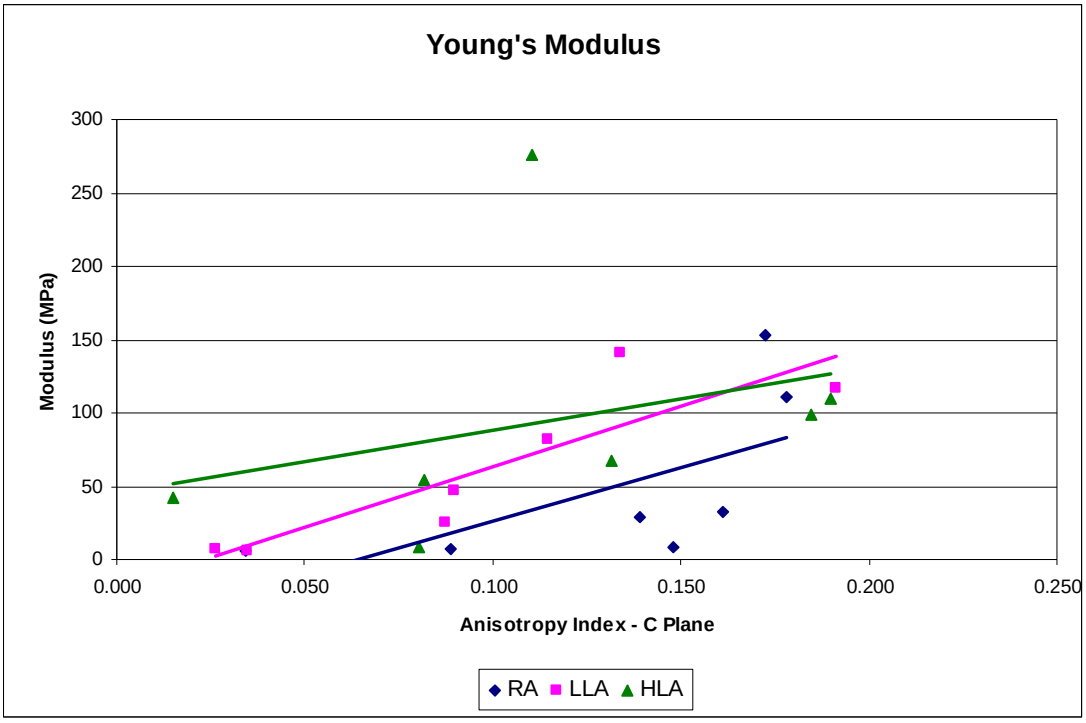

Figure B17: Young's modulus versus anisotropy in the C-plane.

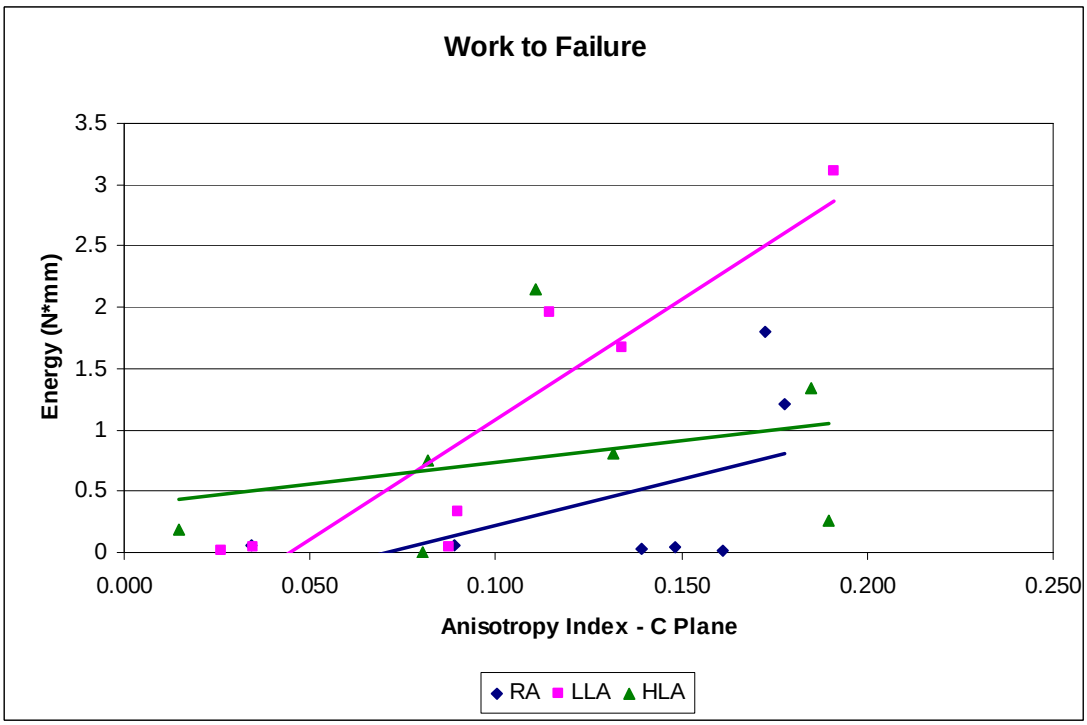

Figure B18: Work to failure versus anisotropy in the C-plane.

REFERENCES

1. Converse, G.L., Yue, W., Roeder, R.K. "Processing and Tensile Properties of Hydroxyapatite-Whisker-Reinforced Polyetheretherketone", *Biomaterials* 2007; 28: 927-935.
2. Kikuchi, M., Itoh, S., Ichinose S., Shinomiya K., Tanaka, J. "Self-organization Mechanism in a Bone-like Hydroxyapatite/Collagen Nanocomposite Synthesized In-vitro and its Biological Reaction In-vivo", *Biomaterials* 2001; 22: 1705-1711.
3. TenHuisen, K.S., Martin, R.I., Klimkiewicz, M., Brown, P.W. "Formation and Properties of a Synthetic Bone Composite: Hydroxyapatite-Collagen", *Journal of Biomedical Material Research* 1995; 29: 803-810.
4. Du, C., Cui, F.Z., Feng, Q.L., Zhu, X.D., de Groot, K. "Tissue Response to Nano-hydroxyapatite/collagen Composite Implants in Marrow Cavity", *Journal of Biomedical Material Research* 1998; 42: 803-810.
5. Du, C., Cui, F.Z., Zhu, X.D., de Groot, K. "Three-dimensional Nano-HAp/collagen Matrix Loading with Osteogenic Cells in Organ Culture", *Journal of Biomedical Material Research* 1999; 44: 407-415.
6. Martin, R.B., Burr, D.B., Sharkey, N.A. Skeletal Tissue Mechanics, Springer, New York; 2004.
7. Sauer GR and Wuthier RE. "Fourier Transform Infrared Characterization of Mineral Phases Formed During Induction of Mineralization by Collagenase-released Matrix Vesicles in Vitro", *The Journal of Biological Chemistry* 1988; 263:13718-13724.
8. Johnsson MS-A and Nancollas GH. "The Role of Brushite and Octacalcium Phosphate in Apatite Formation", *Critical Reviews in Oral Biology & Medicine* 1992; 3:61-82.
9. Bradt J-H, Mertig M, Teresiak A, Pompe W. "Biomimetic Mineralization of Collagen by Combined Fibril Assembly and Calcium Phosphate Formation", *Chemistry of Materials* 1999; 11:2694-2701.

10. Kikuchi M, Itoh S, Ichinose S, Shinomiya K, Tanaka J. "Self-organization mechanism in a bone-like hydroxyapatite/collagen nanocomposite synthesized in vitro and its biological reaction in vivo", *Biomaterials* 2001; 22:1705-1711.

11. Orme CA and Giocondi JL. Model Systems for Formation and Dissolution of Calcium Phosphate Minerals. In: Behrens P and Baeuerlein E, editors. Handbook of Biomineralization. Weinhein: Wiley-VCH; 2007. pg 135-157.

12. Eanes ED, Termine JD, Posner AS. "Amorphous Calcium Phosphate in Skeletal Tissues", *Clinical Orthopaedics and Related Research* 1967; 53:223-235.

13. Termine JD and Posner AS. "Calcium Phosphate formation in vitro: I. Factors Affecting Initial Phase Separation", *Archives of Biochemistry and Biophysics* 1970; 140:307-317.

14. Termine JD and Posner AS. "Calcium Phosphate formation in vitro: II. Effects of Environment on Amorphous-Crystalline Transformation", *Archives of Biochemistry and Biophysics* 1970; 140:318-325.

15. Blumenthal NC and Posner AS. "Hydroxyapatite: Mechanism of Formation and Properties", *Calcified Tissue Research* 1973; 13:235-243.

16. Eanes ED, Termine JD, Nylen MU. "An electron Microscopic study of the Formation of Amorphous Calcium Phosphate and its Transformation to Crystalline Apatite", *Calcified Tissue Research* 1973; 12:143-158.

17. Betts F, Blumenthal NC, Posner AS, Becker GL, Lehninger AL. "Atomic Structure of Intracellular Amorphous Calcium Phosphate Deposits", *Proceedings of the National Academy of Science USA* 1975; 72:2088-2090.

18. Blumenthal NC, Betts F, Posner AS. "Stabilization of amorphous calcium phosphate by Mg and ATP", *Calcified Tissue Research* 1977; 23:245-250.

19. Christoffersen J, Christoffersen MR, Kibalczyc W, Andersen FA. "A Contribution to the Understanding of the Formation of Calcium Phosphates", *Journal of Crystal Growth* 1989; 94:767- 777.

20. Zhou H, Zhang D, Guo L, Li H. "The Synthesis and Phase Transformations of Calcium-Deficient Apatite With Different Ca/P Ratios", *American Journal of Applied Sciences* 2006; Special Issue: 1-4.

21. Mahamid J, Aichmayer B, Shimoni E, Ziblat R, Li C, Siegel S, Paris O, Fratzl P, Weiner S, Addadi L. "Mapping Amorphous Calcium Phosphate Transformation into Crystalline Mineral from the Cell to the Bone in Zebrafish Fin Rays", *PNAS Biophysics and Computational Physics* 2010; 107:6316–6321.

22. Glimcher MJ, Bonar LC, Grynpas MD, Landis WJ, Roufosse AH. "Recent Studies of Bone Mineral: Is the Amorphous Calcium Phosphate Theory Valid?" *Journal of Crystal Growth* 1981; 53:100-119.

23. Grynpas MD, Bonar LC, Glimcher MJ. "Failure to Detect an Amorphous Calcium-Phosphate Solid Phase in Bone Mineral: A Radial Distribution Function Study", Calcified *Tissue International* 1984; 36; 291-301.

24. Wuthier RE, Rice GS, Wallace JEB, Weaver RL, Legeros RZ, Eanes ED. "In Vitro Precipitation of Calcium Phosphate Under Intracellular Conditions: Formation of Brushite from an Amorphous Precursor in the Absence of ATP", Calcified *Tissue International* 1985; 37:401-410.

25. Allen MA, Prissel MM, Young MJ, Douglas T. Constrained Metal Oxide Mineralization: Lessons from Ferritin Applied to other Protein Cage Architectures. In: Behrens P and Baeuerlein E, editors. Handbook of Biomineralization. Weinhein: Wiley-VCH; 2007. pg 313-333.

26. Simpson DR. "Effect of pH and Solution Concentration on the Composition of Carbonate Apatite", *The American Mineralogist* 1967; 52:896-902.

27. Katz EP. "The Kinetics of Mineralization *In Vitro*. I. The Nucleation Properties of 640-angstrom Collagen at 25 Degrees", *Biochim. Biophys. Acta* 1969; 194:121–129.

28. Blumenthal NC, Cosma V, Gomes E. "Regulation of Hydroxyapatite Formation by Gelatin and Type I Collagen Gels", *Calcified Tissue International* 1991; 48:440–442.

29. Glimcher MJ, Hodge AJ, Schmitt FO. "Macromolecular Aggregation States in Relation to Mineralization: The Collagen–Hydroxyapatite System as Studied *In Vitro*", *Proceedings of the National Academy of Science USA* 1957; 43:860–867.

30. de Jong AS, Hak TJ, van Duijn P. "The Dynamics of Calcium Phosphate Precipitation Studied with a New Polyacrylamide Steady State Matrix-Model: Influence of Pyrophosphate Collagen and Chondroitin Sulfate", *Connective Tissue Research* 1980; 7:73–79.

31. Hunter GK, Nyburg SC, Pritzker KP. "Hydroxyapatite Formation in Collagen, Gelatin, and Agarose Gels", *Collagen Relat. Res* 1986; 6:229–238.

32. Glimcher MJ. "Mechanism of Calcification: Role of Collagen Fibrils and Collagen–Phosphoprotein Complexes *In Vitro* and *In Vivo*", *Anatomical Record* 1989; 224:139–153.

33. Wang L and Nancollas GH. "Pathways to Biomineralization and Biodemineralization of Calcium Phosphates: The Thermodynamic and Kinetic Controls", *Dalton Transactions* 2009; 2665–2672.

34. Christiansen D and Silver FH. "Biomimetic Mineralization of an Aligned, Self-assembled Collagenous Matrix", *Materials Research Society Symposia Proceedings* 1992; 255:367-374.

35. Sun X-D, Zhou Y-L, Ren J-Y, Cui F-Z, Li H-D. "Effect of pH on the Fibroin Regulated Mineralization of Calcium Phosphate", *Current Applied Physics* 2007; 7S1:e75–e79.

36. Lawson AC and Czernuszka JT. "Collagen–Calcium Phosphate Composites", *Proc Instn Mech Engrs* 1998; 212(Part H):413-425.

37. Lawson AC and Czernuszka JT. "Production and Characterization of a Collagen-Calcium Phosphate Composite for use as a Bone Substitute", *Material Research Society Symposia Proceedings, Materials Research Society* 1999; 550:273-278.

38. Tadic, D., Peters, F., Epple, M. "Continuous Synthesis of Amorphous Carbonated Apatites", *Biomaterials* 2002; 23: 2553-2559.

39. Martin, R.B., Lau, S.T., Mathews, P.V., Gibson, V.A. Stover, S.M. "Collagen Fiber Organization is Related to Mechanical Properties and Remodeling in Equine Bone. A Comparison of Two Methods", *J. Biomechanics* 1996; 29(12): 1515-1521.

40. Banglmaier, R.F. and VandeVord, P.J. "Mechanical Properties of a Hydroxyapatite-Collagen Composite", *Society for Biomaterials Annual Meeting and Exposition* 2009; April 22-25, San Antonio, Texas.

41. Rho, J-Y., Kuhn-Spearing, L., Zioupos, P. "Mechanical Properties and the Hierarchical Structure of Bone", *Medical Engineering & Physics* 1998; 20: 92–102.

42. Mann, S. Biomineralization: Principles and Concepts in Bioinorganic Materials Chemistry. R.G. Compton, S.G. Davies, J. Evans (eds.), Oxford University Press, New York; 2001.

43. Bullough P. "Atlas of Orthopaedic Pathology", New York: Gower Medical Publishing; 1992.

44. Schaffler, M.B., Burr, D.B., Frederickson, R.G. "Morphology of the Osteonal Cement Line in Human Bone" *Anatomical Record* 1987 3: 223-228.

45. Ascenzi, A. and Bonucci, E. "The Ultimate Tensile Strength of Single Osteons", *Acta Anatomica* 1964; 58: 160-183.

46. Ascenzi, A. and Bonucci, E. "The Tensile Properties of Single Osteons", *Anatomical Record* 1967; 158: 375-386.

47. Ascenzi, A. and Bonucci, E. "The Compressive Properties of Single Osteons", *Anatomical Record* 1968; 161: 377-391.

48. Ascenzi, A. and Bonucci, E. "The Shearing Properties of Single Osteons", *Anatomical Record* 1972; 172: 499-510.

49. Giraud-Guille, M.M. "Twisted Plywood Architecture of Collagen Fibrils on Human Compact Bone Osteons", *Calcified Tissue International* 1988; 42: 167-180.

50. Marotti, G. and Muglia, M.A. "A Scanning Electron Microscope Study of Human Bony Lamellae. Proposal for a New Model of Collagen Lamellar Organization", *Archives of Italian Anatomy and Embriology* 1988; 93: 163-175.

51. Martin, R., Farjanel, J., Eichenberger, D., Colige, A., Kessler, E., Hulmes, D.J.S., Giraud-Guille, MM. "Liquid Crystalline Ordering of Procollagen as a Determinant of Three-dimensional Extracellular Matrix Architecture", *Journal of Molecular Biology* 2000; 301: 11-17.

52. Giraud-Guille, MM., Besseau, L., Herbage, D., Gounon, P. "Optimization of Collagen Liquid Crystalline Assemblies: Influence of Sonic Fragmentation", *Journal of Structural Biology* 1994; 113: 99-106.

53. Ascenzi, MG., Ascenzi, A., Benvenuti, A., Burghammer, M., Panzavolta, S., Bigi, A. "Structural Differences Between ''Dark'' and ''Bright'' Isolated Human Osteonic Lamellae", Journal of Structural Biology 2003; 141: 22–33.

54. Gibson, V.A., Stover, S.M., Martin, R.B., Gibeling, J.C., Willits, N.H., Gustafson, M.B., Griffin, L.V. (1995) "fatigue Behavior of the equine Third Metacarpus: Mechanical property analysis", *Journal of Orthopaedic Research*, 13: 861-868.

55. Xia, Y., Moody, J. B., Burton-Wurster, N., Lust, G. "Quantitative *In Situ* Correlation Between Microscopic MRI and Polarized Light Microscopy Studies of Articular Cartilage", *Osteoarthritis and Cartilage* 2001; 9**:** 393–406.

56. Skedros, J.G., Mendenhall, S.D., Kiser, C.J., Winet, H. "Interpreting Cortical Bone Adaptation and Load History by Quantifying Osteon Morphotypes in Circularly Polarized Light Images", *Bone* 2009; 44: 392–403.

57. Boyde, A. and Riggs, C.M. "The Quantitative Study of the Orientation of Collagen in Compact Bone Slices", *Bone* 1990; 11: 35-39.

58. Ascenzi, MG. and Lomovtsev, A. "Collagen Orientation Patterns in Human Secondary Osteons, Quantified in the Radial Direction by Confocal Microscopy", *Journal of Structural Biology* 2006; 153: 14–30.

59. Ascenzi, MG., Gill, J. Lomovtsev, A. "Orientation of Collagen at the Osteocyte Lacunae in Human Secondary Osteons", *Journal of Biomechanics* 2008; 41: 3426–3435.

60. Underwood, E.E. Quantitative Stereology, Reading, MA: Addison-Wesley; 1970.

61. Odgaard, A. "Three-Dimensional Methods for Quantification of Cancellous Bone Architecture", *Bone* 1997; 20: 315–328.

62. Geraets, W.G. "Comparison of Two Methods for Measuring Orientation", *Bone* 1998; 23: 383–388.

63. Chaudhuri, S., Nguyen, H., Rangayyan, R.M., Walsh, S., Frank, C.B. "A Fourier Domain Directional Filtering Method for Analysis of Collagen Alignment in Ligaments", *IEEE Trans Biomed Eng* 1987; 34: 509–518.

64. Petroll, W.M, Cavanagh, H.D., Barry, P., Andrews, P., Jester, J.V. "Quantitative Analysis of Stress Fiber Orientation During Corneal Wound Contraction", *J Cell Sci* 1993; 104: 353–363.

65. Pourdeyhimi, B., Dent, R., Davis, H. "Measuring Fiber Orientation in Nonwovens. III. Fourier Transform", *Textile Research Journal* 1997; 67: 143–151.

66. Marquez, J.P. "Fourier Analysis and Automated Measurement of Cell and Fiber Angular Orientation Distributions", *International Journal of Solids and Structures* 2006; 43: 6413–6423.

67. Whitehouse, W.J. "The Quantitative Morphology of Anisotropic Trabecular Bone", *Journal of Microscopy* 1974; 101: 153–168.

68. Harrigan, T.P. and Mann, R.W. "Characterization of Microstructural Anisotropy in Orthotropic Materials Using a Second Rank Tensor", *Journal of Materials Science* 1984; 19: 761–767.

69. Cowin, S.C. "Wolff's Law of Trabecular Architecture at Remodeling Equilibrium", *Journal of Biomechanical Engineering* 1986; 108: 83–88.

70. Odgaard, A., Kabel, J., van Rietbergen, B., Dalstra, M., Huiskes, R. "Fabric and Elastic Principal Directions of Cancellous Bone are Closely Related", *Journal of Biomechanics* 1997; 30: 487–495.

71. Sander, E.A. and Barocas, V. H. "Comparison of 2D Fiber Network Orientation Measurement Methods", *Journal of Biomedical Materials Research* 2009; 88A: 322–331.

72. Burger, W. and Burge, M.J. Digital Image Processing: An Algorithmic Introduction using Java. 1st Ed. Springer, New York; 2008. p 343-366.

73. Kuhn-Spearing L, Rey C, Kim HM, Glimcher MJ. Synthesis and Processing of Nanocrystalline Powder, Bourell DL, (ed.), The Minerals, Metals and Materials Society, Warrendale, PA, USA; 1996.

74. Termine, J.D. and Posner, A.S. "Infrared Analysis of Rat Bone: Age Dependency of Amorphous and Crystalline Mineral Fractions. *Science* 1966; 153: 1523–1525.

75. Mahamid, J. Sharir, A., Addadi, L., Weiner, S. "Amorphous Calcium Phosphate is a Major Component of the Forming Fin Bones of Zebrafish: Indications for an Amorphous Precursor Phase", *Proceedings of the National Academy of Science* 2008; 105(35): 12748-12753.

76. Connolly, J. "Introduction Quantitative X-Ray Diffraction Methods", Retrieved 11-23-2011, http://epswww.unm.edu/xrd/xrdclass/09-Quant-intro.pdf.

77. Markovic, M., Fowler, B.O., Tung, M.S. "Preparation and Comprehensive Characterization of a Calcium Hydroxyapatite Reference Material", Journal of Research of the National Institute of Standards and Technology 2004; 109(6): 553-568.

78. Klug HP and Alexander LE. X-ray Diffraction Procedures: for Polycrystalline and Amorphous Materials. John Wiley & Sons, 2nd Ed., 1974.

79. Bragg, W.L. The Crystalline State, Vol. 1, A General Survey. Bell, G., London; 1949; pg 189.

80. van der Meulen, M.C.H., Jepsen, K.J., Mikic, B. "Understanding Bone Strength: Size isn't Everything", *Bone* 2001; 29(2): 101-104.

81. Reilly, D.T., Burstein, A.H., Frankel, V.H. "The Elastic Modulus for Bone", *Journal of Biomechanics* 1974; 7: 271-275.

82. Reilly, D.T. and Burnstein, A.H. "The Elastic and Ultimate Properties of Compact Bone Tissue", *Journal of Biomechanics* 1975; 8: 393-405.

83. Hayes, W.C. and Gerhart, T.N. "Biomechanics of Bone: Applications for Assessment of Bone Strength", Peck, W.A. (ed.) Bone and Mineral Research, Elsevier Science Publishers, Amsterdam; 1985.

84. Fan, Z., Swadener, J., Rho, J., Roy, M., Pharr, G. "Anisotropy Nanoindentation Properties of Human Cortical Bone", *Orthopaedic Research Society 47th Annual Meeting*, San Francisco, CA, Feb. 2001; 25-28.

85. Burstein, A.H., Currey, J.D., Frankel, V.H., Reilly, D.T. "The Ultimate Properties of Bone Tissue: The Effects of Yielding", *Journal of Biomechanics* 1972; 5: 35-44.

86. Moyle, D.D., Welborn, J.W., Cooke, F.W. "Work to Fracture of Canine Femoral Bone. *Journal of Biomechanics* 1978; 11: 435-440.

87. Moyle, D.D. and Bowden, R.W. "Fracture of the Human Femoral Bone", *Journal of Biomechanics* 1984; 17: 203-213.

88. Lanyon, L.E. and Bourn, S. "The Influence of Mechanical Function on the Development and Remodeling of the Tibia: An Experimental Study in Sheep", *Journal of Bone and Joint Surgery (Am)* 1979; 61A: 263-273.

89. Riggs, C.M., Vaughan, L.C., Evans, G.P. Lanyon, L.E., Boyde, A. "Mechanical implications of Collagen Fibre Orientation in Cortical Bone of the Equine Radius", *Anatomical Embryology* 1993; 187: 239-248.

90. Skedros, J.G., Dayton, M.R., Sybrowskyi, C.L., Bloebaum, R.D, Bachus, K.N. "Are Uniform Regional Safety Factors an objective of Adaptive Modeling/Remodeling in Cortical Bone", *Journal of Experimental Biology* 2003; 206: 2431-2439.

91. Landis, W.J. Librizzi, J.J., Dunn, M.G., Silver, F.H. "A Study of the Relationship Between Mineral Content and Mechanical Properties of Turkey Gastrocnemius Tendon", *Journal of Bone Mineral Research* 1995; 10: 859-867.

92. Abe, H.K. and Sato, M. (eds.) Data Book on Mechanical Properties of Living Cells, tissues, and Organs. Springer, Tokyo, Berlin; 1996.

93. Gosline, J., Lillie, M. Carrington, E., Guerette, P., Ortlepp, C., Savage, K. "Elastic Proteins: Biological Roles and Mechanical Properties", *Phil. Trans. R. Soc. Lond*. B, 2002; 357: 121–132.

94. Gao, H., Ji, B., Jager, I., Arzt, E., Fratzl, P. "Materials Become Insensitive to Flaws at Nanoscale: Lessons from Nature", *Proceedings of the National Academy of Sciences* 2003; 100(10): 5597-5600.

95. Gao, H. and Ji, B. "Nanoscale Mechanical Properties in Bone and Dentin", *2003 Summer Bioengineering Conference*, Key Biscayne, FL, June 25-29; 2003.

96. Jager, I. and Fratzl, P. "Mineralized Collagen Fibrils: A Mechanical Model with a Staggered Arrangement of Mineral Particles", *Biophysical Journal* 2000; 79: 1737-1746.

97. Gutsman, T., Fantner, G.E., Kindt, J.H., Venturoni, M., Danielsen, S., Hansma, P.K. "Force Spectroscopy of Collagen fibers to Investigate Their Mechanical Properties and Structural Organization", *Biophysical Journal* 2004; 86:3186-3193.

98. Nalla, R.K. Kinney, J.H. Ritchie, R.O. "Effect of Orientation on the In Vitro Fracture Toughness of Dentine: The Role of Toughening Mechanisms" *Biomaterials* 2003; 24: 3955-3968.

99. Wang, X., Bank, R.A., Tekoppele, J.M., Agrawal, C.M. "The Role of Collagen in Determining Bone Mechanical Properties", *Journal of Orthopaedic Research* 2001; 19:1021-1026.

100. Wang, X., Shen, X., Li, X., Agrawal, C.M. "Age-Related Changes in the Collagen Network and Toughness of Bone", *Bone* 2002; 31: 1-7.

101. Yeni, Y.N., Fyhrie, D.P. "Collagen Bridged Microcrack Model for Cortical bone Tensile Strength", *Proceedings of the Bioengineering Conference BED (ASME)* 2001; New York, NY.

102. Landis, W.J. "The Strength of a Calcified Tissue Depends in Part on the Molecular Structure and Organization of its Constituent Mineral Crystals in the Their Organic Matrix", *Bone* 1995; 16(5): 533-544.

103. Kikuchi, M., Ikoma, T., Itoh, S., Matsumoto, H.N., Koyama, Y., Takakuda, K., Shinomiya, K., Tanaka, J. "Biomimetic Synthesis of Bone-Like Nanocomposites Using the Self-Organization Mechanism of Hydroxyapatite and Collagen", *Composites Science and Technology* 2004; 64: 819-825.

104. Elliot JC. "Recent Progress in the Chemistry, Crystal Chemistry and Structure of the Apatites", *Calcified Tissue Research* 1969; 3:293-307.

105. Posner AS. "Crystal Chemistry of Bone", *Physiological Reviews* 1969; 49:760-792.

106. Boskey AL and Posner AS. "Conversion of Amorphous Calcium Phosphate to Microcrystalline Hydroxyapatite. A pH-Dependent, Solution-Mediated, Solid-Solid Conversion", *The Journal of Physical Chemistry* 1973; 77:2313-2317.

107. Dragoe N. "PowderV2: A Suite of Applications for Powder X-ray Diffraction Calculations", *Journal of Applied Crystallography* 2001; 35:535.

108. A.S.T.M. card files No. 9-432 (HAP).

109. Hanawalt, J.D., Rinn, H., Frevel, L.K. Ind. Eng. Chem., Anal, Ed. 1938; 10: 457.

110. A.S.T.M. card files No. 9-80 (DCPA), No. 9-348, and 9-169 (α and β-TCP), No. 9-77 (DCPD), No. 19-272 (CAP, carbonated apatite), No. 26-1056 (OCP).

111. Harding IS, Rashid N, Hing KA. "Surface Charge and the Effect of Excess Calcium Ions on the Hydroxyapatite Surface", *Biomaterials* 2005; 26:6818–6826.

112. Liu X, Shieh SR, Fleet ME, Zhang L, He Q. "Equation of State of Carbonated Hydroxylapatite at Ambient Temperature up to 10 GPa: Significance of Carbonate", *American Mineralogist* 2011; 96:74–80.

113. Teng S-H, Lee E-J, Wang P, Shin D-S, Kim H-E. "Three-Layered Membranes of Collagen/Hydroxyapatite and Chitosan for Guided Bone Regeneration", *Journal of Biomedical Materials Research Part B: Applied Biomaterials* 2008; 87B:132–138.

114. Sang L, Huang J, Luo D, Chen Z, Li X. "Bone-like Nanocomposites Based on Self-assembled Protein-based Matrices with Ca2+ Capturing Capability", *Journal of Material Science: Materials in Medicine* 2010; 21:2561–2568.

115. Zhang Y, Reddy VJ, Wong SY, Li X, Su B, Ramakrishna S, Lin CT. "Enhanced Biomineralization in Osteoblasts on a Novel Electrospun Biocomposite Nanofibrous Substrate of Hydroxyapatite/Collagen/Chitosan", *Tissue engineering: Part A* 2010; 16:1949-1960.

116. Chung FH. "Quantitative Interpretation of X-ray Diffraction Patterns. I. Matrix-flushing Method of Quantitative Multicomponent Analysis", *Journal of Applied Crystallography* 1974; 7:519-525.

117. Combes C and Rey C. "Amorphous Calcium Phosphates: Synthesis, Properties and Uses in Biomaterials", *Acta Biomaterialia* 2010; 6:3362–3378.

118. Fleet ME and Liu X. "Local Structure of Channel Ions in Carbonate Apatite", *Biomaterials* 2005; 26:7548–7554.

119. Fleet ME and Liu X. "Coupled Substitution of Type A and B Carbonate in Sodium-bearing Apatite", *Biomaterials* 2007; 28:916-926.

120. McConnell D. "Precipitation of Phosphates in a Primeval Sea", *Science* 1973; 181:582.

121. McConnell D. "Crystal Chemistry of Hydroxyapatite: Its Relation to Bone Mineral", *Archives of Oral Biology* 1965; 10:421-431.

122. Aizawa M. et. al. "Syntheses of Calcium-deficient Apatite Fibers by a Homogeneous Precipitation Method and Their Characterizations", *Journal of the European Ceramic Society* 2006; 26:501-507.

123. Ivanova, T.I., Frank-Kamenetskaya, O.V., Kol'tsov, A.B., and Ugolkov, V.L. (2001) "Crystal Structure of Calcium-Deficient Carbonated Hydroxyapatite. Thermal Decomposition", *Journal of Solid State Chemistry* 2001; 160, 340–349.

124. Harper RA and Posner AS. "Measurement of Non-Crystalline Calcium Phosphate in Bone Mineral", *Proceedings of the Society for Experimental Biology and Medicine* 1966; 122:137-142.

125. Matsushima N, Tokita M, Hikichi K. "X-ray Determination of the Crystallinity in Bone Mineral", *Biochimica et Biophysica Acta* 1986; 883:574-579.

126. Dorozhkin SV. "Amorphous Calcium (Ortho)Phosphates", *Acta Biomaterialia* 2010; 6:4457–4475.

127. Gebhardt, W., 1906. "Ueber funktionell wichtige Anordnungsweisen der feineren und gr€oberen Bauelemente des Wirbeltierknochens. II. Spezieller Teil. l. Der Bau der Haverssohen

Lamellensysteme und seine funktionelle Bedeutung", *Arch. Entwickl. Mech. Org.* 1906; 20: 187–322.

128. Oldenbourg, R., and Mei, G. "New Polarized Light Microscope with Precision Universal Compensator", *Journal of Microscopy* 1995; 180 (Pt. 2): 140–7.

129. Arokoski, J.P., Hyttinen, M.M., Lapvetelainen, T., Takacs, P., Kosztaczky, B., Modis, L., Kovanen, V., Helminen, H.J "Decreased Birefringence of the Superficial Zone Collagen Network in the Canine Knee (Stifle) Articular Cartilage After Long Distance Running Training, Detected by Quantitative Polarized Light Microscopy", *Ann Rheum Dis* 1996; 55: 253–64.

130. Skedros, J.G., Dayton, M.R., Sybrowsky, C.L., Bloebaum, R.D. Bachus, K.N. "The Influence of Collagen Fiber Orientation and Other Histocompositional Characteristics on the Mechanical Properties of Equine Cortical Bone", *The Journal of Experimental Biology* 2006; 209: 3025-3042.

131. Tadic, D. and Epple, M. "Mechanically Stable Implants of Synthetic Bone Mineral by Cold Isostatic Pressing", *Biomaterials* 2003; 24: 4565-4571.

132. Pol, H.V., Joshi, Y.M., Tapadia, P.S., Lele, A.K., Mashelkar, R.A. "A Geometrical Solution to the Sharkskin Instability", *Ind. Eng. Chem. Res.* 2007; 46: 3048-3056.

133. Achilleos, E., Georgiou, G.C., Hatzikiriakos, S.G "On Numerical Simulations of Polymer Extrusion Instabilities", *Applied Rheology* 2002; 12: 88-104.

134. Miller, E. and Rothstein, J.P. "Control of the Sharkskin Instability in the Extrusion of Polymer Melts Using Induced Temperature Gradients", *Rheol Acta* 2004; 44: 160–173.

135. Gonzalez-Murillo, C.E. "Physical Properties of Unfired, Extruded Clays Reinforced with Low Cost Additives", Transfer Report, University of Bath, 2008.

136. Cogswell, F.N. "Stretching Flow Instabilities at the Exits of Extrusion Dies", *J Non-Newton Fluid* 1977; 2: 37–47.

137. M. Gelinsky, M. Welzel, P.B., Simonc, P., Bernhardt, A., Koenig, U. "Porous Three-Dimensional Scaffolds Made of Mineralised Collagen: Preparation and Properties of a

Biomimetic Nanocomposite Material for Tissue Engineering of Bone", *Chemical Engineering Journal* 2008; 137: 84–96.

138. Yunoki, S., Ikoma, T., Tsuchiya, A., Monkawa, A., Ohta, K., Sotome, S., Shinomiya, K., Tanaka1, J. "Fabrication and Mechanical and Tissue Ingrowth Properties of Unidirectionally Porous Hydroxyapatite/Collagen Composite", *Journal of Biomedical Materials Research, Part B: Applied Biomaterials* 2007; 80B: 166–173.

139. Hine, P.J., Tsui, S-W., Coates, P.D., Ward, I.M., Duckett, R.A. "Control of fibre orientation during the melt extrusion of short glass fibre reinforced polypropylene." *Proceedings ISATA Conference – Materials for Energy-Efficient Vehicles – Glass Technlogies* 1996; Paper Number 1996-25-0114: 1099-1105.

140. de Koker, D. and van Zijl, G.P.A.G. "Extrusion of Engineered Cement-Based Composite Material", *6th RILEM Symposium on Fiber-Reinforced Concretes (FRC) - BEFIB 20 - 22 September, Varenna, Italy* 2004; 1301-1310.

141. Banse, X., Sims, T.J., Bailey, A.J. "Mechanical Properties of Adult Vertebral Cancellous Bone: Correlation with Collagen Intermolecular Cross-links", *J Bone Miner Res* 2002; 17: 1621–8.

142. Burr, D.B. "The Contribution of the Organic Matrix to Bone's Material Properties", *Bone* 2002; 31: 8–11.

143. Nyman, J.S., Roy, A., Tyler, J.H., Acuna, R.L., Gayle, H.J., Wang, X. "Age-Related Factors Affecting the Postyield Energy Dissipation of Human Cortical Bone", *J Orthop Res* 2007; 25: 646–55.

144. Wang, X.D., Masilamani, N.S., Mabrey, J.D., Alder, M.E., Agrawal, C.M. "Changes in the Fracture Toughness of Bone May not be Reflected in its Mineral Density, Porosity, and Tensile Properties", *Bone* 1998; 23: 67–72.

145. Ascenzi, A. "The Micromechanics Versus the Macromechanics of Cortical Bone–A Comprehensive Presentation", *Journal of Biomechanical Engineering* 1988; 110: 357–63.

146. Evans, F.G., Vincentelli, R. "Relations of the Compressive Properties of Human Cortical Bone to Histological Structure and Calcification", *Journal of Biomechanics* 1974; 7: 1–10.

147. Reilly, D.T. and Burstein, A.H. "The Elastic and Ultimate Properties of Compact Bone Tissue", *Journal of Biomechanics* 1975; 8: 393–405.

148. Reilly, D.T. and Burstein, A.H. "The Mechanical Properties of Cortical Bone", *Journal of Bone Joint Surgery* 1974; 56-A: 1001–22.

149. Friess, W. "Collagen – Biomaterial for Drug Delivery", *European Journal of Pharmaceutics and Biopharmaceutics* 1998; 45: 113–136.

150. Powell, H.M. and Boyce, S.T. "EDC Cross-linking Improves Skin Substitute Strength and Stability", *Biomaterials* 2006; 27: 5821–5827.

151. Wojdyr, M. "Fityk : A General-Purpose Peak Fitting Program", *Journal Applied Crystalography* 2010; 43: 1126–1128.

152. de Guzman, R.C., Loeb, J.A., VandeVord, P.J. "Electrospinning of Matrigel to Deposit a Basal Lamina-Like Nanofiber Surface", *Journal of Biomaterials Science* 2010; 21: 1081–1101.

153. Deshpande, A.S. and Beniash, E. "Bio-inspired Synthesis of Mineralized Collagen Fibrils", *Cryst Growth Des*. 2008; 8(8): 3084–3090.

154. Koutsopoulos, S. "Synthesis and Characterization of Hydroxyapatite Crystals: A Review Study on the Analytical Methods", Journal of Biomedical Materials Research. 2002; 62: 600–612.

ABSTRACT

ENHANCING THE MECHANICAL PROPERTIES OF A HYDROXYAPATITE-COLLAGEN BONE SURROGATE

by

RICHARD F. BANGLMAIER

August 2012

Advisor: Dr. Pamela J. VandeVord

Major: Biomedical Engineering

Degree: Doctor of Philosophy

The synthesis of biomimetic hydroxyapatite-collagen composites is desirable from the perspective of graft elimination and load-bearing support when treating damaged or diseased bone. Bone is an organized network of carbonated hydroxyapatite mineralized collagen, whose strength and toughness is dependent on the organized array of mineralized collagen fibers that align with applied physiologic stresses. The apatitic calcium phosphate phase, hydroxyapatite, is promising for the biomimetic mineralization of collagen. Hydroxyapatite-collagen composites are osteoconductive and resorbable. However, the mechanical properties of these composites are one or more orders of magnitude less than bone. The aim of this study was to produce a bone-like hydroxyapatite-collagen composite with an induced collagen fiber alignment in order to improve the mechanical properties of the composite. In this study, environmental and temporal effects on the synthesis of a hydroxyapatite-collagen composite were characterized and compared to bone. Three dimensional hydroxyapatite-collagen composite scaffolds were fabricated by a combined extrusion and compaction process producing three different levels of collagen fiber alignment, which were quantified and correlated to the resultant mechanical properties. The levels of collagen fiber alignment corresponded to an expected random

alignment, low longitudinal alignment, and high longitudinal alignment. The results showed that a bone-like hydroxyapatite-collagen composite is best synthesized in physiologic to alkaline pH (7.4 – 8.0) and allowed to react for 6 hours. Composite scaffolds fabricated with the low longitudinal alignment method produced the highest degree of alignment among the fabrication methods. Degree of collagen alignment produced the best strain and toughness responses. Compaction aided strength related mechanical properties. This study gives proof of concept for a collagen fiber alignment process and indicates that the mechanical properties of a three dimensional HAp/C composite scaffold fabricated by this process are dependent on the degree of collagen fiber alignment.

AUTOBIOGRAPHICAL STATEMENT

In 1993 Richard Banglmaier received his B.S. degree in Mechanical Engineering from GMI Engineering & Management Institute and in 1999 he earned his M.S. degree in Mechanics from Michigan State University. Mr. Banglmaier conducted research into human injury tolerance and biomechanics at Ford Motor Company for 7 years, after his M.S. degree. Most recently, he has been the Resident Research Coordinator at Henry Ford Hospital since 2008. In this position, he has been conducting research on the biomechanics of femoral neck fracture repair devices and on the effects of advanced glycation end-product (AGE) crosslink breakers on the mechanical response of cortical bone graft tissues, at the Bone & Joint Center. In 2003, Mr. Banglmaier began investigating methodologies to induce preferential alignment of collagen fibers in a hydroxyapatite composite. Currently, Mr. Banglmaier is a Doctoral Candidate of Biomedical Engineering at Wayne State University researching the mechanical properties and characteristics of hydroxyapatite/collagen composite scaffolds for bone repair. Mr. Banglmaier has published over 15 peer reviewed articles and abstracts.

Mr. Banglmaier's research interests are in bone mechanics and orthopaedic tissue engineering. Specifically, his interests are the material property and mineral characterization of hydroxyapatite/collagen composites and engineered bone analogues for fracture repair.